



University  
of Glasgow

Cudden, Judith Rose (2002) *An investigation of braided river dynamics using a new numerical modelling approach*. PhD thesis.

<http://theses.gla.ac.uk/5421/>

Copyright and moral rights for this thesis are retained by the author

A copy can be downloaded for personal non-commercial research or study, without prior permission or charge

This thesis cannot be reproduced or quoted extensively from without first obtaining permission in writing from the Author

The content must not be changed in any way or sold commercially in any format or medium without the formal permission of the Author

When referring to this work, full bibliographic details including the author, title, awarding institution and date of the thesis must be given

**An investigation of braided river dynamics  
using a new numerical modelling approach.**

**Judith Rose Cudden**

Submitted for the degree of Doctor of Philosophy

University of Glasgow  
Department of Geography and Topographic Science

July 2002

© Judith R. Cudden 2002

## DECLARATION OF ORIGINALITY

Except where specific reference is made to other sources the work presented in this thesis is the original work of the author. It has not been submitted in part or in whole for any other degree.

A handwritten signature in cursive script that reads "J. R. Cudden". The letters are fluid and connected, with a prominent loop at the end of the name.

Judith R. Cudden, July 2002

## ABSTRACT

*Braided Cascade* has been developed from *Cascade* (Braun and Sambridge, 1997), a long-term ( $dt = 100$  years) numerical model that simulates long-term landscape evolution. Herein it has been modified and applied to relatively short term process modelling of the evolution of complex river topography, discharge and sediment load of braided rivers. *Braided Cascade* is synthesisist in spirit, there is no detailed hydrodynamic component to the model, a realistic simplification at the time scales considered. The major advantage of the model is the incorporation of an irregular time-varying grid using a triangulated irregular network (TIN) to represent a terrain surface. Advantages of using TINs include the ability to solve problems with non-rectangular geometries and/or boundary conditions and the ability of river segments to form in all directions. The model routes water from node to node based on the local topographic slope. Sediment transport depends on the local stream power. Nodal elevation changes after each iteration according to the difference between the amount of sediment entering and leaving the node. Model output includes spatial and temporal (at one point) water discharge, bedload sediment transport, as well as maps of channel networks, erosion and deposition throughout the reach.

Sensitivity analysis indicated that the most significant parameters for braiding are erosion length scale, splitting ratios and the allowance of the model to deposit sediment. Therefore an imbalance in the amount of sediment the river is carrying and the carrying capacity AND a reworking of the deposits is needed for a braided network to form.

Model results were compared to field and flume data using dynamical systems methods. Quantitative analysis was undertaken using an automated box counting-transfer distance method. Flume data indicates that, as the number of channels in the flume increases, probability density functions of the transport rates become positively skewed and the transport rates become more variable but the frequency of fluctuations decreases. Using dynamical systems methods it was found that for a given discharge, planforms with a similar number of channels are more statistically similar than networks with a greater difference in channel number. Field data from a single anabranch of a braided channel network indicate that the distribution of transport rates is qualitatively similar to those produced by flume experiments with braided channel networks. However quantitative analysis using the modified box counting technique revealed that the field data sets are dissimilar to each other and also to the flume runs. Time series data sampled from one point in a single anabranch therefore have a different internal structure than spatially integrated data obtained by trapping sediment across the entire braidplain width.

Sediment output from model runs indicate that the similarities between model data and other data sets are weak and all runs tended to reach static equilibrium. *Braided Cascade* therefore failed to adequately reproduce realistic data sets. It was found that the differences between model results and the flume data indicate that the model does not always match the physical systems as closely as physical systems match each other.

# TABLE OF CONTENTS

		Page number
<b>Abstract</b>		i
<b>Acknowledgements</b>		xi
<b>Chapter 1: Introduction</b>		
1	Introduction	1
<b>Chapter 2: Approaches to modelling braided rivers.</b>		
2		4
2.1	Introduction	4
2.2	Definition of Braiding	4
2.2.1	Mechanisms of braid development	6
2.3	Bedload transport through braided reaches	8
2.3.1	Spatial and temporal scales of bedload variability	8
2.3.2	Bedload probability density functions	9
2.3.3	Mechanisms of bedload pulsing	14
2.3.4	Summary	16
2.4	Spatial scaling, self-affinity and self-organisation in braided rivers	16
2.4.1	Summary	19
2.5	Approaches to investigating braided rivers	20
2.5.1	Field investigations	20
2.5.2	Modelling of braided rivers	22
2.5.2.1	Physical modelling	23
2.5.2.2	Numerical modelling	24
2.5.3	Reductionist and small-scale investigations	25
2.5.4	Synthesist and larger scale numerical modelling	26
2.5.4.1	Random Walk Models	26
2.5.4.2	Limitations of random walk models	32
2.5.5	Deterministic models	32
2.5.5.1	SIBERIA (Willgoose et al., 1991a-d, 1994)	33
2.5.5.2	Howard's (1994, 1997) model	35
2.5.5.3	<i>Cascade</i> (Braun and Sambridge)	37
2.5.5.4	Channel Hillslope Integrated Landscape Development model (CHILD) (Tucker et al., 1999)	38
2.5.5.5	Deterministic models. A summary	39
2.5.6	Cellular automata models	39
2.5.6.1	Cellular automata models of braided river evolution	41
2.5.6.2	Summary	46
2.6	Conclusions	47
<b>Chapter 3: Numerical modelling and the development of <i>Braided Cascade</i></b>		
3.1	Introduction to Braided Cascade	51
3.2	Philosophies of numerical modelling	53
3.3	Finite element and finite difference models	54
3.4	The model grid	55
3.5	Routing of flows on the grid	57
3.6	Flow directions	58
3.7	Node ordering – the <i>Cascade</i> algorithm	61
3.8	Water routing and runoff	63
3.8.1	Donor nodes with two downhill receiving nodes	65
3.8.2	Donor nodes with two uphill receiving nodes	68

3.8.3	Donor nodes with one downhill and one uphill receiving node, or donor nodes with only one receiving node	69
3.9	Sediment routing	69
3.10	Erosion length scales	73
3.10.1	Spatial lag effects in bed load sediment transport	73
3.10.2	Temporal lag	76
3.11	Deposition	77
3.12	Numerical method used to solve the channel transport equation	77
3.13	Boundary conditions	79
3.14	Scales used in Braided Cascade	80
3.15	Summary of model development	81
<b>Chapter 4. Data used in model validation.</b>		
4.1	Fieldwork program and instrumentation	83
4.2	Sediment characteristics	85
4.3	Point bedload sampling – Helley Smith sampling	88
4.4	Summary of field data collection	90
4.5	Flume data (Zarn 1997)	90
4.6	Summary of Chapter 4	92
<b>Chapter 5. Sensitivity analysis</b>		
5.1	Introduction: what is sensitivity analysis and why is it necessary?	93
5.2	Experimental design and control run: simulation of the idealised Arolla case	94
5.2.1	Boundary and initial conditions	97
5.2.2	Spatial lag effects: the erosion length scale for alluvial material	98
5.2.3	Notional grain size	99
5.2.4	Discharge splitting ratios	99
5.2.5	The effect of lateral erosion	99
5.2.6	Grid gradient	100
5.3	Results from the control run	100
5.4	Sensitivity analysis	105
5.4.1	Variation of spatial length scale - spatial lag	105
5.4.2	The effect of no deposition	124
5.4.3	Discharge splitting ratios (values of <i>qratio</i> and <i>upratio</i> )	127
5.4.4	Lateral sediment transport	139
5.4.5	Gradient of the grid	154
5.5	Discussion	160
5.5.1	Model parameter values	161
5.5.1.1	Erosion length scale and fluvial transport	161
5.5.1.2	Deposition	162
5.5.1.3	Flow splitting ratios	162
5.5.1.4	Lateral transport (Diffusivity)	163
5.5.1.5	Grid gradient	163
5.5.1.6	Sediment input	163
5.6	Conclusions	163
<b>Chapter 6. Testing <i>Braided Cascade</i></b>		
6.1	Introduction	165
6.2	Linking spatial and temporal bedload transport variability	165
6.2.1	Flume data: Zarn (1997)	166
6.2.2	Field data: Arolla 1999	194
6.2.3	Braided Cascade runs	201
6.2.3.1	Model results	203
6.2.3.1.1	Run1	203
6.2.3.1.2	Run2	208
6.2.3.1.3	Run3	214

6.2.3.1.4	Comparisons of all <i>Braided Cascade</i> runs	221
6.3	Discussion and summary of Chapter 6.	223
<b>Chapter 7. Conclusions and Recommendations</b>		
7.1	Introduction	226
7.2	Model development: Braided Cascade	228
7.3	Model sensitivity analysis	230
7.3.1	Parameter values	230
7.3.2	Comparison of model data with field and flume data	231
7.3.3	Summary of conclusions	231
7.4	Braided river modelling: recommendations for future work	231
<b>References</b>		234
<b>Appendix: Cascade authorship and Fortran code</b>		248

## LIST OF FIGURES

### Chapter 2. Approaches to modelling braided rivers.

2.1.	Relative bedload transport rates vs. distance along a (primary) dune with secondary bedforms according to Hamamori's assumptions.	11
2.2.	Generalised Hamamori pdfs for selected values of $m$ .	12
2.3.	Measured and simulated pdfs of relative bedload transport rate for two experiments (experimental data from Hoey 1989; Hoey and Sutherland, 1991).	14
2.4.	Water and sediment routing in the Murray and Paola (1994, 1997) cellular automata braided river model.	43

### Chapter 3. Numerical modelling and the development of *Braided Cascade*.

3.1.	Flow chart showing the sequence of computation in the model.	52
3.2.	Schematic illustration of model grid components.	56
3.3.	2D schematic illustration of flow routing along the TIN node network. Schematic diagram of flow splitting between two receiver nodes.	59
3.4.	An example of a DEM input into <i>Braided Cascade</i> to illustrate problems with node ordering encountered by the bucket passing algorithm (BPA).	64
3.5.	Flow chart showing computations involved in iterations to calculate distribution of water between receiver nodes according to water surface slope.	68
3.6.	Bedload discharge as a function of stream power in the braided rivers used to generate the constant and exponent for the sediment transport equation.	72
3.7.	Schematic diagram of water surface, node elevation and bedrock-alluvial interface.	79
3.8.	Schematic illustration of a typical model grid used for generic runs of the model.	80

### Chapter 4. Data used in model validation.

4.1.	Position of survey transects, bridge site and Wolman count sites shown on contour map of reach on 16/7/99.	84
4.2.	Surface and subsurface bulk samples, Arolla 1999.	87
4.3.	Time series of unit bedload transport ( $\text{g m}^{-1} \text{s}^{-1}$ ), 18/7/99.	89
4.4.	Time series of unit bedload transport ( $\text{g m}^{-1} \text{s}^{-1}$ ), 20/7/99.	89

### Chapter 5. Sensitivity analysis.

5.1.	Diagram of the triangulated grid used in sensitivity analysis.	97
5.2.	Diagram of the control run showing channel evolution.	101
5.3a.	Histogram of overall erosion /deposition experienced by each node for the control run (with no sediment input at the upstream end of the grid).	102
5.3b.	Cumulative frequency curve of erosion / deposition in the control run.	102
5.4.	Diagram showing channel evolution for the control run with sediment added at the upstream boundary.	103
5.5.	Time series of sediment outflux for the control run with and without sediment input, after every 1000 iterations.	104
5.6.	Disequilibrium between transport capacity and actual transport rate as defined by the erosion length scale.	106
5.7.	Diagram showing channel evolution for a run with the erosion length scale equal to 0.00001.	107
5.8.	Diagram showing channel evolution for a run with the erosion length scale equal to the nodal density.	108

5.9.	Diagram showing channel evolution for a run with the erosion length scale equal to 50.	109
5.10	Diagram showing channel evolution for a run with the erosion length scale equal to 100 times the nodal density.	110
5.11	Diagram showing channel evolution for a run with the erosion length scale equal to the length of the grid.	111
5.12a.	Cumulative frequency curve of water depth for runs of different length scales.	113
5.12b.	Histograms of proportion of nodes with different water depth after 50 000 iterations for runs with different erosion length scales and no sediment input.	113
5.13.	Time series of sediment outflux from runs with different erosion length scales.	115
5.14.	Diagram showing channel evolution for a run with the erosion length scale equal to 0.00001 and sediment input at the upstream boundary.	117
5.15.	Diagram showing channel evolution for a run with the erosion length scale equal to the nodal density and sediment input at the upstream boundary.	118
5.16.	Diagram showing channel evolution for a run with the erosion length scale equal to 100 times the nodal density and sediment input at the upstream boundary.	119
5.17.	Diagram showing channel evolution for a run with the erosion length scale equal to the length of the grid and sediment input at the upstream boundary.	120
5.18a.	Cumulative frequency curve of water depth for runs of different length scales and sediment input.	121
5.18b.	Histograms of proportion of nodes with different water depth after 50 000 iterations for runs with different erosion length scales and sediment input.	122
5.19.	Time series of sediment outflux from runs with different erosion length scales and sediment input.	123
5.20.	Diagram showing channel evolution for a run with no sediment deposition.	126
5.21.	Time series of sediment outflux from the control run and a run with no deposition.	127
5.22.	Diagram showing channel evolution for a run with qratio and upratio set to 0.5.	129
5.23	Diagram showing channel evolution for a run with qratio and upratio set to 0.95.	130
5.24.	Diagram showing channel evolution for a run with qratio = 0.8 and upratio = 0.95.	131
5.25.	Diagram showing channel evolution for a run with qratio = 0.95 and upratio = 0.8.	132
5.26.	Diagram showing channel evolution for a run with qratio and upratio set to 0.95 and sediment input at the upstream end of the grid.	133
5.27.	Diagram showing channel evolution for a run with qratio = 0.8 and upratio = 0.95 sediment input at the upstream end of the grid.	134
5.28	Diagram showing channel evolution for a run with qratio = 0.95 and upratio = 0.8 sediment input at the upstream end of the grid.	135
5.29a.	Cumulative frequency curve of water depth for runs with different qratio and upratio values and no sediment input.	136
5.29b.	Histograms of proportion of nodes with different water depth after 50 000 iterations for runs with different qratio and upratio values and no sediment input.	136
5.30a.	Cumulative frequency curve of water depth for runs with different qratio and upratio values and sediment input.	137
5.30b.	Histograms of proportion of nodes with different water depth after 50 000 iterations for runs with different qratio and upratio values and with sediment input.	138
5.31	Diagram showing channel evolution for a run with diffusion turned on.	144
5.32	Diagram showing channel evolution for a run with diffusion turned on and sediment input at the upstream end of the grid.	145

5.33	Diagram showing channel evolution for a run with diffusion set to $1 \times 10^{-6} \text{ m}^3 \text{ s}^{-1}$ .	146
5.34	Diagram showing channel evolution for a run with diffusion set to $1 \times 10^{-7} \text{ m}^3 \text{ s}^{-1}$ .	147
5.35	Diagram showing channel evolution for a run with diffusion set to $1 \times 10^{-8} \text{ m}^3 \text{ s}^{-1}$ .	148
5.36	Diagram showing channel evolution for a run with diffusion set to $1 \times 10^{-6} \text{ m}^3 \text{ s}^{-1}$ and sediment input.	149
5.37	Diagram showing channel evolution for a run with diffusion set to $1 \times 10^{-7} \text{ m}^3 \text{ s}^{-1}$ and sediment input.	150
5.38	Diagram showing channel evolution for a run with diffusion set to $1 \times 10^{-8} \text{ m}^3 \text{ s}^{-1}$ and sediment input.	151
5.39a.	Cumulative frequency curve of water depth for runs with different diffusion constants and no sediment input.	152
5.39b.	Histograms of proportion of nodes with different water depth after 50 000 iterations for runs with different diffusion constants and no sediment.	153
5.40	Time series plots of sediment outflux from the grid for runs with diffusion erosion switched on and the control run (NO diffusion).	153
5.41	Diagram showing channel evolution for a run with slope set to 0.01.	155
5.42	Diagram showing channel evolution for a run with slope set to 0.01 and sediment input.	156
5.43	Time series of sediment outflux for the control run and runs with slope equal to 0.01.	157
5.44	Diagram showing channel evolution for a run with slope set to 0.01 and total discharge of $17.13 \text{ m}^3 \text{ s}^{-1}$ .	158
5.45	Diagram showing channel evolution for a run with slope set to 0.02 and total discharge of $8.565 \text{ m}^3 \text{ s}^{-1}$ .	159
5.46	Time series of sediment outflux from the grid for runs with slope and discharge but the same discharge-slope product.	160

## Chapter 6. Testing Braided Cascade.

6.1	Histograms of unit bedload transport rates in experiments of Zarn (1997)	167
6.2	Time series of unit bedload transport rate for Zarn's (1997) runs grouped according to discharge.	169
6.3	Cumulative sediment transport curves for all Zarn's (1997) runs.	170
6.4	Average unit sediment transport rate versus average number of channels for each discharge (Q).	172
6.5	Mean unit bedload transport rate versus discharge for different flume widths.	172
6.6	Autocorrelation functions of the linear residuals of the bedload transport time series.	176
6.7	Partial autocorrelation functions of the linear residuals of the bedload transport time series.	178
6.8	Time series of bedload transport rate for run 30_7 plotted in state space with a delay of 1.	182
6.9	Time series data for run 30_7 plotted as z scores and rotated clockwise so that the 1:1 line is now horizontal.	182
6.10	Schematic diagram of the appearance of a bedload pulse in state space.	186
6.11	Crossing period versus discharge for runs grouped by flume width.	187
6.12	State space plots of t versus t+1 for all runs grouped by discharge.	189
6.13	Schematic diagram of weighted node movement between cells on the state space plot.	191
6.14	Time series of unit bedload transport rate from Arolla, 18/7/99.	194
6.15	Time series of unit bedload transport rate from Arolla 20/7/99.	194
6.16	Histograms of unit bedload transport rate from Arolla.	196
6.17	Correlograms for Arolla data.	198

6.18	Partial autocorrelations for Arolla data.	198
6.19	Rotated state space plot of $t$ versus $t + 1$ for Arolla data, 18/7/99.	199
6.20	Rotated state space plot of $t$ versus $t + 1$ for Arolla data, 20/7/99.	200
6.21	Time series of sediment ouflux from the grid for a run with a single channel.	204
6.22	Histogram of sediment ouflux from model run 1 with a single thread channel.	204
6.23	Correlogram for <i>Braided Cascade</i> Run 1.	206
6.24	Partial autocorrelation function for <i>Braided Cascade</i> Run 1.	206
6.25	Sediment ouflux from <i>Braided Cascade</i> Run 1 plotted in state space.	207
6.26	Time series of sediment ouflux from the grid for <i>Braided Cascade</i> Run 2.	208
6.27	Plots of water depth on the grid at different times throughout Run 2.	209
6.28	Histograms of relative frequency of water depths on each grid at varying times throughout Run 2.	211
6.29	Histogram of sediment ouflux from <i>Braided Cascade</i> run 2 with a braided channel pattern.	212
6.30	Correlogram for <i>Braided Cascade</i> Run 2.	213
6.31	Partial autocorrelation function for <i>Braided Cascade</i> Run 2.	213
6.32	Sediment ouflux from <i>Braided Cascade</i> Run 2 plotted in state space.	214
6.33	Time series of sediment ouflux from the grid for <i>Braided Cascade</i> Run 3.	215
6.34	Histogram of sediment ouflux from <i>Braided Cascade</i> run 3 with a braided channel pattern.	216
6.35	Plots of water depth on the grid at different times throughout Run 3.	217
6.36	Histograms of relative frequency of water depths on each grid at varying times throughout Run 3.	218
6.37	Correlogram for <i>Braided Cascade</i> Run 3.	219
6.38	Partial autocorrelation function for <i>Braided Cascade</i> Run 3.	219
6.39	Sediment ouflux from <i>Braided Cascade</i> run 3 plotted in state space	220
6.40	Cumulative sediment output from <i>Braided Cascade</i> runs.	222

## LIST OF TABLES

### Chapter 2. Approaches to modelling braided rivers.

2.1.	Summary of braiding mechanisms.	7
2.2.	Hierarchical bedform classification for bedload pulses and bed waves.	9
2.3.	Selected small-scale field investigations of sediment transport in braided rivers.	21
2.4.	Sediment routing rules in the cellular automata braided river model of Murray and Paola (1994, 1997).	43

### Chapter 3. Numerical modelling and the development of *Braided Cascade*.

3.1.	Summary of receiving nodes and flow directions.	60
3.2.	Classification of receiver nodes and water distribution in <i>Braided Cascade</i> .	70
3.3.	Values of the constant and exponent to 3 significant figures (in Hoey <i>et al.</i> , 2001).	72
3.4.	Model parameters, dimensions, values and units.	81

### Chapter 4. Data used in model validation.

4.1.	Details of the study reach.	84
4.2.	D50 and D95 percentiles for Wolman counts at five different locations on the braidplain.	85
4.3.	Maximum clast size and total mass sampled for surface and subsurface bulk samples.	87
4.4.	Percentiles of bulk grain size distribution data in mm and in psi units.	87
4.5.	Bias and precision of bulk samples calculated according to the method of Ferguson and Paola (1997).	87
4.6.	Characteristics of the bedload sampling programme.	88
4.7.	Bedload sample weights (g) collected, summary of grain size characteristics of bedload and summary of bedload transport rate characteristics.	90
4.8.	Summary of Zarn's (1997) flume data	91
4.9.	Bedform development in the flume runs of Zarn (1997)	92

### Chapter 5. Sensitivity analysis.

5.1.	Summary of conditions experienced by the proglacial stream of the Haut Glacier d'Arolla, July 18 <sup>th</sup> - 20 <sup>th</sup> 1999.	95
5.2.	Parameter values for the control run and alternative values used in sensitivity analysis.	95
5.3.	Details of runs with different length scales for erosion.	112
5.4.	Percentage dry area after 50 000 timesteps in runs with different erosion length scales and NO sediment input.	114
5.5.	Details of the total amount of erosion / deposition for runs with different erosion length scales.	115
5.6.	Percentage dry area after 50 000 timesteps in runs with different erosion length scales and WITH sediment input.	122
5.7.	Details of the total amount of erosion / deposition for runs with different erosion length scales and with sediment input (to 3 s.f.).	123
5.8.	Summary of test runs using different values of the discharge ratios $Q_r$ and $Q_{ru}$ .	127
5.9.	Percentage dry area after 50 000 timesteps in runs with different discharge ratios with and without sediment input.	137
5.10.	Details of runs with different diffusion coefficients.	143

5.11	Details of runs with different slope and discharges but equal discharge-slope products.	160
5.12	The effect of model conditions on channel network patterns.	164

## Chapter 6. Testing Braided Cascade

6.1	Variability of bedload transport rates across the flume runs of Zarn (1997).	171
6.2	Results of fitting AR(1) models to residuals from linear regression applied to each data set of Zarn (1997).	180
6.3	Summary statistics of z scores for runs grouped by discharge.	184
6.4	Proportion of each type of movement between data points in state space.	186
6.5	Matrix of RelaxIV results for runs with grouped by discharge.	192
6.6	Summary of unit bedload transport rates at Arolla, 1999.	195
6.7	Summary statistics of z scores for Arolla 1999 data sets.	197
6.8	Proportion of each type of movement between data points in state space for field data from Arolla 1999.	197
6.9	Summary statistics of first order autoregression models fitted to the data from Arolla 1999.	199
6.10	Matrix of results of Arolla field data compared to Zarn's (1997) flume data using RelaxIV.	200
6.11	Run conditions for long <i>Braided Cascade</i> runs.	202
6.12	Variability of sediment outflux from Run 1.	205
6.13	Summary statistics of AR(1) regression for <i>Braided Cascade</i> run 1.	207
6.14	Variability of sediment outflux from Run 2.	210
6.15	Proportion of dry nodes on the grid at certain times throughout <i>Braided Cascade</i> Run 2.	210
6.16	Summary statistics of AR(1) regression for <i>Braided Cascade</i> run 2.	212
6.17	Proportion of dry nodes on the grid at certain times throughout <i>Braided Cascade</i> Run 3.	215
6.18	Variability of sediment outflux from Run 3.	216
6.19	Summary statistics of AR(1) regression for <i>Braided Cascade</i> run 3.	220
6.20	Summary statistics of z scores for <i>Braided Cascade</i> runs.	221
6.21	Proportion of each type of movement between data points in state space for <i>Braided Cascade</i> runs.	221
6.22	Matrix of RelaxIV results for Braided Cascade runs.	222
6.23	Matrix of RelaxIV results for Braided Cascade runs.	223

## ACKNOWLEDGEMENTS

I would like to gratefully acknowledge the supervision and support that I have received from Dr. Trevor Hoey, without whom none of this would have been possible. I would like to thank Professor Paul Bishop for introducing me to the *Cascade* model and Benno Zarn for allowing me to use his data. This study was funded by various means. For two years of this work I was employed as a Research Assistant on a NERC grant (grant number GR3/11373), other funding came from a one-year University Scholarship. A Carnegie Grant contributed towards fieldwork costs.

Field assistance in Arolla was provided by Pete Chung, Sally Gemmell and Louise Sime. Computing and technical assistance was provided by Stewart McNeill of the Department of Computing Sciences at the University of Glasgow.

I would like to thank my friends in Glasgow who helped make my three years there a very worthwhile experience, especially flatmates Ruth, Dave, Melv and Keith and also Jo, Ian, Steve, Anne and Karin for various curries and Friday nights out.

I have to say also big thank you to my family for their continual support and last but by no means least Rob Bryant for his continual support and for putting up with me!

## CHAPTER 1.

### INTRODUCTION.

Research into the dynamics of water, sediment transport and channel network evolution in braided rivers has increased greatly during the past twenty years. Field measurements, physical models and numerical modelling have all been adopted to try to gain greater insight into processes controlling the dynamics of braided rivers, the development of braiding through sediment erosion, entrainment and deposition, and the geometry of braided river deposits. However, it may be argued that this research has not yet led to a comparable advance in understanding of the spatial aspects of sediment transport in dynamic gravel-bed rivers at the reach scale, a scale lying in between that of point measurements and large scale measurements.

Knowledge of the processes of channel change and sediment transport in modern braided rivers is vital for geomorphologists, engineers and geologists, and is important for the interpretation of ancient braidplains and sedimentary deposits, as well as the prediction of subsurface geometry and facies (Ashmore, 1993, 2001; Bristow and Best, 1993). Ancient braidplains form sedimentary sequences that constitute valuable aquifers, hydrocarbon reservoirs and sites for heavy mineral accumulation. These diverse applications make knowledge of the mechanics and deposits of braided rivers most important and yet, compared to meandering river systems, braided rivers are comparatively understudied. Braided systems are highly dynamic making direct study difficult thus many aspects of their functioning are poorly understood.

Hydraulic and sedimentological models provide a framework in which to conceptualise and investigate the relationship between flow hydraulics and sediment transport. In the study of braided rivers, hydraulic models have been applied at many spatial scales, from the small-scale evaluation of turbulent structures in flow in short river reaches, typically in one bar-chute complex (e.g.

Lane and Richards, 1998), to the large-scale evolution of braiding (e.g. Murray and Paola, 1994, 1997). However, with the exception of Webb (1994, 1995) and Murray and Paola (1994, 1997), references to reach scale modelling in the literature have tended to have been drawn from studies that have not specifically set out to quantify the geomorphic processes responsible for braided network generation (e.g. Howard *et al.*, 1970; Krumbein and Orme, 1981). Of those numerical modelling studies that address reach scale processes (Webb, 1994, 1995; Murray and Paola, 1994, 1997), the models developed have been generic in nature and physically simplistic. Whilst the models simplicity does not necessarily invalidate them, their usefulness still has to be proven.

Very few larger scale numerical models have been developed that have incorporated field data collected from braided rivers, an exception is the model of Thomas and Nicholas (2002) but to date this model routes water only (no sediment transport rules are included). Within most numerical models braiding develops upon a flat plain according to rules specified in the model. Indeed, with the exception of Brasington *et al.* (2000) and Lane (2001) there are very few high density field data sets of morphological change collected from braided networks at spatial scales of over one bar-chute complex and temporal scales of over one flow event. Such models and data sets would provide a useful tool in developing understanding of braiding processes.

The overall aim of this study is to bridge the divide between small and large-scale approaches (but using an essentially large-scale generic approach) by developing a robust sediment transfer model with realistic data inputs and a greater degree of physical realism (hydraulic and sedimentological conditions) than those previously developed. Specifically the aims of this study are:

- To develop a numerical model that can simulate the evolution of braided channel networks;
- To incorporate physically realistic transport rules for water and sediment;
- To test the sensitivity of model parameters;

- To use the model to answer specific questions about the formation and evolution of braided channel networks in order to gain insight into the mechanics of braided rivers, for example to attempt to understand the relationship between unsteady sediment transport and morphology.
- To investigate the relationship between spatial and temporal structure in bedload transport using the model results and results from a physical modelling study.

Chapter 2 will review relevant literature and formalise the specifications of the study. Chapter 3 describes the development of the modelling approach; the data used to validate the model is introduced in Chapter 4. The model will be tested by sensitivity analysis to establish optimal parameter values for braiding, (Chapter 5), and in Chapter 6 specific experiments will be conducted with the model using the initial and boundary conditions established in Chapter 5. Conclusions and ideas for future work are discussed in Chapter 7.

## CHAPTER 2.

### APPROACHES TO MODELLING BRAIDED RIVERS.

#### 2.1. Introduction

Braided river reaches and braided alluvial systems are abundant in many environments and are characterised by their multiple alluvial channels. Paola (1996) notes that braided rivers exhibit structural stability while the detailed configurations of an active stream are constantly changing. The division and joining of channels and the associated divergence and convergence of flow contributes to high rates of erosion, sediment transport and deposition, and frequent channel switching and migration. The highly active nature of braided rivers poses interesting problems to many disciplines. Knowledge of the processes of channel change and sediment transport in modern braided rivers are vital before any engineering work is carried out and are important for the interpretation of ancient braidplains and sedimentary deposits (Bridge 1993; Bristow and Best 1993). Ancient braidplains form sedimentary sequences that constitute valuable aquifers, hydrocarbon reservoirs and sites for heavy mineral accumulation. An understanding of modern processes in braided rivers is therefore important for geomorphologists, engineers and geologists. Numerical modelling of braided rivers offers the potential to determine which processes are essential to describe river braiding, and should be useful to estimate the relative importance of the contributing processes (McArdell and Faeh, 2001).

#### 2.2. Definition of braiding.

The form of a natural channel when viewed in plan falls within a continuum of channel patterns that have been classified into straight, meandering braided and anastomosed. The term 'braided' has been given several definitions in the literature. Leopold and Wolman (1957) described the braided river as 'one which flows in two or more anastomosing channels around alluvial islands', while Lane (1957) reported that a braided stream is characterised by having a number of

alluvial channels with bars and islands between meeting and dividing again, and presenting from the air the intertwining effect of a braid.'

This chapter will review past investigations on braided rivers, focusing on larger scale modelling techniques. A brief review of field and small-scale modelling investigations will precede the larger scale modelling review. Firstly though a short description of braiding mechanisms and sediment transport through braided reaches will be given.

Research into the processes initiating and controlling braiding has increased greatly during the past 25 years. Field measurements, physical models and numerical modelling have been adopted to in order to gain greater insight into processes controlling the dynamics of braided rivers, the development of braiding through sediment erosion, entrainment and deposition, and the geometry of their deposits. Early work on braided rivers focused on channel pattern. Leopold and Wolman (1957) demonstrated by laboratory simulation that braids could form without fluctuations in discharge, and put forward a discriminant function that separated braids from meanders based on channel slope and bankfull discharge. The work has since been refined by numerous other workers, for example Schumm (1977) distinguished between braided rivers that at low stage have islands of sediment or semi-permanent vegetation and anastomosing rivers that have branches with individual channel patterns. Henderson (1961) took grain size into account and Kirkby (1972) considered the effects of bed roughness. In parallel, geologists have constructed models of braided sedimentary sequences. The models of braided alluvium reviewed by Miall (1977) were based on the deposits of modern braided rivers but were used to explain the origins of ancient deposits. Sedimentary factors also influence channel pattern. Anastomosing rivers are generally agreed to have stable banks with individual channels showing little tendency to migrate (Knighton and Nanson, 1993). Van den Berg (1995) discriminated between sinuous single thread and braided channels in a plot of specific stream power against median grain size. As boundary resistance increases

through either more cohesive banks or coarser bed material, a greater stream power is required for the onset of braiding.

However, Sapozhnikov and Fofoula-Georgiou (1996) note that there is a significant lack of quantitative studies of pattern in braided rivers; the existing models and frameworks are mostly qualitative. With the exception of the early work by Howard *et al.* (1970) it is only recently that some more quantitative studies have been carried out. Therefore there is scope to improve the understanding of the formation and evolution of braided patterns.

### **2.2.1 Mechanisms of braid development.**

Braiding may develop in more than one way and different modes of braiding occur in distinctive hydraulic conditions and sediment supply. Most theories of braiding development are based on qualitative observation and description, either in flume experiments or in the field. Ashmore (1991a) identified four mechanisms by which braiding may be initiated, to which Ferguson (1993) added a fifth (see Table 2.1).

From Table 2.1 it can be seen that channel geometry and flow and bedform symmetry seem to be the controlling factors distinguishing which mechanism initiates braiding. Instability of flow and sediment transport appears to be at the root of all of the mechanisms, except central bar braiding, which is often an isolated occurrence of purely depositional origin (Ashmore, 1991a). All other processes, except avulsion, involve an element of reworking of the initial deposits by secondary flows that are sufficiently competent to propagate braiding downstream as well as to modify the form of the initial deposit. The loss of flow competence and the migration of bedload sheets appear to be the key to explaining when braiding occurs. The susceptibility of bars to dissection by flow is another important factor in the initiation and maintenance of braiding.

Mechanism name	Mechanism type	Brief description of mechanism	Hydraulic and channel conditions	Upstream bar geometry	Workers
1. Central bar deposition	Depositional	Coarse bedload stalls in the channel due to local flow instability and subsequent bedload is trapped and deposited.	Identified by Leopold and Wolman (1957). In flume experiments for central bar deposition to occur shear stress near to the threshold for bedload transport was needed (Ashmore, 1985a). Rundle (1985a, b) argues that this mechanism is unlikely to occur, as the bar cannot grow outside the shelter of the obstruction.		Leopold and Wolman (1957) Rundle (1985a, b) Ashmore (1991a)
2. Transverse bar conversion	Erosional	Flow division over isolated slip face bar formed in the channel.	Symmetrical bars may be favoured in wider channels where double row bars instead of alternating bars may occur (Ferguson, 1993).	Symmetrical bars.	Ashmore (1991a) Ferguson (1993)
3. Chute cutoff	Erosional	Development of chutes across stalled, previously migratory, alternating point bars.	Similar to 3 but differing in upstream bar configurations.	Asymmetrical bars.	Ashmore (1991a) Ferguson (1993)
4. Multiple dissection of lobate bar	Erosional	Lobate bars are ephemeral features constructed at a preceding phase of deposition at a flow expansion and are generally rapidly dissected into longitudinal forms (Rundle 1985a, b)	Rundle (1985a, b) states that this mechanism is the most probable mechanism of braiding in New Zealand gravel bed rivers.  Uncommon in flume experiments, only occurring in runs with high width to depth ratio (Ashmore, 1991a). May be due to the inadequate flume width for the depth of the water, or to the use of steady flow in the experiments, which may have precluded the deposition of a lobate bar.		Rundle (1985a, b) Ashmore (1991a)
5. Avulsion	Erosional	The relatively rapid switching of course from one channel to another.	In flume experiments, avulsion occurred under a variety of circumstances and did not necessarily involve reoccupation of a well-defined abandoned channel, but, under peak flow, often involved the incision of completely new channels (Ashmore, 1982).		Ashmore (1982) Ferguson (1993)

Table 2.1. Summary of braiding mechanisms.

### **2.3. Bedload transport through braided reaches.**

Sediment transfer through braided reaches is important if medium and long-term understanding of the process of braiding is to be achieved. However braided streams are characterised by complex and transient morphology and associated spatial and temporal changes in bedload transport rate (Goff and Ashmore, 1994). The range of literature is such that it is not possible to review it all; (for a review of the main studies see Gomez (1991)), the main aims of this section are:

1. definition of temporal and spatial scales of bedload unsteadiness and probability distribution functions for bedload;
2. identification of the range of mechanisms that may produce bedload variability in braided reaches.

#### **2.3.1. Spatial and temporal scales of bedload variability.**

There is strong empirical evidence that bedload is frequently transported in waves generated within the braided system or introduced from without in both natural rivers (Griffiths, 1979; Church and Jones, 1982, Meade, 1985; Ashworth and Ferguson, 1986; Hoey, 1992; Lane *et al.*, 1996), and laboratory flumes (Ashmore, 1988, 1991a, b, Hoey and Sutherland 1991; Young and Davies, 1991). A bed wave has been defined as an increase in sediment storage in a reach relative to either that reach at proceeding and succeeding times or relative to adjacent upstream and downstream reaches at the same time (Hoey and Sutherland 1991). In addition, a bedload pulse is defined as a temporal variation in the rate of bedload transport at a particular site (part of whole of channel cross-section), from a minimum to a maximum and back to a minimum. This has no spatial implications and is only used with reference to the process of bedload transport (Hoey and Sutherland 1991).

Bedload pulses and bed waves can be considered to be bedforms and may occur at different scales: mega-, macro-, meso- or micro-scale (Hoey, 1992; Nicholas *et al.*, 1995). Table 2.2 presents a hierarchical bedform classification for bedload

pulses and bed waves. The mega-scale features are controlled by the geomorphological regime of the channel (Hoey, 1992), encompass several reaches ( $10^3$  m) and operate over timescales of several years; typical bed features include groups of bars or complex bar assemblages (Griffiths, 1979; Church and Jones, 1982). The macro-scale is spatially of the order of channel width ( $10^1$  to  $10^3$  m) and temporally of days (flood duration) and features bars: meso-scale features are predominantly influenced by local hydraulics (Hoey, 1992) have the smallest bedforms and a time scale of hours (Church and Jones, 1982; Gomez *et al.*, 1989; Hoey and Sutherland, 1991).

Pulse class	System scale	Wavelength (m)	Timescale	Typical features
Instantaneous (microform)	Grain size	-	$\ll t_e$	-
Mesoform	Flow depth	$10^{-1} - 10^2$	$\approx t_e$	particle clusters
Macroform	Channel width	$10^1 - 10^3$	$\geq t_e$	gravel sheets, unit bars, complex bars
Megaform	Several channel widths	$> 10^3$	$\gg t_e$	bar assemblages

Table 2.2 Hierarchical bedform classification for bedload pulses and bed waves (After Jackson, 1975; Church and Jones, 1982; Hoey, 1992; Griffiths, 1993).

Note:  $t_e$  is the event time (the time taken for a flood to pass through a reach).

Bedload pulses and waves can be generated in one of two ways. Exogenous/allo-pulses are produced by sources of sediment from outside the channel that induce wavelike behaviour (e.g. Gilbert, 1917, Pickup *et al.*, 1983, James, 1989, 1991a, 1991b; Madej and Ozaki 1996; Wathen and Hoey, 1998). Base level changes, tectonic behaviour and volcanic behaviour can also generate exogenous pulses. Endogenous/autopulses are produced by processes occurring within the channel and are formed of alluvial material (e.g. Griffiths, 1979, 1993; Meade, 1985; Kuhnle and Southard, 1988; Ashmore 1991b; Benda and Dunne, 1997a, b).

### 2.3.2. Bedload probability density functions.

Knowledge of the range of bedload transport rates is important to aid in the understanding of channel morphometric processes in contemporary and palaeochannels, to maintain acceptable channel conditions, and in the informed

planning of river use. With the realisation that the transport of bedload is highly variable, a generalised probability distribution function (pdf) that describes the variability of the transport process would be useful. Many well-defined probability distributions have been used to describe hydrologic processes, for example the normal and log-normal distributions have been commonly used, however neither have any basis in the theory of bedload transport and both are based on samples from a homogeneous population. Pdfs have been developed for bedload transport and two will be described below.

The Hamamori (1962) pdf was derived to explain transport fluctuations in flume experiments with sand and is a theoretical treatment of bedload transport under constant flow conditions. The pdf is based on the presumption that bedload transport is associated with the passage of dunes, which are assumed to move downstream at a constant speed without changing shape. Propagation of the primary dune is assumed to occur in response to movement of smaller secondary dunes, which climb the upstream slope of the primary dune and cascade over its crest. The spatial distribution of bedload transport rates is reflected in the movement of these secondary dunes, conceptualised in Hamamori's analysis as a series of similar triangles. Hamamori also assumed that the mean bedload transport rate for each triangular element is equal to half the maximum rate for that element, and the overall mean transport rate for the primary dune is equal to half the mean rate for the element at the dune crest (Figure 2.1). Therefore, relative bedload transport rates may be observed to vary from 0 to 4. Carey and Hubbell (1986) extended Hamamori's analysis to the case of bedforms whose shape changes over time, by assuming that the amplitudes of the oscillations in bedload transport rates form a continuous, non-uniformly increasing function from the trough to the crest of the primary dune. The function is written as:

$$y' = Y(x/L)^m, m \geq 0 \quad (2.1)$$

Where  $y'$  equals the amplitudes of the oscillations in bedload transport rates from dune trough to dune crest,  $x$  is the distance along the base of the dune and  $L$  is the

surface length of the primary dune.  $y' = 0$  at  $x = 0$  and  $y' = Y$  at  $x = L$ . The function is raised to a power  $m$ : when  $m = 1$ , the distribution is Hamamori's distribution, when  $m < 1$  the dune height is increasing, there are fewer lower relative bedload transport rates more higher rates and when  $m > 1$  the dune height is decreasing, there are fewer higher transport rate values and more lower rates. An example of generalised Hamamori pdfs for selected values of  $m$  may be seen in Figure 2.2.

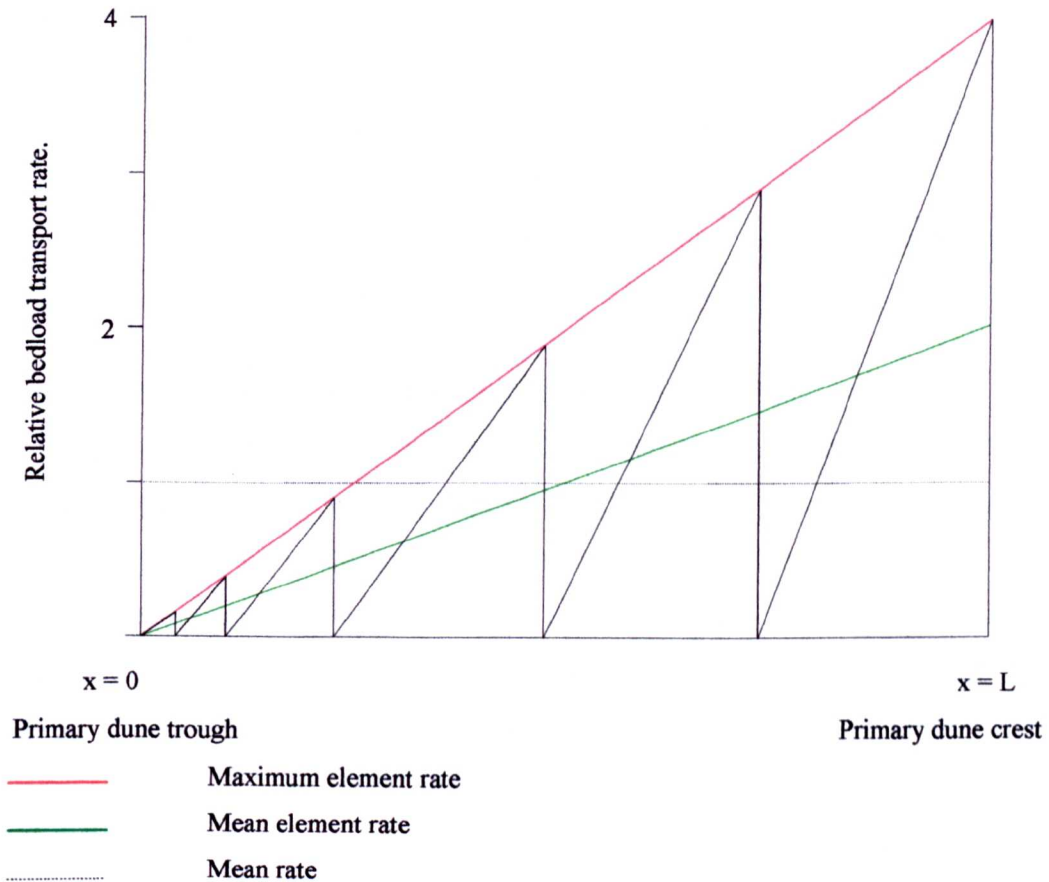


Figure 2.1. Relative bedload transport rates vs. distance along a (primary) dune with secondary bedforms according to Hamamori's assumptions. The maximum relative transport rate is 4.

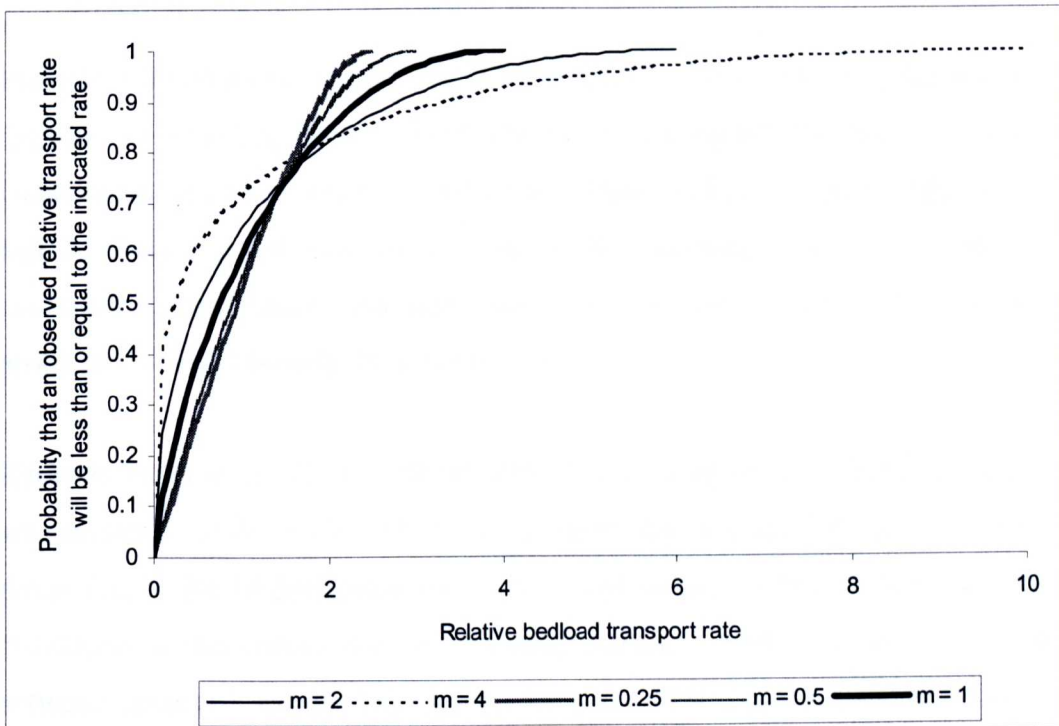


Figure 2.2. Generalised Hamamori pdfs for selected values of  $m$ .

In contrast to Hamamori's approach that is based on bedform migration, Einstein (1937) developed a pdf, derived from flume experiments using a gravel and sand mixture that is based on the consideration of individual particles. The movement of a single grain was described in terms of a series of relatively short random-length steps, each of which is followed by a rest period of random duration. Steps and rest periods are each assumed to follow an exponential distribution. Einstein applied these observations to the distance a particle moves within a given time and also to how much sediment will be caught in a trap within a given time. The distribution of the sampled bedload transport rates is related to both the length of the sampling time and to the average amount of time that particles spend at rest (or conversely the rate at which the load is being transported). Thus for any given bedload transport rate a relatively short sampling interval will tend to give a widely spread distribution of relative transport rates with higher numbers of zero values, because the behaviour of a small number of particles is being observed. A relatively long sampling interval will lead to a narrower distribution with fewer zero values as lots of particles are being observed. In other words, sampling over progressively longer time intervals tends to average out the higher frequency temporal variations in bedload transport rates.

Einstein's distribution function might be expected to best serve the case where the duration of sampling time is short enough to distinguish the higher frequency components in a time series, or conversely where bedload transport rates are low and incoherent grain motions dominated the sampling sequence. Hamamori's probability distribution function best fits averaged data where bedform propagation controls bedload transport rate.

Recently Hoey *et al.* (2001), recognising that existing pdfs for bedload transport are essentially of descriptive utility for cross-section averaged transport in braided rivers due to the inappropriateness of the assumptions on which they are based, developed a theoretical pdf for bedload transport based on the relationship between observed spatial distributions of shear stress and channel morphology. The theory suggests that the statistical structure of bedload time series may be explicable in terms of spatial distributions of controlling variables, for example shear stress and channel width. The theory has not been tested in the field; however, results using spatially and temporally integrated flume data, (from Hoey 1989 and Hoey and Sutherland, 1991), show that stochastic sampling from channel width and shear stress pdfs improves the prediction of relative transport rates relative to using cross-section averaged shear stress. However there are some departures from observations when transport rates are high and the results suggest that it is possible to begin to formally relate temporal and spatial sediment transport patterns in braided streams in a way that has some generality.

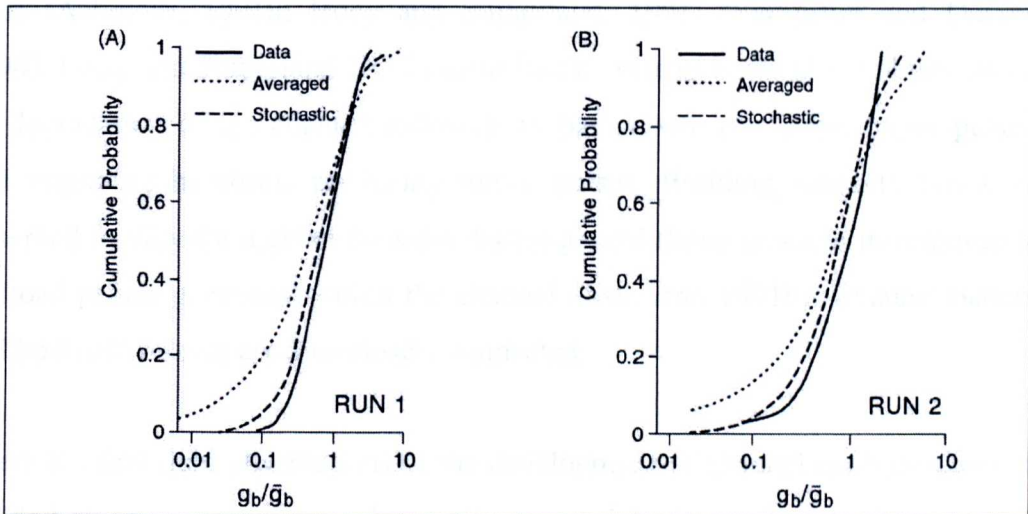


Figure 2.3. Measured and simulated pdfs of relative bedload transport rate for two experiments (experimental data from Hoey 1989; Hoey and Sutherland, 1991).

### 2.3.3. Mechanisms of bedload pulsing.

Observations of variations in bedload transport rates in both natural streams and in the laboratory have been made since at least the early 1900s (e.g. Gilbert, 1917). In single channel flume experiments and field investigations bedload variability has been found to be associated with the passage of bedforms, be they large single grains (Kuhnle and Southard, 1988), dunes (Einstein 1937; Meade, 1985; Gomez *et al.*, 1989; Kuhnle *et al.*, 1989), alternate bars (Gomez *et al.*, 1989), or low relief bedload sheets (Iseya and Ikeda, 1987; Kuhnle and Southard, 1988; Whiting *et al.*, 1988).

In braided rivers the creation, migration and destruction of complex bar assemblages have been related to the production of sediment pulses, even when the reach remains in equilibrium. In flume experiments with braided channels bedload pulses have been observed under constant discharge conditions and constant sediment feed rate (e.g. Hoey and Sutherland, 1991; Young and Davies, 1991; Warburton and Davies, 1994), or recirculation (Ashmore, 1988, 1991b). Higher frequency pulses have been observed at higher transport rates and were associated with the passage of bedforms (Young and Davies, 1991). Observations have linked upstream channel geometry and the variability of bedload transport

rates (Ashmore, 1991b; Hoey and Sutherland, 1991; Warburton and Davies, 1994). Hoey and Sutherland (1991) identified a cycle of bedload variability based on degradation of the channel followed by bar growth producing major pulses, and migrating bedforms producing minor pulses. Braiding intensity has been observed to vary for a given constant discharge and flume gradient in response to bedload pulses generated within the channel (Ashmore, 1991b). Channel pattern and bedload transfer are thus closely connected.

There are few field observations of the development of channel configurations in braided rivers and no standard quantitative models for predicting flow patterns and rates of channel change (Ferguson and Ashworth, 1992). The nature of braided rivers can render the measurement of spatially distributed variables (e.g. channel and bed morphology, flow measurements) difficult. Data on the movement of bedload in braided rivers is difficult to obtain and therefore scarce. Methods used to obtain data on bedload movement, include indirect measurement techniques such as tracer studies (Laronne and Duncan, 1989), morphological methods using aerial photographs (Carson and Griffiths, 1989) or repeated surveying techniques (Goff and Ashmore, 1994).

From aerial photograph work on the Waimakariri River, New Zealand, Carson and Griffiths (1989) found that considerable quantities of bed material were moved by lateral bank scour in braid bends and subsequent downstream deposition on bar heads. However, using daily topographic surveys of the Sunwapta River, Alberta, Canada, Goff and Ashmore (1994) indicated that patterns of erosion and deposition are more complicated than those suggested by Carson and Griffiths (1989). Both lateral bank scour and bed scour were observed to occur and deposition was primarily by unit bar migration along the main anabranches. Laronne and Duncan (1989) used cross section surveys, aerial photographs, scour chains and magnetic tracer particles to study bed material mobilisation in two areas of a wide gravel river in New Zealand. The lower reach, an aggrading narrow channel with fine textured alternate bars and two braids at most, was found to be completely mobilised as the magnitude of flow events

increased. However the upper stable reach, often braided at low flow with well-developed longitudinal bars of fine gravel and an armoured channel, had stable bar remnants at higher flows. The width reduction from the upper to lower reach was forced by flood banks and lead to different results from the findings of Church (1983) for a wandering gravel-bed river (the Bella Coola) in Canada. Here the bulk of the mobile sediment was contained in discrete laterally unstable "sedimentation zones" which were separated by stable reaches. The sedimentation zones were located upstream of, or opposite tributary alluvial fans, in braided reaches. In contrast the stable reaches were confined to a well-armoured single channel, with only minor accumulations of sediment in bars.

#### **2.3.4. Summary.**

Sediment transport in gravel-bed rivers, both single channel and braided, has been observed to vary considerably in both field and flume experiments. Pulses may be exo- or endo-genetic and may occur on a variety of scales. In single channels, the passage of bedforms has been associated with bedload pulses and bed waves in both field and flume experiments. Probability distribution functions to describe variability of bedload transport rates have been developed. In braided reaches the local variability in channel pattern and stream morphology is closely linked to the bedload input from upstream and therefore the bedload transport rate. However this general description of the transfer pattern probably belies the complicated nature of the process in reality and in particular cases.

#### **2.4. Spatial scaling, self-affinity and self-organisation in braided rivers.**

In a linear stability model of braiding Parker (1976) modelled the response of an initially straight channel to perturbations in sediment and water transport and found that the width-depth ratio is the main control on instability. The perturbations are modelled as sine waves and an initially dominant wavelength can be identified. However, Paola (2001) points out that although Parker's theory works well for the initiation of braiding, by the time braiding is fully developed

the system is no longer linear and the dominant wavelength may become replaced by different ones, or none may dominate.

The presence of scaling in a phenomenon means that statistical properties of the phenomenon at one scale relate to its statistical properties at another scale via a transformation that involves only the ratio of the two scales. This implies a certain invariance of the phenomenon under magnification or contraction (scale invariance). Objects showing the same spatial scaling in all directions are termed self-similar fractals and can be characterised by their fractal dimension,  $D$ . However, it is more usual for scaling to be different in different directions (anisotropic scaling). Such objects are called self-affine fractals and are characterised by two fractal dimensions: the local fractal dimension,  $DL$  and the global fractal dimension,  $DG$ , (Mandelbrot, 1982, 1986).

Sapozhnikov and Foufoula-Georgiou (1996) analysed three braided rivers of different scales and sedimentological characteristics (the Aichilik and Hulahula in Alaska and the Brahmaputra in Bangladesh) using the logarithmic correlation integral (LCI). It was found that, despite their different scales, (the braidplain widths vary from 0.5 – 15 km) and bed materials (gravel to sand) the three rivers exhibited anisotropic scaling or self-affinity in the downstream and cross-stream directions. They concluded that this result may indicate the presence of universal features in the underlying mechanisms responsible for the formation of braided rivers, however more rivers need to be studied.

Dynamic (space-time) scaling can be considered as the evolution of a fractal object of fractal dimension  $D$ , in time, if the evolution is such that the object preserves its fractal dimension. The object is thus statistically invariant. However larger objects will evolve more slowly than smaller objects, even if they are larger areas of the same object. If a dynamic exponent exists such that the time dimension can be re-scaled depending on the ratio of the spatial scales of the objects in question, so that the rate of evolution is the same in both (or all) cases, the system can be considered to have dynamic scaling (Sapozhnikov and

Foufoula-Georgiou, 1997, Paola and Foufoula-Georgiou, 2001). In the case of braided rivers, this would imply that a smaller part of a braided river evolves identically (in the statistical sense) to a larger one provided that the time is renormalised by a factor depending on the spatial scale of those parts.

Sapozhnikov and Foufoula-Georgiou (1997) analysed the evolution of an experimental braided river produced in a flume for dynamical scaling. It was found that the river exhibited dynamic scaling with the dynamic exponent taking a low value. In terms of the physical processes governing braided river dynamics, the low dynamic exponent was interpreted thus:

- if the spatial scale were increased, the evolution of the system would slow down by a factor defined by the spatial scale raised to the power of the dynamic exponent. In other words, it implies that the lifetime of the channels in a braided river system scales with channel size;
- the low value of the dynamic exponent indicates a relatively weak dependence of the rate of evolution on the spatial scale; and
- the low value of the dynamic scaling indicates a strong correlation between the evolution of large and small channels within a braided river system. This leads to the conjecture that the evolution of small channel patterns is to a great extent forced by the evolution of larger channels.

The presence of dynamic scaling may be used as a tool to shed light upon the space-time dynamics of braided river evolution by examining statistical similarities between patterns at smaller space-time scales and those at larger space-time scales. The dynamic scaling relationship can also be used to predict long-term changes of the systems at larger spatial scales on the basis of monitored short-term changes at a smaller spatial scale. In addition, Sapozhnikov and Foufoula-Georgiou (1997) argue that dynamic scaling may also indicate that braided rivers may be in a critical state and behave as self-organised critical systems.

The self-organised criticality (SOC) concept introduced by Bak *et al.* (1987) states that many non-linear systems with extended degrees of freedom self-organise into

a critical state in a natural way i.e. without any tuning parameter (e.g. temperature) needed to bring traditional equilibrium systems to a critical state. Sapozhnikov and Fofoula-Georgiou (1997) argue that braided rivers may be self-organised critical systems because braided rivers are non-linear systems; have a large number of degrees of freedom (the number of degrees of freedom can be thought of as the number of variables needed to uniquely define the state of the system mathematically); show collective behaviour, which is a crucial feature of systems in a critical state; exhibit spatial scaling and undergo significant changes over a wide range of scales even when they are in statistical equilibrium.

Therefore, a self-organised critical system will reach a statistically stationary state where rearrangements in the system (for example changes in sediment transport) take place on any length scales and time scales, limited only by the size of the system. So a self organised critical state is an attractor for the dynamics of the system (Tang and Bak, 1988).

#### **2.4.1. Summary.**

Although the initial development of a braided pattern from a straight channel does appear to involve a single dominant wavelength, as described in stability theories (e.g. Parker, 1976), the picture for fully developed braiding is quite different. The original regular pattern of bars breaks up into a complex network of bars and channels on many length scales. The spatial pattern of braided rivers is self-affine and their temporal dynamics are consistent with self-organised critical behaviour. Self-affine systems have no characteristic length scaling (up to the scale of the whole system). These results suggest that braided rivers do not possess characteristic length scales, either when viewed as static spatial patterns, or in terms of their temporal evolution (Sapozhnikov *et al.*, 1998). The apparent scale-invariance of the braided pattern would seem to have implications for the mechanisms involved in determining evolution of the braided morphology. Sapozhnikov *et al.* (1998) note that such scale invariance across a range of scales has several fundamental implications:

1. they may indicate the presence of universal features in the underlying mechanisms responsible for the spatial structure of braided rivers and suggest that this structure is due to the self-organising nature of the flow and sediment flux rather than to specific local external influences;
2. knowledge of which geometric attributes are scale invariant or scale dependant is useful when applying models of braided alluvial architecture deduced from one system to another of a completely different size; and
3. since these scale invariances are properties of real braided rivers, any model of a braided river that tries to simulate braided river patterns should also reproduce them.

## **2.5. Approaches to investigating braided rivers.**

### **2.5.1. Field investigations.**

Undertaking any field research in a braided river is difficult due to the complex interaction between process and braid morphology. Field studies have frequently been used in a reductionist framework to study particular aspects of the physics of braided rivers as they operate at a point scale, or in the context of idealised uniform flow (Ferguson and Ashworth, 1992). Small-scale field investigations into spatial patterns of bedload transport rate, sorting, channel morphology, velocity, and shear stress have commonly been undertaken around chute-bar complexes within one anabranch of a braided river (e.g. Ferguson, *et al.*, 1989; Ashworth *et al.*, 1992a, 1992b; Bridge and Gable, 1992; Ashworth and Ferguson, 1986; Lane *et al.*, 1994, 1995 see Table 2.3). As the detail in field measurement increases, the temporal scale of the measurement tends to decrease.

Larger scale field investigations of braided rivers have focused on downstream and lateral changes in channel planform and sediment transport using aerial photographs and/or repeated surveying of cross sections to try to identify areas of erosion and deposition, and so calculate the sediment budget of the reach in question (e.g. Griffiths, 1979; Church, 1983; Carson and Griffiths, 1989; Laronne and Duncan, 1989; and Goff and Ashmore, 1994). Survey locations may be

Workers	River	Length of study reach	Measurements taken	Main findings.
Ashworth et al., (1992a)	Sunwapta River, Alberta, Canada (proglacial).	50m	Grain size distribution of bed material, bedload and bar head deposition	Low transport rates and only weak evidence to suggest size selection at either entrainment or during transport or deposition.
Ashworth et al., (1992b)	Sunwapta River, Alberta, Canada (proglacial).	50 m around a chute-bar complex.	BLTR, grain size, velocity.	Total bedload transport rate and flow competence influenced by the chute bar unit morphology but overall bedload grain size remained constant throughout the reach.
Ashworth and Ferguson (1986)	Lyngdalselva, Arctic Norway (proglacial).	Approx. 50 m (reach A)	Spatial and temporal variations in channel morphology, velocity and shear stress, bedload transport rate and bedload and bed material grain size distributions.	Almost equal mobility for large and small particles, so transport rate increased with shear stress. However down-reach and down-bar fining indicated size selective transport.
Bridge and Gabel (1992)	Braided reach of the low sinuosity Calamus River, Nebraska Sandhills, USA.	Approx 900 m around a vegetated mid-channel bar.	Channel geometry, flow velocity, sediment transport and deposition.	Patterns of velocity, depth, water surface slope, bed shear stress, BLTR and mean grain size around the mid-channel bar can be accurately predicted using theoretical models of flow, bed topography and sediment transport rates in single river bends applied to each channel around the bar. However was not possible to predict flow and bed topography in areas of flow convergence or divergence.
Lane et al., (1994, 1995)	Proglacial Haut d'Arolla, Switzerland.	50 m around a mid-channel bar (20 m sub-reach used to estimate BLTR).	Morphological estimation of BLTR using terrain models of river bed morphology.	A combination of photogrammetry and rapid tacheometric survey can be used to estimate reach scale bedload budgets and within reach spatial patterns of transport. Very detailed measurements needed.

Table 2.3. Selected small scale field investigations of braided rivers.

BLTR = bedload transport rate.

kilometres apart and repeated over time scales ranging from daily to several years. Sediment budget studies have identified areas of erosion and deposition within the catchment and the importance of storage in the history of sediment movement through a reach, however mapping areas of scour and aggradation from aerial photographs cannot reveal scour or fill within the channel.

Recently remote sensing techniques have been successfully applied to the study of gravel-bed rivers. Digital photogrammetry and digital image analysis have been used to provide information on bed morphology over a wide range of scales (Lane 2001). Two-dimensional image analysis has been applied to the analysis of channel planform, water depth mapping and particle size estimation. Three-dimensional analyses have been used to create digital elevation models from photogrammetry, which have been used to measure bedforms in both flume (see Lane 2001) and field (Westaway *et al.*, 2000) situations.

The field strategies outlined above have yielded greater understanding of the erosion, entrainment and deposition of sediment in braided rivers. Remote sensing techniques allow measurement of channel planform and three-dimensional morphology. However, it may be argued that they have not yet led to a comparable advance in understanding of the spatial aspects of sediment transport in dynamic gravel-bed rivers at the reach scale, a scale lying in between that of point measurements and large scale measurements.

### **2.5.2. Modelling of braided rivers.**

Hydraulic and sedimentological models provide a framework in which to conceptualise and investigate the relationship between flow hydraulics and sediment transport. The scientific literature of the past 25 years contains a large number of reports dealing with the application of physical and numerical models to the assessment of the evolution of braided river networks and the transfer of sediment therein. However, modelling relationships between processes and

channel morphology in braided channels is difficult due to the complexity of both sediment dynamics and flow hydraulics.

### **2.5.2.1. Physical modelling.**

A physical model is a scaled representation of a hydraulic flow situation. In the past, physical modelling of braided rivers received less attention than that for single and meandering channels, despite the fact that the hydraulic and sedimentological inter-relationships in braided rivers are very complicated with substantial feedback mechanisms (Ashworth and Ferguson, 1986), making numerical modelling problematic (especially in three-dimensions). However, non-uniform flow (convergence and divergence around bars), mixed size bed material (ranging over several orders of magnitude in size), and spatial and temporal variability in channel response to flood events lead to difficulties in making detailed and representative quantitative measurements even under simplified laboratory conditions. Despite this, scale modelling has led to some major advances in understanding braided river processes.

Physical models have been used to study bar growth and the mechanisms of braiding, flow dynamics and morphology of channel confluences and diffluences, the importance of chute and lobe unit in controlling local sediment budgets, sediment sorting and deposition in alternate or single bar braid reaches and the relationship between bedload pulses and cycles of aggradation and degradation (e.g. Leopold and Wolman, 1957; Mosley, 1976; Ashmore, 1982, 1988, 1991a-b; Ashmore and Parker, 1983; Southard *et al.*, 1984; Best, 1986, 1988; Hoey and Sutherland, 1991; Ferguson and Ashworth, 1992; Ashworth *et al.*, 1994; Ashworth, 1996; and Lisle *et al.*, 1997). Physical laboratory models have been very useful at giving insight into whole river sediment transport and changes in channel planform but are too shallow and rapidly changing to easily make distributed spatial measurements (Ferguson and Ashworth, 1992).

### 2.5.2.2. Numerical modelling.

As computing capacity has improved, the use of numerical models in fluvial geomorphology has increased considerably. The benefits of numerical modelling include an improved understanding and simulation of key processes in one- two- or three-dimensions, and insight into the distribution of processes within the landscape (Bates and Lane, 1998). Paola (2001) identifies two approaches to numerical modelling, reductionist and synthesist.

A reductionist approach to modelling starts with the governing equations and makes approximations until one arrives at a system that is solvable with whatever means are available. An unstated assumption of this standard approach is that the fewer the fundamental equations that need to be simplified the better (Paola, 2001). The reductionist view states that it is only through specifying in detail the many processes active in nature and the parameters of their mathematical formalisation that landscape evolution can be understood.

The synthesist approach is rooted in the idea of 'emergent' phenomena (Paola, 2001). Emergent phenomena are aspects of complex-systems dynamics that arise from the interactions of the parts but that could not readily be deduced from studying the dynamics of the parts separately. Synthesist models often make assumptions about the underlying processes such as water flow and erosion in order to gain simplicity at the expense of realism. While they were popular at a time when computer power was more limited, they were to some extent eclipsed as more detailed simulation became more possible. There has however been a recent revival of interest in such models due to the comparative ease with which many features of their behaviour can be understood and also to suggestions that some aspects of system behaviour may be comparatively independent of the details of the model, i.e. display self organised criticality. (Barzini and Ball, 1993). Synthesist approaches to modelling include cellular automata models that are developed to predict the overall style of river behaviour, however they are generic and are not readily applicable to specific sites.

### 2.5.3 Reductionist and small-scale investigations.

Computational fluid dynamics (CFD) models have been available since the early 1970s. However, continual improvements in process representation within the models have progressively improved their appeal (Bates and Lane, 1998). The models solve the Navier-Stokes equations, and may allow some modification by the user so enabling the study of sediment transport and possibly channel change (for a recent, detailed description of the basic principles of CFD modelling, see Lane, 1998). A number of CFD models are commercially available (e.g. FLUENT, STREMR) and previous studies have applied these models to single channel reaches (e.g. Hodkinson, 1996; Hodkinson and Ferguson, 1998). Recently CFD models have been applied to braided channel reaches, typically around bar-chute complexes (e.g. Lane and Richards, 1998; Nicholas and Sambrook Smith, 1999), and the small-scale application of many CFD models has successfully predicted short-term river behaviour in short, narrow channels at scales of 1-10 m (e.g., Lane and Richards, 1998). While these models are useful in identifying small-scale processes, extending this approach in space and time is computationally very difficult, and requires a high level of field data for verification. While remote sensing techniques are able to capture large amounts of data (see Westaway *et al.*, 2000), there is an issue with data quality that must be addressed (see Lane 2000).

Recent advances in two-dimensional (Lane and Richards, 1998) and three-dimensional (Nicholas and Sambrook Smith, 1999) modelling of flow hydraulics in multi-channel systems may in future allow a physically based treatment of these processes (Nicholas, 2001). However while such schemes may be appropriate for use in modelling process-form interactions at the scale of the bar-pool unit, they are both computationally expensive and demanding in terms of their data requirements. Consequently one-dimensional models may remain more effective tools for use in the derivation of bedload flux estimates at the reach scale, provided that such models are modified to incorporate the effects of the

spatial variability in flow and sediment transport processes that characterise braided streams (c.f. Paola, 1996).

McArdell and Faeh (2001) have developed a reductionist numerical model of braiding in which the flow is represented via the depth-averaged shallow-water equations. Model results were compared to published laboratory experiments on braiding (Fujita, 1989 in McArdell and Faeh, 2001) and it was found that, whilst the model initially underpredicted the distance between bar tops and scour pool bottoms, over time in a simulation the agreement improved.

#### **2.5.4. Synthesisist and larger scale numerical modelling.**

The use of physically based numerical models of braided systems at the larger scale has been attempted. These models make assumptions about the underlying processes such as water flow and erosion in order to gain simplicity at the expense of realism. A “random walk” approach has been used to produce two-dimensional braided patterns (e.g. Howard *et al.*, 1970), and simple numerical models (e.g. Barzini and Ball, 1993; Murray and Paola, 1994, 1997) have demonstrated that the apparently stochastic behaviour of braided river processes may reflect a simple non-linear relationship between stream power and bedload transport. Approaches to modelling braided rivers are examined in more detail below.

##### **2.5.4.1. Random Walk Models.**

Random walk models are geometric or topological models in which channel networks are formed by a series of steps of random orientation. The models do not incorporate the altitude dimension. Networks are developed sequentially and proceed downstream; the models usually contain rules to constrain channel orientation. Random walk models allow streams to move in two lateral directions and also to bifurcate. As these options are available at each grid node, channels will also coalesce, leading to a braided channel pattern. Random walk models

have been developed by Howard, *et al.* (1970), Krumbein and Orme (1972), Rachoki (1981), and Webb (1994, 1995).

Howard *et al.* (1970) developed four random walk models on rectangular grids with no lateral boundaries. Instead, a weighting factor was used to constrain the overall width of the system. The lateral movement of channels and the occurrence of branching were randomly determined by a probability function. Channels joined or bifurcated according to a series of rules with the restriction that no more than three channels intersected at a given step. Comparing output with dimensionless parameters validated the model. Howard *et al.* (1970) found that the model with the most restrictive rules for channel bifurcation and the largest step lengths produced the best match with their observed data for 26 braided rivers in the USA.

Krumbein and Orme (1972) developed two random walk models on a diamond shaped grid, similar to those developed by Howard *et al.* (1970). The models incorporated parallel reflecting boundaries and channels joined wherever they intersected. The probability of channels bifurcating was scaled by discharge (in the first model), or by the reciprocal of the number of channels (in the second model). Models were tested using the theoretical proportions of link types (defined by Smart and Moruzzi, 1971) to judge the topological adequacy of the simulated systems. Within a braided channel network four types of links have been defined. Links may start at either a joint (J), where two channels merge into one, or a fork (F), where a channel bifurcates. Links may terminate at either a joint or fork, leading to four link types: FF, FJ, JF and JJ (e.g. JF means that the link begins where two channels join together and ends where the channel bifurcates). Smart and Moruzzi (1971) show that when the number of bifurcations equals the number of junctions, the proportions of each type of link are  $FF = 0.22$ ,  $FJ = 0.44$ ,  $JF = 0.11$ ,  $JJ = 0.22$ . The second model was found to agree well with field data from the Santa Clara River, California. However, after short runs of the first model and longer runs of both models (referred to but not published) both models tended to converge onto one link type (JF links); the exact ratios were not

published. Krumbein and Orme (1972) therefore concluded that both of the modelling approaches were unacceptable.

Rachoki (1981) proposed a random walk model on a diamond shaped grid to represent the channels spreading out from the apex of an alluvial fan. Each channel had the same probability of flowing in one of three ways (to the left, right or bifurcating). No boundaries are defined; the overall width of the system can continue to increase. The model was used to investigate the coverage of fan surface with braided channels, the probability of reoccupation of preserved channels during subsequent flow events, the degree of system development and the distribution of flow, however no formal validation was performed.

Webb (1995) applied the link type measurement approach of Krumbein and Orme (1972) to the models of Howard *et al.* (1970) and Rachoki (1981). Both were found to contain approximately the correct percentage of JF type links but a higher proportion of FJ links. Webb (1995) concluded that all three models fail to reproduce accurately the theoretical link-type ratios.

The results of the above models are interesting as the spatial patterns produced by the models match those of real rivers when compared using a variety of averaged statistics even though, as the authors point out, the models are purely geometric and do not simulate any of the physical processes of a real river. The results imply that standard, topologically based statistics are not very sensitive test of model dynamics (Paola, 2001). According to Webb (1995), the models of Howard *et al.* (1970), Krumbein and Orme (1972) and Rachoki (1981) share three limitations:

1. the lateral motion of a channel in each time step is constrained to a fixed grid spacing, thus limiting the scale of the resolution and the variability of motion in the lateral direction;
2. none of the models can accommodate the effects of channel width on the location or frequency of intersections; and
3. none of the models include estimates of channel depth necessary to describe the associated topographical (geomorphological) surface adequately.

Webb (1995) claims to have overcome the above limitations via a random walk model, BCS (Braided Channel Simulator). The model has been used to produce two-dimensional and three-dimensional braided networks, hereafter referred to as BCS-2D and BCS-3D respectively.

BCS-2D is a random walk approach to modelling a two-dimensional braided pattern. However, unlike the models of Howard *et al.* (1970), Krumbein and Orme (1972) and Rachoki (1981) BCS-2D incorporates both hydraulic geometry of stream channels and an adaptive grid allowing flexible lateral movement, width and depth of each section of the channel system. This accounts for the limitations of the previous models. BCS-2D allows a user-specified number of channels upstream, each of which is randomly assigned a portion of total stream discharge.

The braided network is developed within a rectangular space having lateral no-flow boundaries. At each iteration, channels are extended a fixed distance in the longitudinal direction and a variable distance in the transverse direction. The transverse shift is randomly chosen from a uniform distribution with a range determined from a specified channel sinuosity. All channels have a finite width, depth and velocity based on the individual channel discharge and user-specified hydraulic channel geometrical relationships. At each step, channels that intersect (no more than two at a time) are joined to form a single channel with the combined discharge of the two joining channels, and consequently a different width, depth and velocity. After all intersecting channels are joined a certain number of the remaining channels are chosen to bifurcate or split based on a user-specified bifurcation probability. A random percentage of the discharge in the original channel is assigned to each of the two new channels and their shape is determined using the hydraulic geometry relations. Thus discharge is conserved throughout the network.

A three-dimensional topographic surface is developed from channel location along with total width and depth. Absolute elevations are assigned to nodes within

a square topographical grid equal to the depth of the channel link (if any) at the node. All nodes outside a channel are assigned an elevation equal to the elevation of the original surface. All channels are assumed to have a parabolic shape.

The calibration criteria for BCS are either generic (applicable to all braided rivers) or site specific. Site-specific indices were derived from Mosley's (1982) study of the Ohau River, New Zealand, and include topological measures derived from aerial photographs of the river. Model calibration was undertaken by taking the arithmetic average of 30 runs and comparing the result with calibration targets. A formal sensitivity analysis found that the most significant input parameters are the bifurcation probability and the step size.

Although BCS-2D greatly improves upon previous random walk models, the model contains some problems. Shortcomings of BCS-2D include:

- the model is constrained to a rectangular study area with parallel lateral confining boundaries;
- although the initial number of channels can be specified, their locations are randomly chosen by the model; and
- the model assumes no control on channel location by pre-existing topography (i.e. the random walk has no topographical weighting).

In his 1994 paper, Webb extended BCS-2D to allow the generation of multiple topographic surfaces. The new model, BCS-3D, is a geometrically based model that produces three-dimensional facies distributions of braided river systems. A random walk algorithm produces two-dimensional braided surfaces with each channel segment assigned characteristics including channel width, depth, velocity and sediment type. Sediment type is linked to Froude number. Each topographic surface is generated separately then the surfaces are stacked to form a three-dimensional framework of sediment packages.

BCS-3D differs from BCS-2D by the following additions:

1. a weighting function constrains the location of simulated channels based on the topography of the previous surface. A measure of topographic control is thus placed on a channel via the elevation of previous surfaces. The first surface to be simulated has a weighting factor of zero, allowing it to be randomly simulated. The weighting factor of subsequent surfaces is determined by comparison of the current and previous discharge;
2. the model includes variables to constrain the variability of discharge and the variability of mean surface offset (aggradation). The average vertical offset for the stacking of surfaces is user-specified. The final offset is a percentage of the average vertical offset equal to the ratio of the current discharge to the average discharge;
3. parameters to allow variability in the hydraulic geometry relationships used to define channel shape. The variables that define the relationship of width, depth and velocity to discharge are derived empirically from field data; and
4. a definition of sediment units based on a Froude-number scale. Assignment of sediment units is based on a measure of flow energy at each point on the surface. The sediment units of interest are defined by the user along with a scaling factor for discharge that determines the total discharge (the channel forming flow rate). The discharge at deposition is some fraction of the channel-forming discharge.

A composite set of field data was developed from data collected by others (Mosley, 1982; Brierley, 1989), and was used to derive input parameters and to calibrate the model. Mosley's data contains geomorphological information on the channel network of the Ohau River, New Zealand; calibration targets used were the same as for BCS-2D. Brierley's data consists of quantitative information on abundance and vertical transition of sediment units in the Squamish River, British Columbia. Both rivers are of the Donjek type (Miall, 1978), consisting of fine gravel and sand deposits in well-developed channels. The model was formally sensitivity tested.

The calibrated model has been used to examine the effect of spatial patterns in hydrofacies on contaminant transport (Anderson *et al.*, 1999), to simulate groundwater flow through each sequence of sediments and to trace the movement of imaginary particles through the representations of the two deposits.

#### **2.5.4.2. Limitations of random walk models.**

Random walk models are two-dimensional topological models, which are statistical in nature, and may produce fractal structures closely resembling many planar features of real river networks (Rodríguez-Iturbe and Rinaldo, 1997). Even though random walk models may reproduce topologically based statistics, their purely statistical nature does not provide insight into the geomorphic processes responsible for network generation. In a random walk model network evolution is viewed as a growth process, with channels proceeding a fixed distance downstream at every step. The frequency of channel bifurcations is usually determined by user-defined statistical rules and channel confluences and diffluences are usually set at a fixed angle, determined by the shape of the grid. There is no topographic control over braidplain formation.

The models of Webb (1994, 1995) go some way to account for the problems described above. These models use an adaptive flexible grid to create a more realistic braidplain by linking dynamic processes with hydraulic geometry relationships. However, even though Webb has extended his two-dimensional model to simulate three-dimensional deposits, the process used to simulate the first surface (the only surface in the two-dimensional model), which exerts a topographic control over the surfaces above, is a purely random process.

#### **2.5.5. Deterministic models.**

A deterministic model is one that does not include random variables (i.e. variables that are represented by probability density functions). Deterministic models can produce apparently stochastic behaviour if the system is sufficiently complex, a

phenomenon known as “chaos” (Paola, 2000). These models have deterministic driving mechanisms although they operate under variable conditions, either for the variable or for the initial or boundary conditions (Howard 1994; Rodríguez-Iturbe and Rinaldo, 1997). The models incorporate the altitude dimension, as a fundamental part of their structure, and include models of erosion and the evolution of river networks. The rivers produced are not braided, however the approaches allow for growth and meaningful three-dimensional river basin structures. The models reviewed in this section are large-scale landscape evolution models, however they are relevant to the discussion as they include fluvial transport equations.

#### **2.5.5.1. SIBERIA (Willgoose *et al.*, 1991a-d, 1994).**

Willgoose *et al.* (1991a-d, 1994) have developed a large-scale two-dimensional geomorphological model (SIBERIA) of catchment evolution involving channel network growth and elevation evolution. The model, based on a finite-element rectangular grid, includes overland and channelised flows, a channel initiation function (cif), and a fluvial transport formulation that depends non-linearly on discharge and local slope, (i.e. stream power, Kooi and Beaumont, 1994)

Elevation within the catchment is simulated by a mass transport continuity equation. Mass transport processes considered include fluvial sediment transport (modelled by the Einstein-Brown equation) and mass movement mechanisms, (soil creep, rainsplash, landsliding and tectonic uplift). The model makes an explicit distinction between sediment transport processes operating in channels and those on hillslopes. Within channels fluvial sediment transport processes dominate; on hillslopes, diffusive mass transport is more important and may dominate.

A channel is formed, or a channel head advances upstream, when the selected flow and transport mechanisms which constitute the cif exceed a pre-determined threshold value. Erosion within a channel is greater than on the hillslope, leading

to preferential erosion in the channel and a convergence of flow on hillslopes towards channels, triggering channel head advance. Channel heads can only advance, and channels cannot shift their planar position, therefore once formed the channel exists forever. These restrictions are not believed to be critical because the elevation equation is a mean equation so for compatibility the mean channel network should be used (fluctuations in channel head position over short timescales are ignored), and although channels meander about their floodplain, the general position of the valley floor is more or less fixed. The channelisation equation has two stable attractors that correspond to a point in space being channelised or not. When the cif exceeds the threshold for channelisation, the equation becomes unstable and goes into transition i.e. it tends towards the other stable solution. In other words, once a threshold has been exceeded, that point in the catchment goes into transition from a hillslope to a channel. During this transition sediment transport processes are intermediate between that for a hillslope and that for a channel, however the model is insensitive to the exact form of these processes (Willgoose *et al.*, 1991a).

A drainage direction is assigned to each node according to the steepest slope to the next node (a node can only drain to one other node), and the contributing area to each node is calculated. From the contributing areas and flow and sediment, continuity equations for flow and sediment are written. The areas and the steepest slopes are used to evaluate the cif and therefore determine the areas of active channel network growth. The model is transport limited, i.e. it assumes that there are adequate supplies of erodible materials in the catchment, thus rivers always transport at capacity. It is therefore applicable where stream channels are alluvial in character (Ibbitt *et al.*, 1999).

Model runs commence with random elevations assigned to an initially flat grid, and erodibility, runoff, and channel initiation function, threshold all considered to be spatially uniform. Rodríguez-Iturbe and Rinaldo (1997) note that no thorough study of the effects of randomness on these properties has been performed, but the results of Willgoose *et al.* (1991a-c) suggest that for equal coefficients of

variation, and flat conditions, randomness in the initial elevations is the most important variable.

SIBERIA was tested by comparing its ability to simulate the channel network properties of a drainage basin in New Zealand (the Ashley River basin) with that of an optimal channel network model (OCN), an energy model that minimises the overall energy expenditure of the network within a given catchment boundary. It was found that in general and using spatially uniform inputs, neither model successfully replicated the prototype river basin. The best results from SIBERIA-generated networks were obtained using a non-additive area-slope relationship and a realistic tectonic history of the basin. SIBERIA results are thus sensitive to the form of the network used to initialise simulations (Ibbitt *et al.*, 1999).

#### **2.5.5.2. Howard's (1994, 1997) model.**

Howard (1994) proposed a high-resolution, process-based simulation model of slope and channel development at the basin scale incorporating creep and threshold erosion as well as detachment- and transport-limited fluvial processes. The model of Howard (1994) contrasts with that of Willgoose *et al.* (1991a-d, 1994) in several major respects. The Willgoose model assumes flow (overland and in channels) is transport limited, whereas the model of Howard (1994) assumes that erosion in many locations, particularly in headwaters, is supply limited. The constraint on landscape evolution is the rate at which material can be detached. The model is therefore most appropriate to areas of hard geology where the streams flow over exposed bedrock (Ibbitt *et al.*, 1999).

Simulations take place on a finite-difference square matrix cell within each both channel and slope processes occur. This is in contrast to the Willgoose model in which individual simulation cells are either channels or slopes, and leads to a simpler set of governing equations.

Channel operations are simplified to a sub-grid cell process; whatever the embedded width of the active channel possibly existing in the cell, it is specified to be less than the width of the cell (Howard, 1994). Both mass wasting and fluvial transport/erosion, whatever their relative importance, occur in each cell. It is assumed that all runoff becomes concentrated into a single permanent or ephemeral channel running the length of the cell with a gradient equal to the overall slope gradient and that all fluvial erosion within the cell occurs in the channel. Values for width and depth are calculated using empirical relationships. The use of the activation function in the model of Willgoose *et al.* (1991a-d, 1994) automatically defines the channel network and drainage density; in the model of Howard (1994) the location of channel heads is defined by a morphometric criterion.

Most runs start with a planar surface with a random elevation perturbation superimposed. Lateral boundaries are periodic for water and sediment; the upper boundary is assumed impenetrable by water, sediment and regolith and the lower boundary is assumed level with a specified elevation. The lower boundary can be lowered at a constant rate for steady state drainage basin development. Therefore it is like a constant lowering of base level. Internal cells may donate to only one of their eight neighbours. Sediment and water leave cells via the steepest slope, taking into account the difference in distance between diagonal cells.

Fluvial erosion is advective and incorporates two processes: erosion is detachment-limited in steep channels flowing on bedrock or regolith in which the bedload sediment flux is less than capacity load; in lower gradient alluvial channels, fluvial erosion is transport-limited. In this respect, the model differs from Willgoose's model.

The model can be run with alluvial or non-alluvial channels. For alluvial channels the potential rate of fluvial erosion is equal to the spatial divergence of the volumetric unit bed sediment transport rate (Howard *et al.*, 1994, 1997). Non-

alluvial channels are defined as those in which the bedload sediment flux is less than a capacity load. Such channels may be flowing on bedrock or regolith.

Results of model runs were compared with fieldwork from badlands developed in Macos Shale near Cainville, Utah (Howard, 1997). The modelling results support the field interpretation (Howard, 1986 in Howard, 1997) of erosional history and controls on slope morphology. However the model parameters have not been directly validated and calibrated by field observations.

### **2.5.5.3. *Cascade* (Braun and Sambridge 1997).**

*Cascade* is an ANSI-standard Fortran surface process model which uses an irregular, adaptive finite-difference triangulated grid (Delaunay triangulation) to represent the land surface. Large-scale, long-term landform evolution is assumed to be controlled by short-range hillslope and long-range fluvial transport. Two types of hillslope processes are included: continuous slow processes such as soil creep are modelled using a linear diffusion parameter and mass wasting is modelled by imposing a slope threshold when this is exceeded the slope is brought back to the threshold by moving material down the slope (Braun and Sambridge 1999). Long-range fluvial transport is controlled by the carrying capacity of the rivers; *Cascade* differs from most other long-term landscape evolution models in its treatment of river erosion as being linearly dependent on discharge and local slope, and includes a length scale for bedrock incision. Surface runoff at a point on the mesh is routed downslope towards one neighbouring node via the edge with the steepest slope. If a node lies at a point of minimum elevation the water may either evaporate away or a lake may form, depending on the algorithm invoked (Braun and Sambridge 1997). If the carrying capacity of the river is greater than the material available for transport, erosion will occur and vice versa. For long-term landscape evolution on large spatial scales, orographic rainfall effects and tectonic processes (flexural isostasy) is included. In this study *Cascade* has been altered to produce *Braided Cascade*, and will be further discussed in Chapter 3.

#### **2.5.5.4. Channel Hillslope Integrated Landscape Development model (CHILD) (Tucker *et al.*, 1999).**

The CHILD model is designed to simulate the evolution of fluvially dominated landscapes formed chiefly by physical erosion and may be thought of as an extension to the *Cascade* model (Braun and Sambridge 1997). It simulates the development of two general types of process: “fluvial” processes, which encompass erosion or deposition by runoff (including slope wash, and channel and rill erosion), and “hillslope” processes, which includes weathering, creep and other slope transport processes. Like *Cascade*, the model is based on an irregular finite-difference mesh; this is based on the method of Braun and Sambridge (1997). The model allows for stochastic rainfall forcing, stream meandering and dynamic remeshing, overbank deposition, multiple sediment sizes and the ability to track the deposition of sediment layers at each point in the landscape. CHILD therefore differs from the models of Willgoose *et al.* (1991) and Howard (1994, 1997) as these models only allow for uniform rainfall, no stream meandering, one sediment size, no overbank deposition and no sediment tracking facility. Following Braun and Sambridge (1997) (the *Cascade* model), rivers are defined via the route with steepest descent; lakes may form or the runoff may evaporate. One of four alternative runoff-generation models may be used to compute surface runoff from drainage area, allowing the user to choose a method appropriate to the environment of interest.

No explicit distinction is made between erosion by overland flow and that by fully channelised flow. Sediment transport by hillslope processes is modelled using a diffusion equation. Like Howard (1994) the model distinguishes between detachment of material from a streambed and transport of the detached material. The maximum detachment rate depends on local slope and discharge. If the sediment transport capacity exceeds the sediment influx, the rate of water erosion is equal to the maximum detachment rate (the detachment-limited case). However if sufficient sediment is available for transport, streams are assumed to be at carrying capacity (the transport-limited case).

### **2.5.5.5. Deterministic models. A summary.**

The deterministic models of Willgoose *et al.* (1991a-d, 1994), Howard (1994) Braun and Sambridge (1997) and Tucker *et al.* (1999) are useful tools in the investigation of landscape evolution. The models use accurate in the descriptions of different processes affecting fluvial erosion, and the complexity of the possible scenarios for landscape evolution is clear and likely to be realistic (Rodríguez-Iturbe and Rinaldo, 1997). However, they do not clarify the linkages between fundamental aspects of the dynamics and the existence of general types of scaling relationships in the elements of the network and the landscape itself. The indefinite persistence of initial conditions, common to all deterministic models and the need to tune the large numbers of parameters required to describe the many natural processes introduce important elements of arbitrariness.

Willgoose's and Howard's approaches agree with the reductionist, process orientated tenet to which most geomorphology is committed (Rodríguez-Iturbe and Rinaldo, 1997; Paola, 2000). As such it is only through specifying in detail the many processes active in nature and the parameters of their mathematical formalisation that landscape evolution can be understood.

### **2.5.6. Cellular automata models.**

Cellular automata are mathematical idealisations of physical systems in which space and time are discrete and physical quantities take on a finite set of discrete values (Wolfram, 1983, 1984). An automaton can be generalised to any system that has a finite number of internal states and moves between those states by following specified rules (Lucas, 2000). A cellular automaton consists of a regular uniform lattice with a discrete variable at each site (or cell). The state of a cellular automaton is completely specified by the values of the variables at each site. A cellular automaton evolves in discrete time steps, with the value of a particular site being determined by the previous values of a neighbourhood of sites around it. The neighbourhood of a site is typically taken to be the site itself and all immediately adjacent sites, however it can be extended to "close" (including

neighbour's neighbours) or "global" (anywhere in the system). The values of the sites evolve synchronously in discrete time steps according to a definite set of local rules (Smith, 1991).

Physical systems containing many discrete elements with local interactions are often conveniently modelled as cellular automata. Any physical system satisfying differential equations may be approximated as a cellular automaton by introducing finite differences and discrete variables (Wolfram, 1983, 1984). The trajectories of the system can be plotted in the 'state (or phase) space' i.e. a space that has an axis or dimension for each important variable except time. Each point represents a state of the system at one instant and, as the system changes with time, it will trace out a path in the state space. In almost all cases, cellular automaton evolution is irreversible so that the trajectories merge with time, and after many time steps, trajectories starting from almost all initial states become concentrated onto "attractors" (Wolfram 1983, 1984), although if the systems are non-linear, deterministic, they may diverge from very similar initial states. These attractors typically contain only a very small fraction of possible states. Evolution to attractors from arbitrary initial states allows for "self-organising" behaviour, in which structure may evolve at longer time scales from structureless initial states. The nature of attractors determines the form and extent of such structures. Wolfram (1983, 1984) suggests that many cellular automata (perhaps all) can be grouped into four classes based on their qualitative patterns:

- Class 1. Point attractors. The system freezes into a fixed state after a short time (the transient behaviour).
- Class 2. Limit cycles. The system cycles between several states in a regular fashion (i.e. it develops periodic behaviours, which then repeat continuously). A loop will be traced out in state space.
- Class 3. Chaotic. The system becomes aperiodic, continuously changing in unpredictable and random ways. A random pattern appears and so-called 'strange attractors' are formed (a strange attractor characterises a system that never returns to the same place, e.g. the Lorenz (1963) attractor).

- **Class 4. Structured.** The system can develop highly patterned but unstable ways. Computationally rich, this type of system denotes an automaton between states 2 and 3 – at the edge of chaos. (The edge of chaos can be simply defined as a system midway between stable and chaotic domains. It is characterised by a potential to develop structure over many different scales and is an often-found feature of those complex systems whose parts have some freedom to behave independently).

Therefore, there is order in state space even if normal space appears chaotic. Many different realisations of the same dynamical system, while exhibiting different sequences of values, will sketch out the same attractor when plotted in state space.

Cellular automata models have been widely applied to many biological systems and ecological and population modelling (e.g. the “Game of Life” where site values represent states of living cells or groups of cells). In a geomorphological context, cellular automata models have been applied to the erosion of landforms (Smith 1991), landscape evolution (Chase, 1992), the evolution of an upland drainage basin (Coulthard *et al.*, 1998, 1999) and the evolution of generic braided river networks (Murray and Paola 1994, 1997). The last example will be explored in more detail.

#### **2.5.6.1. Cellular automata models of braided river evolution.**

Murray and Paola (1994, 1997) developed a cellular model that simulates the evolution of a braided network. The model uses a square lattice and the real variables defined on the lattice are bed elevation, water discharge and sediment discharge. These variables and all other model parameters are specified in arbitrary units. Most runs start with uniform slope and white-noise elevation perturbations are placed on the grid to give a random initial topography.

Each iteration begins with the introduction of units of water in some or all of the cells at the upstream end of the lattice. The water moves downstream row by row and can be distributed from one cell to one or more of the three downstream neighbouring cells. River patterns are not predicted spontaneously. In this respect the model resembles a random walk model, however the movement of water is determined by local gradient, not a purely statistical rule, and fluxes of water and sediment are determined by the previous values of the adjacent neighbourhood of eight cells. The model does not allow the formation of lakes and all water entering a cell leaves it during that iteration. The iteration ends when water reaches the downstream end of the lattice when the elevation of each cell is adjusted. It should be noted that as discharge is conserved, depth is not predicted explicitly.

Water and sediment are conserved: i.e. there is no net gain or loss in the model. Water transports sediment from cell to cell according to one of six different rules used (Table 2.4.), which involve local discharge or the local stream power index (local discharge multiplied by local slope). Two rules incorporate a sediment-transport threshold  $Th$ , which is defined as being approximately half of the local stream power. Elevation changes are dependent on the difference between the total amount of sediment entering and leaving a cell. Lateral erosion or channel bank erosion, may occur and sediment can be transported from lateral neighbour cells with higher elevation. This occurs regardless of whether the neighbour cells contain water so that any channel bank can erode.

$Q_{si} = K[Q_i]^m$	$Q_s$ rule 1
$Q_{si} = K[Q_i S_i]^m$	$Q_s$ rule 2
$Q_{si} = K[Q_i(S_i + C_s)]^m$	$Q_s$ rule 3
$Q_{si} = K \left[ Q_i S_i + \varepsilon \sum_{j=1}^3 Q_{uj} S_{uj} \right]^m$	$Q_s$ rule 4
$Q_{si} = K[Q_i(S_i + C_s) - Th]^m$	$Q_s$ rule 5
$Q_{si} = K \left[ Q_i S_i + \varepsilon \sum_{j=1}^3 Q_{uj} S_{uj} - Th \right]^m$	$Q_s$ rule 6

Table 2.4. Sediment routing rules in the cellular automata braided river model of Murray and Paola (1994, 1997).

$Q_{si}$  = the amount of sediment transferred to downstream neighbour  $i$  from the cell in question.  
 $K$  = a constant adjusted so that the elevation changes by at most a few percent of the mean elevation difference between rows in each time step;  $Q_i$  = discharge;  $S_i$  = slope;  $C_s$  = the order of the average slope;  $m$  = a constant  $> 1$ , usually 2.5;  $\varepsilon \approx 0.3$ ;  $Th$  = sediment transport threshold, around half the typical stream power.

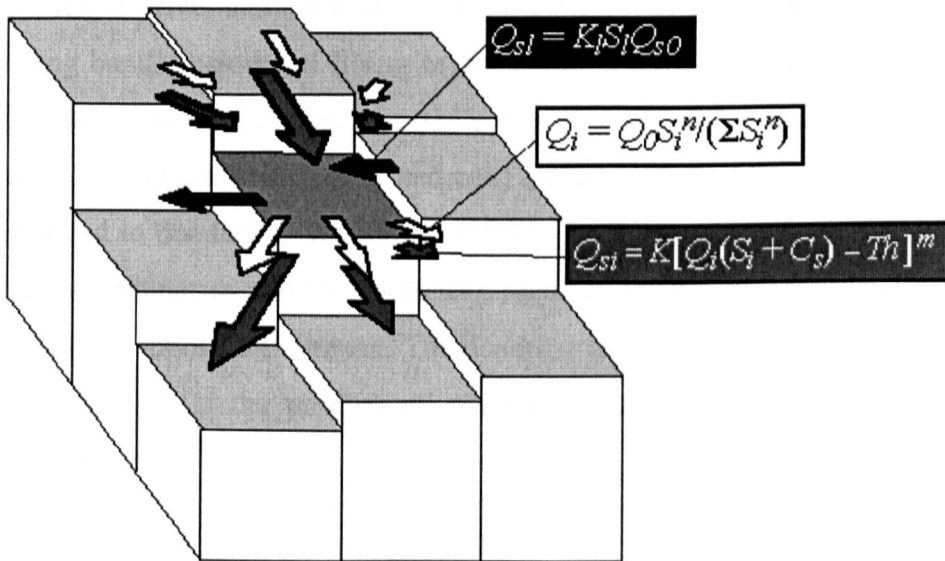


Figure 2.4. Water and sediment routing in the Murray and Paola (1994, 1997) cellular automata braided river model. Water fluxes are shown as white arrows, direct sediment flux as grey arrows and lateral sediment transport as black arrows. Rules for water transport ( $Q_i$ ), ( $Q_0$  is the discharge coming from the target cell); direct sediment transport ( $Q_{si}$  – rule 5) and lateral sediment transport ( $Q_{s1}$ ) are given in boxes.  $K_1$  is a constant,  $S_1$  is the lateral slope and  $Q_{s0}$  is the direct sediment transport in the target cell. From Paola (2001).

In a standard run, the model boundaries are high sidewalls containing the flow. In most runs the elevation of the first and last rows of cells are fixed, simulating the rigid side and end walls of laboratory flume experiments.

The simple, deterministic interactions of the model produce spatial patterns and temporal dynamics that are qualitatively realistic. The system reaches a dynamic equilibrium in which all sediment supplied is passed through to the downstream end. The pattern never repeats itself but is statistically steady (Paola, 2001).

The Murray and Paola (1994, 1997) model suggests that, for braiding to occur, it is crucial to have a topographically driven flow expansion and contraction and non-linear sediment transport law that couples these to changes in bed elevation. Experiments with the model show that if the sediment flux is linear, braiding does not develop. Lateral bedload flux is essential to maintain braiding, as model runs without this ability tend to drift into a 'canyon' state with one very deep channel from which the river can not escape (Paola, 2001). Lateral transport prevents this by forcing bank erosion and filling in narrow high-velocity zones. Changing the transport law from flux-limited (for non-cohesive materials) to detachment limited (for cohesive materials including bedrock) causes the channel pattern to switch from braided to dendritic. The braided topology, which balances confluences and diffluences (tributaries and distributaries), requires equal measures of erosion and deposition: reversible entrainment. The dendritic topology, which has confluences (tributaries) only, is the product of one-way erosion: irreversible entrainment (Paola, 2001).

Neither the patterns produced by the model nor those in real braided rivers have an obvious characteristic length (Sapozhnikov and Foufoula-Georgiou, 1996). The model remains statistically stable over time and the spatial patterns produced match those of real rivers when compared using a variety of averaged geometric statistics (after Howard *et al.*, 1970) although it was noted that such comparisons do not necessarily discriminate well between patterns generated by different model runs.

Spatial patterns produced by the model were analysed using dynamical systems methods (delay co-ordinate embedding) by plotting the position of the system in state space (Murray and Paola, 1996). Reconstructed three-dimensional state-space plots were produced showing the total width of all active channels at each cross-section versus the total width of the previous two cross sections for different sediment transport rules. The shapes of the plots were analysed qualitatively by comparing the plots to those derived from a real river (the Aichilik River, Alaska). A two-dimensional state-space plot was then constructed by plotting each width versus the last. Quantitative analysis was undertaken using a box counting method to provide a measure of the difference between two plots. Using both qualitative and quantitative analyses it was found that model runs with sediment transport rule 4 gave the best comparison with the prototype river, however runs with sediment transport rules 5 and 6 were not tested.

However, using the state-space method has limitations. The distance (or delay for a time series) between measurements could affect the outcome of a comparison if it is not the same for both series, because using larger distances expands the plot away from the diagonal. If this distance or time delay becomes large, succeeding measurements may become uncorrelated (Murray and Paola, 1996).

Sapozhnikov *et al.* (1998) present a method for braided stream model validation based on the sequential organisation and the hierarchical organisation of their plan patterns. The method is an extension of that used by Murray and Paola (1996) and uses results from their model using sediment rules 3 and 4, and data from other prototype rivers (the Aichilik and Hulahula Rivers in Alaska and the Brahmaputra River, Bangladesh). State-space plots of total widths were constructed in two dimensions (i.e. by plotting total width versus the previous value). It was found that areas of dense data are similar indicating similar sequences of widths suggesting that fundamentally similar mechanisms operate in all of these braided streams (Sapozhnikov *et al.*, 1998).

Differences between plots and real rivers indicate that the model does not always match the real rivers as closely as real rivers match each other (Sapozhnikov *et al.*, 1998). Fractal analysis carried out on traced discharge patterns of the model found that the model rivers exhibit fractal behaviour up to the scale of their width. A logarithmic correlation integral (LCI) was applied to determine the type of fractal scaling and it was found that, at long runs when braiding is fully developed, the model rivers are self-affine objects showing a high degree of anisotropic scaling. Islands in the modelled rivers were analysed using the LCI method for fractal scaling and it was found that the scaling anisotropy of the islands was lower than the modelled rivers. This agrees with previous results obtained for natural rivers (Sapozhnikov and Fofoula-Georgiou, 1996).

Thomas and Nicolas (2002) have applied cellular automata modelling to a specific site. The model is similar to that of Murray and Paola (1994, 1997); a square lattice is used, however flow is split between five downstream neighbour cells allowing for lateral transfer of water at angles of up to 60°. Water is routed according to energy slope so water heights are calculated, and sediment routing is not included. The model has been used to route water through a DEM of a section of the braided Avoca River, New Zealand. Resulting simulated flow patterns show that the model is capable of replicating the patterns observed in the field and the predictions of a more sophisticated two-dimensional hydraulic model at higher flows.

#### **2.5.6.2. Summary.**

The Murray and Paola (1994, 1997) model is synthesisist in spirit (Paola, 2000); the braid pattern emerges from a highly simplified model of the dynamics. In this model braiding is an emergent behaviour (i.e. it is a property contained by the whole, which does not exist in terms of the parts or the vocabulary appropriate to them; Lucas, 2000) of the system of shallow water dynamics and sediment-flux equations. There is still vigorous debate about whether the pattern formation

requires an approach explicitly based on emergence, or can be better modelled with conventional “reductionist” techniques (Paola, 2001).

Dynamical systems methods have been applied to the model results. State-space plots indicate that, qualitatively, the total width of modelled rivers compares well to prototype rivers with similar sequences of widths suggesting that fundamentally similar mechanisms operate in all of these braided streams. Quantitative analysis found that the differences between plots and real rivers indicate that the model does not always match the real rivers as closely as real rivers match each other. Fractal analyses indicate that the model rivers show self-affine scaling for both the river as a whole and the island size.

Numerical models by Murray and Paola (1994) and Barzini and Ball (1993) produce braiding which is qualitatively comparable to prototype rivers, however, these models are generic and work at long time scales. The application of the model of Thomas and Nicholas (2002) to field data goes some way to addressing the problem of generic models, however this model routes water only. Therefore, there remain no standard quantitative models for predicting the methods of, and the spatial distribution of, channel change, sediment transport or flow patterns in braided rivers (Ferguson and Ashworth, 1992).

## **2.6. Conclusions.**

Braided rivers are highly dynamic systems characterised by high rates of erosion, sediment transport and deposition. Despite the importance of braided rivers to the work of geomorphologists, engineers, sedimentologists, and geologists, braided rivers have been less extensively studied than single channel rivers due to the difficulties in undertaking fieldwork in a rapidly changing environment. The studies of braided river evolution to date have been mostly qualitative in nature.

Fieldwork in braided river systems has generally been carried out in a reductionist framework with the scale of investigation typically one bar-chute complex.

Froude-scale models have provided useful qualitative data on braided river evolution and whole reach scale sediment transport, however there is a difficulty in making distributed spatial measurements in a shallow, rapidly changing flume environment.

The adoption of numerical modelling approaches to dynamic gravel-bed rivers is a fairly recent phenomenon, with the aim of improving understanding over a range of scales. Paola (2001) notes that braided networks fall in a 'grey area,' i.e. they are systems of moderate complexity the best approach is not obvious. Approaches to modelling braided rivers have fallen within either a reductionist or synthesist tenet, both having advantages and disadvantages. Reductionist models contain very detailed equations of the system under study, however they are data intensive and, to date have only been applied in very small spatial and temporal scales due to the difficulty of solving complex equations on a constantly deforming domain. Within synthesist models the governing equations of the system are simplified, with interactions between parts of the system producing emergent phenomena. However, synthesist models tend to work in arbitrary units and it may be argued that the act of simplifying the system reduces understanding of the systems component parts. In the context of this work the styles of numerical models reviewed may be either adopted or rejected depending on their application to and results from braided river modelling:

### 1. CFD models.

CFD follow the reductionist tenet of model development. They are grounded in classical mechanics and solve the Navier-Stokes equations in three dimensions. They have been proved capable of simulating the dynamics of fluid flow over a wide variety of situations. However, there are problems in coupling these models with sediment transport to simulate evolving channel patterns. This is partly because sediment transport can lead to the redefining of the mesh of the model, which is highly time consuming and computationally difficult. Modelling fully developed braiding using CFD techniques is therefore hindered by the difficulty of solving the non-linear systems equations on a complex, constantly deforming

domain. At present, CFD models are therefore computationally restricted to modelling fluid flow in a confined area. For this reason CFD-type modelling has been rejected as a method of modelling braided rivers at large spatial and temporal scales.

## 2. Topological (random walk) models.

Random walk models produce the planar features of braided systems, and may reproduce topologically based statistics, however they give no insight into the geomorphic processes responsible for network evolution. However, they do not contain any physical flow routing rules and sediment is not routed. To understand more fully about the braiding process more physically realistic flow routing should be included and sediment routing should be included. This approach to modelling braided rivers has therefore been rejected.

## 3. Deterministic models of landscape evolution.

These models allow for growth and meaningful three-dimensional river basin structures. However, the models need detailed specification of the dominant dynamics and the calibration of the relative importance of many processes and it is not practical for large basin-scale models to simulate three-dimensional flow around clasts. However the introduction of irregular triangulated grids which would allow rivers to form in all directions would be beneficial to a braided river model.

## 4. Cellular automata models.

Cellular automata models have been applied to the evolution of braided river networks (Murray and Paola, 1994, 1997; Thomas and Nicholas 2002). These models are synthesist in spirit, the braid pattern emerging from a highly simplified model of the dynamics. This approach to modelling braided rivers has advantages in that it replaces the computationally hard problem of solving the shallow water equations on complex, changing topographical domain with simple, algebraic flow (and sediment) routing rules that capture the main effect of topography in spreading and concentrating the flow. Simple rule-based water (and sediment)

routing schemes make it possible to attempt to simulate geomorphic processes over greater temporal and spatial scales than is possible when using approaches involving the solution of the Navier-Stokes equations. However the accuracy of such simple rule-based schemes is limited by the square grids used in the models: when water is routed downstream from one cell to the next the magnitude of the lateral flows may be restricted. In spite of this, simplified cellular models can reproduce many features of braiding, but the parameters may be difficult to constrain. (Paola, 2001). However the advantages of this modelling approach outweigh the disadvantages when modelling geomorphic process over large temporal and spatial scales and on deforming grids. Therefore a similar approach to modelling braided river networks has been adopted in this thesis.

The main interest of this study is to develop an approach to modelling the evolution of a braided network that lies between the two modelling ideologies of reductionist and synthesist outlined above. The model will be an adaptation of the long-term landscape evolution model *Cascade* (Braun and Sambridge 1997) and will be based on an irregular triangulated grid. However only the gridding routines will be preserved, the flow routing and sediment transport routines will be re-written to take account of flow bifurcations and the shorter temporal and spatial application of braided river models. A simplified flow and sediment routing scheme will be developed based on the rule-based rules of the cellular automata models but incorporating physically realistic hydraulic conditions and the option for the incorporation of field data. The triangulated grid will allow lateral flows in all directions solving the problem of the square grids of the cellular automata models. This work will extend present modelling capability beyond the present generation of very detailed small-scale models to larger scale robust models with realistic data inputs and applicability beyond the field site. The development of the model is outlined in Chapter 3.

## CHAPTER 3.

### NUMERICAL MODELLING AND THE DEVELOPMENT OF *BRAIDED CASCADE*.

#### 3.1 Introduction to *Braided Cascade*.

*Cascade* (Braun and Sambridge, 1997) is a physically based finite difference model developed to simulate long-term ( $10^6 - 10^7$  years) landscape evolution. The model simulates long-term changes in land surface elevation and the consequent effects on channel network growth. The model tracks a number of basic state variables that determine the depth of erosion or deposition at each point during a given iteration, including elevation and slope. Changes in elevation are modelled by continuity equations for water and sediment transport; elevation changes result from local imbalances in sediment transport as well as tectonic elevation changes.

This version of the model *Braided Cascade*, builds on the irregularly discretised version of the landscape evolution model *Cascade* (Braun and Sambridge, 1997). The incorporation of an irregularly discretised grid differentiates *Cascade* from other landscape evolution models e.g. those of Willgoose *et al.* (1991a-d, 1994) and Howard (1994, 1997). *Cascade* assumes that landscape evolution on tectonic timescales and large spatial scales occurs via two types of processes: short-range (diffusive) hillslope processes and long-range (advective) channelised water flow (Braun and Sambridge, 1997). *Braided Cascade* works at much shorter length and timescales and allows simulation of long braided river reaches (Figure 3.1). The modelling approach is simplified and takes no account of detailed flow hydraulics or of sediment grain sizes. The intention is to model the overall spatial patterns of sediment transport, deposition and erosion and to analyse these in terms of their net statistical properties, rather than to produce accurate predictions of processes at particular localities. Model output includes maps of sediment erosion,

deposition, shear stress and stream power achieved throughout the modelled reach.

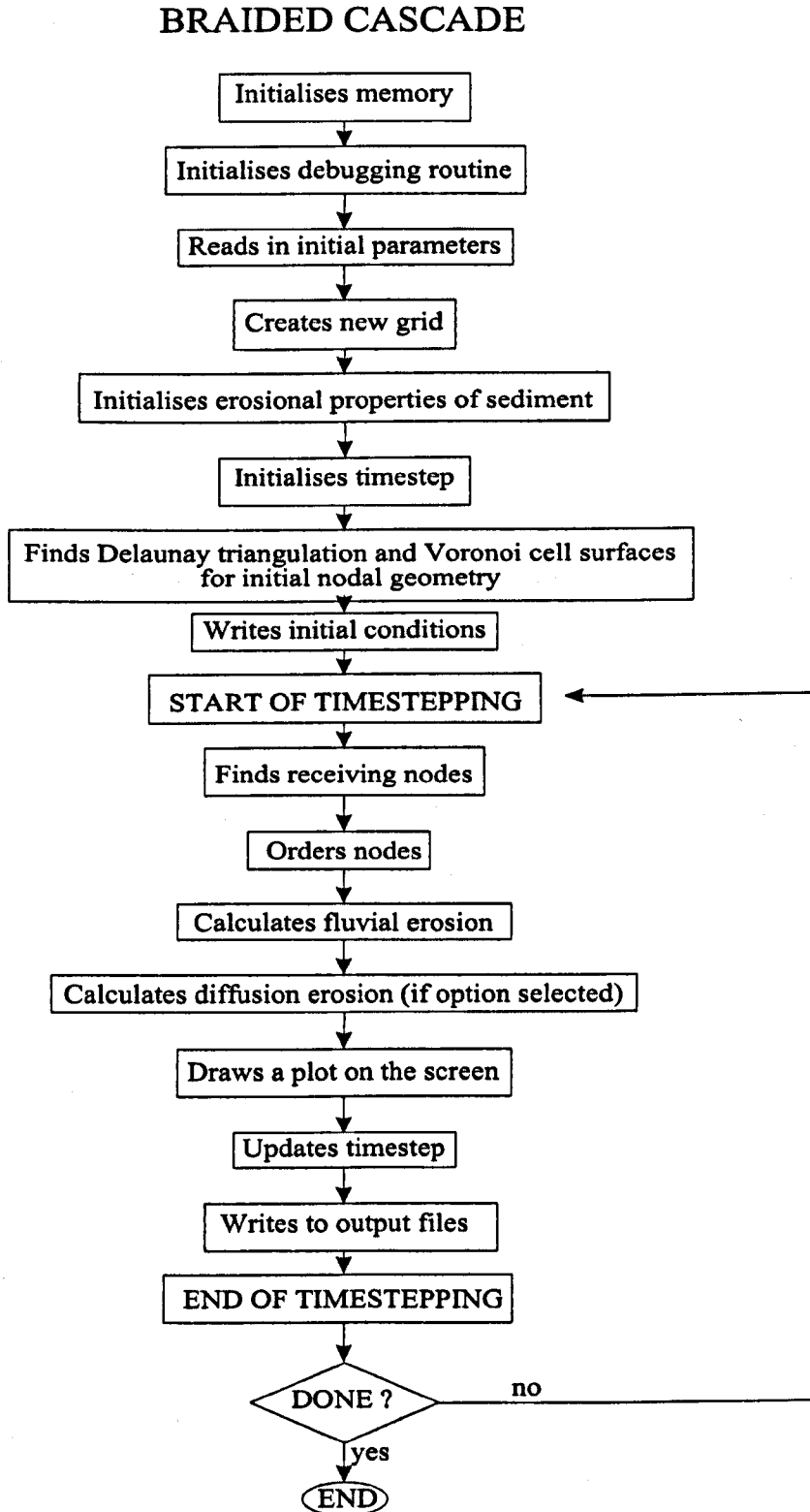


Figure 3.1. Flow chart showing the sequence of computation in the model.

*Braided Cascade* is similar in approach to the cellular automata model of Murray and Paola (1994, 1997) designed to predict the overall evolution and development of braided channel networks. However *Braided Cascade* is more sophisticated in terms of topography and fluid dynamics than the Murray and Paola (1994, 1997) model.

### **3.2. Philosophies of numerical modelling.**

Paola (2001) identified two alternative approaches to modelling stream braiding, termed *reductionist* and *synthesist*. A reductionist approach to modelling starts with the governing equations and makes approximations until one arrives at a system that is solvable with whatever means are available. An unstated assumption of the standard approach is that the less the fundamental equations need to be simplified the better (Paola, 2001). The long-term landscape evolution models of Willgoose *et al.* (1991a-d, 1994) and Howard (1994, 1997) agree with the reductionist, process orientated tenet to which most geomorphology is committed (Rodríguez-Iturbe and Rinaldo, 1997; Paola, 2000). The reductionist view states that it is only through specifying in detail the many processes active in nature and the parameters of their mathematical formalisation that landscape evolution can be understood. An example of a reductionist approach to modelling braided rivers is the model of McArdell and Faeh (2001) where the flow computations are based on the two-dimensional shallow water equations, solved using a finite volume technique.

However Paola (2001) notes that the traditional reductionist approach to modelling is being challenged. The synthesist approach is rooted in the idea of 'emergent' phenomena (Paola, 2001). Emergent phenomena are aspects of complex-systems dynamics that arise from the interactions of the parts but that could not readily be deduced from studying the dynamics of the parts separately. The heart of the synthesist approach to modelling multi-scale systems lies in the fact that behaviour at a given level in the hierarchy of scales may be dominated by

only a few crucial aspects of the dynamics at the next level below (Paola 2001). Therefore when modelling using the synthesist approach it is sensible to focus only on the few key aspects of the lower-level behaviour that matter, and any lower-level dynamics would be represented in a higher level model by a relatively simple set of equations or rules that summarise the crucial dynamics. Synthesist approaches to modelling include cellular automata models that are developed to predict the overall style of river behaviour, however they are generic and are unable to be applied to specific sites. An example of a synthesist approach to modelling braided rivers is the model of Murray and Paola (1994, 1997) where the braid pattern emerges from a simplified model of the dynamics.

In *Braided Cascade* there is no detailed hydrodynamic component to the model, which is a realistic simplification at the timescales considered (1 year). In this respect *Braided Cascade* may be classed as a synthesist model in spirit; the braid pattern emerges from a simplified model of the dynamics. Braiding is therefore an emergent behaviour (Lucas, 2000).

### **3.3. Finite element and finite difference models.**

Finite element methods can be used to study the evaluation of the cause and effect of forcing functions on a system (Desai, 1979). The basic concept underlying finite element analysis is the principle of discretisation, the division of the working area into smaller, more manageable particles. The aim of the process is to combine the understanding of individual components and obtain an understanding of the whole or continuous system. The system is approximated by differential equations. Finite difference methods differ from finite element approaches in that the derivatives in the differential equations are approximated by expressions using differences between the values of the dependent variable at selected points of a grid. The differential is thus replaced by a number of algebraic equations.

Many current finite element and finite difference models successfully predict short-term river behaviour at scales of 1-10 m, but require high-density survey and hydraulic information to run successfully. Many models efficiently route water over fixed beds and cover large areas. However the level of complexity reached when sediment is routed and the bed starts to evolve requires a high degree of sophistication to model successfully and some models may be unsuitable. Therefore such models may be unsuitable for studying medium and large rivers over longer timescales. These larger scales have been modelled generically, enabling investigation of the overall style of river behaviour. The computational structure of such models requires major modification if they are to be applied to specific sites. *Braided Cascade* employs a finite difference method to evaluate channel network evolution at scales greater than those of a few reaches and therefore extends the modelling capability beyond the present generation of very detailed small-scale models.

### 3.4. The model grid.

The model domain implemented in *Cascade* consists of a set of points  $N$  that are connected to form a mesh of triangles. Grid points (nodes) are connected using the Delaunay triangulation (Voronoi 1908, Delaunay 1934). A triangulation satisfies the Delaunay criterion when the circumcircles of the triangles formed do not enclose any other data points. A Delaunay triangulation minimises the maximum internal angle of the elements and produces the most “equable” triangulation of a given set of points.

Each node,  $N_i$  is associated with a surrounding Voronoi polygon. The Voronoi polygon for a node is the area within which the arbitrary point  $q$  would be closer to node  $i$  than to any other node on the grid. The boundaries between Voronoi polygons are lines of equal distance between adjacent nodes (Figure 3.2). Each Voronoi polygon has surface area  $A_i$  and the vertices of the Voronoi polygons coincide with the circumcenters of the triangles and have degree three: i.e. they are the common intersection of exactly three edges of the Voronoi diagram (Lee and

Preparata 1984). In general each triangle is associated with one and only one Voronoi vertex. The dual of the Voronoi diagram is the Delaunay triangulation. (Dual means to draw a line segment between two Voronoi vertices if their Voronoi polygons have a common edge). For details of the Delaunay triangulation method used in *Cascade* see Braun and Sambridge (1997).

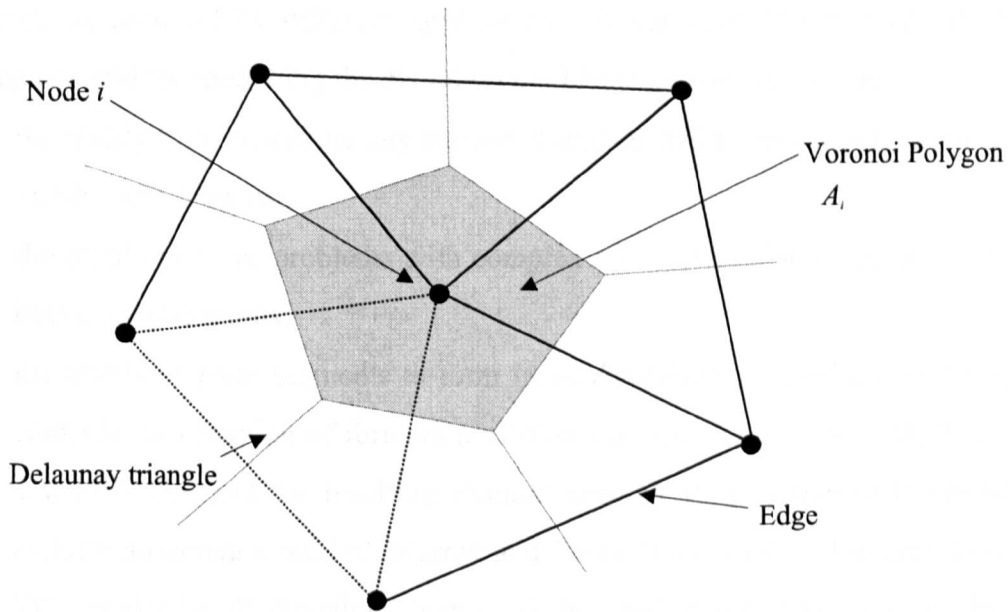


Figure 3.2. Schematic illustration of model grid components.

The original version of *Cascade* created a new mesh for every run. Within *Braided Cascade*, the mesh handling routines now have the capability to either read in an existing mesh in the form of  $x$ ,  $y$  and  $z$  co-ordinates (e.g. from a DEM) or to create a new surface with white noise random topography. A new mesh creating routine has also been added to *Braided Cascade* to enable easy specification and alteration of grid parameters (length, width, slope, and amplitude of white noise). When creating a new surface within *Braided Cascade* the user can specify grid dimensions, slope and amplitude of the white noise random topography. The mesh handling routines are also designed to allow for dynamic point addition while preserving the Delaunay triangulation (see Braun and Sambridge, 1997). This is significant as *Braided Cascade* may be run with an adapting grid; as the bed topography evolves the computational grid develops to

reflect areas of greatest erosion and deposition, thus nodal density may vary across the grid.

A triangulated irregular network (TIN) therefore represents the terrain surface. Current algorithms usually model terrain using either a regular grid structure or a TIN. One advantage of using a TIN is the fact that the organisation of hierarchies of multiple TINs, with respect to their resolution, can provide generalisations or details as required by different applications. Advantages of using an adapting irregular grid for modelling the evolution of channel networks include:

- the ability to approximate any surface at any desired tolerance with a minimal number of polygons;
- the ability to solve problems with complex non-rectangular geometries and/or boundary conditions;
- the ability of river segments to form in all directions. A regular grid strongly controls the direction of formation of river segments (e.g. N-S, E-W, NE-SW and SW-NE), and the resulting channel network (this is true of the braided cellular automata model of Murray and Paola 1994, 1997). However using a TIN results in all directions being equally used if the slope is equal in all directions (Braun and Sambridge, 1997); and
- the use of a dynamically adapting mesh makes it possible to vary the spatial resolution across the landscape. For example, spatial resolution may be increased around channels and kept low in areas experiencing only diffusive mass transport.

Elevation and other state variables are computed at the nodes rather than within the triangles (a finite-difference rather than a finite-element approach).

### **3.5. Routing of flows on the grid.**

*Cascade* employs a Voronoi based approach to drainage networks and flow routing (water and sediment fluxes). Any flow originating within a node's

Voronoi polygon is routed downstream along the steepest edges that are connected to that node. Therefore, the contributing area at node  $i$  is equal to the sum of the Voronoi areas of all nodes upstream of  $i$  (including  $i$  itself). An advantage of this approach is that it lends itself to finite-difference modelling, because each node has a unique watershed and drainage direction applied to it. The primary disadvantages are that drainage boundaries are defined by Voronoi polygons rather than by triangles and that flow pathways and gradients are forced to follow triangle edges (Figure 3.3).

### 3.6. Flow directions.

In the original version of *Cascade* one receiving node was found for each donor node; the receiving node was the node with the steepest downhill slope from the donor. However to allow for braiding, channels need to be able to bifurcate. It was therefore necessary make alterations to the code to allow two potential receiving nodes to be found.

To identify flow directions the two steepest channel bed slopes from a node  $i$  to its neighbours  $j$  and  $k$  are identified and the nodes  $j$  and  $k$  are stored as receiver nodes of node  $i$  (Figure 3.3 and Table 3.1). If both receiving nodes are downslope from the donor node (i.e. both of the channel bed slopes to the receiving nodes are positive) the receivers are stored in the order of steepest positive slope.

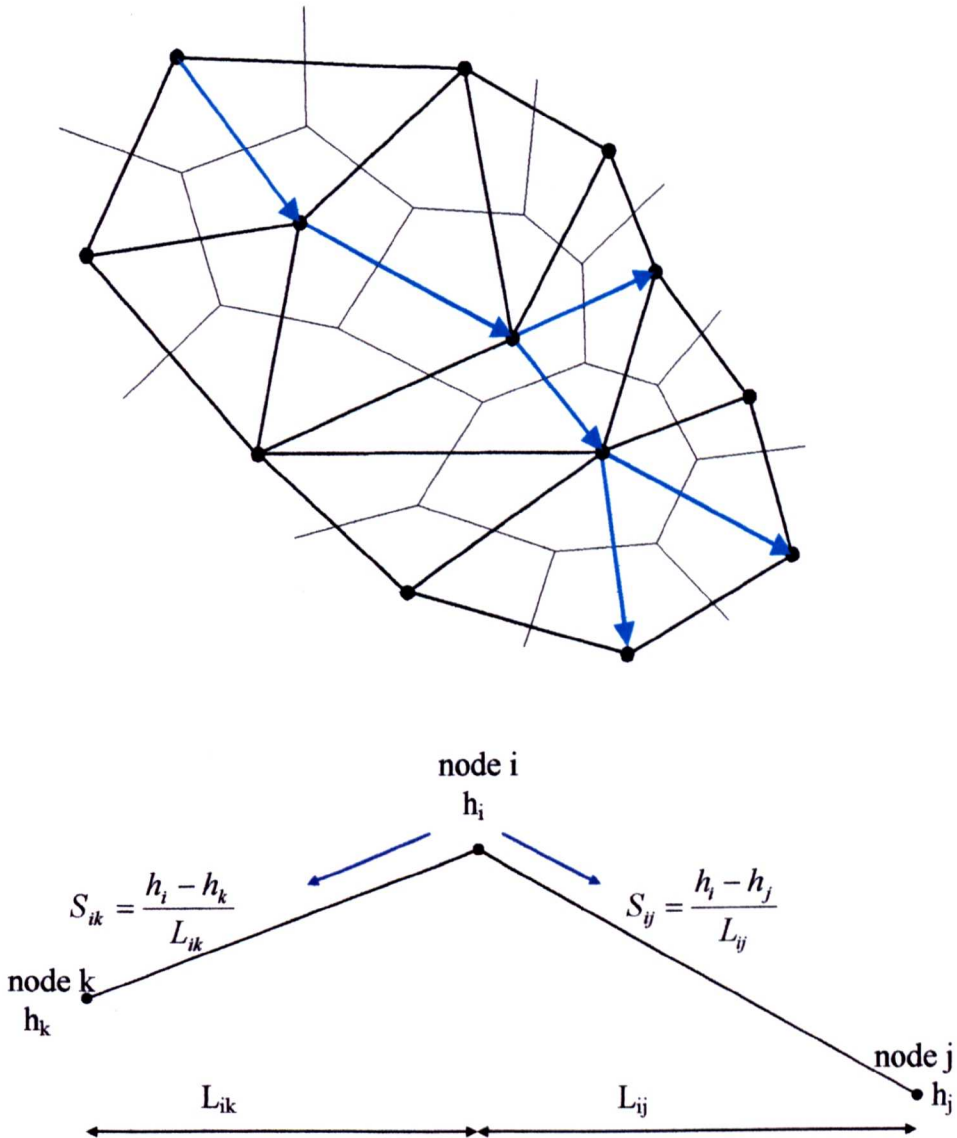


Figure 3.3. **TOP:** 2D schematic illustration of flow routing along the TIN node network. Blue lines are flow pathways. **BOTTOM:** Schematic diagram of flow splitting between two receiver nodes.  $i$ ,  $j$  and  $k$  are nodes,  $h_i$ ,  $h_j$  and  $h_k$  are the elevations of nodes  $i$ ,  $j$  and  $k$  respectively.  $L_{ij}$  is the distance between nodes  $i$  and  $j$ ,  $L_{ik}$  is the distance between nodes  $i$  and  $k$ .  $S_{ij}$  is the slope between nodes  $i$  and  $j$  and  $S_{ik}$  is the slope between nodes  $i$  and  $k$ .

In the case of the donor node being a point of local minimum elevation the least steep negative channel bed slopes to two neighbouring nodes are identified and these nodes are stored as receiving nodes. This scenario is included because in prototype braided rivers ponding does not often occur; flow momentum or a positive water surface slope usually drives water up a negative bed slope. Uphill receiving nodes are stored in the order of least steep negative slope. In the case of a channel bed slope having a gradient of exactly zero, the value of the slope is set

to 0.000001 to avoid the problem of numerical instabilities in the water and sediment routing routines.

Receiving nodes identified.	Receiving nodes stored.	Ordering of receiving nodes by slope.	Schematic diagram of water routing.
Both receivers downhill (slope to both receivers are positive).	j, k	$S_j, S_k > 0$	
One receiver downhill, one uphill or with a zero slope.	j	j	
Two uphill receivers (slopes to both receivers are negative).	j, k	$S_j < S_k < 0$	
One receiving node with zero slope, one with an uphill slope (negative slope).	j	$S_j = 0.000001$	

Table 3.1. Summary of receiving nodes and flow directions.  $S_{j,k}$  = slope from donor node to receiving node j or k. Black arrows indicate that water is routed to the receiving node; grey arrows indicate that water is not routed to the receiving node even though the receiving node has been identified.

Every link is given a characteristic channel length,  $L_{ij}$  or  $L_{ik}$ , defined as the distance between the provider node (node  $i$ ) and receiver node ( $j$  or  $k$ ), and slope,  $S_i$ , defined as the height difference between the donor and receiver nodes divided by the length (Figure 3.3). Every node also has a surface area, which is the area of the Voronoi polygon,  $A_i$ .

### 3.7. Node ordering – the *Cascade* algorithm.

At every time step, discharge and sediment load at each node are updated. The original version of *Cascade* ordered nodes using the *Cascade* algorithm (Braun and Sambridge, 1997). This was deemed computationally more efficient than a complete re-ordering of all nodes at every timestep. The *Cascade* algorithm operates by proceeding through the nodes so that when the height of node  $i$  is updated, the heights of nodes upstream of node  $i$  have already been updated, and their contributions to the sediment load and water flux have already been computed (Braun and Sambridge, 1997). This was achieved by giving each node a parcel of water and determining which nodes are able to donate the water to downstream nodes (a bucket passing algorithm). Any nodes that did not receive any water were ordered first (these are nodes of local maximum elevation). Nodes that received water were then ordered (channel nodes) by listing all nodes in each channel separately according to the position in the channel in which they were located (i.e. from channel head to channel output) and finally, and nodes that are “self-donors”, i.e. nodes of local minimum elevation and have no downhill receivers and nodes on boundaries were ordered (if the boundaries are not periodic). Nodes were therefore organised in the order:

- local maximum nodes (nodes that do not receive water from any other nodes but can donate water to other nodes);
- nodes in channels (nodes that receive water from upstream nodes and can donate water);
- self-donors (these nodes receive water from upstream nodes but cannot donate to other nodes as they have local minimum elevation), and boundary nodes.

The bucket-passing algorithm is computationally efficient and gave the correct results when implemented in the original version of *Cascade* where only one receiving node was identified. However, when dealing with channel bifurcations and two downhill receiving nodes the problems were encountered. The bucket passing algorithm was unable to deal with two receiving nodes and classified the

second downstream receiving node identified as a channel head (i.e. a node of local maximum elevation) as it deemed that the donor node would pass all of its water to the first receiver identified (i.e. water is passed along the steepest slope between donor and receiver nodes). Nodes are listed in order from channel head to channel output for each channel; therefore the second receiving node was placed near the start of the ordering with all of the other nodes classified as channel heads. No water would therefore be passed to the second receiving node as the node had been identified as a node of local maximum elevation and previously listed in the ordering. Therefore channels downstream from any second receiving nodes would remain dry (see Figure 3.4).

Uphill receiving nodes also caused problems as the bucket passing algorithm can only pass water along positive slopes (i.e. to downhill receiving nodes). Therefore in scenarios in which a donor node has two uphill receiving nodes the donor node would not pass water but would store water and create a “lake” and the node would be classified as a self-donor. As *Braided Cascade* can identify uphill receiving nodes and therefore contains no ponding of water this was producing incorrect results.

Therefore for runs on flume-like slopes, with a slope gradient in the x direction, a new node ordering routine was implemented. Node ordering is now achieved by ordering all the nodes in ascending order by their x co-ordinate. Nodes at the top of the slope will be the ones with the smallest x co-ordinate value. Therefore nodes are ordered uphill to downhill according to the average grid slope. This ordering routine requires a complete ordering of all the nodes at each time step. This is slightly less computationally efficient than the *Cascade* algorithm and causes each timestep to be processed at a slightly slower speed than if using this algorithm (see Braun and Sambridge (1997) for typical processor time required to perform timesteps). However the new node ordering routine solves the problem of channel bifurcations (see Figure 3.4) and negative slopes to receiving nodes.

### 3.8. Water routing and runoff.

In the original version of *Cascade* water was added to the grid in the form of precipitation, orographically controlled by topography and assuming a prevailing wind direction. In *Braided Cascade* water is input to the grid in the form of a discharge at one or more specified input points along the upstream boundary. At every timestep the program can read in a discharge of water (see Figure 3.4). Discharge may be constant at each timestep or may vary from timestep to timestep (but not within a timestep); therefore hydrographs can be run.

Water routing is based on the water surface slopes between a donor node  $i$  and nodes  $j$  and  $k$  that receive from  $i$ . Water collected at a point on the grid, node  $i$ , is routed downslope to the two receiver(s) of the node, following the edges that have the steepest downhill water surface slope. If a node is a point of local minimum elevation (i.e. a pit) with no downhill route away from the node, water may be routed to the neighbour(s) with the least steep uphill water surface slope; thus the model does not include ponding.

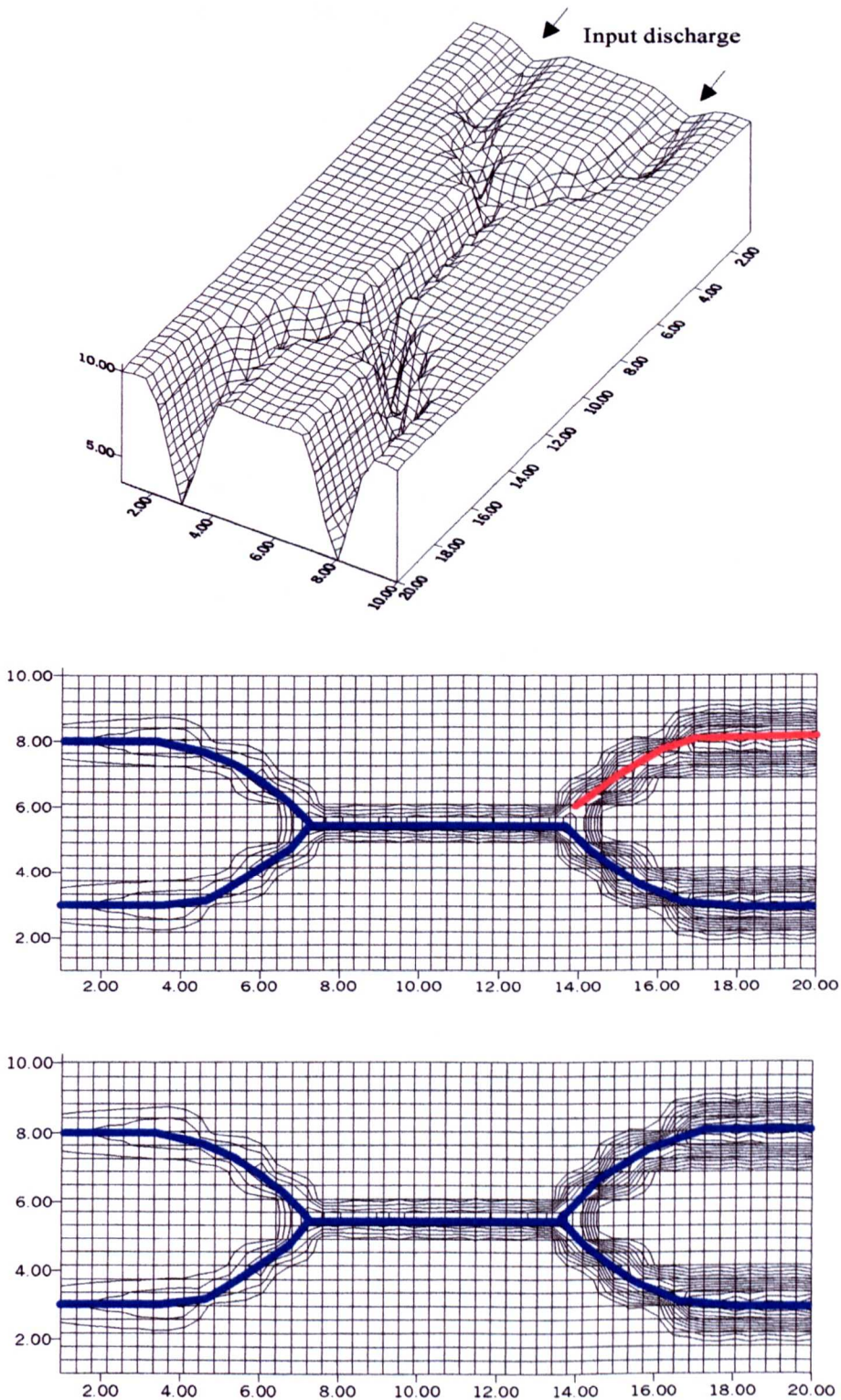


Figure 3.4. An example of a DEM input into *Braided Cascade* to illustrate problems with node ordering encountered by the bucket passing algorithm (BPA). **TOP**: 3D view of DEM on a square grid using Surfer 6 (Golden Software 1994). **MIDDLE**: Channels delineated using the BPA, note that after the bifurcation all water is routed to the first receiver node, the second receiver node is classified as a channel head and does not receive water from upstream, thus the second channel (in red) remains dry. **BOTTOM**: Using the new node ordering gives the correct outcome; water is split between the two channels downstream of the bifurcation. Flow is from left to right for middle and bottom diagrams.

### 3.8.1. Donor nodes with two downhill receiving nodes.

If a node  $i$  donates to two other nodes  $j$  and  $k$ , and  $j$  and  $k$  are both downslope, (i.e. both the channel bed slopes to the receiving nodes are positive), the proportion of the total discharge distributed to each receiving node is calculated using:

$$r_{si} = \frac{S_i^n}{\sum_{j=1,2} (S_j)^n} \quad (\text{Q rule 1})$$

where  $r_{si}$  is the ratio of the channel bed slope from node  $i$  to one of its receiver nodes  $j$ ,  $S_i$  is the channel bed slope from node  $i$  to the receiver node, and  $n$  is a constant taken as 0.5 after Murray and Paola (1994, 1997). The water distribution rules represent an approximation to momentum conservation. Following Murray and Paola (1994,1997) Q rule 1 (and Q rule 2 below) can be derived from the equation of motion for uniform flow in a wide channel:

$$\tau = \rho g h S \quad (3.1)$$

where  $\tau$  is the mean shear stress the flow exerts on the bed (Pa),  $\rho$  is the density of water ( $\text{kg m}^{-3}$ ),  $g$  is acceleration due to gravity ( $\text{m s}^{-2}$ ),  $h$  is water depth (m) and  $S$  is the water surface slope. Combining this with the relationship between  $\tau$  and a representative flow velocity ( $V$ ,  $\text{m s}^{-1}$ ) (Vernard and Street, 1961):

$$\tau = f \rho V^2 / 8 \quad (3.2)$$

(where  $f$  is the (Darcy) friction factor that depends on roughness and Reynolds number) to get:

$$V = C h^{1/2} S^{1/2} \quad (3.3)$$

where  $C = 8g/f$  is the Chezy roughness coefficient, which can be expressed as:

$$C = h^{1/6} / n \quad (3.4)$$

where roughness is given by Manning's  $n$ , assuming a wide flow  $h$  is substituted for  $R$ , the hydraulic radius (m) (Vernard and Street, 1961). Using equations 3.3 and 3.4 and the expression:

$$q = hV \quad (3.5)$$

for the discharge per unit width  $q$  ( $\text{m}^2 \text{s}^{-1}$ ) leads to:

$$q = h^{5/3} S^{1/2} / n \quad (3.6)$$

Using the channel bed slope ratios to both receiving nodes, a discharge ratio,  $Q_r$  (qratio) is computed to determine whether or not the water discharge will be split between the receiving nodes:

$$Q_r = \frac{r_{s1}}{r_{s1} + r_{s2}} \quad \text{where } n=1, 2 \quad (3.7)$$

Where  $Q_r$  is the proportion of water at node  $i$  distributed to the first donor (when  $n = 1$  only) and  $r_{s1}$  and  $r_{s2}$  are channel bed slope ratios for the first and second receiving nodes respectively. Discharge is not split if  $Q_r$  is greater than  $Q_r^* = 0.8$  (i.e. more than 80 % of the water from the donor node goes the first receiving node – this is the node with the steepest downhill slope from the donor node); in this case all water from the donor node is routed to that one receiver node (different values of  $Q_r^*$  have been tested and these are discussed in Chapter 5).

Water at the receiving nodes  $j$  and  $k$  is then calculated by multiplying the water at the donor node  $i$  by the discharge ratios for receiving nodes  $j$  and  $k$  ( $Q_r$  and  $(1 - Q_r)$  respectively).

If discharge from node  $i$  is distributed between the two receiving nodes  $j$  and  $k$ , (i.e.  $Q_r$  is less than 0.8), the program uses the initial distribution ratios based on bed slope and iterates to calculate the proportion that would be routed to each receiving node using the water surface slope (Figure 3.5). Water surface slope is used here in preference to bed surface slope as positive water surface slopes may drive flow across areas of negative channel bed slopes. This is a departure from and improvement on the model of Murray and Paola (1994, 1997) that did not take into account water depth or water surface slopes. Water depth and thus water surface slope is calculated by applying the hydraulic geometry equation of Ergenzinger (1987) to the amount of water at both donating and receiving nodes. The equation was derived for single braids in the Butramo River, Italy, using the standard hydraulic geometry form:

$$h = aQ^b \quad (3.8)$$

where  $h$  = flow depth (m),  $Q$  = discharge ( $\text{m}^3 \text{s}^{-1}$ ), and  $a$  and  $b$  are empirical constants determined by Ergenzinger (1987) (for their values see Table 3.4).

Water surface slope is calculated using the water depth at each node. The water surface slopes between the donor and receiving nodes are used to compute a slope ratio for each node, which is then used to calculate the proportion of discharge to be distributed to each receiving node. This discharge ratio is compared to the ratio calculated using bed slopes and if it is within a given tolerance specified by the user, the amount of water routed to the receiver nodes is calculated using the ratio of water surface slopes. If the difference between the two ratios is greater than the tolerance, the program iterates until the difference between the ratios are within the given tolerance (Figure 3.5).

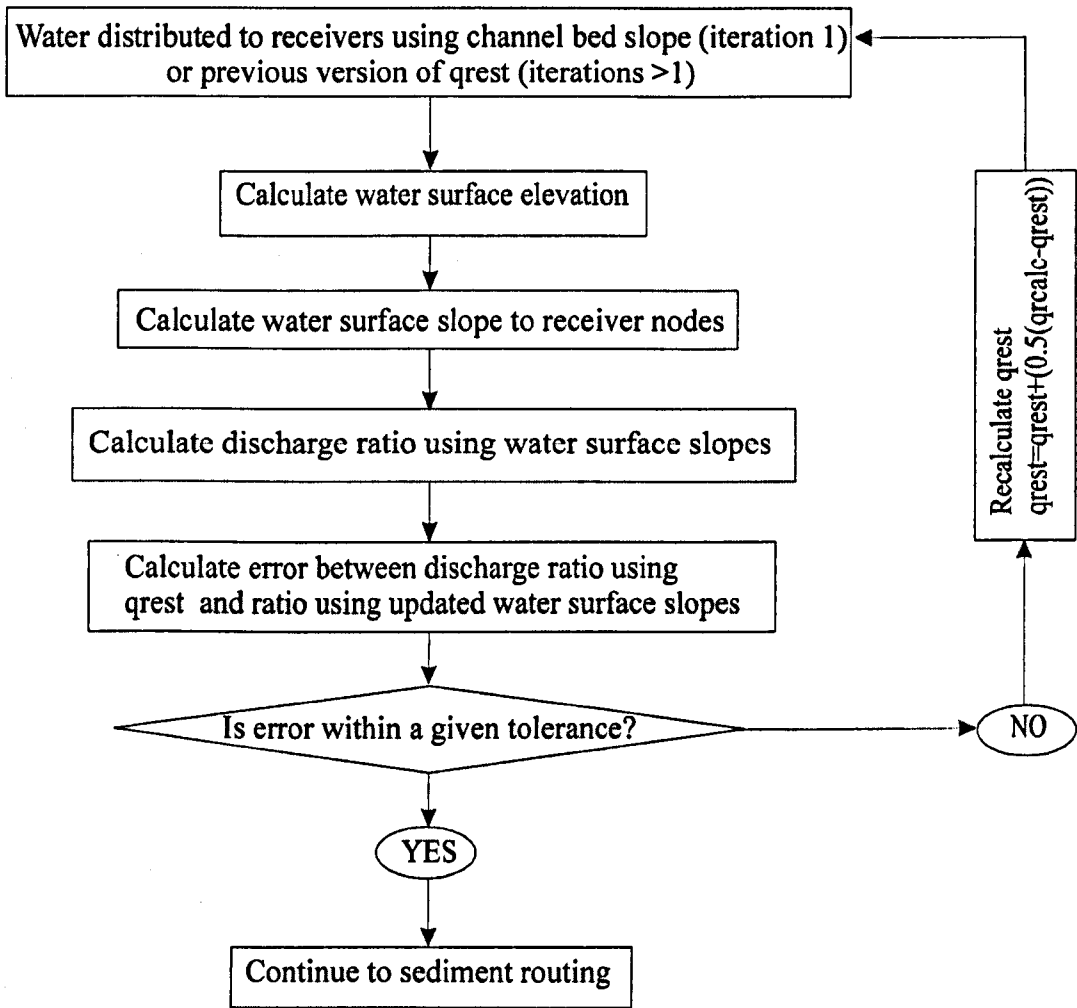


Figure 3.5 Flow chart showing computations involved in iterations to calculate distribution of water between receiver nodes according to water surface slope.

### 3.8.2. Donor nodes with two uphill receiving nodes.

If both channel bed slopes from the donor node to the receivers are negative the proportion of water distributed to each receiver node is calculated according to the equation

$$r_{si} = \frac{[-S]_i^{-n}}{\sum_{j=1,2} ([-S]_j)^{-n}} \quad (\text{Q rule 2})$$

Where  $n$  is the constant described above for Q rule 1.

The discharge ratio, “upratio,” is computed using the channel bed slope ratios for both receiver nodes. Once again if upratio, ( $Q_{ru}$ ), is greater than  $Q_{ru}^*$  (= 0.8 initially), all water is routed to the first receiver node (the node with the least steep negative slope). The value used for upratio has also been subjected to sensitivity analysis and this is discussed in Chapter 5.

Water surface heights at the donor and receiving nodes are then calculated by applying the hydraulic geometry equation (3.8) of Ergenzinger (1987) and the water surface slope between the donor and receiving nodes is calculated. If the water surface slopes to both receiving nodes are positive (downhill) then water at node  $i$  is split using (Q rule 1) and substituting water surface slopes for channel bed slopes. If the water surface slopes to both receiving nodes are negative (uphill) then water at node  $i$  is split using (Q rule 2) and substituting water surface slopes for channel bed slopes. If the water surface slope to one receiving node is positive and the water surface slope to the other receiving node is negative all water from node  $i$  is routed to the receiving node with the positive water surface slope.

### **3.8.3. Donor nodes with one downhill and one uphill receiving node, or donor nodes with only one receiving node.**

If a node  $i$  has one downhill donor  $l$  and one uphill donor  $m$  (based on channel bed slopes) the nodes are stored in order of steepest positive slope so the downhill donor will be stored first. In this case all water is routed to the first receiving node,  $l$ . If the program finds only one donor for node  $i$  (this may occur for nodes near fixed boundaries – nodes on boundaries cannot receive water and sediment), all water is routed from node  $i$  to the receiving node found.

### **3.9. Sediment routing.**

*Cascade* (Braun and Sambridge 1997) was originally developed to simulate long-term landscape evolution, and so modification of some of its algorithms for

sediment transfer is required for application to modelling the development of river bed topography over periods of up to 1 year.

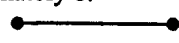
Channel bed slope to 1 <sup>st</sup> receiving node (with sketch of slope).	Channel bed slope to 2 <sup>nd</sup> receiving node (with sketch).	Water distribution rule.
Positive 	Positive 	Q rule 1. Split water if $q_{ratio} < 0.8$ . Then iterate to get water surface slopes.
Negative 	Negative 	Q rule 2. Split water if $u_{ratio} < 0.8$ . Then iterate to get water surface slopes: Both wss positive – split water using Q rule 1. Both wss negative – split water using Q rule 2. One wss positive, one negative – all water routed to node with positive wss.
Positive 	Negative 	All water routed to first receiving node.
Negative 	Positive 	Does not occur as nodes are ranked by positive slope so downhill receivers will be ranked first.
Approximately 0. 	Negative 	All water routed to first receiver.
Negative 	No second receiving node	All water routed to first receiving node.
Positive 	No second receiving node	All water routed to first receiving node.

Table 3.2. Classification of receiver nodes and water distribution in *Braided Cascade*. Wss = water surface slope. By default  $Q_r^* = Q_{ru}^* = 0.8$

Sediment transport by continuous diffusive hillslope processes such as soil creep and raindrop impact is not included in *Braided Cascade*. All sediment is transported within the channel network and is a purely advective process; i.e. diffusion erosion has been turned off from the original version of *Cascade*.

Water transports sediment from node to node according to the local stream power. Stream power is used in preference to shear stress to calculate sediment transport

as water routing is discharge based and channel widths are not known. All sediment is treated as bedload, whereas in the original version of *Cascade* sediment is effectively *total* load. The bedload sediment transport rate is measured by mass (in units of  $\text{m}^3 \text{s}^{-1}$ ); thus, the transport rate implicitly includes channel width. Therefore, there is no correction for width to bedload transport built into *Braided Cascade*. Total stream power is therefore the most reliable basis for calculating sediment transport. The sediment transport equation takes the form:

$$Q_b = K\Omega^m dt \quad (3.9)$$

$Q_b$  is the amount of sediment transported from the node in question (node  $i$ ) to one of the two receiver nodes,  $\Omega$  is stream power ( $\Omega=Q_i S_i \rho$ , where  $S_i$  is the local bed slope,  $Q_i$  is the local discharge,  $\rho$  is the density of water ( $1000 \text{ kg m}^{-3}$ )) and  $dt$  is the time interval. Locally the water surface slope should be used to determine stream power but the model is limited to using channel bed slopes. Transport can occur on negative bed slopes in prototype rivers because momentum can drive the flow across such areas. However, water velocity is not known in the model and bed slopes are used in preference to water surface slopes, (also the occurrence of a negative water surface slope caused numerical instabilities in the sediment transport equations). Values for the constant  $K$  and for the exponent  $m$  are given in Tables 3.3 and 3.4. These values are derived from the bedload sediment from regression analysis of bedload sediment transport ( $\text{kg s}^{-1}$ ) versus stream power ( $\text{kg s}^{-1}$ ) shown in Figure 3.6 for four braided rivers (Belova *et al.*, 1975; Jaoshvili *et al.*, 1976; Jaoshvili and Zenginidze 1981; Davoren and Mosley, 1986; Shvidchenko, 1997; Shvidchenko and Kopaliani, 1998; Hoey *et al.*, 2001). The values of the coefficient and exponent used in the control run were that of the raw data and did not include a threshold sediment transport rate.

Murray and Paola (1994, 1997) note that incorporating a sediment transport threshold into their sediment transport equations did not affect the qualitative results, regardless of the magnitude of the threshold, as long as it was not large

enough to prevent transport altogether in the first iteration. In most model runs they used a threshold of around half the typical stream power. In the data given below two thresholds are shown, however the inclusion of the thresholds did not lead to significantly different results for the regression analyses, therefore the values of the constant and exponent for sediment transport equation were taken from the raw data with no threshold included.

	Coefficient	Exponent	R <sup>2</sup>
Raw data	$2.43 \times 10^{-10}$	3.61	0.876
Best fit with a threshold ( $\Omega_T = 22.8 \text{ kg s}^{-1}$ )	$6.44 \times 10^{-10}$	3.48	0.88
Using a threshold of $\Omega_T = 100 \text{ kg s}^{-1}$	$3.10 \times 10^{-8}$	2.98	0.869

Table 3.3. Values of the constant and exponent to 3 significant figures (in Hoey *et al.*, 2001). The forms of the equation are:  $Q_s = k\Omega^m$  for the raw data and  $Q_b = k(\Omega - \Omega_t)^n$  for equations with a threshold. Where  $k$  is the coefficient,  $Q_b$  is bedload transport,  $\Omega_t$  is the threshold sediment transport, and  $n$  is the exponent.

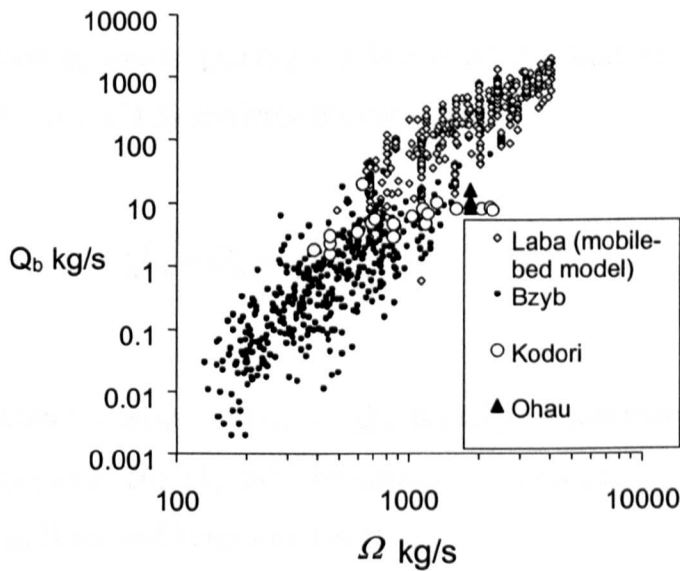


Figure 3.6. Bedload discharge as a function of stream power in the braided rivers used to generate the constant and exponent for the sediment transport equation. Data provided by A. Shvidchenko (pers. comm.) are from Belova *et al.*, 1975; Jaoshvili *et al.*, 1976; Jaoshvili and Zenginidze 1981; Davoren and Mosley, 1986; Shvidchenko, 1997; Shvidchenko and Kopaliani, 1998.

For receiving nodes with a positive channel bed slope the maximum slope for input to the sediment transport equations was fixed at twice the average slope of the grid. This is to avoid out-of control positive feedback creating large scour holes (pits) in the mesh (see also section 3.11 – deposition). *Braided Cascade* contains no temporal lag (see section 3.10.2) so areas of higher erosion will only propagate upstream very slowly over time and tend to create stable areas of very

low elevation with steep slopes surrounding these areas. These steep slopes feed back into the sediment transport equation leading to very high sediment transport rates and thus the low area will get lower. Compare this with the rule for deposition (section 3.11). There is no sediment transport on flat or uphill (negative) channel bed slopes.

In the cellular automata model of Murray and Paola (1994,1997) a value of 2.5 is used for  $m$  which is derived from log-log plots of sediment discharge versus stream power index for several laboratory braided streams measured by Ashmore (1985 in Murray and Paola 1997). Murray and Paola (1994, 1997) also used a value of 5/3 derived from expressing sediment transport formulae using bed shear stress expressed in a form involving stream power.

Sediment transport by mass,  $(Q_{si})$  ( $\text{kg s}^{-1}$ ), is converted to bulk sediment transport (by volume)  $(Q'_{si})$  ( $\text{m}^3 \text{s}^{-1}$ ) by applying the conversion:

$$Q'_{si} = Q_{si} \frac{1}{\rho_s(1-\lambda)} \quad (3.10)$$

where  $Q_{si}$  is sediment transport in  $\text{kg s}^{-1}$ ,  $Q'_{si}$  is sediment transport in  $\text{m}^3 \text{s}^{-1}$ ,  $\rho_s$  is sediment density (set at  $2650 \text{ kg m}^{-3}$ , the density of quartz), and  $\lambda$  is bed porosity (taken as 0.3, e.g. Hoey and Ferguson, 1994).

### 3.10. Erosion length scales.

#### 3.10.1. Spatial lag effects in bed load sediment transport.

Spatial lag effects are defined as the inability of an alluvial system to immediately overcome the presence of constrained sediment boundary conditions (Phillips and Sutherland 1989). Constraints can arise from the presence of a rigid bed upstream of a mobile bed, or sediment inflow rates at the upstream boundary which are lesser or greater than the capacity of the flow to transport sediment. A certain

distance is required before the alluvial system reaches equilibrium, this is termed “spatial lag” (Phillips and Sutherland, 1989).

Local erosion or deposition rate is assumed proportional to the difference between the sediment transport rate and the sediment carrying capacity. The amount of sediment calculated by equation (3.10) is equivalent to a channel carrying capacity (Beaumont *et al.*, 1992; Kooi and Beaumont, 1994). The carrying capacity is compared to the sediment available for transport at each node to determine whether erosion or deposition will take place. It is assumed that the channel network is not forced to carry sediment at the carrying capacity. Therefore, a potential disequilibrium may exist between carrying capacity ( $Q_e$ ) and actual sediment flux ( $Q_i$ ). Following Beaumont *et al.* (1992) and Kooi and Beaumont (1994) if it is assumed that the system evolves towards equilibrium at a rate proportional to the disequilibrium, sediment load along a channel changes according to:

$$\frac{dQ}{dt} = \frac{Q_e - Q_i}{t_f} \quad (3.11)$$

where  $t_f$  is a characteristic reaction time (Beaumont *et al.* 1992; Kooi and Beaumont 1994). If it is assumed that the sediment transport is in steady state, i.e. that there is no local change in sediment flux over time interval  $\Delta t$ ,

$$\frac{dQ}{dt} = 0 \quad (3.12)$$

then:

$$\frac{dQ}{dt} = \frac{dQ}{dt} + v_f \frac{dQ}{dl} = v_f \frac{dQ}{dl} \quad (3.13)$$

where:

$v_f$  = advection velocity of the sediment flux and  $l$  = distance downstream (Beaumont *et al.*, 1992; Kooi and Beaumont, 1994). Under these circumstances the time dependence of erosion or deposition takes the form of a spatial dependence. Therefore for constant advection velocity,  $l$  is a material property equal to the erosion-deposition length scale required for the disequilibrium to be reduced to a factor of  $(1/e)$  when the sediment flux is constant. This leads to the following expression of change in local topography:

$$\frac{\delta h}{\delta t} = -\frac{\delta Q}{\delta l} = \frac{Q_e - Q}{L_{e,d}} \quad (3.14)$$

where

$L_{e,d} (= v_f t_f)$  is a length scale for erosion and deposition.

On the local scale this leads to two situations:

1. If the sediment flux at a node is greater than the carrying capacity (i.e.  $Q_{si} > Q_e$ ), deposition occurs and the local change of height is calculated by:

$$\frac{\delta h}{\delta t} = \frac{Q_{si} - Q_e}{L_d} \quad (3.15)$$

where  $L_d$  is the length scale for deposition. There is also a maximum amount of material that can be deposited at one location during a timestep ( $dh_{max}$ ). This maximum based on the notional grain size that *Braided Cascade* is working with and is set to equal one median grain size per timestep to try to avoid computational instability.

2. If the sediment flux at a node is less than the carrying capacity (i.e.  $Q_{si} < Q_e$ ), erosion occurs and sediment is eroded. The local change in height is calculated by:

$$\frac{\delta h}{\delta t} = \frac{Q_{si} - Q_e}{L_e} \quad (3.16)$$

where  $L_e$  is the length scale for erosion.

Many mathematical models have assumed that the sediment transport capacity of the flow is reached instantaneously at every point in time and space and spatial lag effects are thereby neglected. However when constrained sediment boundary conditions are present, Bell (1980; in Phillips and Sutherland, 1989) has demonstrated that a certain distance is required before the transport capacity is reached, especially under conditions of strong bed degradation (Phillips and Sutherland, 1989). The erosion length scale for alluvial sediment takes account of the spatial lag term in *Braided Cascade*.

The specification of the length scales by the user allows spatial lag to be included in the model. The length scales determine the distance downstream from a point of erosion or deposition that it would take for the sediment transport rate to equal the carrying capacity. The erosion length scale for alluvial material was set at 10 times the mean nodal spacing at the start of each run (Peter Van der Beek, pers. comm.). This is further discussed in chapter 5 when the model parameters are tested for sensitivity.

### 3.10.2. Temporal lag.

Under non-steady flow conditions an alluvial system has been found to be unable to immediately respond to the changing flows. A certain time is required before the bedform geometry, sediment transport rate and flow depth adjust to the new flow regime. This phenomenon is termed “temporal lag” (Phillips and Sutherland, 1990). However *Cascade* and *Braided Cascade* do not take account of temporal

lags and all water entering the grid leaves it during the same timestep. This is equivalent to a steady flow assumption and is common in long-term sediment routing modelling (e.g. Willgoose *et al.*, 1991a-d, 1994).

### 3.11. Deposition.

*Braided Cascade* does not explicitly include grain size. However there is a maximum amount of material that can be deposited at one location during a timestep ( $\delta h_{max}$ ) and this value has been based on the notional grain size that the model has been set to work with (the median grain size from the field site – the proglacial stream of the Haut Glacier d’Arolla – see Section 3.16 for a description of the field site). The inclusion of this rule avoids out-of-control positive feedback occurring as a run progresses, without this rule the topography would eventually consist of an unrealistic collection of deep holes and very high ridges or spires.

### 3.12. Numerical method used to solve the channel transport equation.

The continuity equation for bed material is conventionally written in differential form:

$$\frac{\delta Q_s}{\delta x} = -(1 - \lambda) \frac{\delta h}{\delta t} \quad (3.17)$$

Where  $x$  is the longitudinal co-ordinate in the flow direction  $Q_s$  is sediment transport rate,  $h$  is bed elevation,  $t$  is time and  $\lambda$  is bed porosity.

If the sediment flux at a node (e.g. node  $i$ ),  $Q_i$  is greater than the carrying capacity,  $Q_e$  (i.e.  $Q_i > Q_e$ ) deposition occurs, the node height is updated and sediment is set to the carrying capacity. In finite difference form equation (3.17) can be written:

$$H_{i,2} = H_{i,1} + \frac{Q_i - Q_e}{A_i} \left( \frac{1}{\rho_s(1-\lambda)} \right) \quad (3.18)$$

Where  $H_i$  is the height of node  $i$  at times 2 and 1 respectively, and  $A_i$  is the surface area associated with the node. Streams never carry more than their carrying capacity.

If  $Q_i < Q_e$  erosion occurs and the node height is updated:

$$H_{i,2} = H_{i,1} + \left( \frac{Q_i - Q_e}{A_i} \right) \left( \frac{L_i}{L_{e,a}} \right) \left( \frac{1}{\rho_s(1-\lambda)} \right) \quad \text{if } H_{i,2} > H_{i,0} \quad (3.19)$$

Where  $H_{i,0}$  is the bedrock-sediment interface and  $L_{e,a}$  is an erosion length scale for alluvial material.

The user can fix the thickness of the alluvial material, the position of the interface between alluvium and bedrock. By fixing the bedrock-alluvium interface at a great distance below the surface it is possible to force the model to only erode within the alluvial material. In each run of *Braided Cascade* the bedrock-alluvial interface was positioned at 50 m below the original surface elevation (Figure 3.6). Therefore no erosion occurred in bedrock. However the alluvium-bedrock interface could be used as an analogue for an active layer of different erodibility to the substrate.

Sediment load is adjusted:

$$Q_{ij} = Q_i + (Q_i - Q_e) \left( \frac{L_i}{L_e} \right) \quad (3.20)$$

and the discharge and sediment load are passed to the receiver of node  $i$ . This is computed for all nodes in each timestep and works from the upstream boundary down through the network.

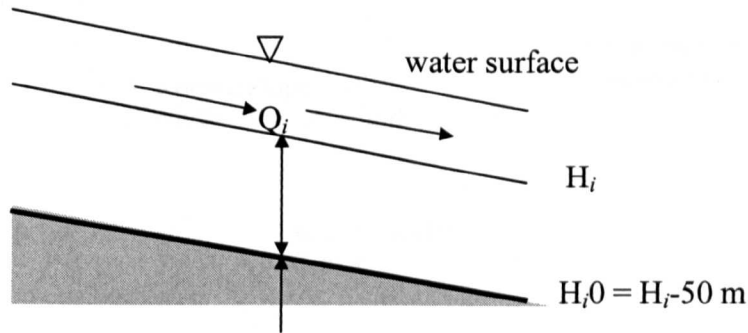


Figure 3.7. Schematic diagram of water surface, node elevation and bedrock-alluvial interface. See text for definition of symbols.

### 3.13. Boundary conditions.

The model underwent sensitivity testing (see Chapter 5) on a rectangular grid with a known slope, white noise random elevation perturbations of known amplitude, and a known nodal density (Figure 3.7). A new subroutine was written to enable the user to easily change any parameters relating to the grid. The upstream boundary condition concerns the water and sediment supply to the upstream end of the grid. Water and sediment may be introduced to any nodes in the first row of the grid. An influx of sediment may or may not be input to the upstream end of the grid. In the case that the sediment influx specified is not equal to the carrying capacity of the flow (i.e. the sediment influx is either greater smaller than the amount of sediment that can be transported in one timestep) this would represent a constrained boundary at the upstream end of the grid.

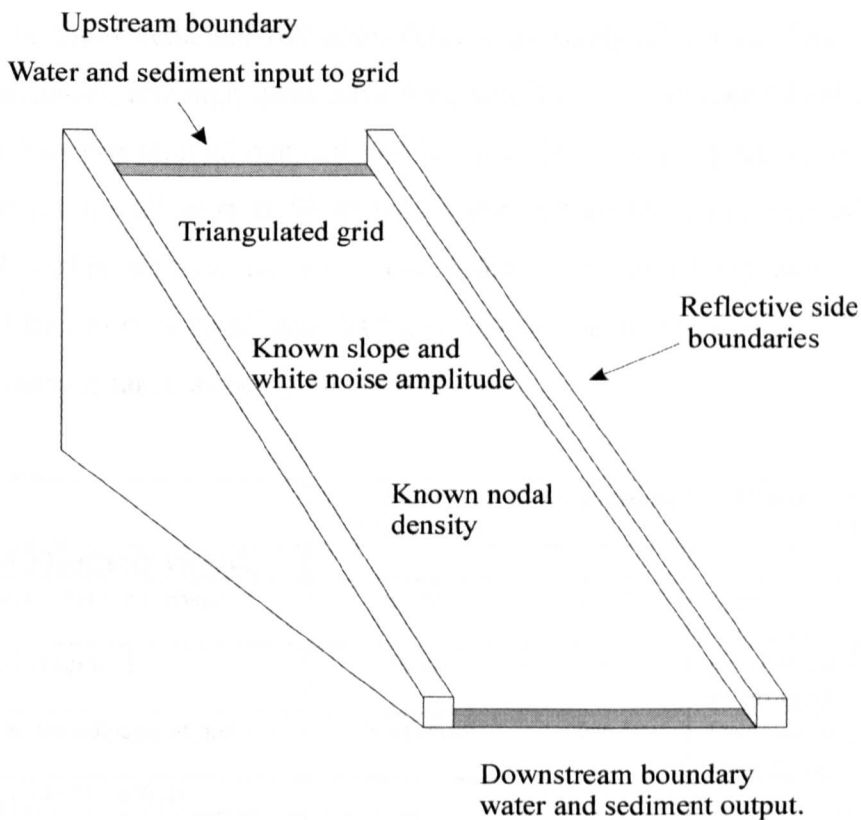


Figure 3.8. Schematic illustration of a typical model grid used for generic runs of the model.

The elevation of first and last rows of the grid may be fixed to simulate the rigid end walls of laboratory experiments or may be allowed to experience erosion and deposition. In the transverse direction, the boundaries are not periodic but are reflective (zero flux boundary condition) and are constrained by high sidewalls to contain the flow, mimicking the sidewalls of a flume, so that the braid plain is constrained within a certain width.

### 3.14. Scales used in Braided Cascade.

Table 3.4 lists default model parameters and their units. Distances in the x-, y- and z- dimensions of the grid are in meters. The model computes the mean nodal spacing ( $\delta$ ) in meters and the Voronoi polygon associated with each node (surfscale), which has dimensions in square meters ( $m^2$ ). Erosion length scales for alluvium and bedrock are defined by the user and were initially set to take the

value of 10 times delta and 100 times delta respectively (P. van der Beek personal communication), although these have been sensitivity tested (see Chapter 4). The interface between alluvial material and bedrock,  $H_i0$ , can be specified by the user and, was set for all runs at 50 m below the surface to ensure that all erosion occurred within alluvial material. The sediment transport equation computes sediment transport in  $\text{kg s}^{-1}$  and discharge is taken as being in  $\text{m}^3 \text{s}^{-1}$ . Therefore, each timestep is taken as being one second.

	Model parameters	Dimensions	Values	Units
<b>SURFACE PROCESS MODEL</b>				
Size of grid (x and y dimensions)	nx, ny	L x L	Specified by user	m x m
Mean nodal spacing, $L_i$	Delta	L	Determined by program	m
Size of Voronoi polygon of node, $A_i$	Surfscale	L x L	Determined by program	$\text{m}^2$
<b>OVERALL DEM / GRID</b>				
Slope, $S_i$	Gradient	-	Specified by user	-
Amplitude of white noise random topography	Ampnoise	L	Specified by user	m
Timestep	dt	T	1	seconds
<b>WATER TRANSPORT* (<math>h=aQ^b</math>)</b>				
Water depth coefficient	a	-	0.16	-
Water depth exponent	b	-	0.37	-
<b>SEDIMENT TRANSPORT (<math>Q_s=K\Omega^m</math>)</b>				
Sediment transport coefficient**	K	-	$2.428 \times 10^{-10}$	-
Sediment transport exponent**	m	-	3.606	-
Maximum amount of material that may be deposited in one timestep (based on grain size at Arolla).	dhmax	L	0.007751	m
Erosion length scales				
Alluvial material	$L_{e,a}$	L	10 x delta	m
Bedrock	$L_{e,b}$	L	100 x delta	m

Table 3.4. Model parameters, dimensions, values and units. All model parameters have uniform values in space and time.

\* Values for coefficient and exponent taken from Ergenzinger (1987).

\*\* From Hoey *et al.* (2001).

### 3.15. Summary of model development.

*Cascade* (Braun and Sambridge, 1997) was developed to simulate long-term landscape evolution. *Braided Cascade* has been developed from the original

model and has been modified so that it can be applied to short term process modelling. Delaunay triangulation is used to generate a computational grid, which minimises the maximum internal angle of the elements. Water is routed through the model from one or more specified input points and flow may divide around bars based on the relative water surface slopes to different possible receiving nodes. Sediment transport is based on local stream power, which is calculated using channel bed slopes. The model incorporates a length scale for erosion but no temporal lags are included, which is equivalent to a steady flow assumption. The model does not explicitly include a sediment size; however there is a maximum amount of material that can be deposited during one timestep and this is equivalent to a notional grain size.

The modelling approach is simplified and takes no account of detailed flow hydraulics. The intention is to model the overall spatial patterns of sediment transport, deposition and erosion and to analyse these in terms of their net statistical properties, rather than to produce accurate predictions of processes at particular localities. In this respect, the modelling approach is synthesist and braiding is an emergent phenomenon.

## CHAPTER 4.

### DATA USED IN MODEL VALIDATION.

To meet the research aims set out in Chapter 1 and to gather data for input to *Braided Cascade* requires the identification of dynamic braided river systems. It was decided to collect field data from a braided river in a proglacial setting. Such a setting has been chosen as proglacial rivers are often braided and competent flows (those able to move sediment) are achieved daily at predictable times.

The proglacial river chosen for this study was that of the Haut Glacier d'Arolla, located above the village of Arolla at the head of the Val d'Herens, Valais, Switzerland. The Haut Glacier d'Arolla is a typical high Alpine glacier, 4 km long with an area of approximately 6.33 km<sup>2</sup> and an altitudinal range of 1000m (Sharp *et al.*, 1993; Nienow *et al.*, 1998). The glacier terminates approximately 2560m above sea level. The glacier is drained by a proglacial stream that enters an intake for the power scheme 950 m from the glacier snout. Stream discharge and meteorological data are provided by Grande Dixence S.A. A brief description of the relevant field data collected and analysed is presented here, for an in depth discussion of bedload sampling and grain size characteristics see Hoey and Cudden (in press).

#### 4.1. Fieldwork program and instrumentation.

Data were collected from a 160 m section of channel within the braided reach of the proglacial river in July 1999. Data were obtained to enable specification of model boundary conditions and to establish the accuracy of model output. The study reach, which was situated approximately 500m from the glacier snout, consists of a braided system with flow diverging and converging around numerous bars. The reach was laterally constrained by a steep ice cliff on the west side of the reach and a moraine ridge to the east (Figure 4.1). The flow then spread through a braided network across an aggrading alluvial plain. In previous years

the reach had been a proglacial lake, however in 1999 the lake had drained creating a wide braid plain. The reach is concave and fines rapidly in the downstream direction. Characteristics of the study reach are given in Table 4.1.

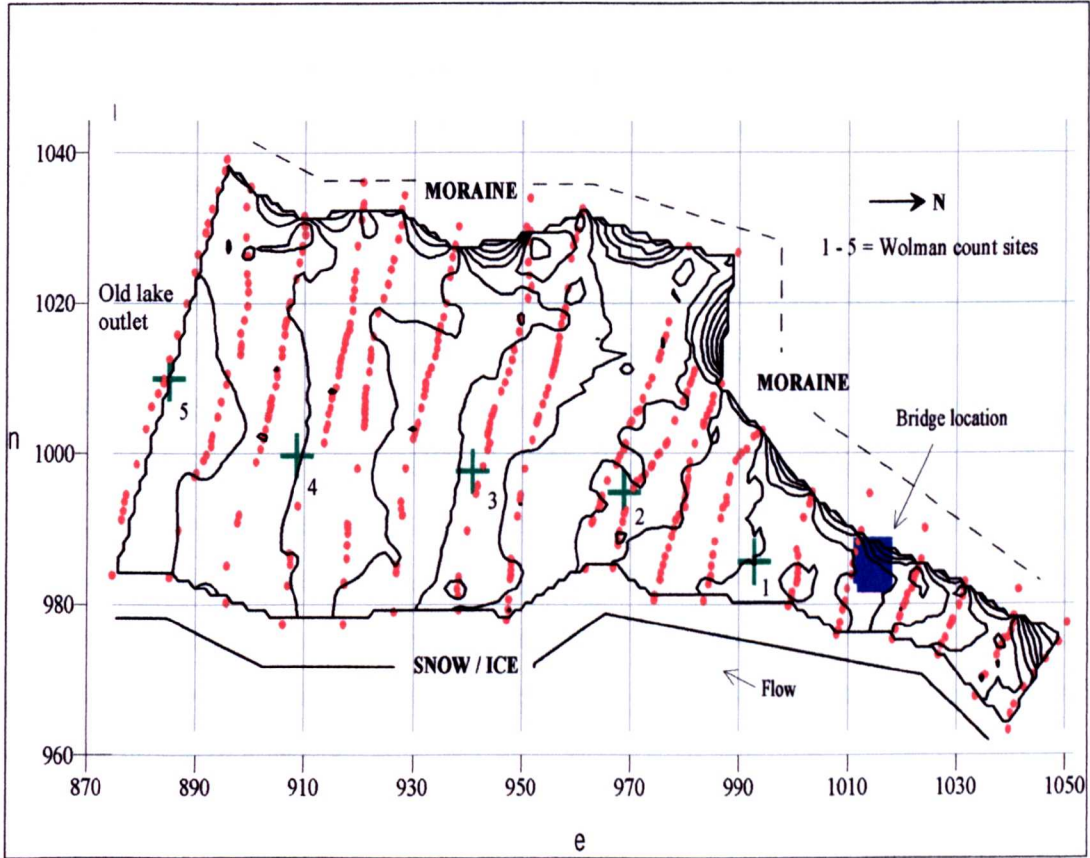


Figure 4.1. Position of survey transects (in red), bridge site (in blue) and Wolman count sites (in green) shown on contour map of reach on 16/7/99. Each grid square is 20m x 20m.

<b>Distance from glacier snout</b>	512 m
<b>Reach length</b>	150 m
<b>Width of anabranch</b>	4.47 m
<b>Slope of thalweg (bridge reach) [18.7.99/20.7.99]</b>	0.0281 / 0.029
<b>Water surface slope [18.7.99/20.7.99]</b>	- / 0.0237

Table 4.1. Details of the study reach.

## 4.2. Sediment characteristics.

The grain size distribution of the whole reach was characterised by surface pebble counts and by both surface and subsurface bulk sampling and sieving. Grid-by-number sampling (Wolman, 1954) is commonly used to characterise the size distribution of exposed fluvial sediments. Individual clasts are classified using square 0.5Ø openings on a template and the results are directly equivalent to conventional bulk sieve analysis of subsurface sediments (Church *et al.*, 1987; Rice and Church, 1996).

It is important that the sample size generates a distribution that is statistically significant. Wolman (1954) recommended a 100 clast sample for a statistically significant estimate of the median grain size ( $D_{50}$ ), however Rice and Church (1996) recommended a sample size of 400 clasts to obtain statistically significant estimates of percentiles of typical fluvial grain size distributions. Precision is not improved greatly with sample sizes greater than 400 clasts (Rice and Church, 1996). Surface pebble count distributions for 5 locations in the braided reach were carried out by randomly sampling at least 400 particles from exposed bars within the braid plain (Table 4.2).

Location	D50 (mm)	D95 (mm)
1	33.93	85.9
2	36.82	85.0
3	35.24	76.4
4	29.21	55.8
5	17.59	35.4

Table 4.2. D50 and D95 percentiles for Wolman counts at five different locations on the braidplain.

Separate bulk samples of surface and subsurface sediment were collected from one exposed bar which was situated upstream of the bridge by combining different subsamples from different points on the bar, using the method of Wolcott and Church (1991). Surface bulk samples were removed to the base of the largest visible clast present at the surface, subsurface samples were excavated from below this level for at least the same depth again.

According to the criteria of Church *et al.* (1987) the largest clast in a sample should comprise  $\leq 0.1\%$  of the sample mass to reliably estimate the parameters of the size distribution. This value is raised to 1% for maximum particle sizes of 32 to 128 mm (Church *et al.*, 1987). However to adhere to this criteria yields sample sizes of over 4800 kg (Table 4.7, Figure 4.6). In order to speed up the field procedure, whilst maintaining a statistically significant representation of the grain size distribution, samples were truncated at 64 mm. All particles greater than 64 mm were measured and weighed in the field. A sub-sample was taken of particles between 64 mm and 8 mm, which was sieved and weighed in the field. Particles below 8 mm were sub-sampled and removed to the laboratory for detailed grain size analysis. The sub-sample mass was determined based on Church *et al.* (1987) by assuming a density of  $2650\text{kgm}^{-3}$  (i.e. quartz) a 64mm clast weighs c.a. 0.36 kg. Thus a sub-sample mass of at least 36kg of all sediment less than 64mm was sieved in the field. This was again truncated at 8mm and a sub-sample of c.a. 400g was removed to the laboratory. These samples were dried, weighed and sieved into half-phi fractions. Bias and precision of the percentiles of the distributions were calculated following Ferguson and Paola (1997).

Surface and subsurface sample data are presented in Figures 4.2 and summarised in Tables 4.3 to 4.5. The particle size distribution of surface and subsurface material shows a mode spanning the 64 – 90 mm size class (surface) and the 90 – 128 mm size class for the subsurface sample. However, the percentage of material in each size class falls away rapidly for the subsurface sample indicating that the large size class are dominated by one or two clasts only. The bed material size distributions are therefore negatively skewed. Negative skewness is common in gravelly bed material (Kondolf and Matthews 1993) and indicates a fine component that is abundant enough to impose a fine tail on the overall distribution but not enough to impose recognisable bimodality (Folk and Ward 1957; Lisle 1995). The ratio of the surface  $D_{50}$  to the subsurface  $D_{50}$  is 2.44 indicating that the channel is armoured.

	Largest clast (g)	Sampled weight (tonnes)	Largest clast as % of sample weight
Surface	4800	0.49	0.97
Subsurface	2058	0.21	0.98

Table 4.3. Maximum clast size and total mass sampled for surface and subsurface bulk samples.

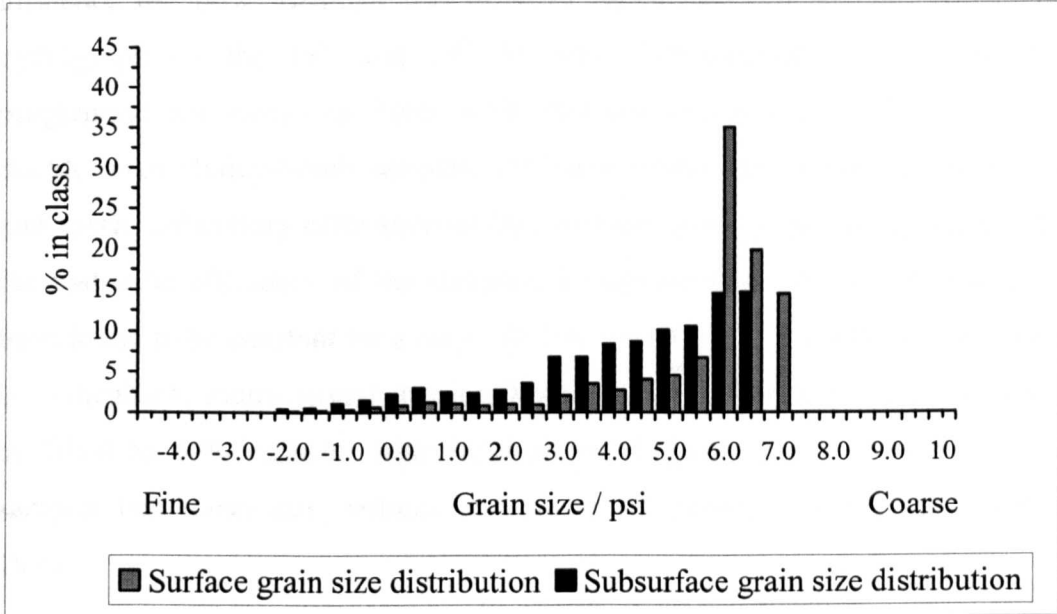


Figure 4.2. Surface and subsurface bulk samples, Arolla 1999.

Percentile	Surface (mm)	Surface (psi)	Subsurface (mm)	Subsurface (psi)
D5	3.54	1.82	1.27	0.34
D16	23.8	4.57	5.51	2.46
D50	77.5	6.28	31.8	4.99
D84	124	6.96	87.8	6.46
D90	143	7.16	101	6.66
D95	161	7.33	114	6.83

Table 4.4. Percentiles of bulk grain size distribution data in mm and in psi units (to 3 s.f.).

	Surface	Subsurface
Total mass sampled (kg)	497.4 (wet weight)	209.2 (wet weight)
Critical sample size for negligible bias for D84 (kg) (Ferguson and Paola, 1997)	181	109
Critical size for onset of improved precision for D84 (kg) (Ferguson and Paola, 1997)	2050	3475
Standard deviation of grain size percentiles.	0.445	0.606

Table 4.5. Bias and precision of bulk samples calculated according to the method of Ferguson and Paola (1997).

### 4.3. Point bedload sampling – Helley Smith sampling.

Point bedload sampling was carried out to investigate sediment transport into the braided reach. Sampling was carried out from a single-span bridge that did not influence the flow. Bedload was sampled throughout the rise and fall of the hydrograph on the 18<sup>th</sup> and 20<sup>th</sup> of July. Characteristics of the sampling programme are shown in Table 4.10. Bedload samples were collected using double sized Helley-Smith samplers (152 mm) fitted with sampler bags of 0.25 mm mesh. Laboratory calibration of Helley-Smith bedload samplers indicate that the hydraulic efficiency of the samplers is approximately 1.54. This value has been found to be constant for a range of flow conditions in experiments, the range is applicable to many natural streams. The study indicates that the sample bag can be filled to 40% capacity with sediment of diameter greater than that of the sampler bag mesh size, without a decrease in hydraulic efficiency (Emmett, 1979).

One sampler was placed on the bed in the middle of the reach in the area of fastest flowing water. The sampler was left on the bed for 2 minutes (18/7/99) and 30 seconds (20/7/99) before being removed, emptied and replaced. Samples were bagged and labelled immediately. Bedload samples from 20/7/99 were brought to the laboratory where they were dried, weighed and sieved into half phi fractions, samples from 18/7/99 were not sieved. A time series of the bedload samples collected is shown in Figures 4.7 and 4.8; summaries of sample weights, bedload transport rates and grain size characteristics of bedload samples are given in Table 4.11. For a full discussion of the causes of the bedload pulses see Cudden and Hoey (in press).

Helley-Smith bedload sampling	18/7/99	20/7/99
Number of samples	55 (54 bagged)	158 (115 bagged)
Sampling interval	120 seconds	30 seconds
Total sampling time	3 hr 13 min	6 hr 2 min
Minimum transport rate (g/m/s)	21.1	13.5
Maximum transport rate (g/m/s)	1964	3735
Mean transport rate (g/m/s)	590	724

Table 4.6. Characteristics of the bedload sampling programme.

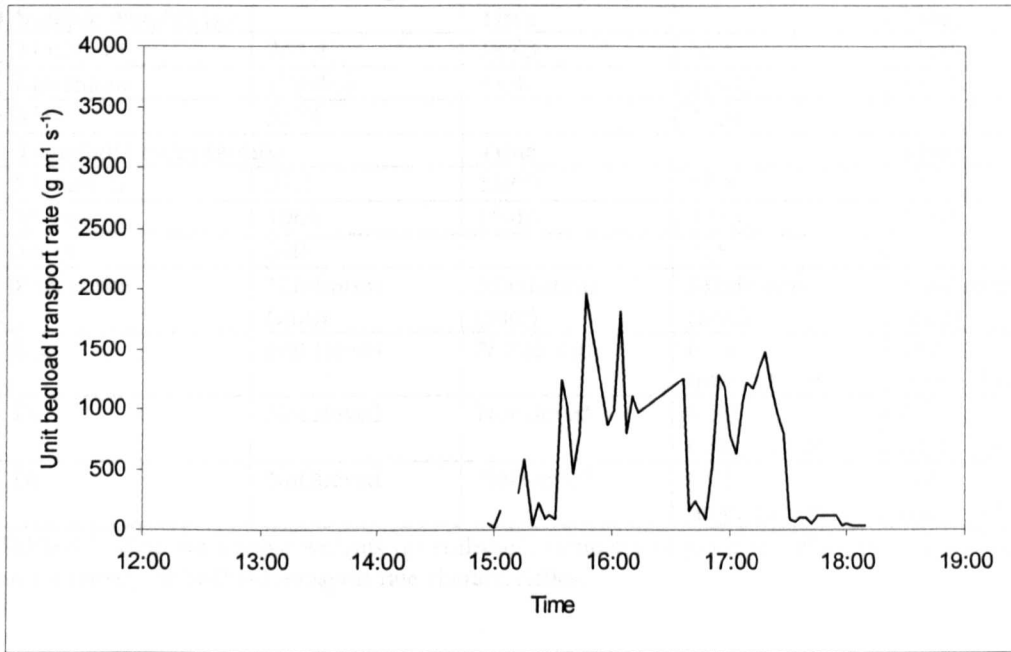


Figure 4.3. Time series of unit bedload transport ( $\text{g m}^{-1} \text{s}^{-1}$ ), 18/7/99.

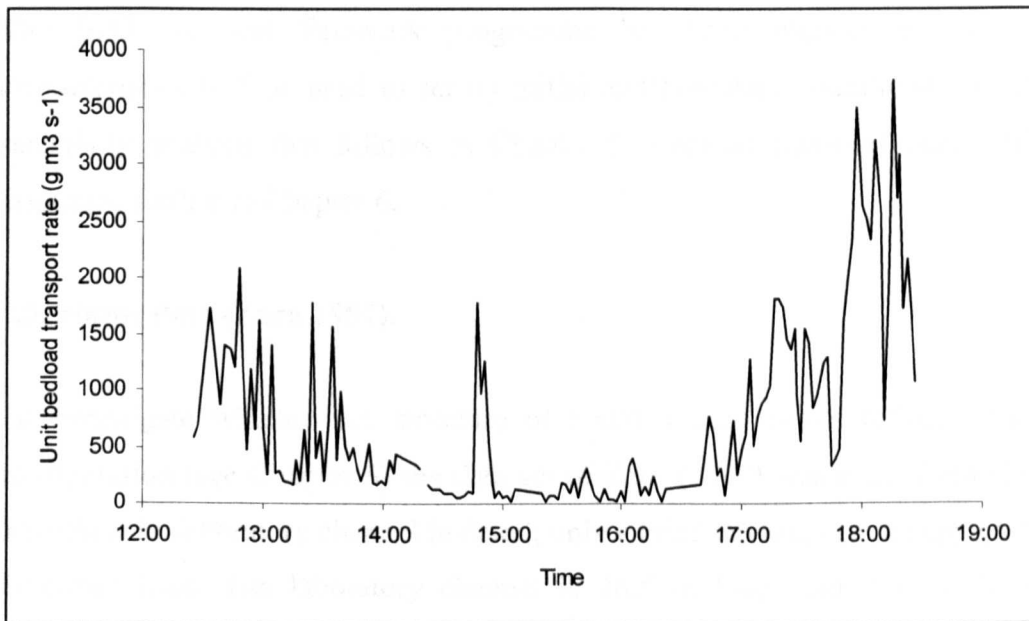


Figure 4.4. Time series of unit bedload transport ( $\text{g m}^{-1} \text{s}^{-1}$ ), 20/7/99.

	18/7/99		20/7/99	
<b>Sample weights (g)</b>		<b>Time</b>		<b>Time</b>
Minimum	263.4	18:03	61.5	15:50
Maximum	17909.4	15:46	17032	18:15
Mean	5574		3304	
<b>Transport rates (g/m/s)</b>		<b>Time</b>		<b>Time</b>
Minimum	21.1	15:00	13.5	15:50
Maximum	1964	15:46	3735	18:15
Mean	590		725	
<b>Percentile</b>	<b>Minimum (mm)</b>	<b>Maximum (mm)</b>	<b>Minimum (mm)</b>	<b>Maximum (mm)</b>
D <sub>50</sub>	Not sieved	Not sieved	0.34 time: (15:56)	45.59 time: (14:55)
D <sub>84</sub>	Not sieved	Not sieved	0.50 time: (15:56)	91.87 time: (14:47)
D <sub>95</sub>	Not sieved	Not sieved	0.71 time: (15:56)	115.4 time: (14:47)

Table 4.7. Bedload sample weights (g) collected, summary of grain size characteristics of bedload and summary of bedload transport rate characteristics.

#### 4.4. Summary of field data collection.

The field site and fieldwork programme has been introduced. Field site characteristics will be used to set up initial and boundary conditions for model sensitivity analysis that follows in Chapter 5. Bedload transport rates will be discussed further in Chapter 6.

#### 4.5. Flume data (Zarn 1997).

To investigate whether the structure of bedload time series reflects channel configuration (see Chapter 6) the data set of Zarn (1997) was used. Zarn (1997) describes the laboratory channel in detail; only a brief summary of the apparatus is described here. The laboratory channel is 26.5 m long, and 3 m wide with adjustable width and slope. Sediment was fed into the upstream end of the channel at a constant rate and was measured at the downstream end of the flume on average just under every 6 minutes. The accuracy of a single bedload measurement was  $\pm 0.5\%$ , the accuracy of the medium bedload transport during an experiment was  $\pm 1\%$  (Zarn, 1997). Laboratory models trap bedload across the entire braid plain width, and provide spatial integration that is not present when point sampling is used (Hoey *et al.*, 2001).

Four sets of runs were conducted using four different widths and four different steady discharges. All runs used the same grain size distribution, with a median grain size ( $D_{50}$ ) of 1.16 mm and  $D_{90}$  of 1.97 mm. All experiments started on a plane bed without any bars or bedforms. Runs are summarised in Table 4.8.

Run name	Discharge ( $l\ s^{-1}$ )	Sediment input rate ( $g\ s^{-1}$ )	Unit bedload transport rate ( $g\ m^{-1}\ s^{-1}$ )			Flume width (cm)	Average number of channels.
			Mean	Median	St. dev.		
30 5	6.89	4	13.5	13.7	3.20	30	1
30 6	4	1.6	5.08	5.07	1.93	30	1
30 7	5	6.3	19.8	19.6	2.95	30	1
30 8	2.37	4	12.7	12.6	2.21	30	1
75 2	4.01	1.6	2.13	2.11	0.92	75	2.28
75 3	4.97	6.3	7.85	7.89	1.78	75	2.34
75 4	2.34	4	5.29	5.20	2.04	75	2.78
75 6	6.89	4	5.59	5.62	1.19	75	1.76
140 1	2.34	4	3.33	3.02	1.85	140	4.6
140 2	4.98	6.3	4.41	4.29	1.75	140	3.86
140 3	3.95	1.6	1.40	1.32	0.77	140	3.88
140 4	6.9	4	3.11	2.88	1.41	140	3.38
250 2	4.02	1.6	1.05	0.89	0.84	250	4.89
250 3	5	6.3	2.80	2.57	1.52	250	5.48
250 4	2.29	4	2.07	1.79	1.40	250	5.98
250 6	6.91	4	2.50	2.26	1.48	250	3.97

Table 4.8. Summary statistics of Zarn's (1997) flume data.

From Table 4.8 it can be seen that channel morphology ranged from a single channel to a braided network, depending on flume width. Zarn (1997) describes the development of bedforms throughout each run, these are summarised in Table 4.9.

Run name	Bedforms
30_5	Dunes
30_6	Two longitudinal ribs
30_7	Transverse bars
30_8	Plane bed
75_2	Transition form of alternate bars and braided network
75_3	Transition form of alternate bars and braided network
75_4	Braided
75_6	Transition form of alternate bars and braided network
140_1	Braided
140_2	Braided
140_3	Braided
140_4	Braided
250_2	Braided
250_3	Braided
250_4	Braided
250_6	Braided

Table 4.9. Bedform development in the flume runs of Zarn (1997).

Variation of transport rate will be described and discussed in Chapter 6.

#### 4.6. Summary of Chapter 4.

This chapter has introduced primary field data and secondary data that will be used in the sensitivity analysis and testing of *Braided Cascade*. Sensitivity analysis follows in Chapter 5, further testing of the model will be undertaken in Chapter 6.

## CHAPTER 5.

### SENSITIVITY ANALYSIS.

#### 5.1. Introduction: what is sensitivity analysis and why is it necessary?

The form of sensitivity analysis used here assesses the effect on model output of a fixed percentage change in each model parameter while holding all the other parameters constant. Alternative methodologies are available (e.g. the Generalised Likelihood Uncertainty Estimation (GLUE) framework, which is based on Monte Carlo simulation for estimating the predictive uncertainty associated with models, Freer *et al.* 1996). Sensitivity analysis is concerned with parameter reliability and estimation and with reason for goodness of fit between model output and real systems. Most sensitivity analysis is concerned with process parameters (i.e. parameters representing processes in the real world). However, a necessary stage in model development is to conduct sensitivity analysis of model parameters (e.g. temporal or spatial steps in the model) and of model boundary conditions, and also of the model structure itself.

It is necessary to quantify parameters in order to specify the equations that make up the model. Where process parameters bear a physical resemblance to the actual attributes of the real system, calibration can be achieved by field measurements. Where this is not the case, they may be evaluated by a procedure known as optimisation (Kirkby *et al.*, 1993). Optimised parameters have no “physical” meaning, the parameter value is chosen to optimise the comparison of the model output with real or expected results.

Sensitivity analysis should be carried out at an early stage in model development, since this will indicate to which of the parameters the model is sensitive, which process parameters may require particular attention in the field and may suggest

possible changes to the model structure whilst this is still feasible (Kirkby *et al.*, 1993). However while a parameter may not be sensitive it may still be important to the overall model performance (Anderson and Burt, 1985).

*Braided Cascade* contains several parameters whose values either have been determined for particular field and / or laboratory conditions or have been determined using *a priori* reasoning. The method adopted when testing the sensitivity of the model is to vary a single parameter at a time from its initial value in a control run, in order to identify which parameters exert the greatest influence over the development of braiding. This chapter investigates the behaviour of *Braided Cascade* as a function of the antecedent configuration, and suggests how the values of the model parameters may be interpreted.

## **5.2. Experimental design and control run: simulation of the idealised Arolla case.**

The model was described in detail in Chapter 3. Simulations have been conducted with a range of model parameter values, and a variety of initial and boundary conditions. As well as addressing model sensitivity, these simulations have implications with regard to several important issues in the evolution of braided networks.

This chapter firstly describes an initial run of the model using reasonable first estimates of parameter values and boundary conditions. This acts as a control run for the sensitivity testing that follows. The aim of the control run is to determine whether using this physically based model can simulate braiding.

The idealised conditions of the control run are based on those measured in the proglacial stream of the Haut Glacier d'Arolla, Valais, Switzerland in July 1999 and previously described in Chapter 4 and in Cudden and Hoey (in press). Table 5.1

summarises the field conditions, Table 5.2 defines parameter values for the control run and alternative values used in sensitivity analysis.

Proglacial stream, Haut Glacier d'Arolla 1999.	
Reach length	150 m
Braidplain width	75 m
Slope of thalweg	0.0281 (18/7/99), 0.029 (20/7/99)
Water surface slope	0.0237 (20/7/99)
D <sub>50</sub> (surface bulk sample)	77.5 mm

Table 5.1 Summary of conditions in the proglacial stream of the Haut Glacier d'Arolla, July 18<sup>th</sup> - 20<sup>th</sup> 1999.

Parameter	Units	Control run value	Alternative values
Reach length	m	250	-
Reach width	m	10	-
Number of nodes in length	-	250	-
Number of nodes in width	-	10	-
Delta (average node spacing)	m	Calculated by program	Calculated by program
Channel bed slope	-	0.02855*	0.01
Amplitude of white noise perturbations	-	0.01 x slope x length	-
Erosion length scale for alluvial material	m	10 x delta**	0.00001, delta, 100*delta, 1000*delta, length of grid
Dhmax	m	0.07751***	0 (no deposition)
Timestep, dt	s	1	-
Discharge input (units per timestep)	m <sup>3</sup> s <sup>-1</sup>	2 units at three nodes on the upstream boundary.	1, 5 units at different nodes on the upstream boundary.
Sediment input at upstream boundary	m <sup>3</sup> s <sup>-1</sup>	0	Sediment equilibrium transport rate at each node receiving water on the upstream boundary.
Splitting parameters qratio and upratio	-	0.8	0.5, 0.95
Diffusion erosion	-	Switched off	Switched on****

Table 5.2. Parameter values for the control run and alternative values used in sensitivity analysis.

\* Average of thalweg slopes for 18/7/99 and 20/7/99

\*\* Peter van der Beek (pers. comm. 2000)

\*\*\* D<sub>50</sub> surface sediment determined by bulk sampling, Arolla 1999.

\*\*\*\* See section 5.4.4 for values of diffusion coefficient.

*Braided Cascade* was set up to perform the control run with the default grid setting as illustrated in section 3.13. The grid is rectangular with the average grid slope based on the field site. Within the rectangular grid, nodes are connected via Delaunay triangulation. As can be seen from Table 5.1 the Arolla reach was 150 m long and 75

m wide. However, the grid for the control run and subsequent sensitivity analyses was defined as being 250 nodes long by 10 nodes wide (Table 5.2 and Figure 5.1). Nodal density was set as being one node per metre (i.e. the length of the grid was therefore set as 250 m with 250 nodes along the length and the width was set as being 10 m with 10 nodes along the width). The nodal density was kept at one node per metre for all runs in the sensitivity analyses. The grid size and nodal density used were designed as a compromise for two reasons:

- to minimise computational time needed to process each timestep, (with a grid of 150 by 75 nodes each timestep was taking over five minutes to be processed);
- to increase the ratio between reach length and braidplain width (with a grid of 150 by 75 nodes the length is only twice the width). This has implications for spatial lag effects, morphological length scales and step lengths, and will be discussed further in section 5.5.1.

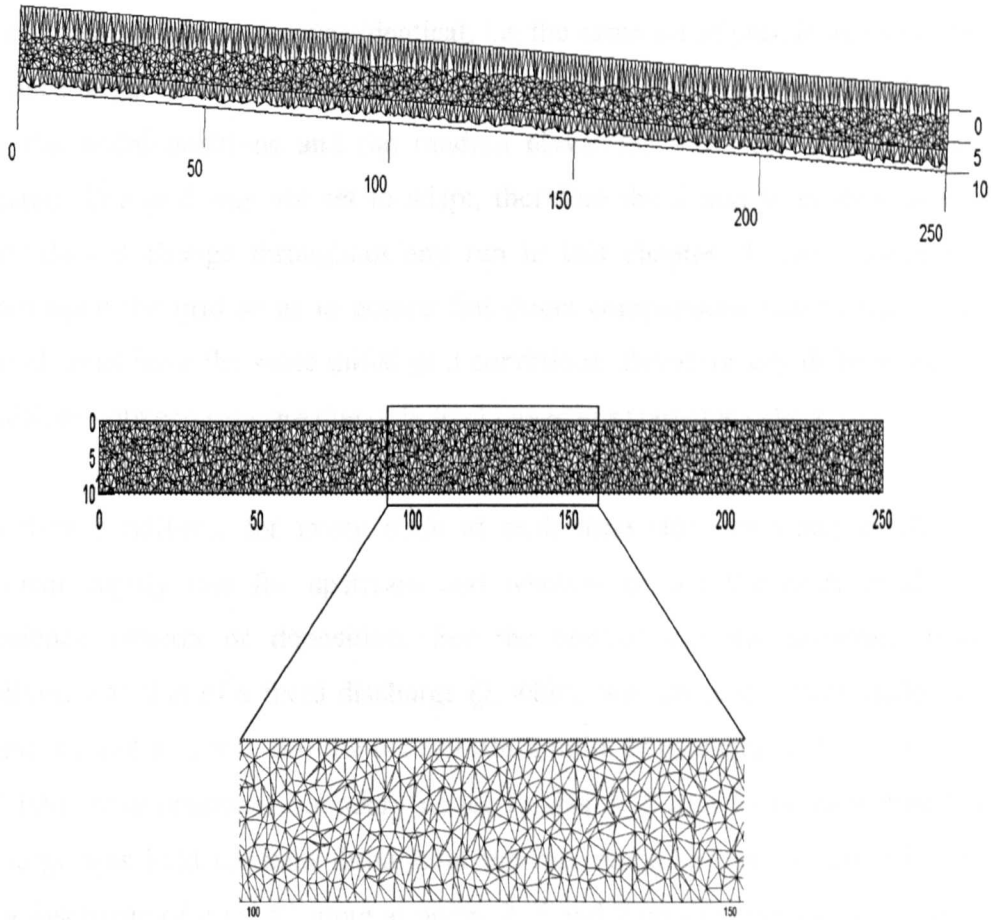


Figure 5.1 Diagram of the triangulated grid used in sensitivity analysis. **TOP**: oblique view of the grid showing the sidewalls. **MIDDLE**: 2-dimensional vertical view of the grid. **BOTTOM**: close up of the grid showing the triangulated network. Water is input at  $x = 0$ . Flow is from left to right.

### 5.2.1. Boundary and initial conditions.

Initial conditions for a run comprise grid dimensions (length, width, slope and amplitude of white noise perturbations). In all cases, the initial and boundary conditions were as follows: the initial condition was a uniform plane of sediment sloped in the  $x$ -direction to which a low level of white noise was added. The amplitude of the white noise was calculated as being 10% of the slope multiplied by the length of the grid. The side boundaries were set as being 100 m higher than the nodes on the braidplain, thus constraining the width of the braidplain (Figure 5.1). Thus, the sidewalls were reflective and constituted a no-flow zone.

For all runs the grid set up was identical, i.e. the same set of pseudo-random numbers was used to generate the white noise for the elevation perturbations. Therefore, for all runs the nodal positions and the random elevations were the same for the first timestep. The grid was not set to adapt, therefore the  $x$  and  $y$ - co-ordinates of the nodes do not change throughout any run in this chapter. These constraints were placed upon the grid so as to ensure that direct comparisons can be made between runs; all runs have the same initial grid conditions, therefore any differences in final conditions between runs are due only to changes in parameter values.

Boundary conditions for every node at each time step are water discharge and sediment supply rate for upstream and whether or not the node is allowed to experience erosion or deposition. For the control run the upstream boundary condition was that of a fixed discharge  $Q$ , which was input at certain nodes, and no sediment input at  $x = 0$ . For the control run 2 units of discharge ( $Q = 2 \text{ m}^3 \text{ s}^{-1}$ ) were read into three upstream boundary nodes (nodes 2, 5 and 7) at each timestep and discharge was held constant throughout the run. All other runs discussed here also had a discharge of  $2 \text{ m}^3 \text{ s}^{-1}$  input at nodes 2, 5 and 7 on the upstream boundary. The effect of unsteady discharge was not considered.

The upstream boundary was allowed to erode, i.e. the elevation of the bed was not fixed. However this chapter also reports simulations with sediment supplied to upstream boundary nodes at a rate equal to the equilibrium sediment transport rate for the first timestep at each node preventing aggradation or degradation at  $x = 0$ . The downstream boundary condition for the control run was that of no erosion or deposition at  $x = nx$  (where  $nx$  is the number of nodes in the  $x$  direction along the grid, in this case 250). This is analogous to the fixed end of a flume. In the first instance each run was set to perform 50 000 iterations (13.8 hours).

### **5.2.2. Spatial lag effects: the erosion length scale for alluvial material.**

For the control run the erosional length scale ( $xlf\_AL$ ) was set to equal 10 times the

average nodal spacing (node spacing is determined by the program). The default value for the erosional length scale was chosen after personal communication with Peter van der Beek (2000) and was set to equal the default value of the length scale used in the original version of *Cascade* when modelling long-term landscape evolution (see Braun and Sambridge 1997). Simulations with differing values of the length scale have been carried out and these are reported in section 5.4.1.

### 5.2.3. Notional grain size.

There is a maximum amount of sediment that can be deposited at one location during one timestep,  $dh_{max}$  (see section 3.11). For the control run, this value was set to equal the median grain size ( $D_{50}$ ) of surface material at Arolla, determined by bulk sampling. *Braided Cascade* operates with one grain size only, it was decided to set the maximum amount of sediment that can be deposited during one timestep equal to a physically realistic grain size, thus the surface  $D_{50}$  from Arolla was used. However simulations were also carried out with no deposition allowed, i.e. the system was purely erosional. These results are discussed in section 5.4.2.

### 5.2.4. Discharge splitting ratios.

In the water routing algorithm discharge is not split if the ratio of the discharges routed to the two receiving nodes ( $q_{ratio} Q_r$ , or  $up_{ratio} Q_{ru}$ ) is greater than 0.8 (see Chapter 3 sections 3.8.1 and 3.8.2). The value of 0.8 was chosen as a first attempt at forcing discharge to split between two receiver nodes; simulations with other values have been carried out and these are reported in section 5.4.3.

### 5.2.5. The effect of lateral erosion.

Lateral sediment transport removes sediment from the banks of a channel, adding it to the sediment load in the channels and widening the channels. *Cascade* incorporates diffusion erosion to model short-range transport processes (for example soil creep, landslides, rainsplash, surface and subsurface wash). Within *Braided Cascade*, the diffusion erosion has been used as an analogue for lateral sediment transport and is

discussed further in section 5.4.4.

### **5.2.6. Grid gradient.**

In the control run the gradient of the grid was set to equal the average slope of the thalweg in the proglacial stream of the Haut Glacier d'Arolla. Simulations with other gradients were undertaken and these are reported in section 5.4.5.

### **5.3. Results from the control run.**

Figure 5.2 shows water depth at each node for the control run after 25 000 and 50 000 timesteps respectively. The initial sheetwash over the whole grid resolves itself into channels and, as the run progresses one meandering channel is created which remains stable at the lower end of the grid for over 25 000 timesteps. At the upper end of the grid the discharge (input at three nodes along the upstream boundary) resolves itself into one main channel with minor secondary channels then between about  $x = 30 - 60$  m water covers the whole of the braidplain. This area remains stable for over 25 000 timesteps although it can be seen that within this stable area water depths at nodes change over time.

The system experienced overall net erosion due to zero sediment input, although the majority of nodes experienced no overall change in elevation (Figure 5.3, Table 5.3). This can be attributed to the fact that once the dominant channel has formed at the downstream end of the grid the flow erodes the bed and carves itself a stable channel with steep banks that trap all the flow, so most of the bed remains dry.

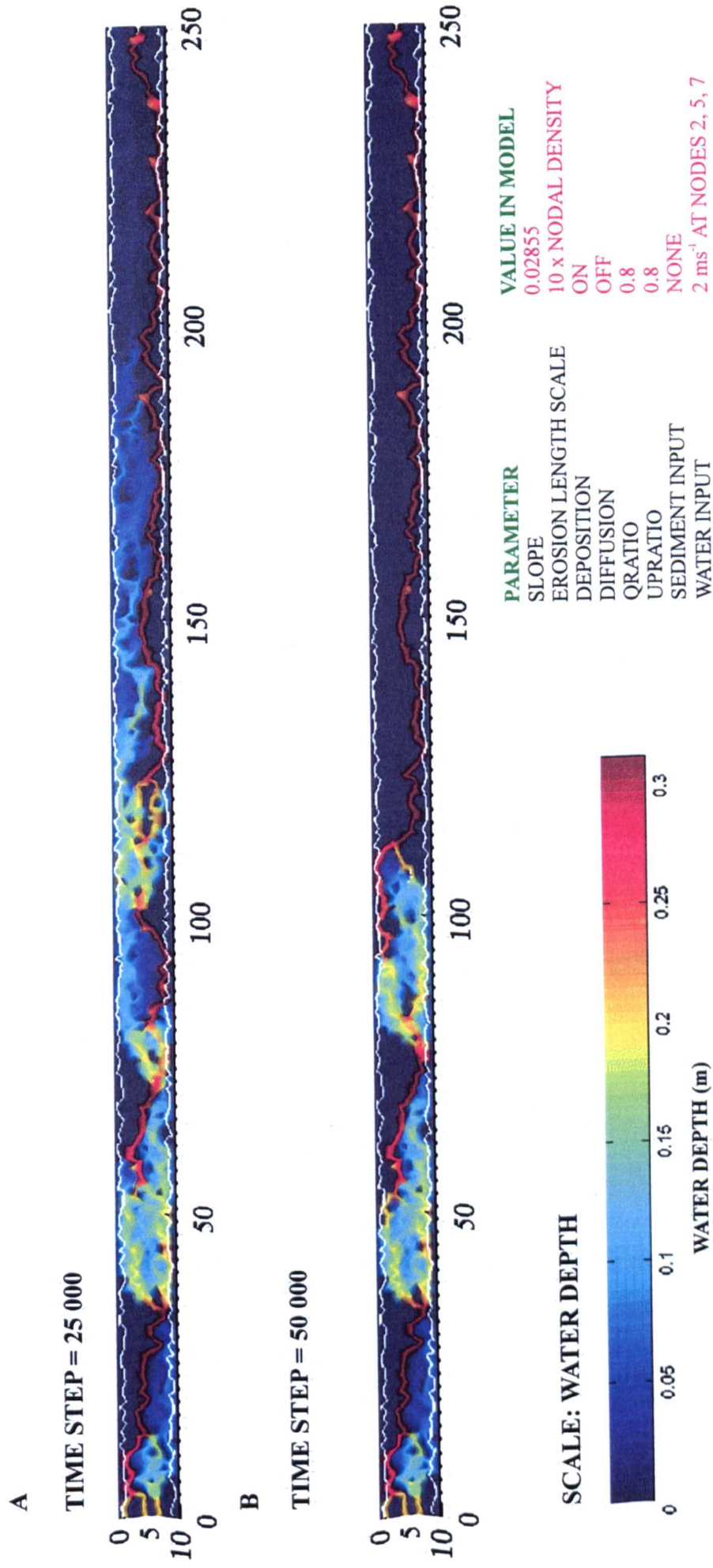


Figure 5.2. Diagram of the control run showing channel evolution. White lines on the diagrams show the side boundaries of the grid. Top: after 25 000 timesteps. Bottom: after 50 000 timesteps. Colour bar indicates water depth. Flow is from left to right.

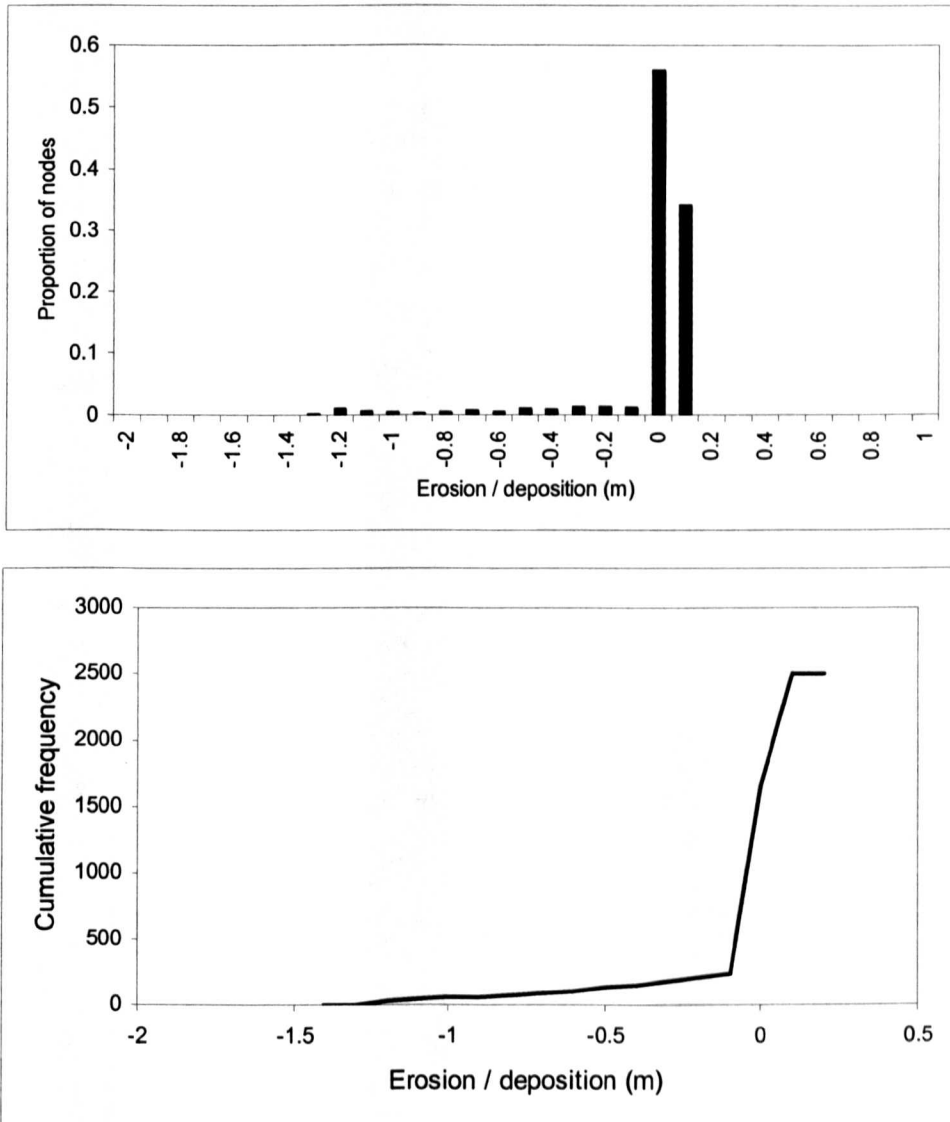


Figure 5.3. a) Histogram of overall erosion /deposition experienced by each node for the control run (with no sediment input at the upstream end of the grid). b). Cumulative frequency curve of erosion / deposition in the control run for node with water (i.e.  $\Delta z \neq 0$ ).

The control run was repeated with sediment added to the upstream end of the grid at every timestep. Sediment was added at the same nodes as water (i.e. nodes 2, 5 and 7). The amount of sediment added was set to equal the equilibrium sediment transport at the node in question for the first timestep. Added sediment volumes did not change at any node on the upstream boundary throughout the run. Figure 5.4 shows the

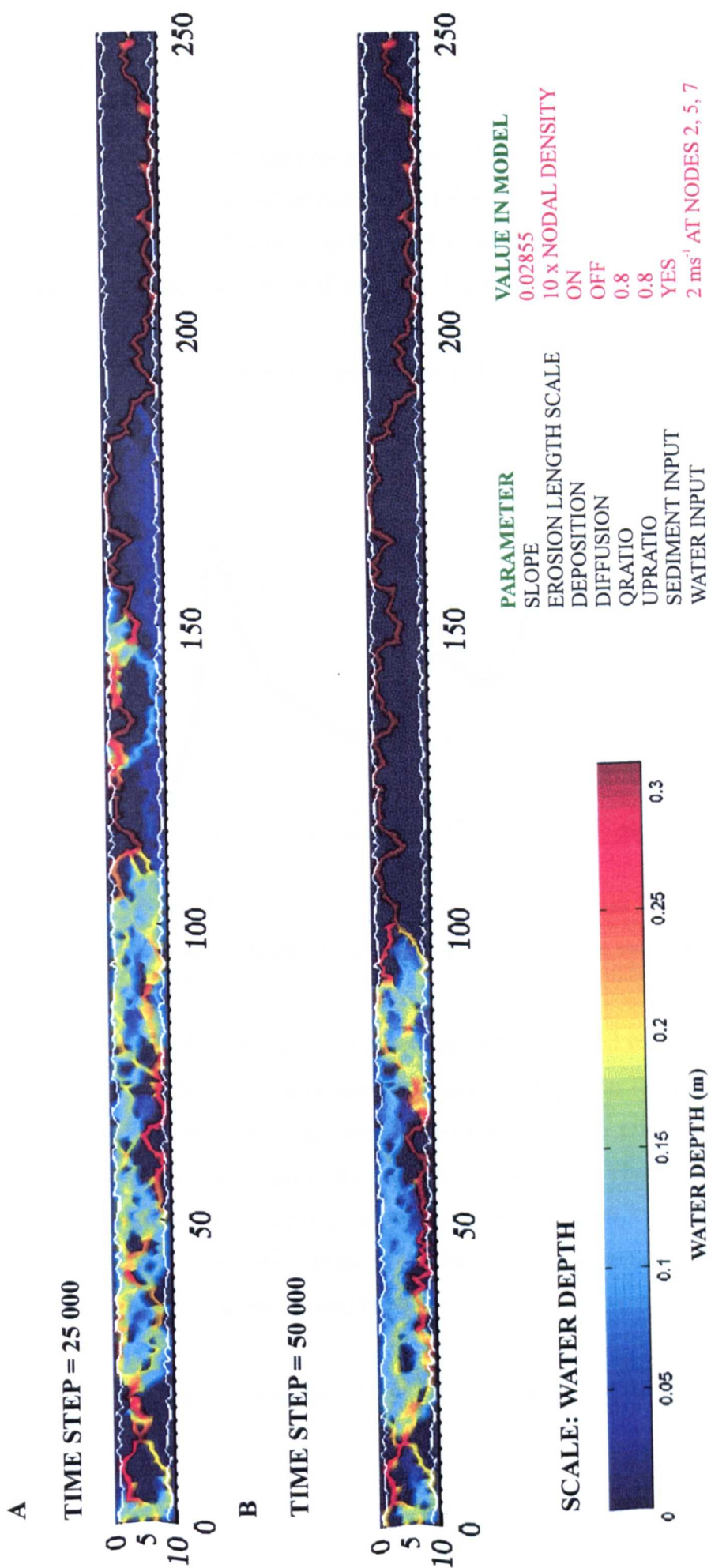


Figure 5.4. Diagram showing channel evolution for a run with sediment input at the upstream end of the grid. Top: after 25 000 timesteps. Bottom: after 50 000 timesteps. Control bar indicates water depth. Flow is from left to right.

spatial distribution of channels on the grid after 25 000 and 50 000 timesteps, Figure 5.5 shows the time series of sediment outflux from the downstream boundary for the control run with and without sediment. The addition of sediment did not significantly alter the spatial distribution of channels (Figure 5.4); channels at the upstream end of the grid (from  $x = 0$  to  $x = 100$ ) were more active than in the control run, however below  $x = 100$  one main channel developed and captured the entire flow.

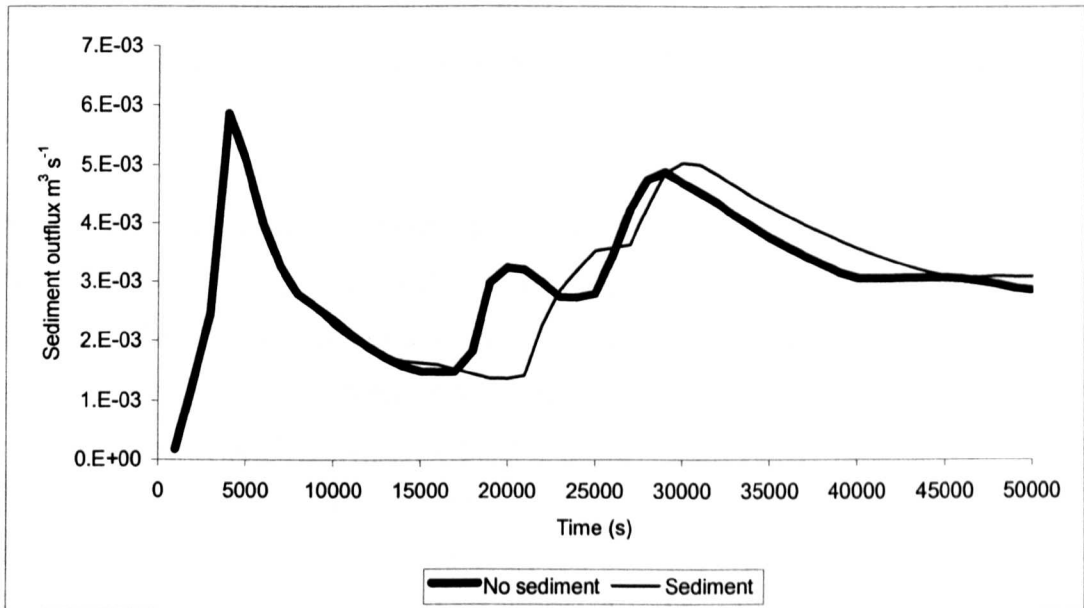


Figure 5.5. Time series of sediment outflux for the control run with and without sediment input, after every 1000 iterations.

The addition of sediment to the upstream end of the grid results in marginally more sediment leaving the downstream boundary of the grid as the run progresses ( $1.54 \times 10^{-1} \text{ m}^3 \text{ s}^{-1}$  for the control run with no sediment and  $1.55 \times 10^{-1} \text{ m}^3 \text{ s}^{-1}$  when sediment is added at the upstream end of the grid). One main channel had formed on the downstream boundary after 3000 iterations and by 4000 iterations this channel had captured most of the flow ( $5.97 \text{ m}^3 \text{ s}^{-1}$  out of a maximum of  $6 \text{ m}^3 \text{ s}^{-1}$ ), leading to a peak outflux of sediment at 4000 timesteps.

Both runs were stopped after 50 000 iterations. If allowed to proceed, it is likely that

in both cases the main channel would have eroded upstream and one channel would be carved down the length of the model grid. Therefore further investigation should be carried out to explore parameter values that lead to braiding.

#### **5.4. Sensitivity analysis.**

Changes in parameter values for runs with upstream boundary conditions of input discharge but no sediment input will be discussed first. The upstream boundary was allowed to erode; therefore, simulations with no sediment input are equivalent to a degradational system.

##### **5.4.1. Variation of spatial length scale - spatial lag.**

As discussed in Chapter 3, section 3.10.1, spatial lag effects are defined as the inability of an alluvial system to immediately overcome the presence of constrained sediment boundary conditions (Phillips and Sutherland 1989). A certain distance, termed “spatial lag,” is required before the alluvial system reaches equilibrium (Phillips and Sutherland, 1989). Spatial lag may also be thought of as a “step length.” The step length method identifies a typical distance of travel between sediment source (erosion) and sediment sink (deposition) and has been applied to meandering (e.g. Neill 1971) and braided channels (e.g. Carson and Griffiths 1989; Ferguson and Ashworth 1992; Goff and Ashmore 1994 - see Chapter 2 section 2.5.1). The loci of erosion and deposition in braided channels are spatially complex but have been identified using frequent resurvey over short periods (Ferguson and Ashworth, 1992), or by making cross-section spacing small enough to identify the downstream trend in loci of erosion and deposition (Griffiths 1979; Ferguson and Ashworth, 1992; Goff and Ashmore 1994).

For the control run the erosion length scale for alluvial material was set at 10 times the nodal density (P. van der Beek, pers. comm. 2000), which was the default value for the long-term landscape evolution version of *Cascade*. The length scale

determines the rate at which the disequilibrium between transport capacity and actual transport rate is reduced i.e. for the control run any disequilibrium that exists between potential carrying capacity of the flow and sediment flux will be reduced to  $1/e$  of the initial volume within 10 node spacings downstream (Figure 5.6). Other numerical models of braided network evolution have neglected spatial lag terms and have assumed that the sediment transport capacity of the flow is reached instantaneously at every point in space and time (e.g. Murray and Paola, 1994, 1997; McArdeell and Faeh, 2001). However, spatial lag may be important as changing the erosion length scale should change the amount of material eroded from each node and the distance downstream that the material is transported before being deposited. If the length scale is small, deposition should occur very near the node from which material has been eroded, and vice versa. To test the sensitivity of the model to spatial lag, the erosion length scale was altered from 0.00001 to 250 (the length of the grid). Zero was not used as this created numerical instabilities in the model, so 0.00001 was used to approximate an instance in which the sediment transport capacity of flow is reached instantaneously in time and no spatial lag effects occur.

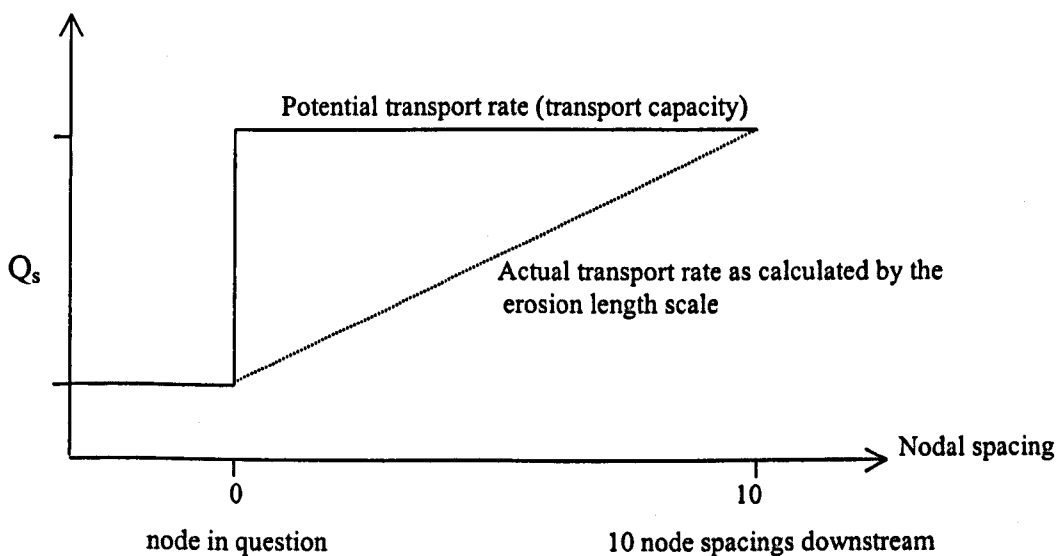


Figure 5.6. Disequilibrium between transport capacity and actual transport rate as defined by the erosion length scale, for an erosion length scale of 10 x the nodal density (i.e. the spacing used in the control run).

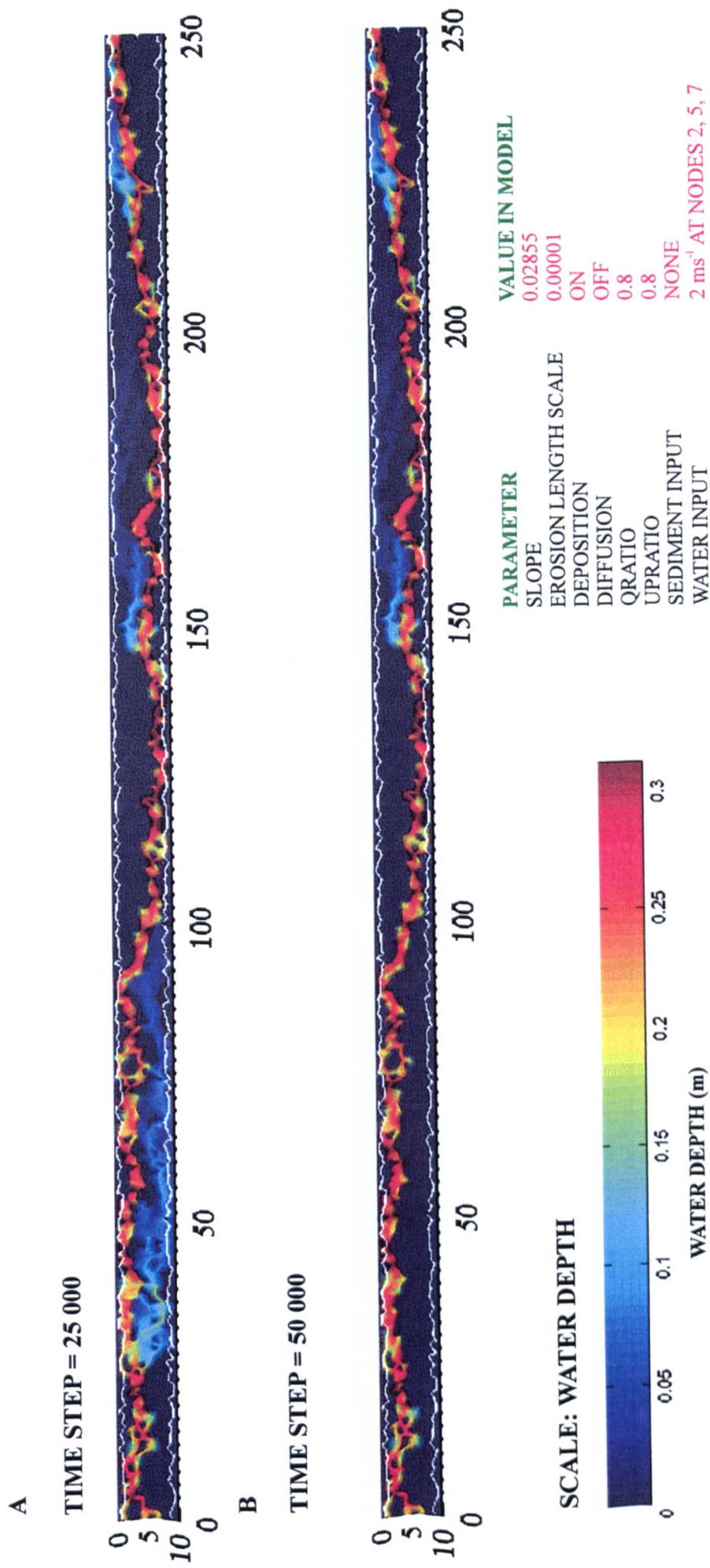


Figure 5.7. Diagram showing channel evolution for a run with the erosion length scale equal to 0.00001. Top: after 25 000 timesteps. Bottom: after 50 000 timesteps. Colour bar indicates water depth. Flow is from left to right.

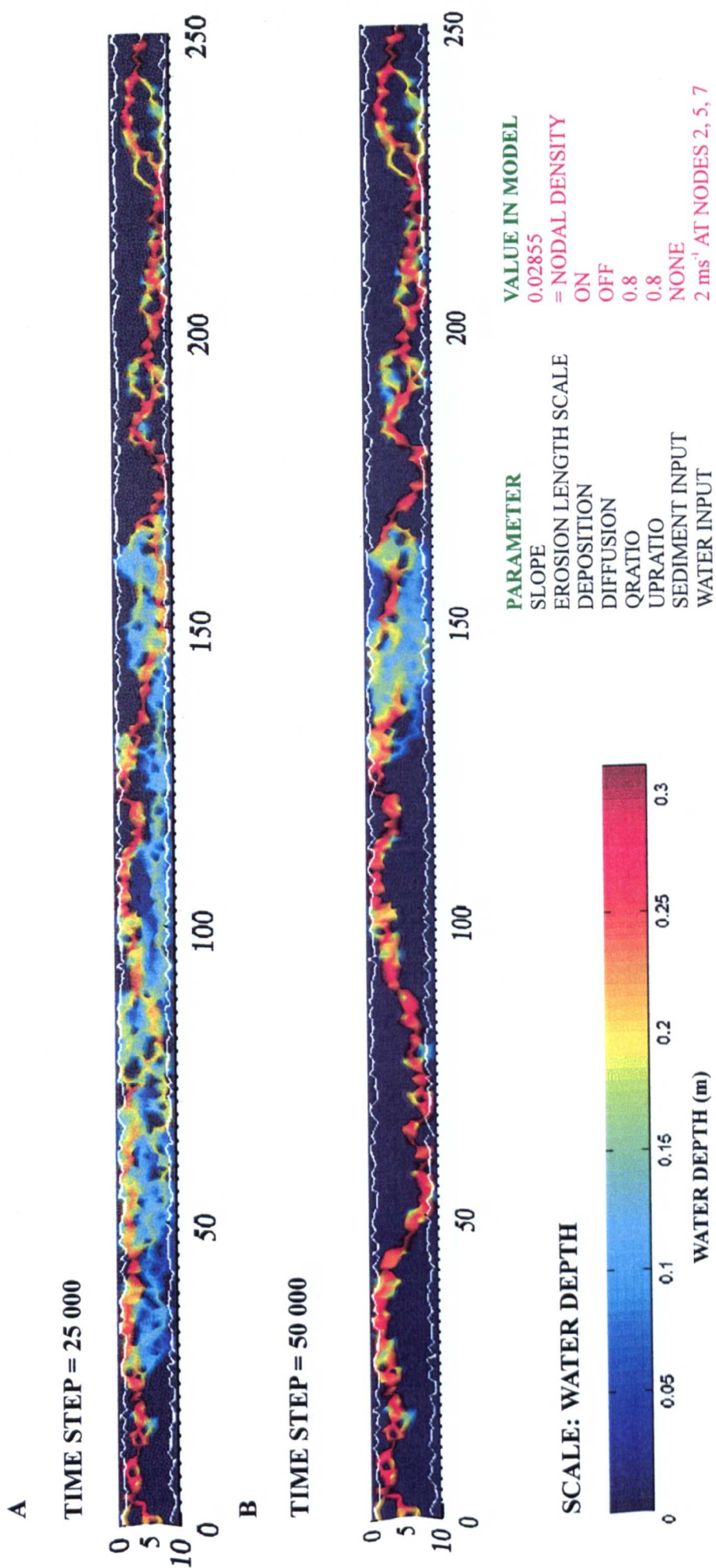


Figure 5.8. Diagram showing channel evolution for a run with the erosion length scale equal to the nodal density. Top: after 25 000 timesteps. Bottom: after 50 000 timesteps. Colour bar indicates water depth. Flow is from left to right.

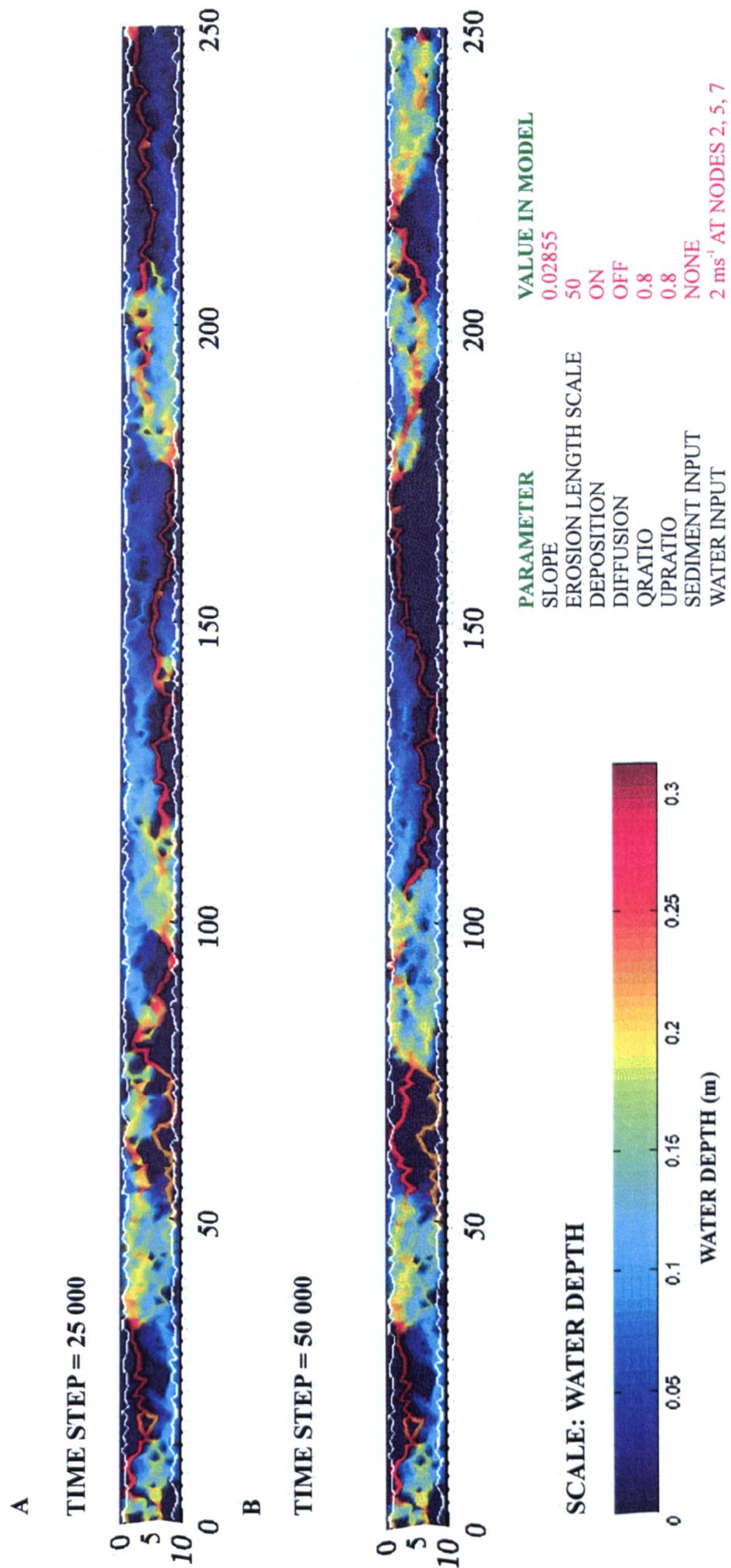


Figure 5.9. Diagram of the control run showing channel evolution for a run with the erosion length scale equal to 50..  
Top: after 25 000 time steps. Bottom: after 50 000 time steps.  
Colour bar indicates water depth. Flow is from left to right.

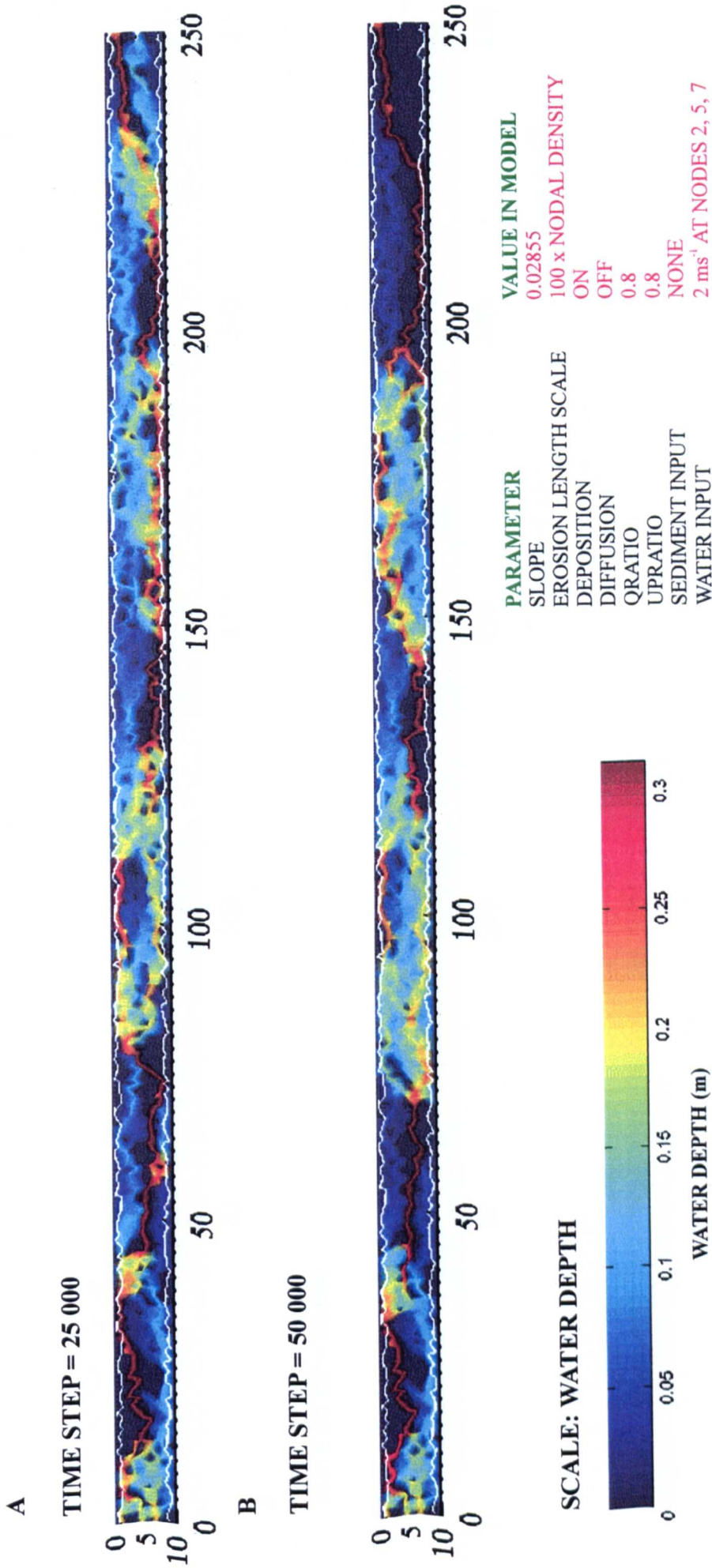


Figure 5.10. Diagram showing channel evolution for a run with erosion length scale equal to 100 times the nodal density. Top: after 25 000 timesteps. Bottom: after 50 000 timesteps. Colour bar indicates water depth. Flow is from left to right.

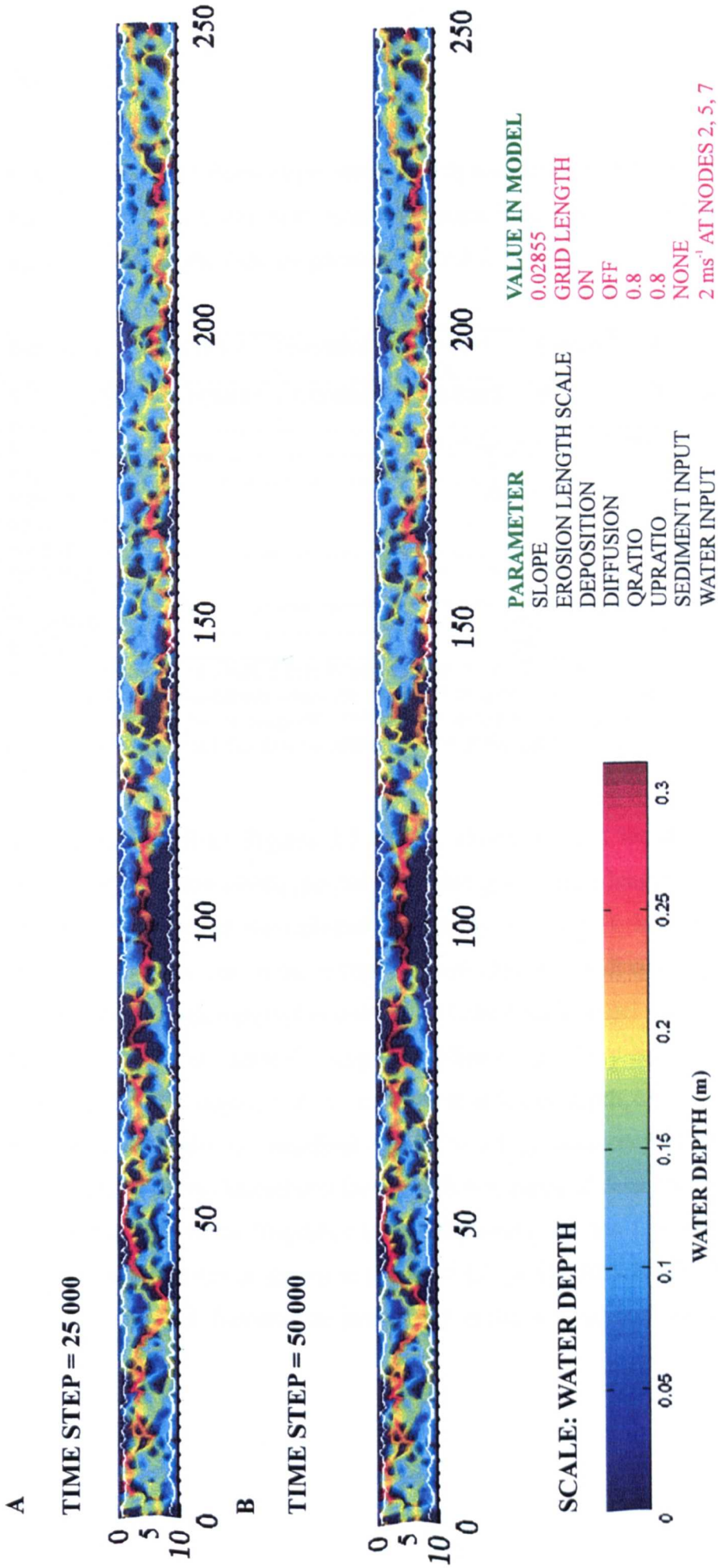


Figure 5.11. Diagram showing channel evolution for a run with the erosion length scale equal to the length of the grid (250). Top: after 25 000 timesteps. Bottom: after 50 000 timesteps. Colour bar indicates water depth. Flow is from left to right.

Figures 5.7 to 5.11 show water depth at each node after 25 000 and 50 000 timesteps for five runs conducted with different erosion length scales (and with no sediment input). Details of the runs are given in Table 5.3.

Run name	Length 1	Length 2	Control run	Length 3	Length 4	Length 5
Erosion length scale (m)	0.00001*	1.00402**	10.0402	50	100.402	250***
Discharge	2 units of water at nodes 2, 5 and 7					
Slope	0.02855					
Splitting ratios (qratio and upratio)	Both 0.8					
Sediment input****	No / Yes					
Deposition	on					
Diffusion	off					

Table 5.3 Details of runs with different length scales for erosion. \*0.00001 is used to approximate zero to avoid numerical instabilities within the model. \*\* Erosion length scale equals average nodal density ( $\Delta$ ; as calculated by the program). \*\*\* Erosion length scale equals grid length. \*\*\*\* One set of experiments was carried out with no sediment input at the top of the grid and one set with sediment input.

As can be seen from Figures 5.7 to 5.11 shorter erosion length scales lead to the erosion of one main stable channel down the grid, longer length scales lead to more channels. The spatial data plotted in Figures 5.7 to 5.11 may be summarised as frequency distributions of water depth in each channel. In all runs, the total volume of water added at each timestep was  $6\text{m}^3\text{ s}^{-1}$ ; if one main channel forms, all water should be captured by this channel. Using the hydraulic geometry equation of Ergenzinger (1987) for water depth,  $6\text{m}^3\text{ s}^{-1}$  equates to a water depth of 0.312 m. Runs with numerous channels (i.e. braiding) will have a high frequency of shallow channels; runs with one main channel will have a high frequency of deep channels. A histogram of water depth versus frequency (as a proportion) for the five runs with different erosion length scales is shown in Figure 5.12. In Figure 5.12 dry areas of the grid have been omitted, however the percentage of dry area for each run is given in Table 5.4.

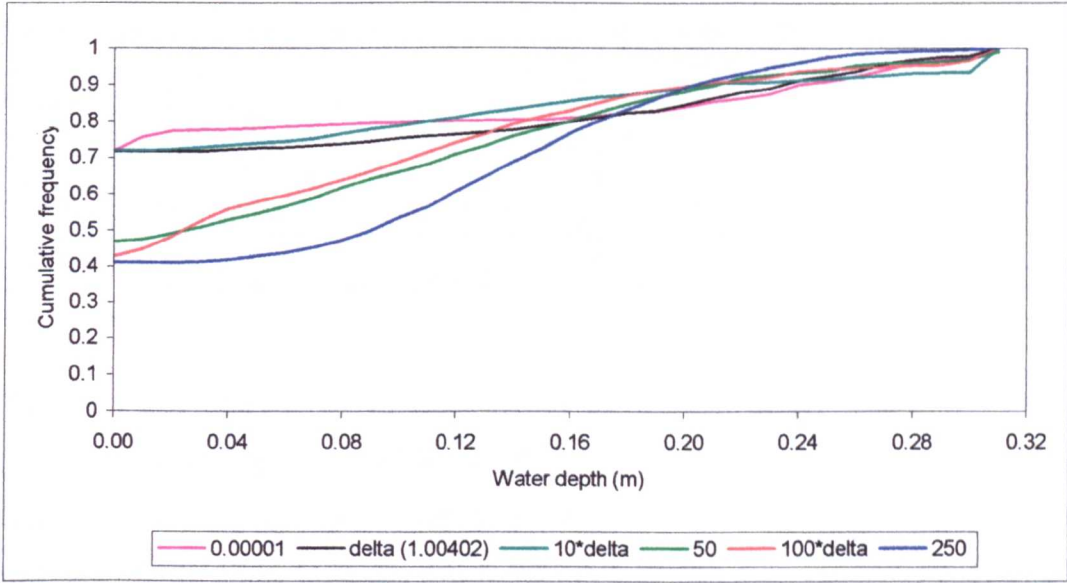
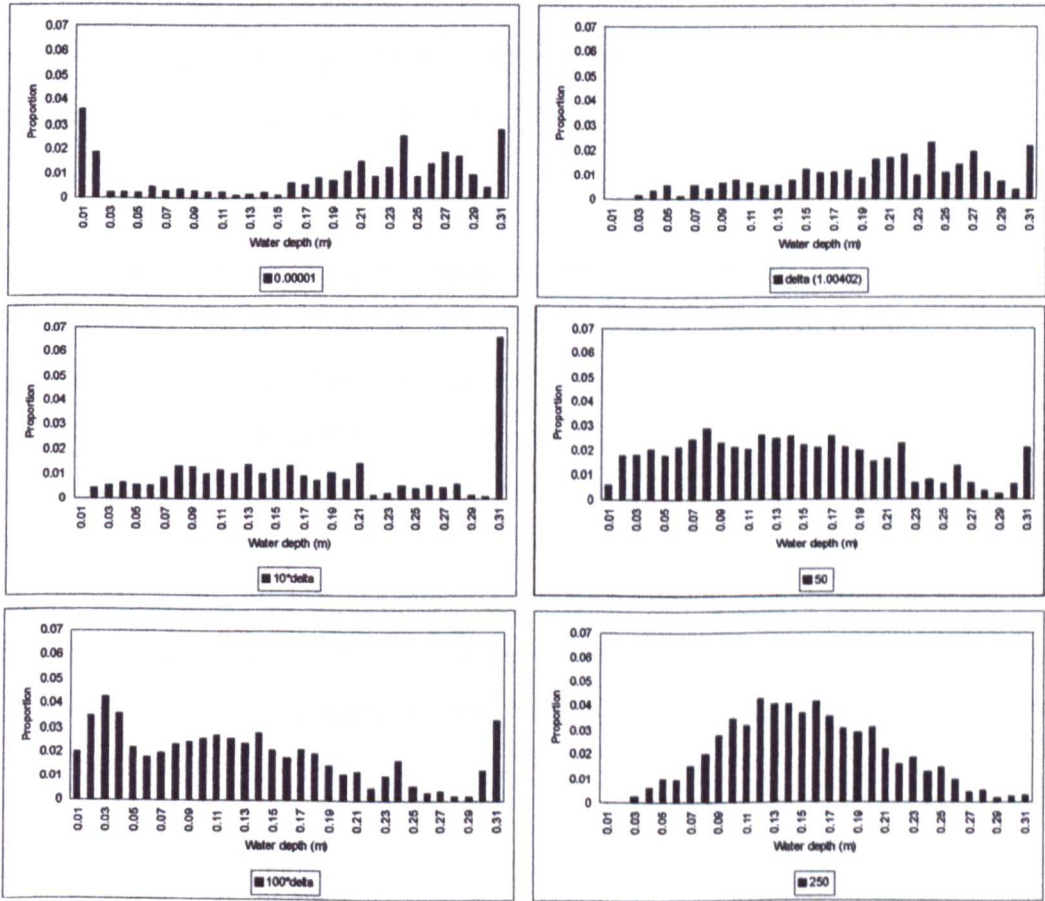


Figure 5.12a. Cumulative frequency curve of water depth for runs of different length scales.



5.12b. Histograms of proportion of nodes with different water depth after 50 000 iterations for runs with different erosion length scales and no sediment input. Dry nodes (i.e. water depth = 0) have been omitted. Bins are in steps of 0.01m. 10\*delta = control run.

Run Name (erosion length scale)	% dry area after 50 000 timesteps. Runs with NO sediment input.
Length 1 (0.00001)	72.1
Length 2 (1.00402)	71.9
Control run (10.0402)	72.0
Length 3 (50)	46.8
Length 4 (100.402)	42.8
Length 5 (250)	41.0

Table 5.4. Percentage dry area after 50 000 timesteps in runs with different erosion length scales and NO sediment input.

Table 5.4 and Figure 5.12 indicate that as the erosion length scale increases, the proportion of the grid covered by water decreases and more shallow channels are formed. There seems to be an abrupt transition in the proportion of dry areas, this transition takes place at length scales between 50 and 100\* $\Delta$ . A small erosion length scale leads to one stable channel eroding on the grid, this channel captures all of the flow leading to a greater frequency of nodes with a high water depth and an increased proportion of dry areas on the grid.

Shorter length scales imply that the model reaches carrying capacity within a very short distance of the node experiencing erosion or deposition, therefore fluvial erosion will be transport limited. Transport of eroded material is capacity-limited and may therefore be intermittent, thus the rate of bed material transport is almost entirely a function of the transporting capacity of the flow (Knighton, 1984). This may be compared with the landscape evolution models of Howard *et al.* (1994, 1997) and Willgoose *et al.* (1991a-d, 1994), neither of which incorporates a spatial lag component. In the model of Howard *et al.* (1994, 1997), fluvial erosion is advective and in alluvial channels fluvial erosion is transport limited. Willgoose's model is transport limited, i.e. it assumes that there are adequate supplies of erodible materials in the catchment.

Run name	Erosion length scale	Minimum (erosion) (m)	Maximum (deposition) (m)	Mean (m)	Standard deviation (m)	Sum (net erosion / deposition)
Length 1	0.00001	-0.510	0.103	-0.0209	0.070	-52.1
Length 2	1.00420	-0.523	0.094	-0.0156	0.061	-39.0
Control run	<b>10.0402</b>	<b>-1.340</b>	<b>0.093</b>	<b>-0.0283</b>	<b>0.220</b>	<b>-132</b>
Length 3	100.402	-0.640	0.101	-0.0082	0.088	-20.5
Length 4	250	-0.187	0.072	0.0004	0.012	1.03

Table 5.5. Details of the total amount of erosion/deposition for runs with different length scales (3 s.f.).

Table 5.5 gives details of the runs in terms of total amounts of erosion and deposition. The grids for all runs except the run with a spatial lag of 250 experience net erosion (Table 5.5), as a result of the upstream boundary condition of an erodible boundary and no sediment input. The greatest amount of erosion occurs during the control run, in which the value of the spatial lag was set to the default value used for the original version of *Cascade*. When the erosion length scale was set to equal the length of the grid, (i.e. 250 m), the grid experienced net deposition, this was also the run with the greatest number of channels at the downstream end of the grid after 50 000 timesteps (Figure 5.11); all other runs created one main channel which was relatively stable at the downstream end.

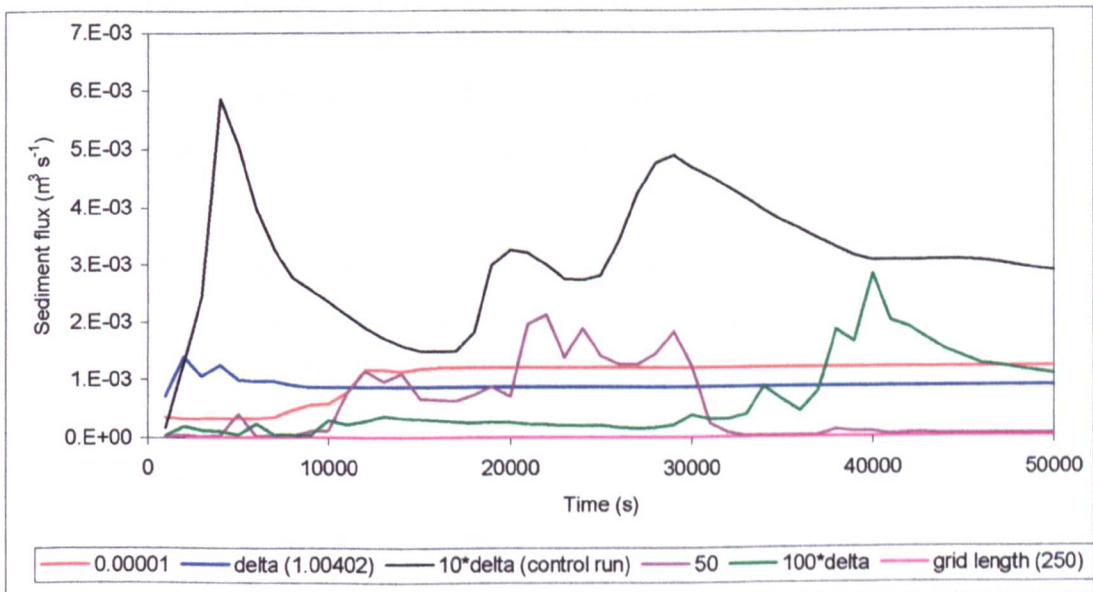


Figure 5.13. Time series of sediment outflux from runs with different erosion length scales.

Figure 5.13 and Table 5.5 show that flux is not a simple result of braiding intensity. Lag effects are not linear; therefore, the maximum erosion in the control run is due to the interaction between spatial lag itself and the effect of the lag on channel pattern. Thus, spatial lag leads to controls on braiding, which in turn control the net sediment output. This suggests that the length scale affects the braiding process but not (directly) the flux. Therefore braiding moderates total flux, however it is difficult at this stage to eliminate spatial lag impacts on total flux.

When sediment outflux from each run is considered (Figure 5.13) it can be seen that the greatest variation in sediment outflux occurs in the control run. When the erosion length scale is very short (0.00001) or very long (250) the model settles into a stable state and sediment outfluxes remain static for long periods. For short spatial lags, (less than or equal to the nodal spacing) the model quickly evolves to a static state with one main channel and a constant sediment output. With an erosion length scale of  $100 \times \Delta$  (100.402) sediment outflux rises to a peak at around 40 000 iterations then decreases towards the end of the run. With a long spatial lag, (e.g. equal to the grid length) many shallow channels are formed but these are stable and the volume of sediment output is small and constant. Therefore, from Figure 5.13 it is clear that only three runs where the channels keep evolving are the control run and the run with erosion length scales equal to 50 and to  $100 \times \Delta$ ; all other runs (i.e. runs with very short or very long spatial lags) tend to settle into static states.

The runs were repeated (excepting run with length scale = 50), with sediment added to the upstream end of the grid at every timestep. The amount of sediment added was constant throughout each run and the same for every run. The sediment added was set to equal the equilibrium sediment transport of the nodes on the upstream boundary for the first timestep in the control run. Therefore, for run under different conditions, sediment input will not be at equilibrium. Figures 5.14 to 5.17 show the spatial distribution of channels in each run after 25 000 and 50 000 timesteps. The results are summarised in Figure 5.18, showing the frequency of water depths at each node

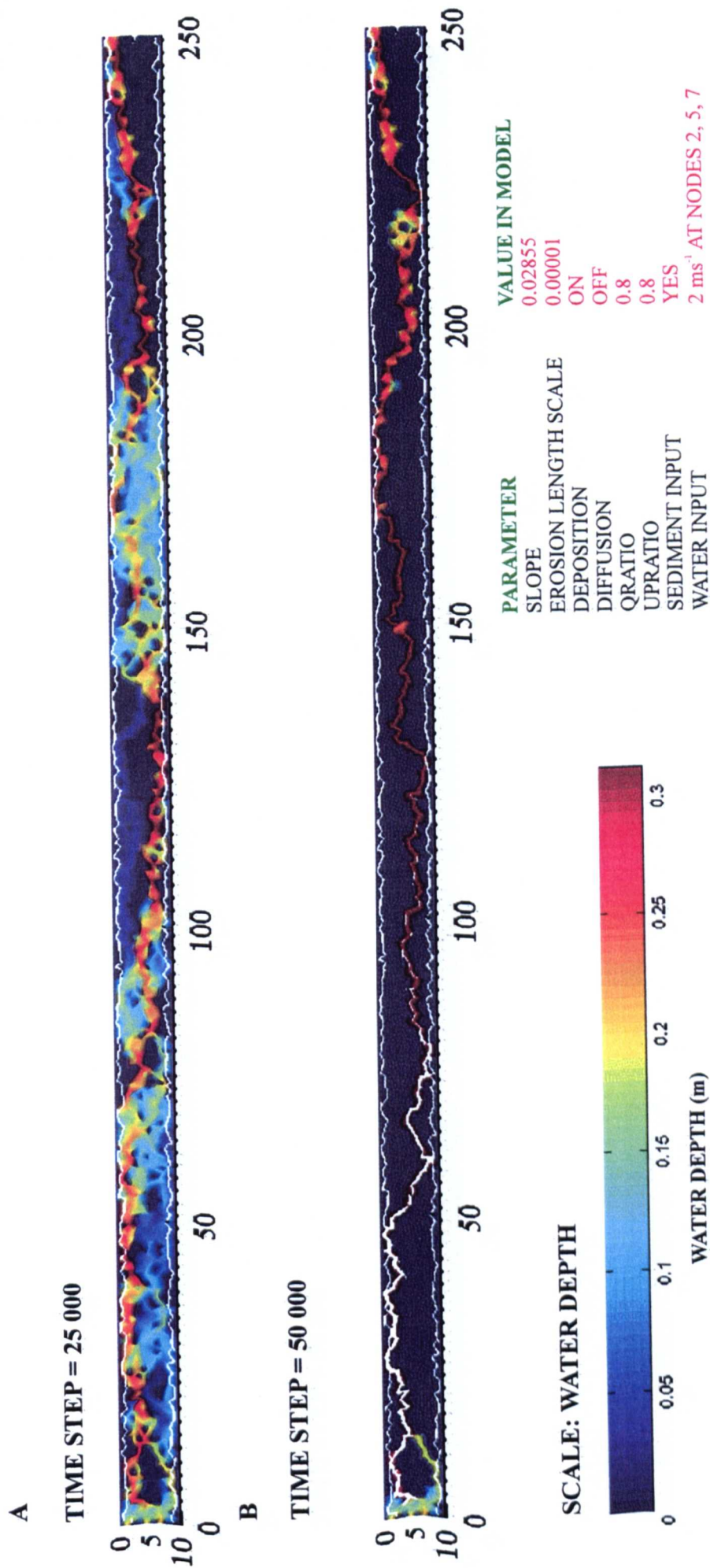


Figure 5.14. Diagram showing channel evolution for a run with the erosion length scale set to 0.00001 and sediment input at the upstream end of the grid.

Top: after 25 000 timesteps. Bottom: after 50 000 timesteps. Colour bar indicates water depth. Flow is from left to right.

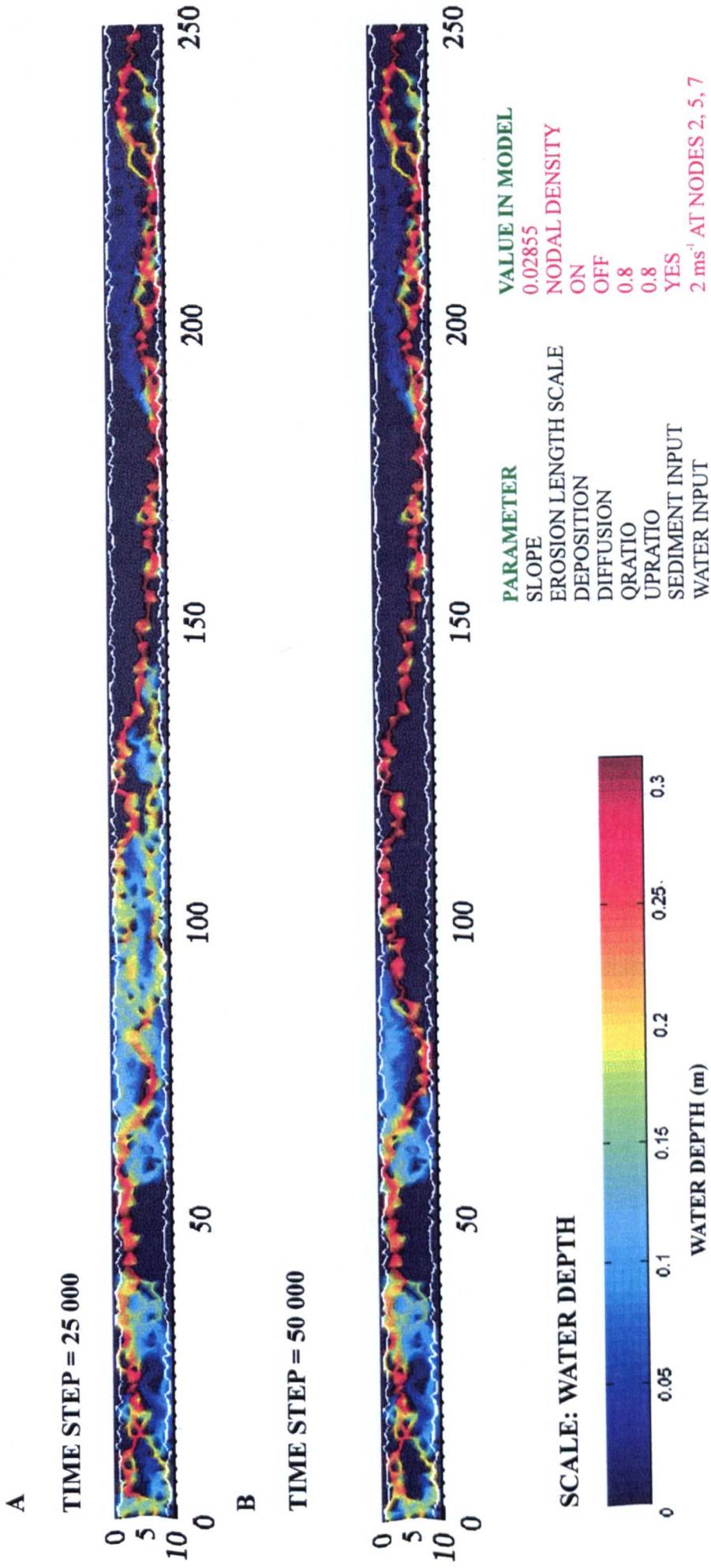


Figure 5.15. Diagram showing channel evolution for a run with the erosion length scale equal to the nodal density and sediment input at the upstream end of the grid.  
 Top: after 25 000 timesteps. Bottom: after 50 000 timesteps.  
 Colour bar indicates water depth. Flow is from left to right.

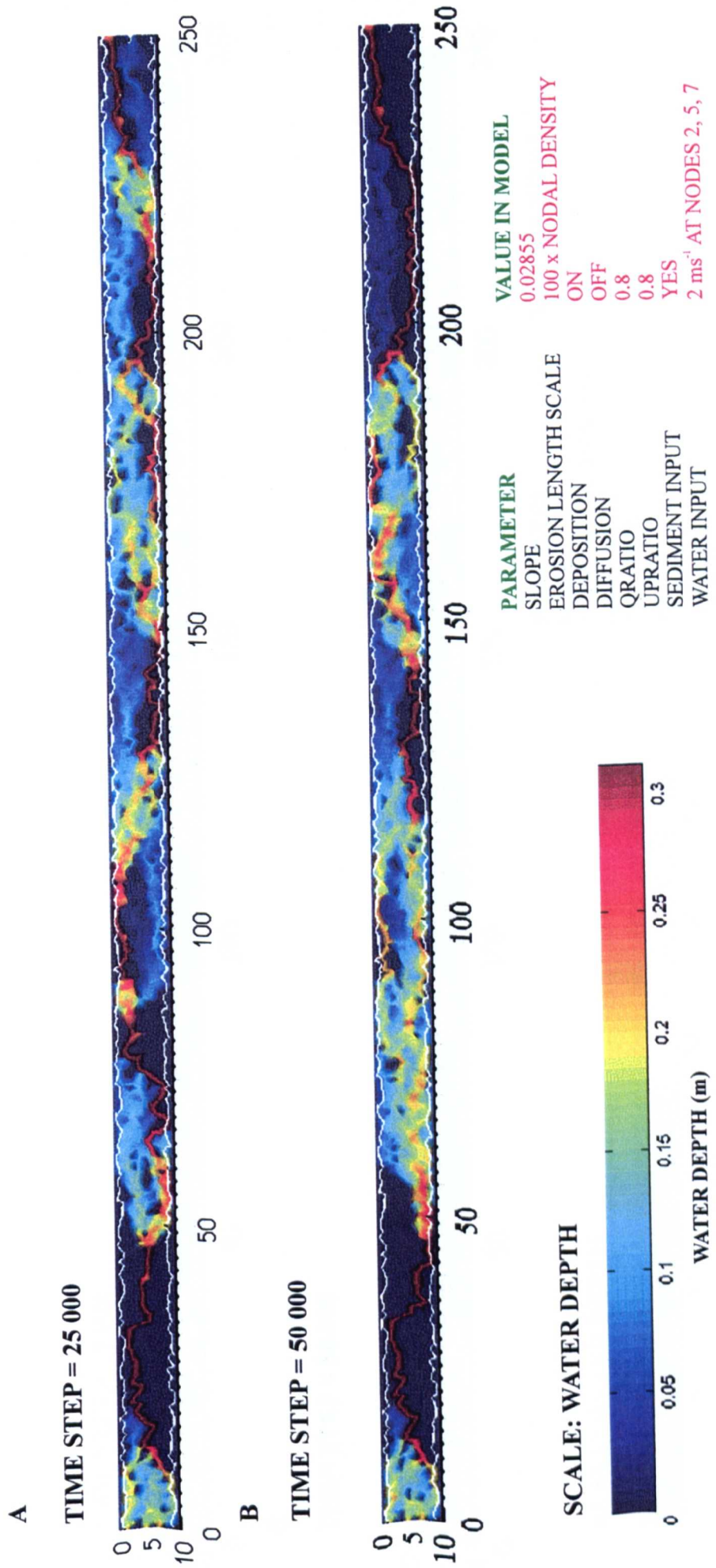


Figure 5.16. Diagram showing channel evolution with erosion length scale equal to 100 times the nodal density and sediment input at the upstream end of the grid. Top: after 25 000 timesteps. Bottom: after 50 000 timesteps. Colour bar indicates water depth. Flow is from left to right.

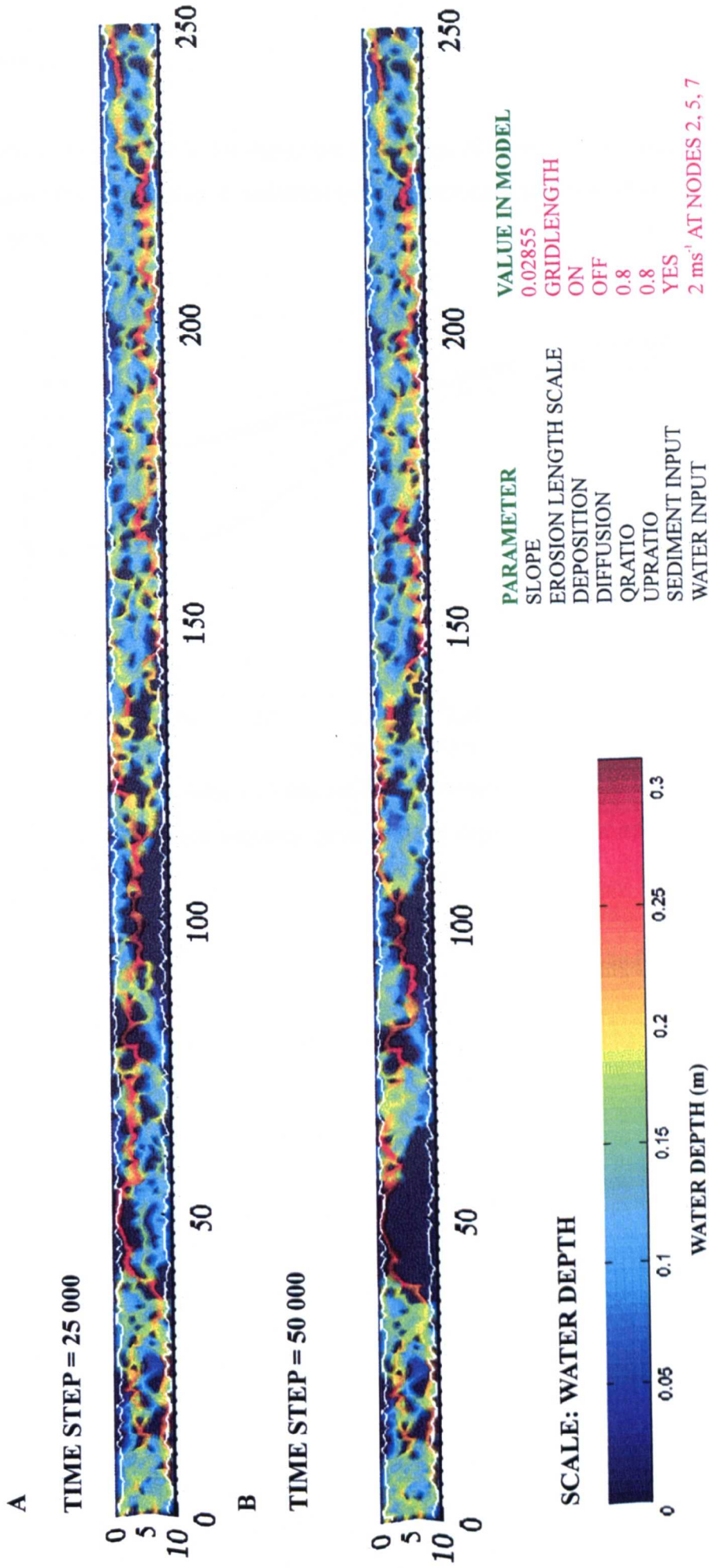


Figure 5.17. Diagram showing channel evolution for a run with the erosion length scale set to the length of the grid and sediment input at the upstream end of the grid.  
 Top: after 25 000 timesteps. Bottom: after 50 000 timesteps.  
 Colour bar indicates water depth. Flow is from left to right.

across the grid. Table 5.6 shows the percentage dry areas of each grid and Figure 5.19 shows the time series of sediment output from each grid for different erosion length scales.

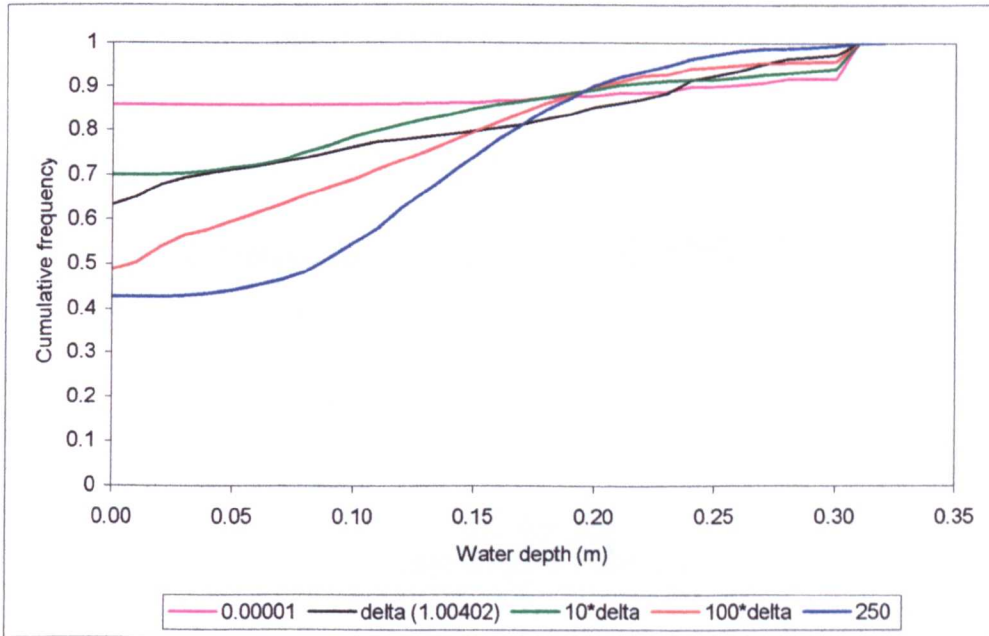
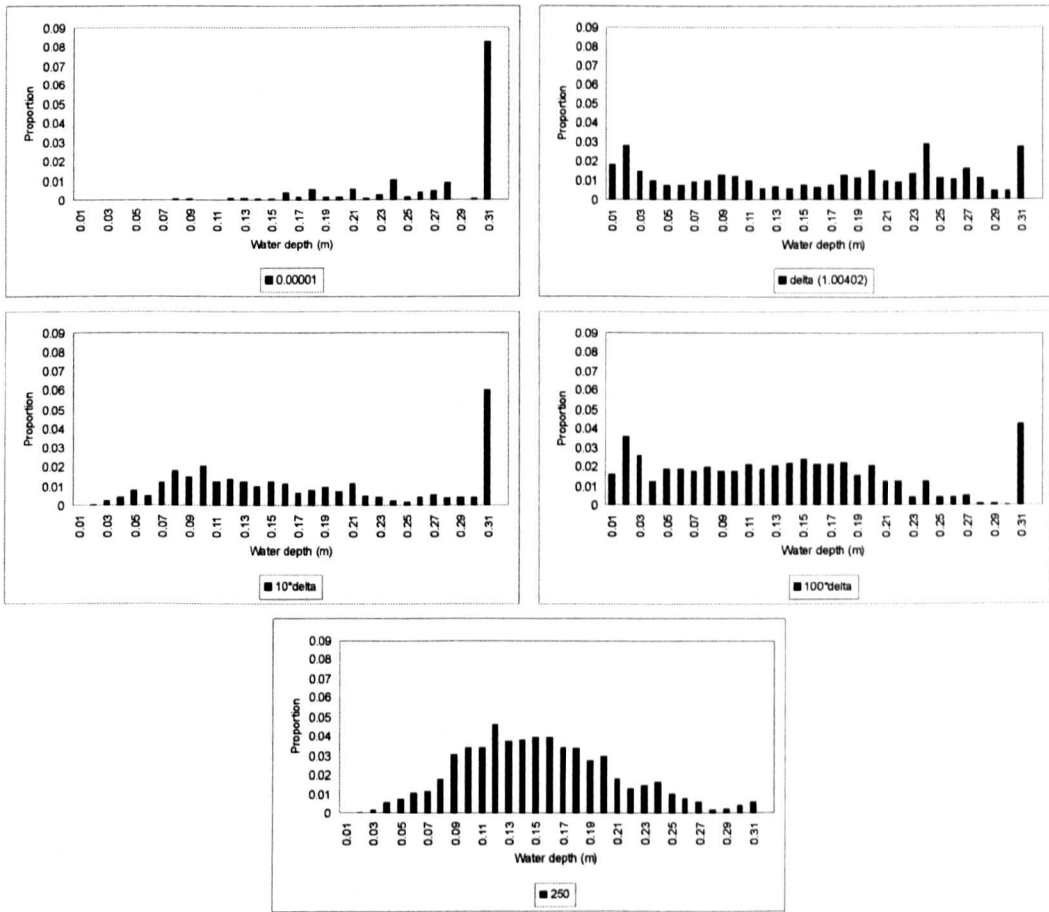


Figure 5.18a. Cumulative frequency curves of water depth for runs of different length scales and sediment input



5.18b. Histograms of proportion of nodes with different water depth after 50 000 iterations for runs with different erosion length scales and sediment input. Nodes with no water have been omitted.

Run Name	% dry area after 50 000 timesteps. Runs WITH sediment.
Length 1 with sediment	85.8
Length 2 with sediment	63.2
Control run with sediment	70.0
Length 4 with sediment	48.8
Length 4 with sediment	42.7

Table 5.6. Percentage dry area after 50 000 timesteps in runs with different erosion length scales and WITH sediment input.

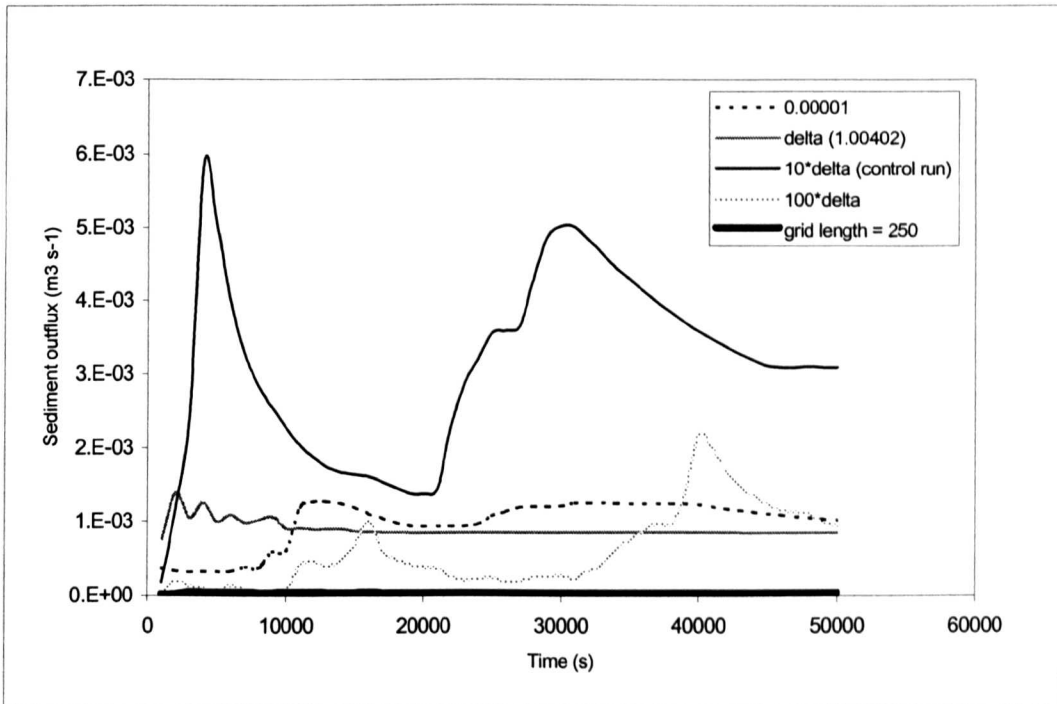


Figure 5.19. Time series of sediment outflux from runs with different erosion length scales and sediment input.

Run name	Erosion length scale	Minimum (erosion) (m)	Maximum (deposition) (m)	Mean (m)	Standard deviation (m)	Sum (net erosion / deposition)
Length 1 (sed)	0.00001	-6.63	69.5*	-0.250	1.83	-625
Length 2 (sed)	1.00402	-0.312	3.46*	-0.00304	0.174	-7.6
Control run (sed)	10.0402	-1.32	3.46*	-0.0374	0.268	-93.5
Length 4 (sed)	100.402	-0.335	3.46*	0.0073	0.194	18.3
Length 5 (sed)	250	-0.232	69.5*	0.0497	1.43	124

Table 5.7. Details of the total amount of erosion / deposition for runs with different erosion length scales and with sediment input (to 3 s.f.). \*Maximum deposition occurred at the upstream end of the grid where the sediment was being added.

The addition of sediment to the grid does not result in significantly different channel patterns (for runs with the same initial conditions). Sediment input results in more active channels at the upstream end of the grid (i.e. the model does not produce one main channel at the upstream end of the grid and channels in this location continue to evolve throughout the run), for longer a duration throughout each run. From Figure

5.19, the total volume of sediment outputted from the model runs is higher for runs with sediment input than for runs without sediment input. However once again Figure 5.19 indicates that for very short and very long erosion length scales the model reaches static states. Table 5.7 indicates that for all runs the maximum deposition occurred at the upstream end of the grid. Very short and very large length scales result in sediment amassing at the upstream end of the grid (Table 5.7); sediment input is obviously not at equilibrium in these conditions. For the other runs a maximum amount of deposition is reached but is moderated by the transport rate, which is in turn affected by the length scale.

Therefore, it can be concluded that significantly different results do occur for runs with different erosion length scales. Very short erosion length scales tend to produce one main stable channel on the grid that captures all of the flow. Sediment output from these runs fluctuates as the channel is evolving then becomes constant when the channel has been eroded. These results indicate that for braiding to occur there must be a large disequilibrium between the sediment available for transport and the transporting capacity of the flow. In other words, in the presence of a constrained upstream boundary, a braided system will evolve if the network is not immediately able to overcome the constraint. However, if the spatial lag is very long, *Braided Cascade* will tend to evolve to a static state with no channel evolution and constant sediment output.

#### **5.4.2. The effect of no deposition.**

Brotherton (1979) differentiates between depositional braiding patterns (which develop in response to depositional induced erosion) and erosional braids which are initiated directly by a discharge with excess shear stress. Paola (2001) and Murray and Paola (1994, 1997) demonstrate the importance of deposition in braiding. Braided networks balance confluences and diffluences (tributaries and distributaries), and require equal measures of erosion and deposition: reversible entrainment. Cohesionless sediments are eroded and redeposited in response to local gradients in

flow strength (Paola 2001). Deposition is the main process for the development of braiding via central bar deposition, however all other mechanisms require erosion and subsequent reworking of deposits (see Chapter 2, Table 2.1). A dendritic topology is the product of irreversible entrainment; once eroded material cannot readily be redeposited (Paola, 2001) and, without redeposition, once the flow gathers it can never split. Murray and Paola (1994, 1997) demonstrated the importance of deposition in the evolution of braided networks in their cellular automata model. If deposition was prevented the drainage system that evolved was dendritic rather than braided; channels formed anywhere on the grid and a dendritic erosion pattern resembling rills developed (Murray and Paola 1994, 1997; Paola, 2001). However, in these experiments water was introduced over the whole grid surface, and not introduced only at the upstream boundary.

A simulation in which there was no deposition was conducted to investigate the role of deposition in producing a braided channel network; Figure 5.20 shows water depth after 25 000 and 50 000 iterations of this run. Water was introduced to the upstream boundary of the grid only. As can be seen from Figure 5.20 one stable main channel is quickly eroded and is stable for over 25 000 iterations. This result is very similar to the control run (Figure 5.20) however the channels in the run without deposition established themselves more quickly due to the fact that all sediment, once entrained, was removed from the system (Figure 5.21). The model results suggest that instead of the ongoing change of the braided system, static dendritic patterns develop without local redeposition. Dendritic channel patterns also formed using the original version of *Cascade* as a long-term landscape evolution model with rainfall over the whole grid (see Braun and Sambridge, 1997).

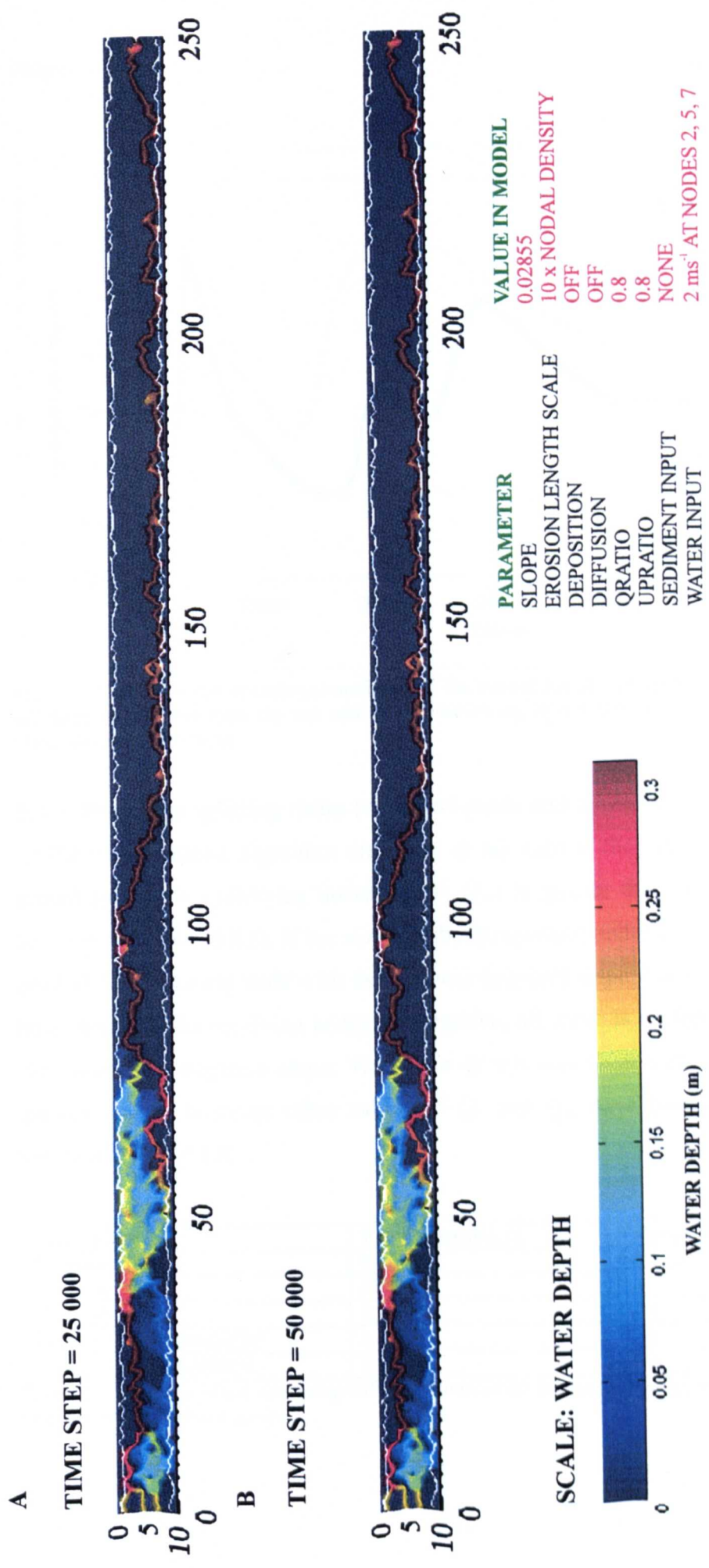


Figure 5.20. Diagram showing channel evolution for a run with no sediment deposition. Top: after 25 000 timesteps. Bottom: after 50 000 timesteps. Colour bar indicates water depth. Flow is from left to right.

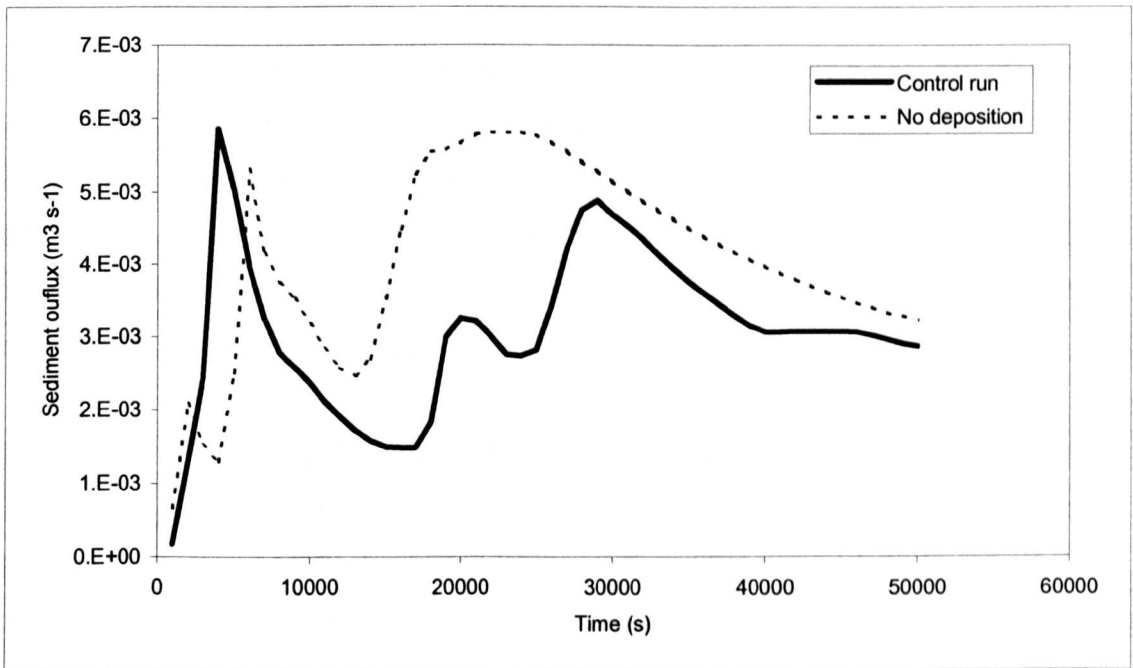


Figure 5.21. Time series of sediment outflux from the control run and a run with no deposition. More sediment is removed from the run with no deposition as, in this run, all sediment entrained was removed from the system.

**5.4.3. Discharge splitting ratios (values of *qratio* and *upratio*).**

In the water routing algorithm discharge is not split if the ratio of the discharges routed to the two receiving nodes ( $Q_r$  or  $Q_{ru}$ ) is greater than 0.8, (see Chapter 3 sections 3.8.1 and 3.8.2). If the slopes to both receiving nodes are positive, all water goes to the receiving node with the steepest downhill slope from the donor node; if both slopes to the receiving nodes are negative, all water is routed to the node with the least steep negative slope. The value of 0.8 was chosen as a reasonable first approximation, however other values of  $Q_r$  and  $Q_{ru}$  have been tested, these are outlined in Table 5.8.

Run name	Value of <i>qratio</i> , $Q_r$	Value of <i>upratio</i> , $Q_{ru}$
Control run	0.80	0.80
Dratio0.95	0.95	0.95
Dratio0.5	0.50	0.50
Qratio0.8 upratio0.95	0.80	0.95
Qratio0.95 upratio0.8	0.95	0.80

Table 5.8. Summary of test runs using different values of the discharge ratios  $Q_r$  and  $Q_{ru}$ . Dratio = both *qratio* and *upratio*.

Values of  $Q_r$  and  $Q_{ru}$  were varied together and individually (Table 5.8) to test whether water routing along positive or negative bed slopes is more important for braiding. In theory the greater the value of the discharge ratios, the easier it should be for discharge to split and be distributed to both receiving nodes and vice versa. This is because it should be unusual to have high slope ratios (unless of course the model has eroded a canyon with steep slopes).

The models of Murray and Paola (1994, 1997) and Thomas and Nicholas (2002) do not have the ability to constrain flow divergence; all water in one cell is split between the three (Murray and Paola, 1994, 1997) or five (Thomas and Nicholas, 2002) downstream cells according to the local bed slope to each downstream cell. The ability to constrain flow divergence is a purely model parameter and has no direct equivalence in prototype rivers, however in practise it may be thought of as a momentum related term. The parameter has been tested to determine it's sensitivity for model output.

Figures 5.22 to 5.25 show results of runs with different values of  $Q_r$  and  $Q_{ru}$  (and with no sediment input), Figures 5.26 to 5.28 show results of the same runs but with sediment input at the upstream end of the grid. The spatial results are summarised in Figures 5.28a-b (runs without sediment) and 5.29a-b (runs with sediment), percentage dry areas of each grid are given in Table 5.9.

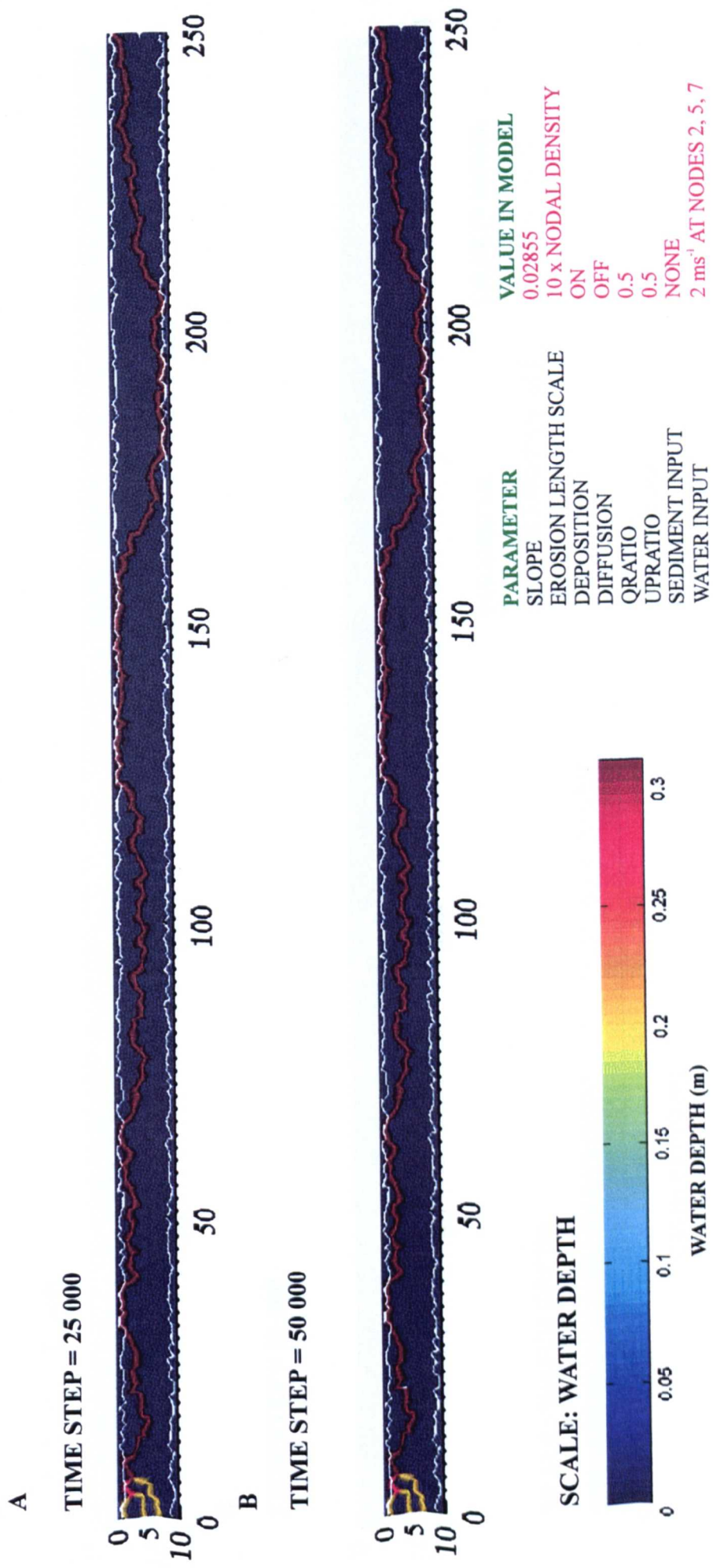


Figure 5.22. Diagram showing channel evolution for a run with qratio and upratio set to 0.5. Top: after 25 000 timesteps. Bottom: after 50 000 timesteps. Colour bar indicates water depth. Flow is from left to right.

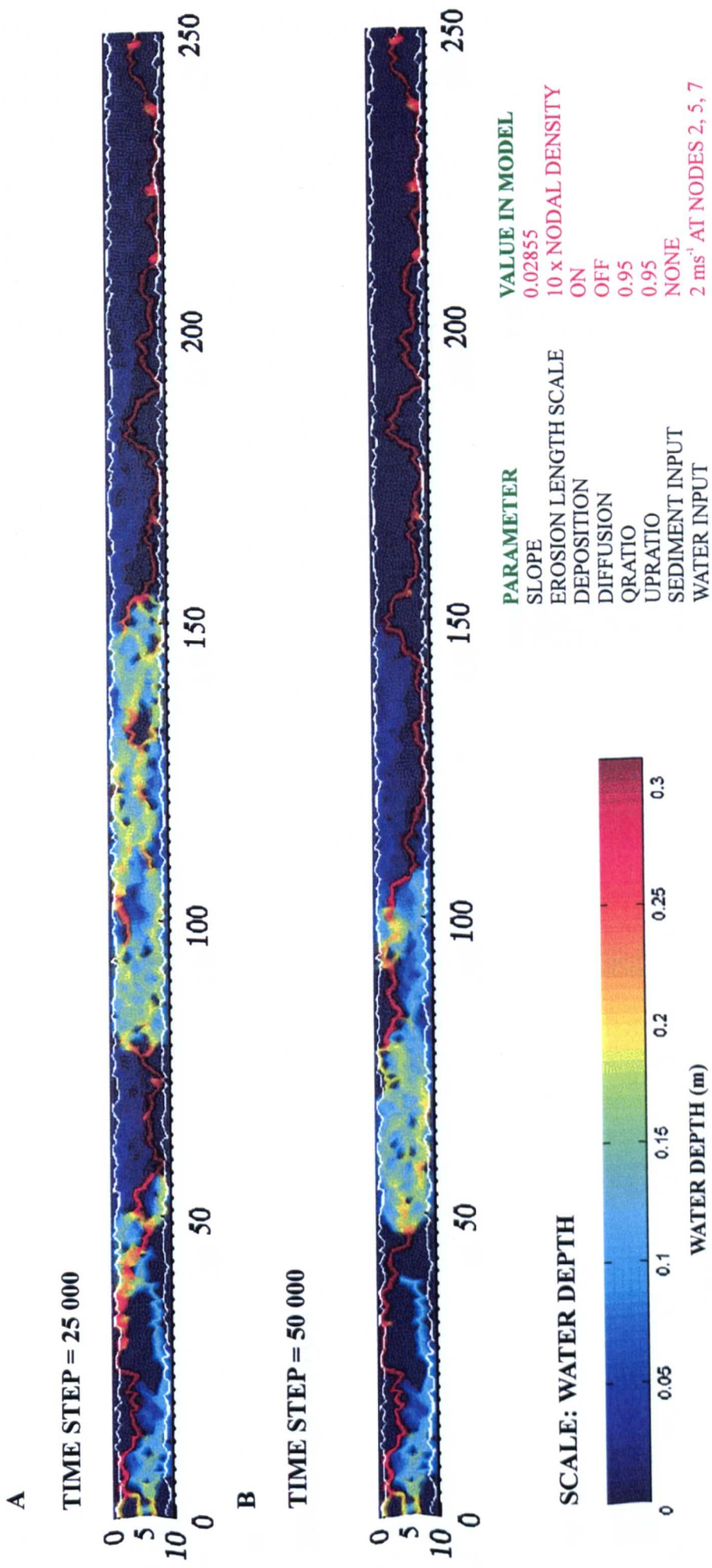


Figure 5.23. Diagram showing channel evolution for a run with qratio and upratio set to 0.95. Top: after 25 000 timesteps. Bottom: after 50 000 timesteps. Colour bar indicates water depth. Flow is from left to right.

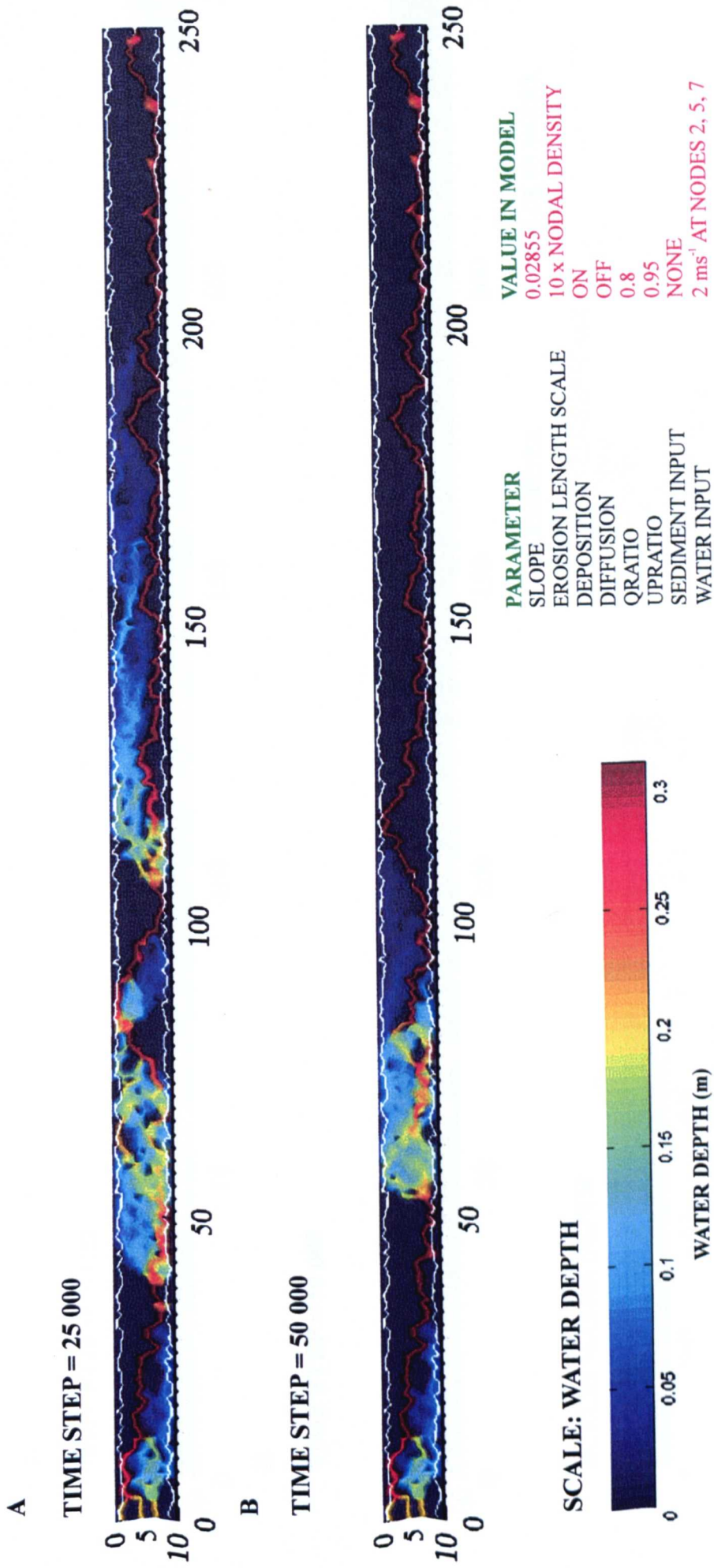


Figure 5.24. Diagram showing channel evolution for a run with qratio = 0.8 and upratio = 0.95. Top: after 25 000 timesteps. Bottom: after 50 000 timesteps. Colour bar indicates water depth. Flow is from left to right.

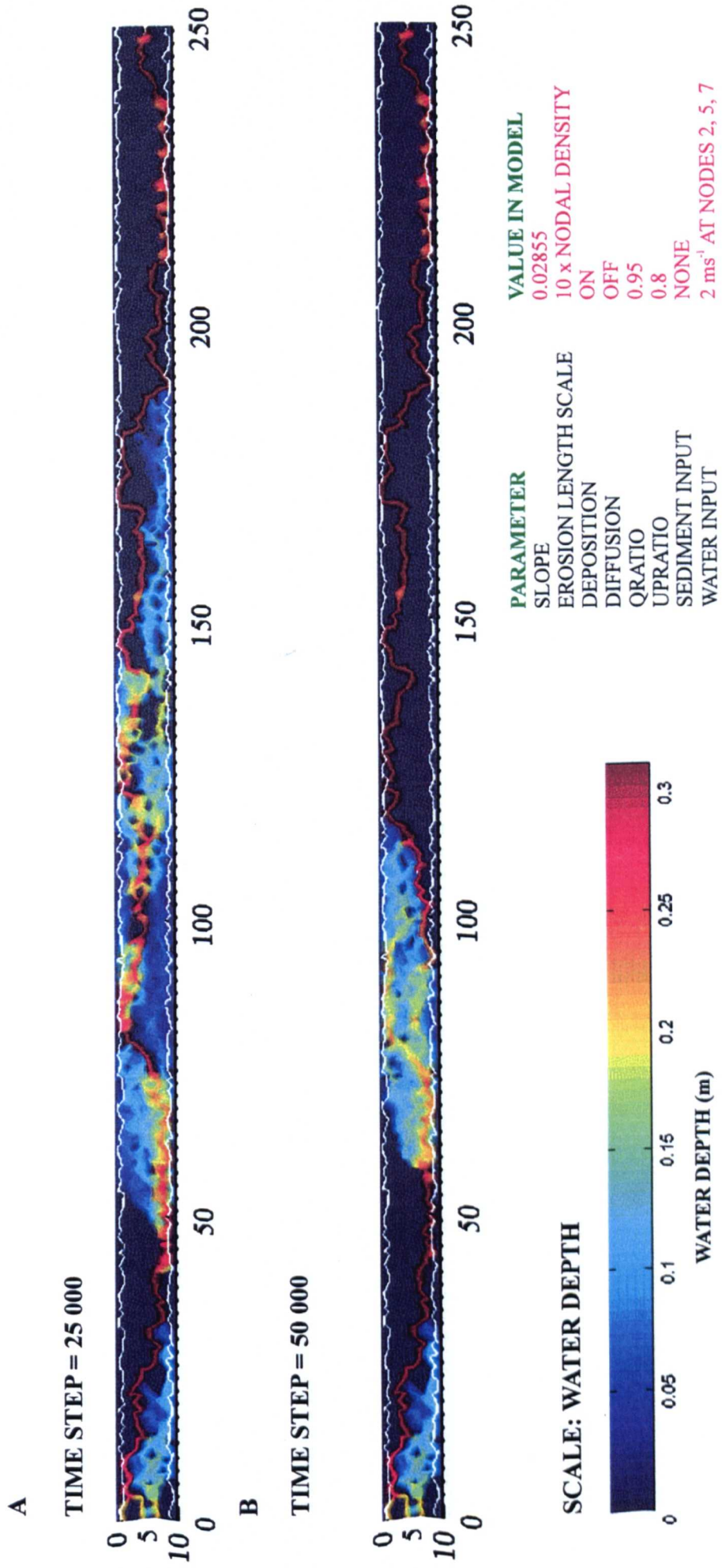


Figure 5.25. Diagram showing channel evolution for a run with qratio = 0.95 and upratio = 0.8. Top: after 25 000 timesteps. Bottom: after 50 000 timesteps. Colour bar indicates water depth. Flow is from left to right.

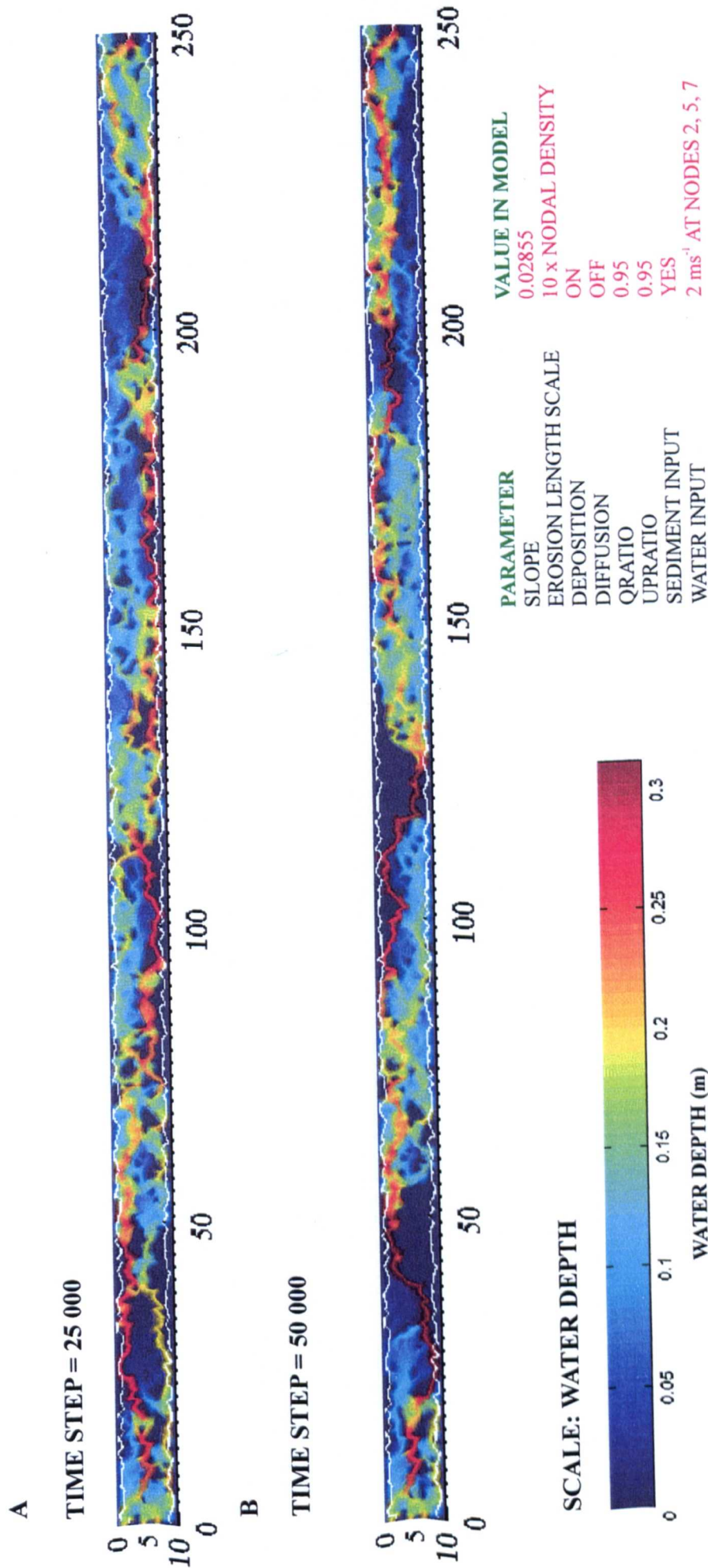


Figure 5.26. Diagram showing channel evolution for a run with qratio and upratio set to 0.95 and sediment input at the upstream end of the grid.  
Top: after 25 000 timesteps. Bottom: after 50 000 timesteps.  
Colour bar indicates water depth. Flow is from left to right.

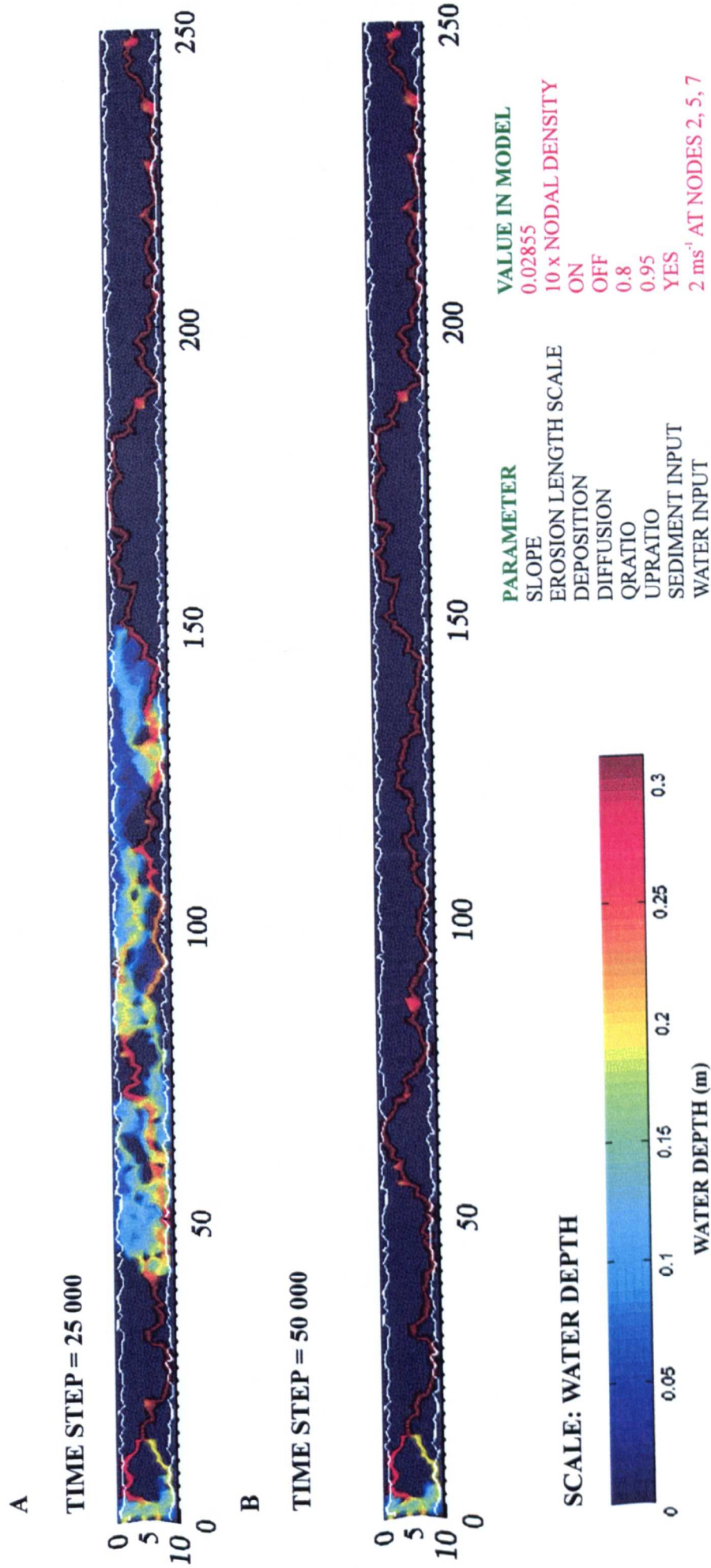


Figure 5.27. Diagram showing channel evolution for a run with  $qratio = 0.8$  and  $upratio = 0.95$  and sediment input at the upstream end of the grid..  
Top: after 25 000 timesteps. Bottom: after 50 000 timesteps.  
Colour bar indicates water depth. Flow is from left to right.

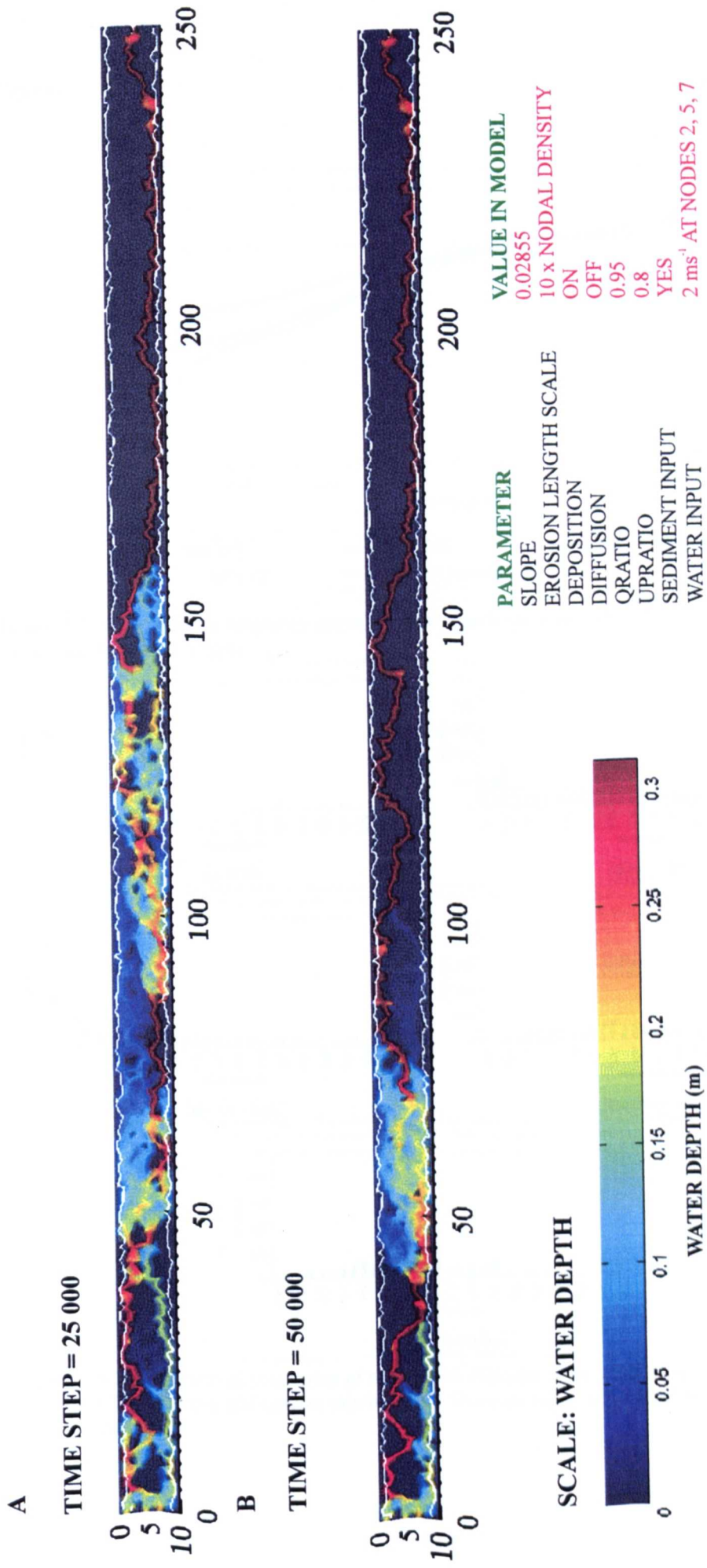


Figure 5.28. Diagram showing channel evolution for a run with qratio = 0.95 and upratio = 0.8 and sediment input at the upstream end of the grid..  
 Top: after 25 000 timesteps. Bottom: after 50 000 timesteps.  
 Colour bar indicates water depth. Flow is from left to right.

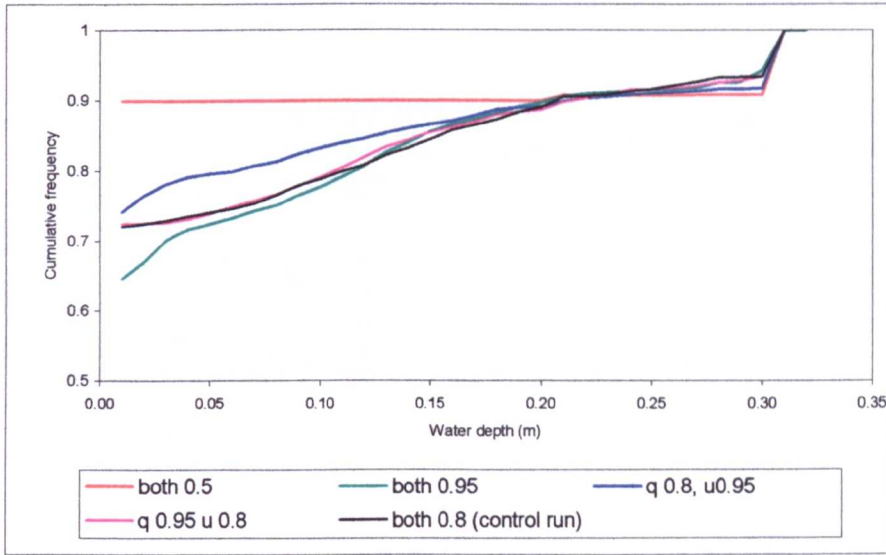


Figure 5.29a. Cumulative frequency curve of water depth for runs with different qratio and upratio values and no sediment input.

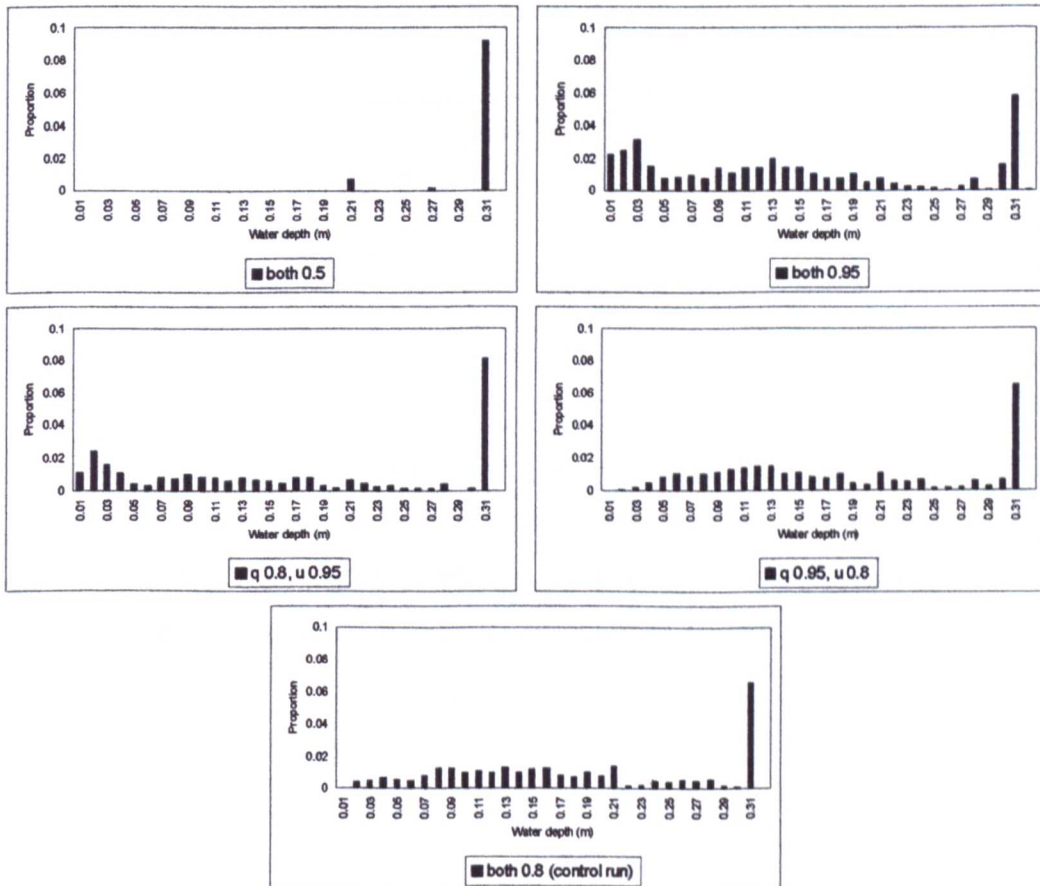


Figure 5.29b. Histograms of proportion of nodes with different water depth after 50 000 iterations for runs with different qratio and upratio values and no sediment input. Dry nodes have been omitted. q= qratio, u = upratio.

Run Name	% dry area after 50 000 timesteps. Runs with NO sediment.	% dry area after 50 000 timesteps. Runs WITH sediment.
Control run	72.0	70.4
Dratio 0.95	62.2	51.0
Dratio 0.5	89.9	-
Qratio 0.8, upratio 0.95	73.0	87.8
Qratio 0.95, upratio 0.8	72.4	75.9

Table 5.9. Percentage dry area after 50 000 timesteps in runs with different discharge ratios with and without sediment input.

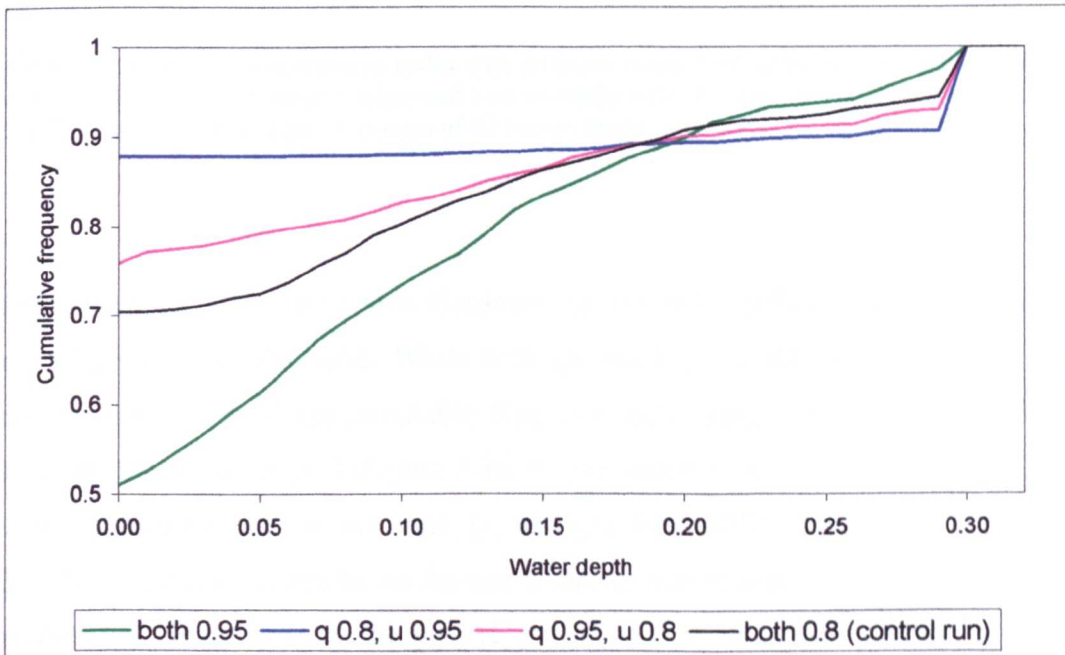
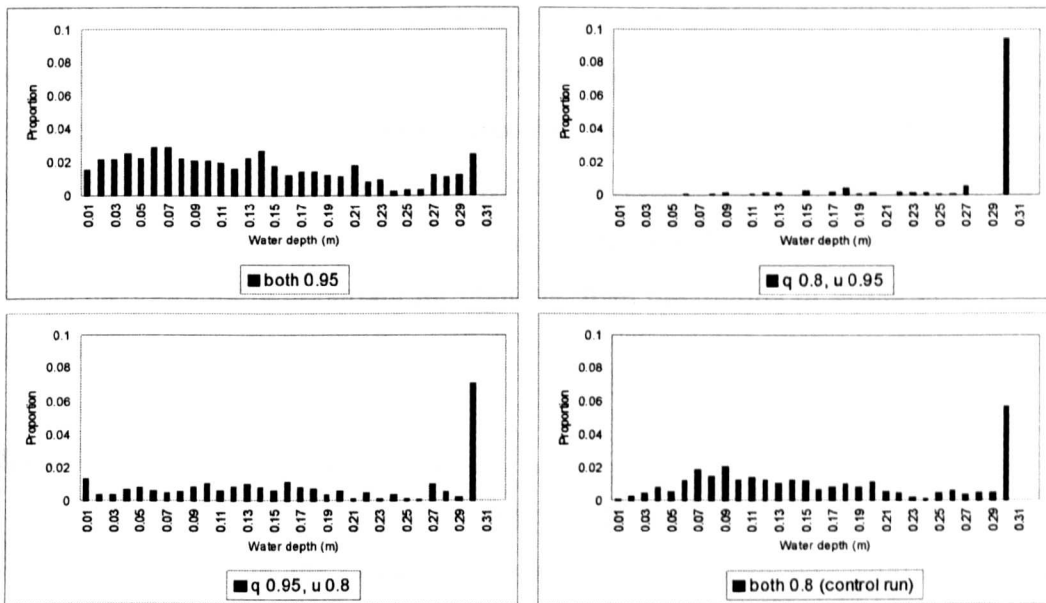


Figure 5.30a. Cumulative frequency curve of water depth for runs with different qratio and upratio values and sediment input.



5.30b. Histograms of proportion of nodes with different water depth after 50 000 iterations for runs with different qratio and upratio values and with sediment input. Nodes with no water (i.e. water depth = 0) have been omitted. Bins are in steps of 0.01m. q= qratio, u = upratio.

From the figures, it can be seen that lower values of  $Q_r$  and  $Q_{ru}$  lead to greater flow convergence and vice versa. When both  $Q_r$  and  $Q_{ru}$  are set to equal 0.5 the flow quickly resolves itself into one stable channel, which incises, captures all the flow and runs the length of the grid (Figure 5.30, no run was carried out  $Q_r$  and  $Q_{ru} = 0.5$  and with sediment input). When both  $Q_r$  and  $Q_{ru}$  equal 0.95 (Figure 5.23) a greater number of shallow channels are formed when compared to the control run, and when sediment is introduced to the grid (Figure 5.26) the channels continue to evolve throughout the course of the run. These results confirm the theory above.

When  $Q_r$  and  $Q_{ru}$  are varied individually the results are more complex. When  $Q_r$  is equal to 0.95 and  $Q_{ru}$  is equal to 0.8 it should be easier for flow to diverge along positive slopes than along negative slopes. From Figures 5.29, and 5.30 it can be seen that compared to the control run, runs with  $Q_r$  equal to 0.95 and  $Q_{ru}$  equal to 0.8 produced more shallow channels. When  $Q_r$  is equal to 0.8 and  $Q_{ru}$  is equal to 0.95

(i.e. it is easier for flow to split along negative slopes than along positive slopes) there are more channels with water depth of approximately 1 to 4 cm (sheet flow) but fewer channels with water depth of approximately 7 to 21 cm when compared to the control run. This is true for both cases (i.e. with and without sediment) and implies that the forcing of water along negative gradients is more important to produce shallow flows, and is therefore more important for braiding, than the routing of water along positive gradients.

#### **5.4.4. Lateral sediment transport.**

Lateral sediment transport removes sediment from the banks of a channel, adding it to the sediment load in the channels and widening the channels. Murray and Paola (1997) report simulations without lateral sediment transport that produce narrower channels that migrate less than those in runs with lateral transport. Murray and Paola (1997) note that in the long term the lateral sediment transport rule is essential for the model to continue to indefinitely exhibit the complex dynamics involving channel switching and channel shifting. Without this rule the model eventually digs itself a canyon that confines the flow, thus reaching a static steady state. The cellular automata model of Thomas and Nicholas (2002) does not include an explicit rule for the transport of sediment on lateral slopes, however as flow is split between five downstream neighbour cells, water may be transported at angles of up to 60 °.

The lateral sediment transport rule in the cellular automata model of Murray and Paola (1994, 1997) applies an algorithm that transports a small amount of sediment from lateral neighbour cells that have higher elevations. This occurs regardless of whether these neighbour cells contain discharge so that any channel bank can erode. The lateral sediment transport rule in the Murray and Paola (1994, 1997) model is based on an expression given explicitly by Parker (1984) for the transverse component of sediment flux  $q_{sl}$ .

$$q_{sl} = \frac{1 + \mu r}{\mu} \left( \frac{\tau_c}{\tau} \right)^{1/2} S_l q_s \quad (5.1)$$

Where:  $l$  denotes the transverse direction,  $r$  is the ratio of lift coefficient to drag coefficient,  $\mu$  is the dynamic coefficient of Coulomb friction,  $\tau_c$  is the critical value of  $\tau$ ,  $S_l$  is the lateral slope and  $q_s$  is the total local sediment flux. Murray and Paola (1994, 1997) neglect the dependence on  $\tau$ , producing:

$$Q_{sl} = K_l S_l Q_{s0} \quad (5.2)$$

where  $Q_{sl}$  is the amount of sediment transported from a lateral neighbour cell into the cell in question,  $Q_{s0}$  is the total sediment load out of the cell in question into the three downstream immediate neighbours and  $K_l$  is a constant adjusted so that  $Q_{sl}$  is on the order of a few percent (the percentage is not explicitly quoted) of  $Q_{s0}$  for typical values of  $S_l$  (Murray and Paola 1997).

An analogue for the above expression exists within some long-term landscape evolution models in the mechanisms used to model short-range transport processes. Short-range transport models represent the cumulative effect of processes (soil creep, landslides, rainsplash, surface and subsurface wash) that remove material from hill and mountain sides and transport it to the valleys. In the long-term landscape version of *Cascade* the sum of the short-range hillslope processes are modelled as a linear diffusion equation in which the rate of change of landscape topography is proportional to the second derivative of topography:

$$\frac{\partial h}{\partial t} = K_D \nabla^2 h \quad (5.3)$$

Where  $K_D$  is a diffusion constant (default value =  $0.3 \text{ m}^2 \text{ a}^{-1}$ , Braun and Sambridge

1997) and  $\nabla^2 h$  is the second derivative of the elevation and the first derivative of local slope. The diffusion equation is solved using a finite element method adapted for a triangulated grid (see Braun and Sambridge 1997). Equation 4 follows the model of Beaumont *et al* (1992) and Kooi and Beaumont (1994) in which the horizontal flux  $s_s$  is related to the local slope,  $\nabla h$  by

$$s_s = -u_s h_s \nabla h \quad (5.4)$$

where  $u_s$  is the transport speed ( $L.T^{-1}$ ) and represents the ease of material transport once it has become fragmented,  $h_s$  is the vertical height scale of the erodible surface boundary layer (the steady state thickness of the boundary layer in which the cohesion has been destroyed by weathering) and subscript  $s$  denotes short range slope processes.  $u_s$  and  $h_s$  may be combined as a single transport coefficient  $K_s = u_s h_s$ . If it is assumed that there is no tectonic transport of the surface material, that volume is conserved and that the effects of solution are negligible, the transport equation can be combined with the continuity equation,

$$\frac{dh}{dt} = -\nabla s_s \quad (5.5)$$

to give the linear diffusion equation for the rate of change of local height, (denudation) in response to erosion by the short range processes,

$$\frac{dh}{dt} = u_s h_s \nabla^2 h \equiv K_D \nabla^2 h \quad (5.6)$$

These equations assume that during the interval  $\Delta t$ , the flux is in a dynamically steady state; that is, it does not vary during  $\Delta t$ . If a neighbouring cell  $i$  is higher than  $j$  (the receiving cell) a volume of material is transported between the two cells in time  $\Delta t$  from cell  $i$  to cell  $j$ . There is no transport upslope to higher cells.

There is currently a debate in the literature as to the value of the diffusion constant used in landscape evolution models. Martin and Church (1997) quote values for the diffusion coefficient implemented in landscape evolution models as ranging from  $10^{-2} \text{ m}^2 \text{ a}^{-1}$  for slow mass movements such as creep (Anderson, 1994; Rosenbloom and Anderson, 1994) to  $5 \times 10^3 \text{ m}^2 \text{ a}^{-1}$  (Flemings and Jordan, 1989 - this value is based on mean regional gradients in mountain belts and basin fill rates and may incorporate both hillslope and fluvial processes). Kooi and Beaumont (1994, 1997) implement diffusivities from  $2 \times 10^{-2} \text{ m}^2 \text{ a}^{-1}$  to  $1 \times 10^2 \text{ m}^2 \text{ a}^{-1}$  that are assumed to represent all slope processes including landsliding; the values at the higher end of the ranges are implemented in humid ranges. Willgoose *et al.* (1991), Tucker and Slingerland (1994) and Rinaldo *et al.* (1995) do not quote diffusivity values adopted in their landscape development models.

Braun and Sambridge (1997) have conducted experiments to test the effect of varying the diffusional constant on the resultant landscape over long-term timescales. A diffusion constant of 0 is equivalent to assuming a very thin regolith and/or sediment cover, or that the landscape is directly carved into resistant bedrock. In long-term landscape experiments, a value of zero for  $K_D$  resulted in very narrow valleys with nearly vertical valley walls (experiment 3 Braun and Sambridge 1997). With a value of  $0.3 \text{ m}^2 \text{ yr}^{-1}$  for  $K_D$  the resultant valleys were wide with convex walls (experiment 1). With a value of  $3 \text{ m}^2 \text{ yr}^{-1}$ , for  $K_D$  valleys were wide with concave downwards walls and the landscape had a low stream density (experiment 4).

Lateral sediment transport was approximated in *Braided Cascade* using the diffusion erosion subroutine in the original version of *Cascade*. The diffusional sediment transport may be thought of as an analogue for lateral sediment transport from channel banks. However by default diffusion occurs everywhere in response to local curvature of slope, even for those cells that have no water.

When choosing a value for the diffusion constant in *Braided Cascade* the default value ( $0.3 \text{ m}^2 \text{ a}^{-1}$ ) was used as a first approximation. For a timestep of one second this is equivalent to  $9 \times 10^{-9} \text{ m}^2 \text{ s}^{-1}$ . Figures 5.31 and 5.32 show the spatial pattern of channels after 25 000 and 50 000 iterations for runs with the diffusion constant set to equal  $9 \times 10^{-9} \text{ m}^2 \text{ s}^{-1}$  and without / with sediment input respectively. Qualitatively comparing the results from these runs with those from the control run (Figures 5.2 and 5.4) indicates that the presence of diffusion erosion does not produce significantly different results. However this may be due to the fact that the diffusion coefficient is small relative to those used in other long-term landscape evolution models. Other values of the diffusion coefficient were tested (Table 5.8).

The values of the diffusion coefficient tested range from the first approximation to  $1 \times 10^{-6} \text{ m}^2 \text{ s}^{-1}$ . This latter value was arrived at by approximating the diffusive sediment velocity was equal to  $50 \text{ m}^2 \text{ yr}^{-1}$  (which equates to  $1.6 \times 10^{-6} \text{ m}^2 \text{ s}^{-1}$ ). This is a large value relative to other diffusivity coefficients used in landscape evolution models and is used here to test the model under extreme conditions.

Run name	Diffusion1	Diffusion2	Diffusion3	Diffusion4	Control run
Diffusion $\text{m}^2 \text{ s}^{-1}$	$9 \times 10^{-9}$	$1 \times 10^{-8}$	$1 \times 10^{-7}$	$1 \times 10^{-6}$	off
Erosion length scale	10.0402				
Discharge	2 units of water at node 2, 5 and 7				
Slope	0.02855				
Splitting ratios (qratio and upratio)	Both 0.8				
Sediment input*	No / Yes				
Deposition	On				

Table 5.10. Details of runs with different diffusion coefficients.

\* One set of experiments was carried out with no sediment input at the top of the grid and one set was carried out with sediment input at the upstream boundary.

Figures 5.33 to 5.38 show the spatial distribution of channels on the grid with and without sediment after 25 000 and 50 000 iterations. From these Figures, it can be seen that with a large diffusion coefficient (i.e.  $1 \times 10^{-6}$ ) all water entering the grid is channelled along the sidewalls. The large diffusion coefficient leads to an increase in

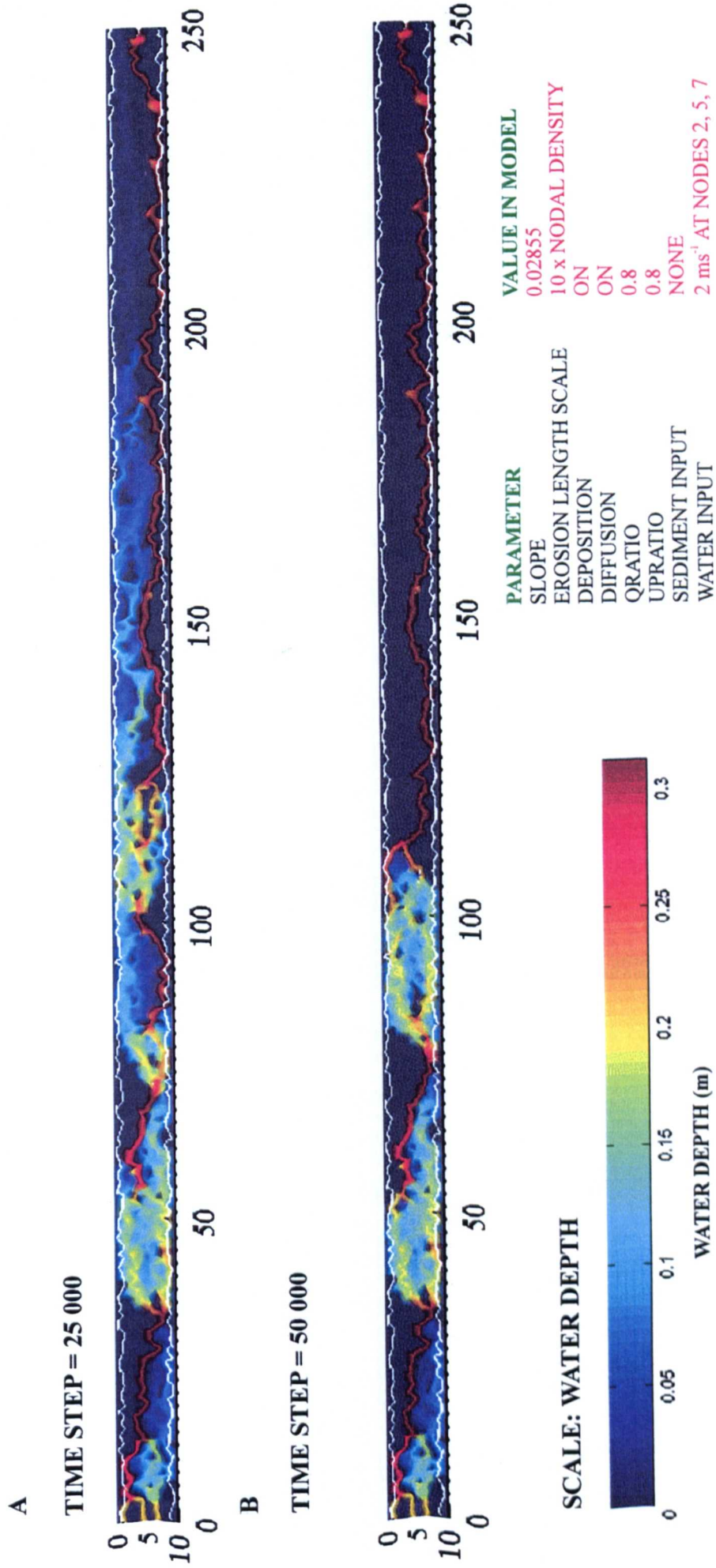


Figure 5.31. Diagram showing channel evolution for a run with diffusion turned on. Top: after 25 000 timesteps. Bottom: after 50 000 timesteps. Colour bar indicates water depth. Flow is from left to right.

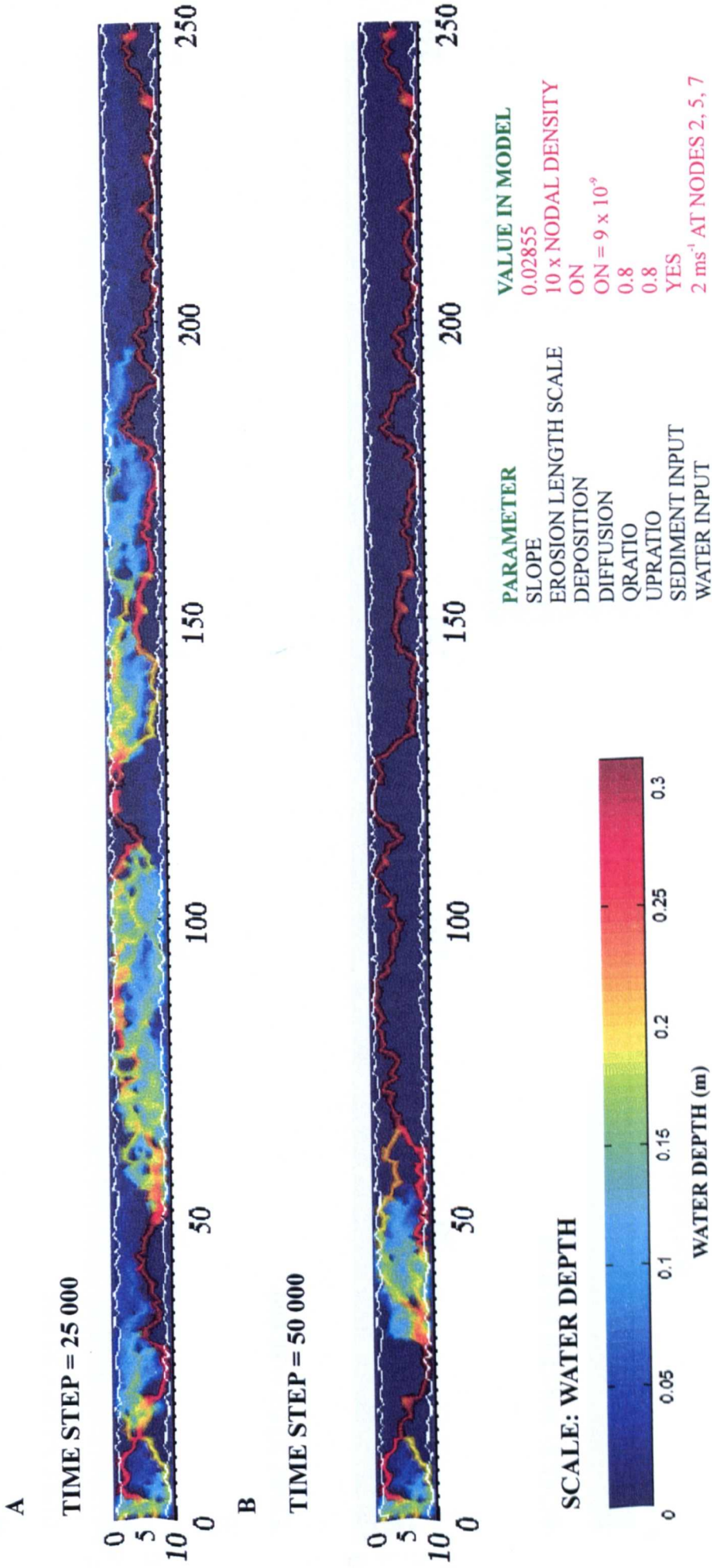


Figure 5.32. Diagram showing channel evolution for a run with diffusion turned on and sediment input at the upstream end of the grid. Top: after 25 000 timesteps. Bottom: after 50 000 timesteps. Colour bar indicates water depth. Flow is from left to right.

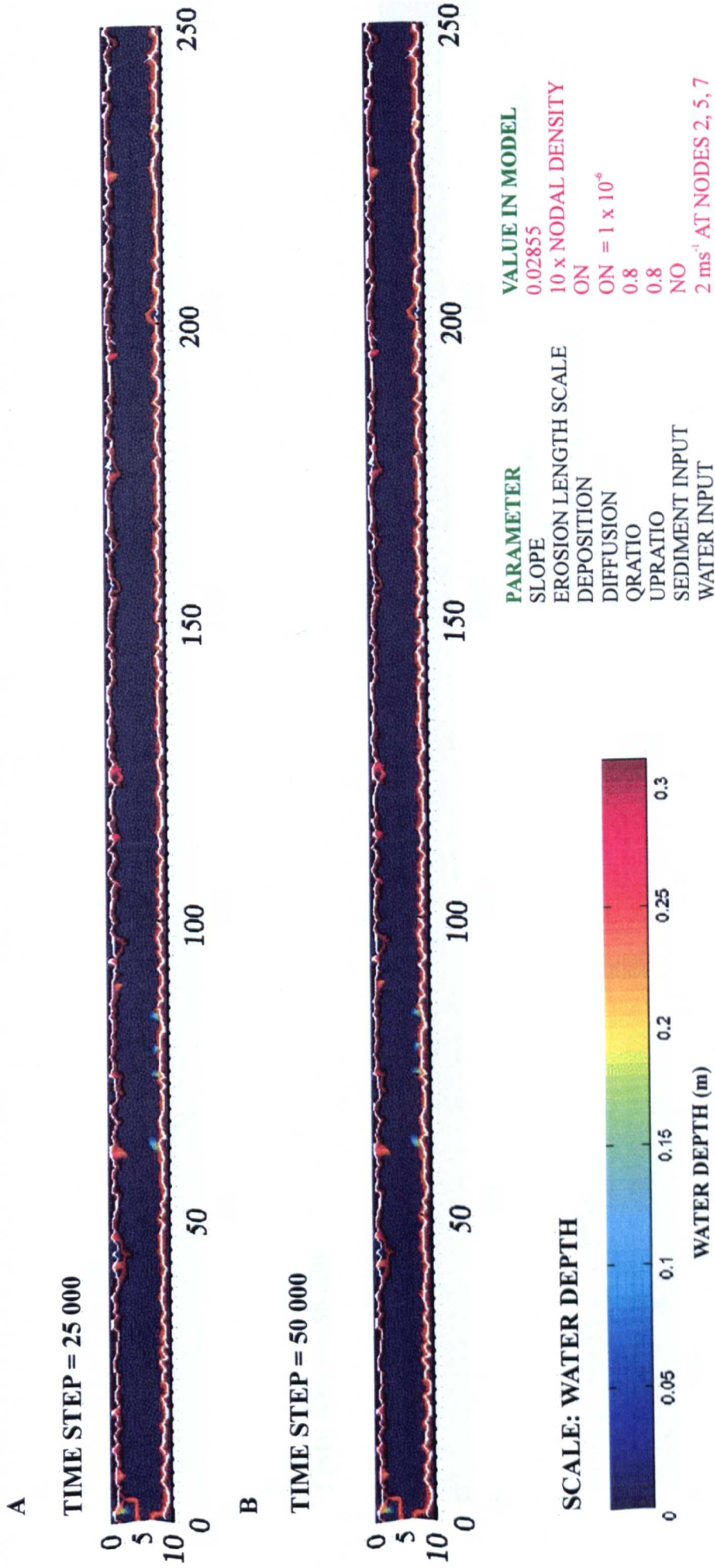


Figure 5.33. Diagram showing channel evolution for a run with diffusion set to  $1 \times 10^{-6}$ . Top: after 25 000 timesteps. Bottom: after 50 000 timesteps. Colour bar indicates water depth. Flow is from left to right.

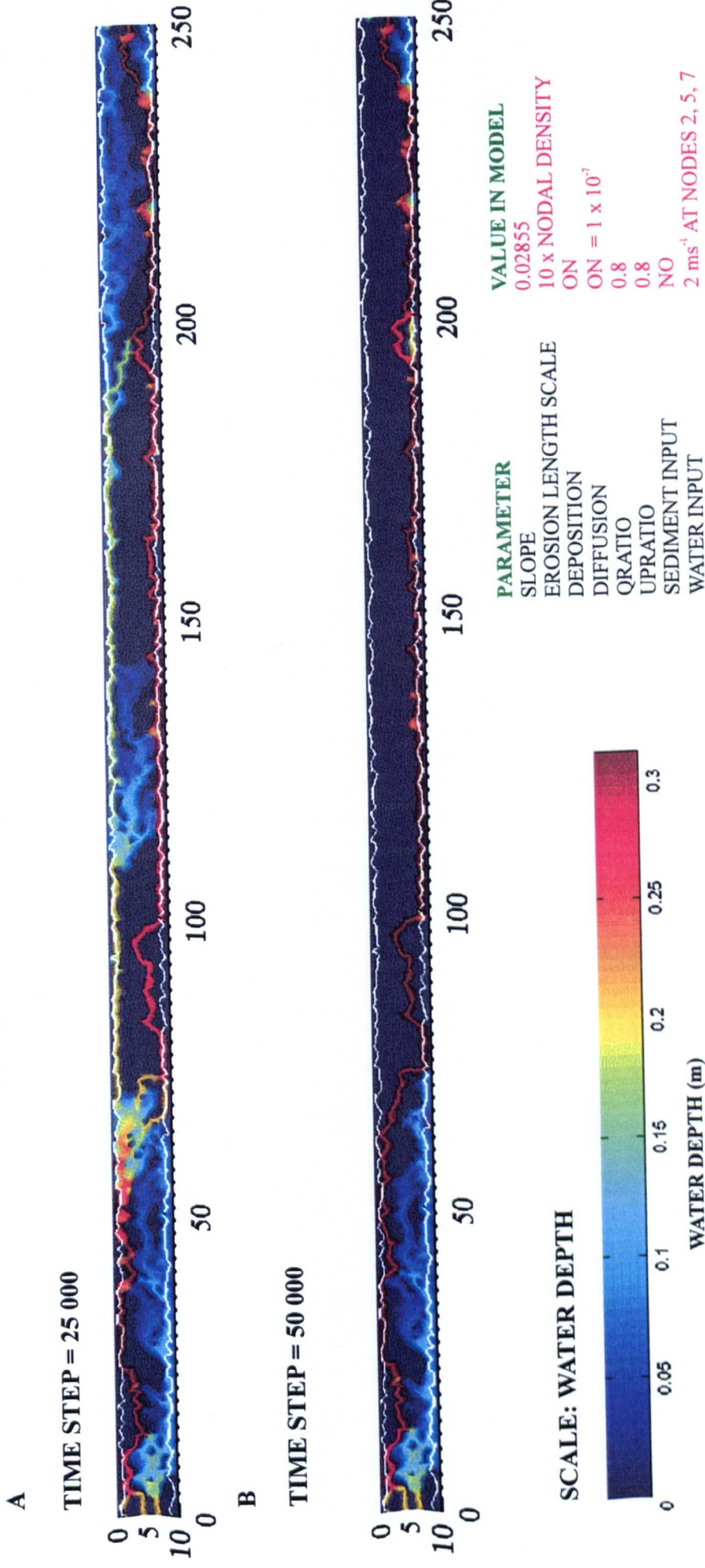


Figure 5.34. Diagram showing channel evolution for a run with diffusion set to  $1 \times 10^{-7}$ . Top: after 25 000 timesteps. Bottom: after 50 000 timesteps. Colour bar indicates water depth. Flow is from left to right.

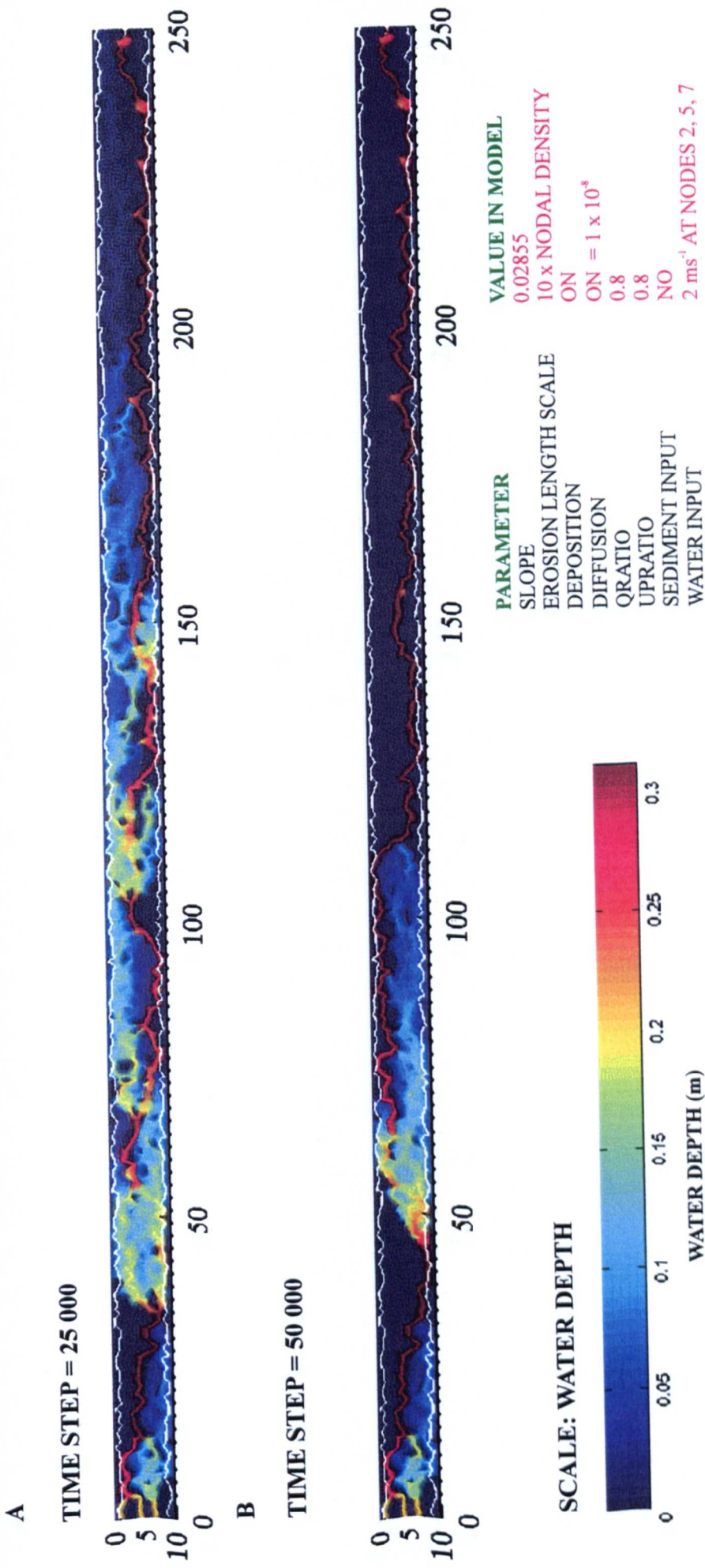


Figure 5.35. Diagram showing channel evolution for a run with diffusion set to  $1 \times 10^{-8}$ . Top: after 25 000 timesteps. Bottom: after 50 000 timesteps. Colour bar indicates water depth. Flow is from left to right.

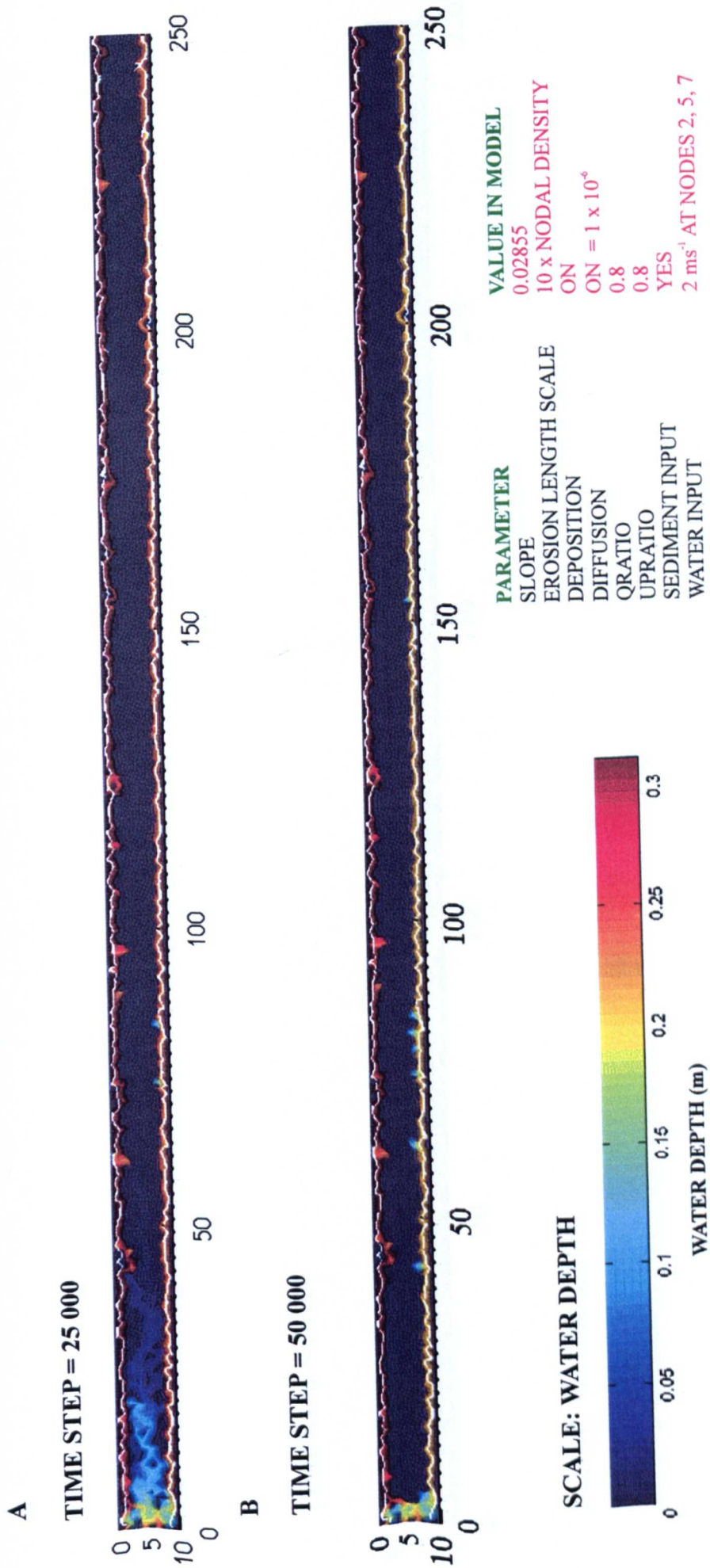


Figure 5.36. Diagram showing channel evolution for a run with diffusion set to  $1 \times 10^{-6}$  and with sediment input at the upstream boundary. Top: after 25 000 timesteps. Bottom: after 50 000 timesteps. Colour bar indicates water depth. Flow is from left to right.

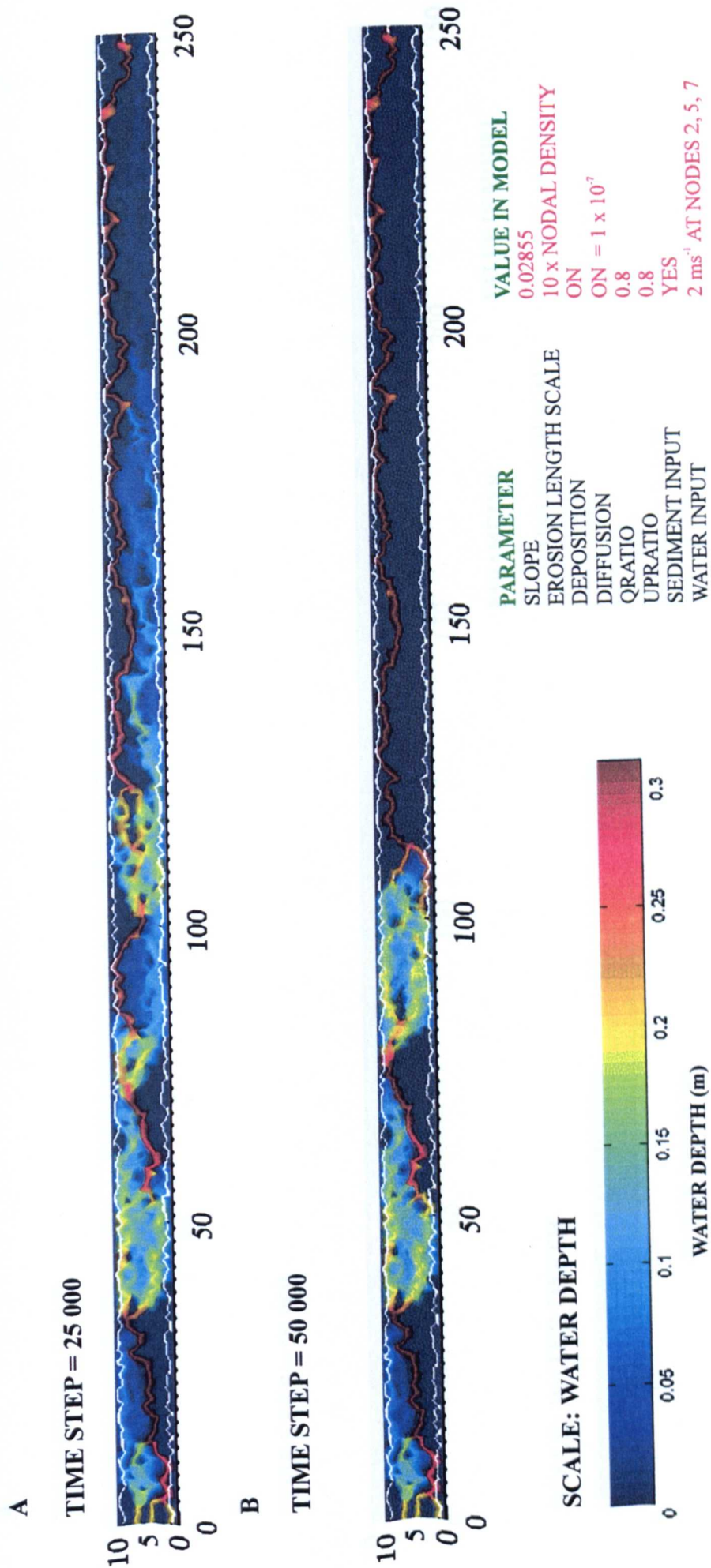


Figure 5.37. Diagram showing channel evolution for a run with diffusion set to  $1 \times 10^{-7}$  and with sediment input at the upstream boundary. Top: after 25 000 timesteps. Bottom: after 50 000 timesteps. Colour bar indicates water depth. Flow is from left to right.

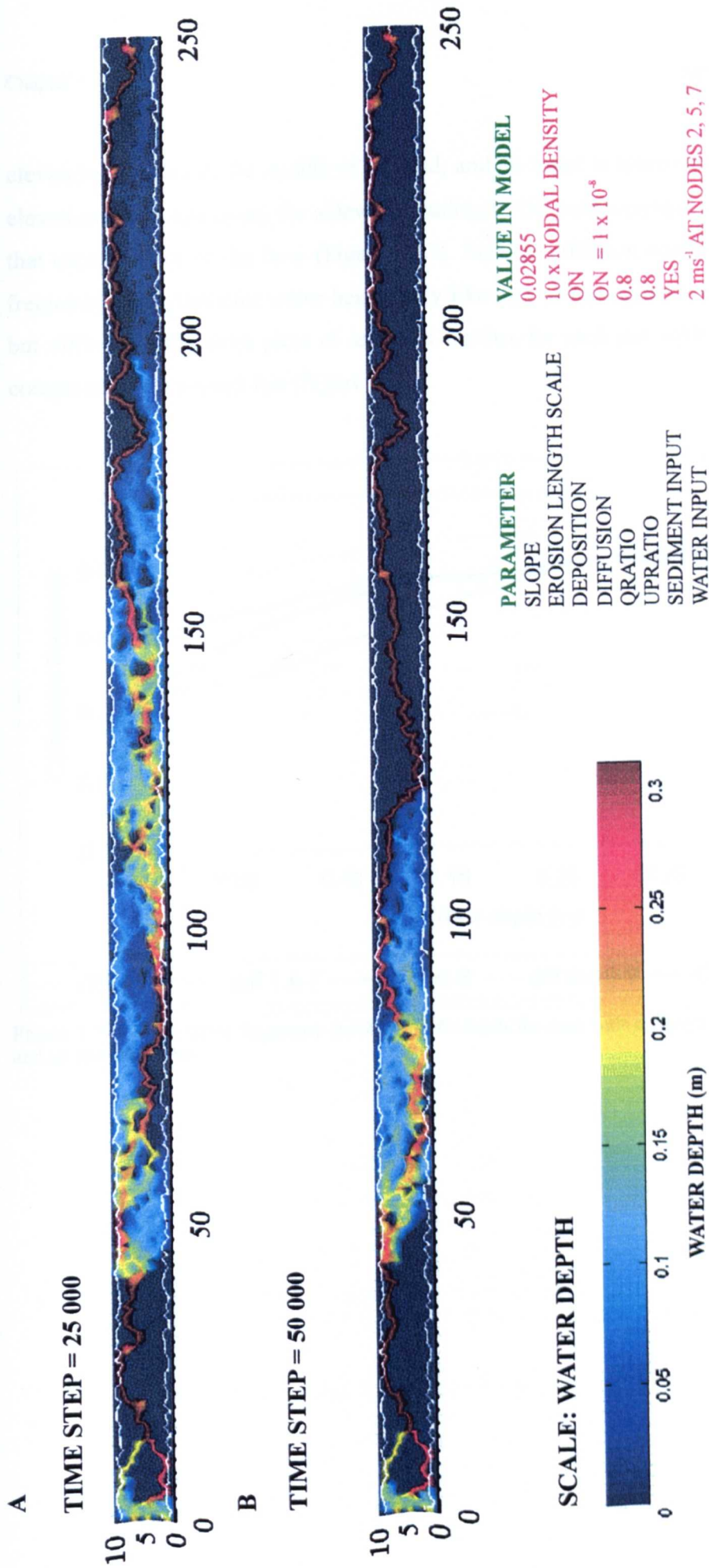


Figure 5.38. Diagram showing channel evolution for a run with diffusion set to  $1 \times 10^{-8}$  and with sediment input at the upstream boundary. Top: after 25 000 timesteps. Bottom: after 50 000 timesteps. Colour bar indicates water depth. Flow is from left to right.

elevation of nodes in the middle of the grid, and all water is routed around the higher elevation nodes and along the sidewalls leading to the predominance of two channels that capture most of the flow (Figure 5.33). Smaller diffusion coefficients produced frequency histograms for water height very like that of the control run (Figure 5.38), but different time series plots of sediment outflux for each run with diffusion when compared to the control run (Figure 5.39).

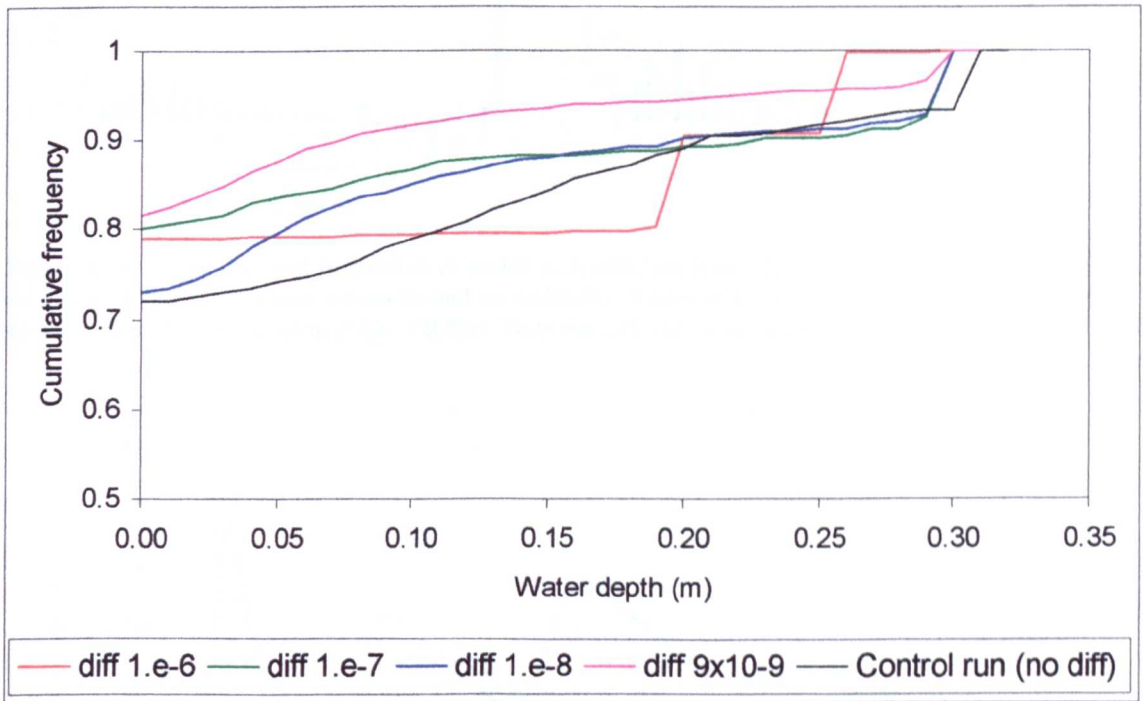


Figure 5.39a. Cumulative frequency curve of water depth for runs with different diffusion constants and no sediment input.

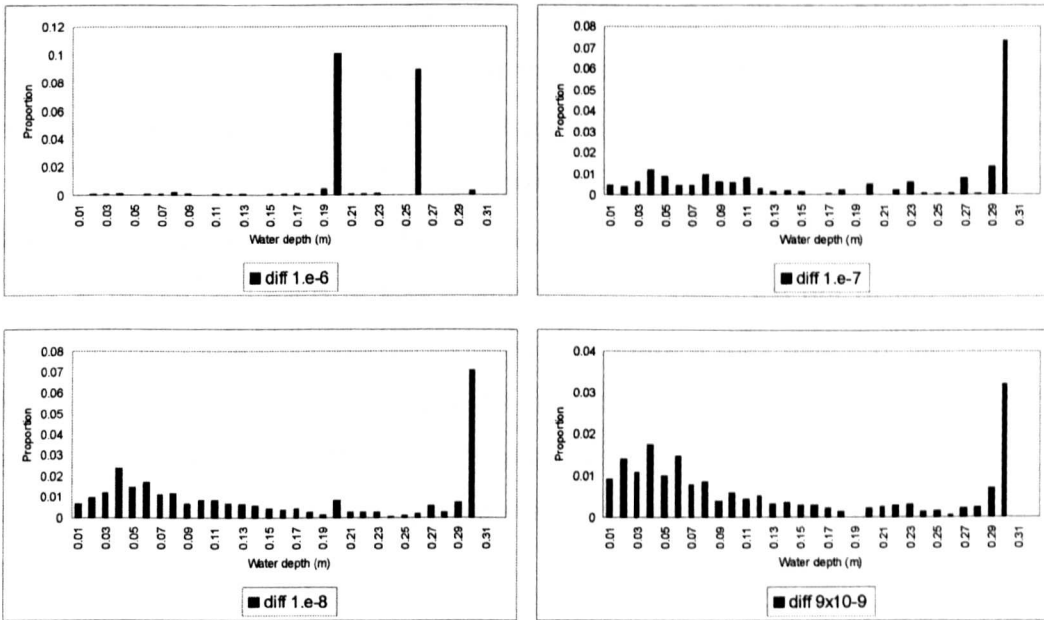


Figure 5.39b. Histograms of proportion of nodes with different water depth after 50 000 iterations for runs with different diffusion constants and no sediment. Nodes with no water (i.e. water depth = 0) have been omitted. Bins are in steps of 0.01m. Note the different vertical scales.

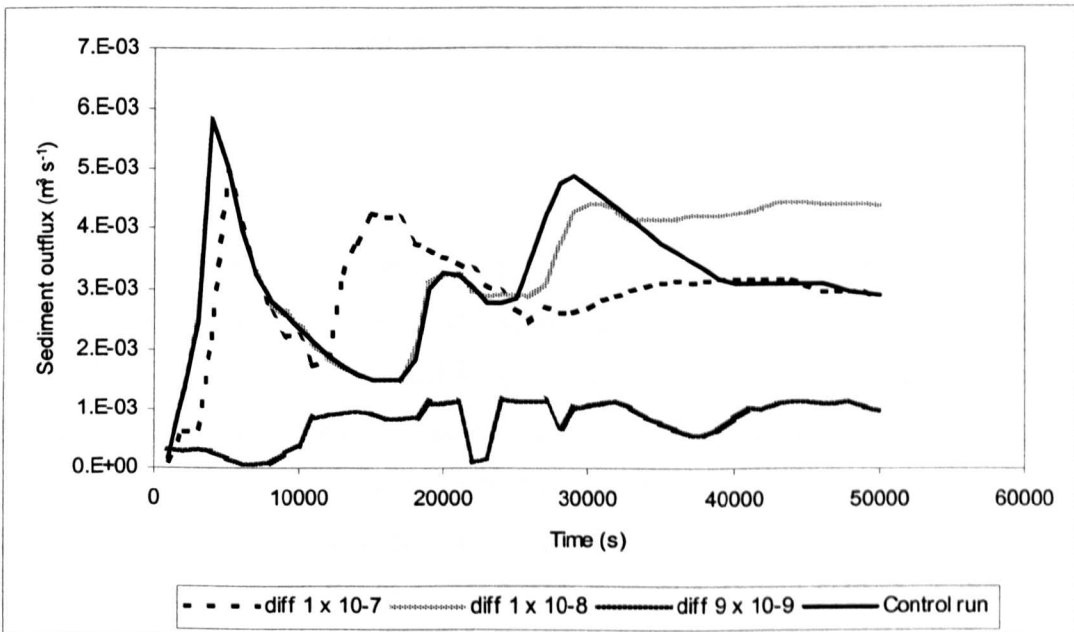


Figure 5.40. Time series plots of sediment outflux from the grid for runs with diffusion erosion switched on and the control run (NO diffusion). No sediment is input at the upstream boundary.

From Figure 5.40 it can be seen that the run with a diffusion coefficient equal to 1 x

$10^{-8} \text{ m}^3 \text{ s}^{-1}$  mirrors the control run (with no diffusion), until after 23 000 iterations when more sediment leaves the grid. At this point, for both runs, there is one main channel at the downstream boundary that contains the entire flow. A higher sediment output for the run with diffusion switched on implies that more sediment is being transported to the channel from the surrounding area. A smaller diffusion coefficient (i.e.  $1 \times 10^{-9} \text{ m}^2 \text{ s}^{-1}$ ) leads to less sediment being transported out of the grid, even when compared to the control run (with no diffusion). It may therefore be concluded that large diffusivity coefficients lead to a greater amount of sediment leaving the grid than for runs with no diffusion, however very small diffusion coefficients may hamper the supply of sediment, even when compared to runs without diffusion erosion.

Therefore a diffusion constant of  $1 \times 10^{-8} \text{ m}^2 \text{ s}^{-1}$  produces similar results to the control run with slightly more braiding, a diffusion constant of  $1 \times 10^{-9} \text{ m}^2 \text{ s}^{-1}$  produces more braiding but less sediment output and a diffusion constant of greater than  $1 \times 10^{-8} \text{ m}^2 \text{ s}^{-1}$  causes excessive concentration of flow into major channels and therefore suppresses braiding.

#### **5.4.5. Gradient of the grid.**

Two runs were performed with the overall grid gradient set to equal 0.01 (the default value for the control run is 0.02855) and sediment input switched off / on. Changing the gradient is straightforward and is specified when the grid dimensions are set up. However the gradient of the grid influences the amplitude of the white noise applied to the grid (this is set to be equal to  $0.01 \times \text{gradient} \times \text{grid length}$ ); therefore for the control run the white noise amplitude is equal to 0.0712, for a run with a gradient of 0.01 the white noise amplitude equals 0.025. Figures 5.41 and 5.42 show the spatial distributions of channels for these runs without and with sediment input; both runs have a large proportion of the grid covered with water and a large number of shallow channels which seem to remain stable throughout the runs and between runs. From Figures 5.41 to 5.42 it can be seen that a decrease in grid gradient leads to the channel

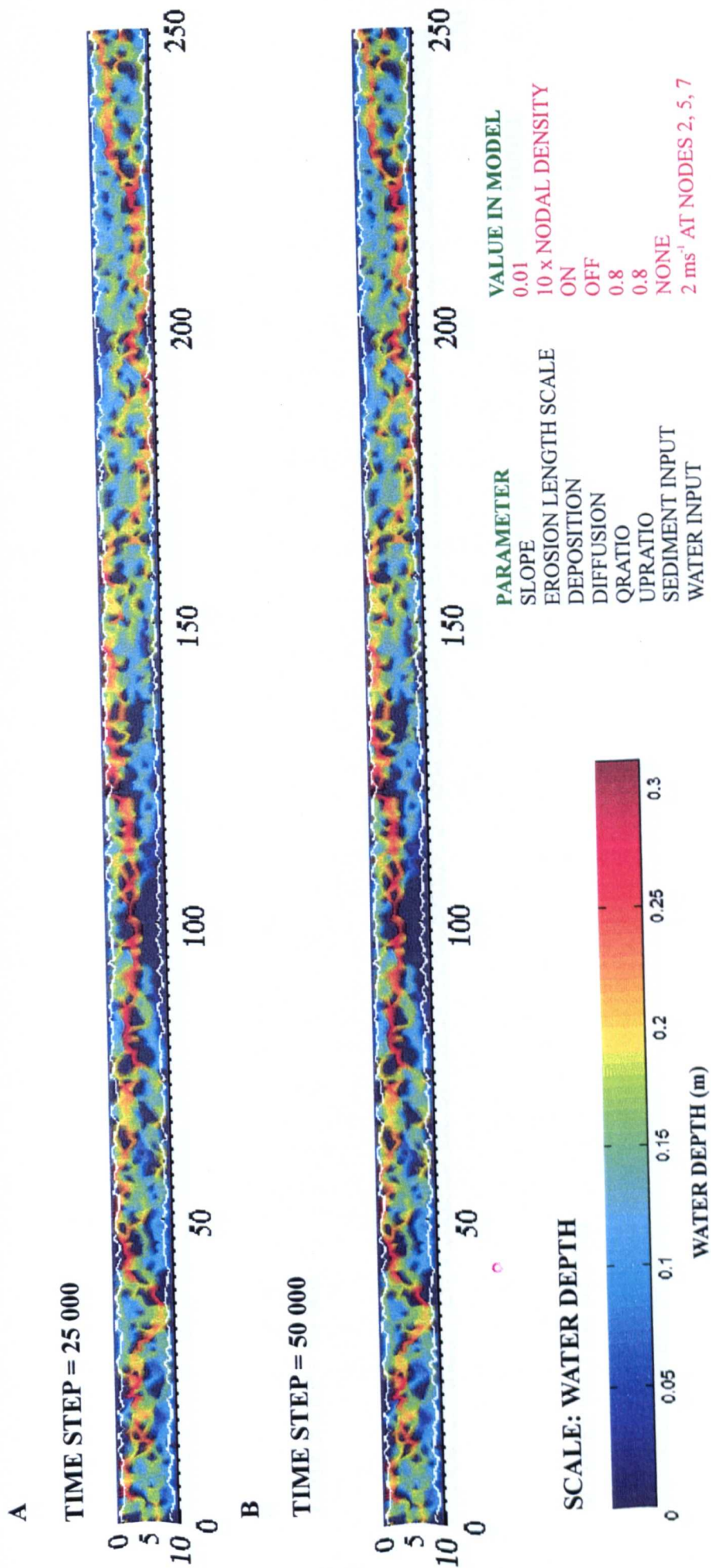


Figure 5.41. Diagram showing channel evolution for a run with slope set to 0.01. Top: after 25 000 timesteps. Bottom: after 50 000 timesteps. Colour bar indicates water depth. Flow is from left to right.

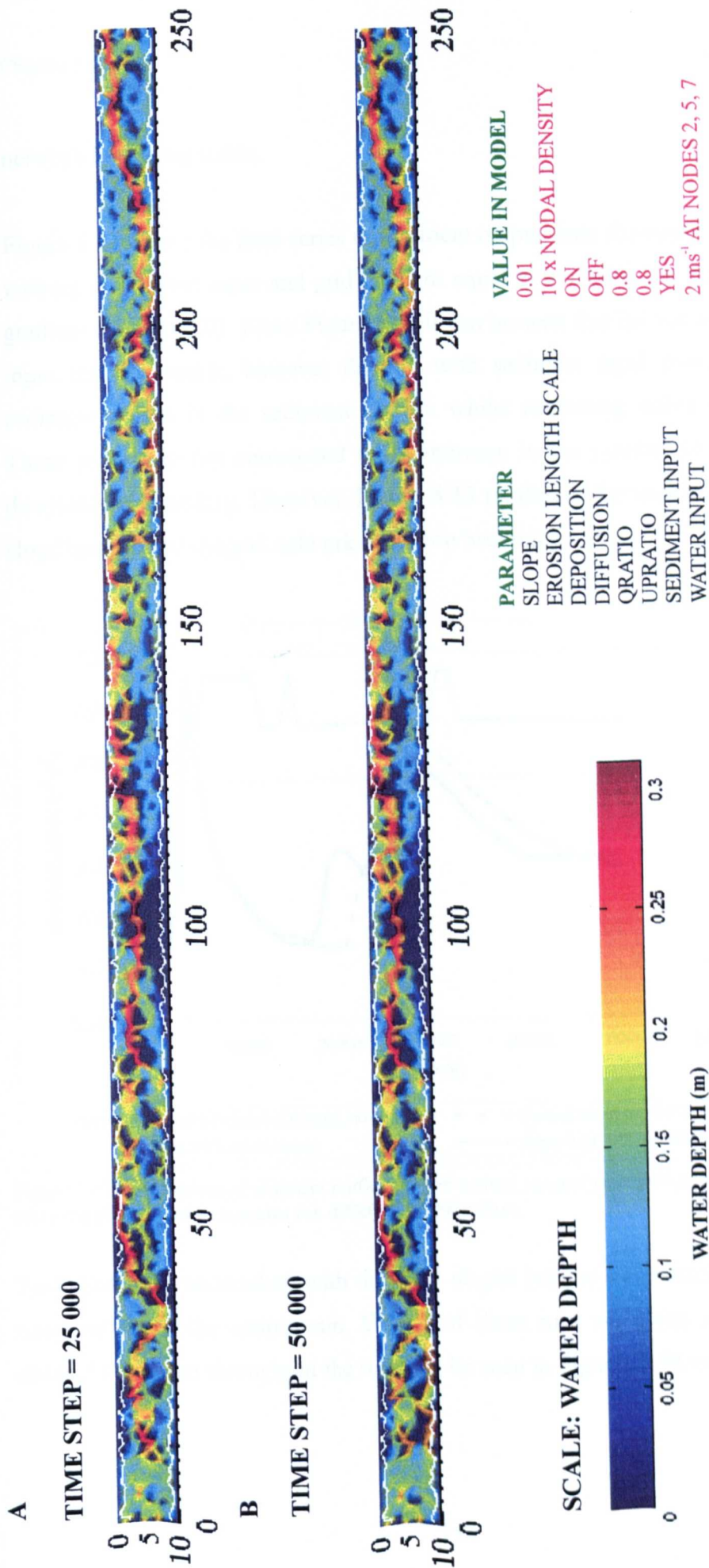


Figure 5.42. Diagram showing channel evolution on a grid with slope equal to 0.01 and with sediment input at the upstream end of the grid. Top: after 25 000 Bottom: after 50 000 timesteps. Colour bar indicates water depth. Flow is from left to right.

network becoming stable.

Figure 5.43 shows the time series of sediment output from the control runs (with and without a sediment input and grid gradient equal to 0.02855) and the runs with grid gradient equal to 0.01. From Figure 5.42 it can be seen that the run without sediment input remains stable, however the run with sediment input experiences discrete sediment pulses in the sediment outflux whilst remaining stable between pulses. These pulses do not correspond to an increase in the number of channels at the downstream boundary. However, Figure 5.43 reinforces the conclusion that a lower slope leads to the channel network evolution becoming stable.

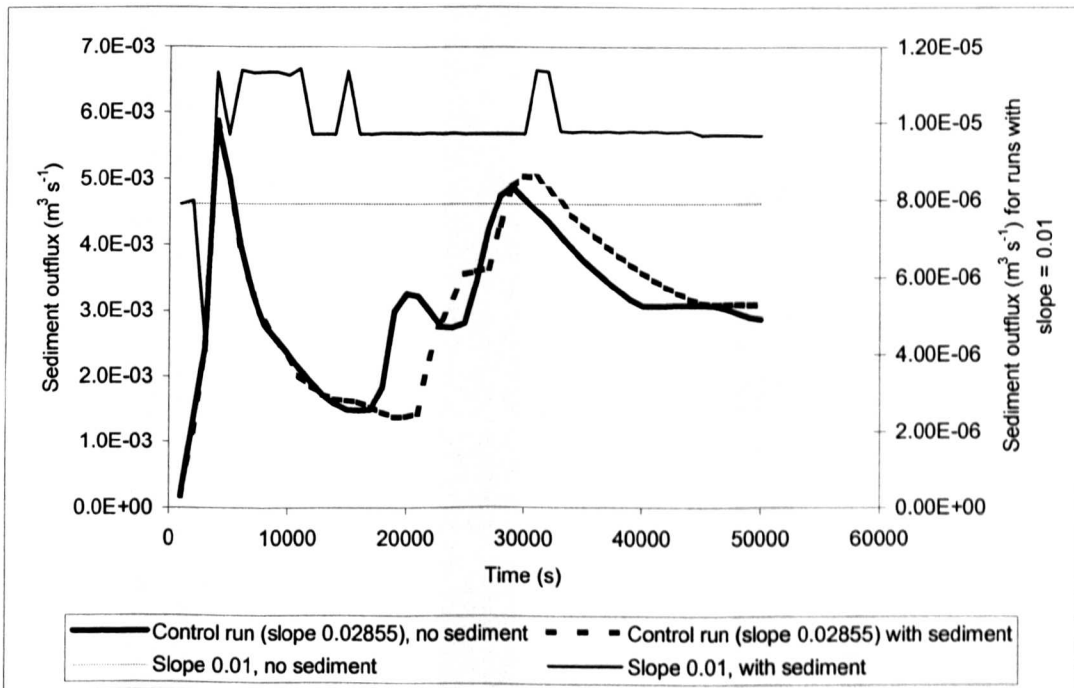


Figure 5.43. Time series of sediment outflux for the control run and runs with slope equal to 0.01. **Note the different y axis scales for different slope values.**

Two runs were undertaken with different slopes but the same discharge-slope (Q-S) combination as the control run. Details of these runs are given in Table 5.11 and channel evolution throughout the runs may be seen in Figures 5.44 and 5.45.

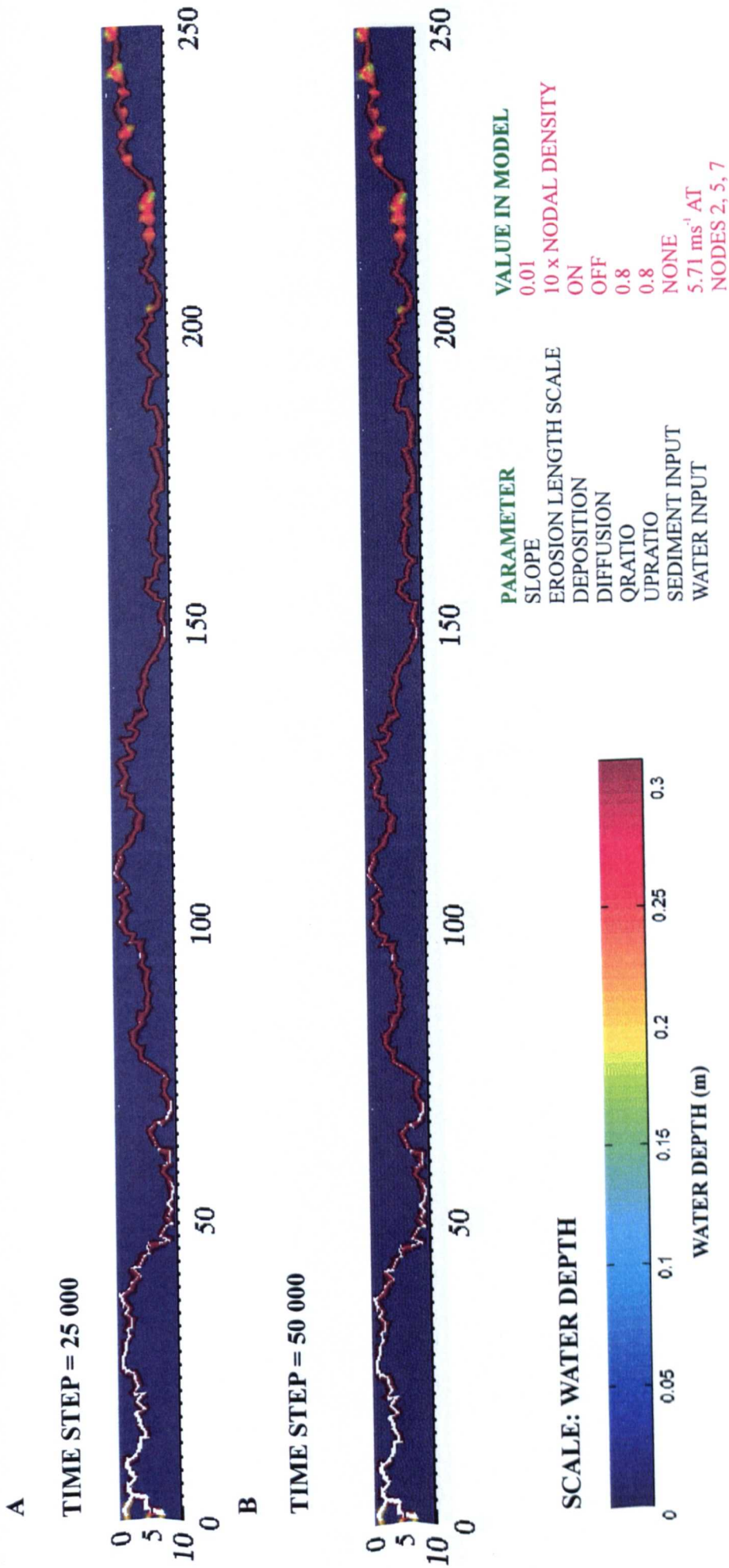


Figure 5.44. Diagram showing channel evolution for a run with slope set to 0.01 and total discharge of 17.13 m s<sup>-1</sup>. Top: after 25 000 timesteps. Bottom: after 50 000 timesteps. Colour bar indicates water depth. Flow is from left to right.

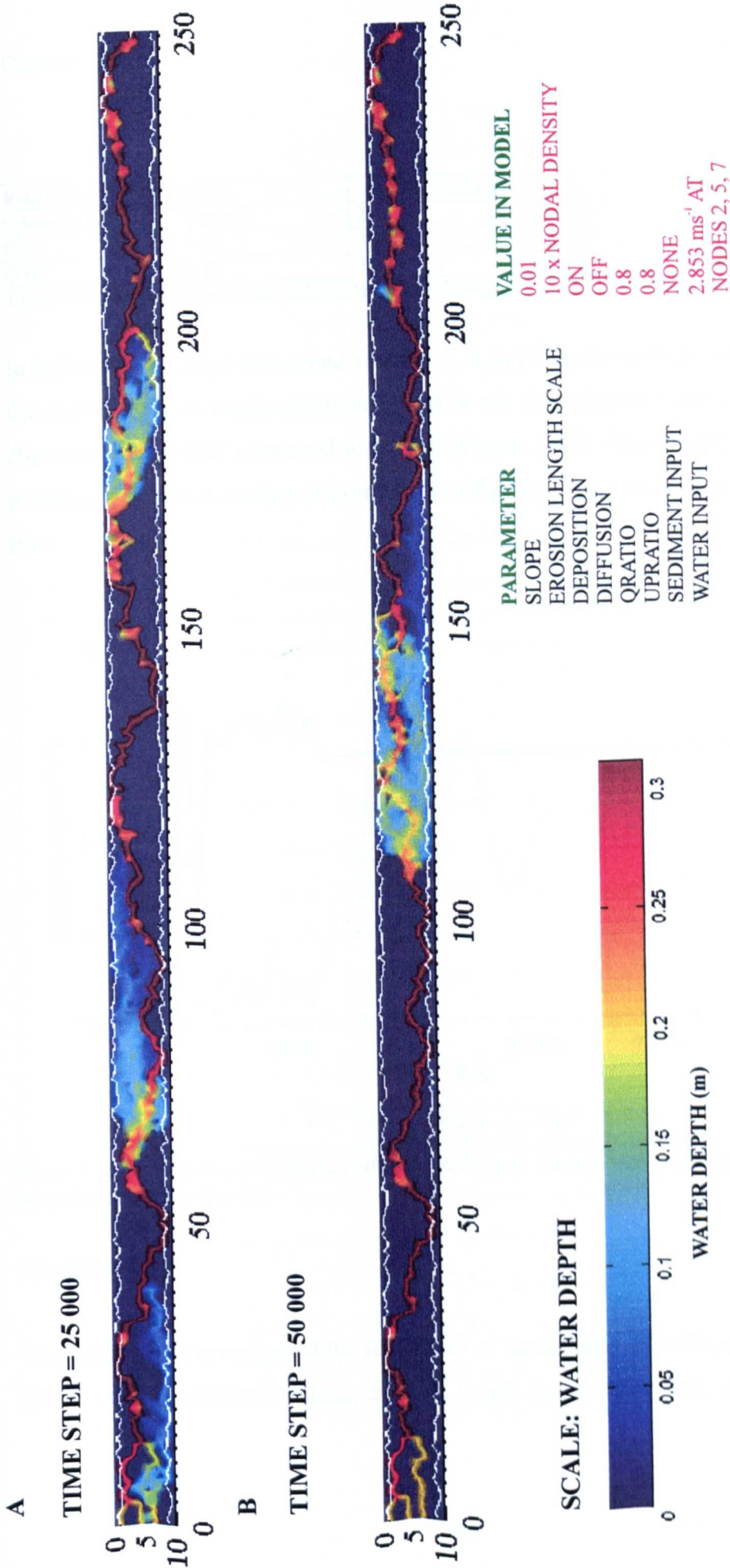


Figure 5.45. Diagram showing channel evolution for a run with slope set to 0.01 and total discharge of 8.56 m s<sup>-1</sup>. Top: after 25 000 timesteps. Bottom: after 50 000 timesteps. Colour bar indicates water depth. Flow is from left to right.

Run name	Slope	Total Q (m3 s-1)	Q*S	Sediment input?
Control run	0.02855	6	0.1713	N
QS1	0.01	17.13	0.1713	N
QS2	0.02	8.565	0.1713	N

Table 5.11. Details of runs with different slope and discharges but equal discharge-slope products.

In both runs discharge was added at nodes 2, 5 and 7 on the upstream boundary (as in the control run). A single channel evolved in run QS1 (Figure 5.44) that was stable, channels in run QS2 continued to evolve (Figure 5.45). This is also evident when examining sediment outflux from each run (Figure 5.46); run QS1 reaches a steady state.

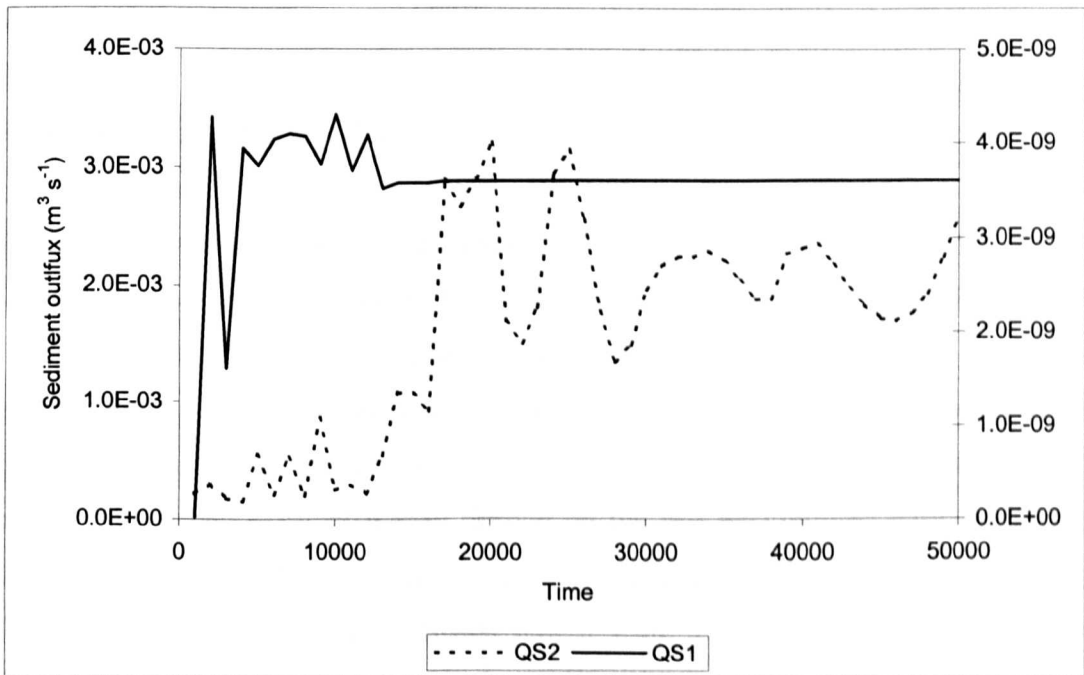


Figure 5.46. Time series of sediment outflux from the grid for runs with slope and discharge but the same discharge-slope product.

### 5.5. Discussion.

This chapter has investigated the sensitivity of the model results for a range of values of the model parameters: slope, erosion length scale, deposition, diffusion (lateral

sediment transport), discharge splitting ratios and sediment input and has investigated the parameter values needed to give styles and timescales for model evolution that are comparable to the evolution of braided channel networks. The results show that most combinations of model parameters produce basic braiding, however the model has a tendency to reach a static state in certain circumstances.

In the absence of measurements of these transport parameters at the necessary temporal and spatial scales in prototype rivers, the parameter values do not have any significance beyond the model. Given the lack of knowledge concerning parameter values in natural systems, the best that can be done is to make approximate estimates of the scale dependence from existing data and to show that these are consistent with the model behaviour.

### **5.5.1. Model parameter values.**

#### **5.5.1.1. Erosion length scale and fluvial transport.**

It is not obvious how to make a useful comparison between the numerical values of the erosion length scales and related empirical or physical parameter values determined by short-time scale and small spatial scale measurements. The erosion length scale likely depends on the cohesive strength of the alluvial material (or detachability), or, in the case of bed material it may depend on the bed packing and structure (these influence the critical shear stress for the bed), this could be seen as a reflectance of the sediment availability. The erosion length scale is a lumped parameter, like a thermodynamic parameter, which reflects the combination of many processes that scale with space and time. It has been shown that erosion length scales of equal to or less than the model nodal density tend to produce one incised stable channel. Long erosion length scales (of the order of the grid length) produce many shallow channels, however the spatial distribution of these channels remains stable for long periods. Therefore the spatial lag needed for braided networks to form and to evolve is of the order of 10 to 100 times the nodal density, implying that there is a disequilibrium

between the sediment available for transport and the transporting capacity of the flow is needed for braided networks to form.

### **5.5.1.2. Deposition.**

Most braiding mechanisms require the deposition of material (e.g. Ashmore, 1991a; Ferguson, 1993) and, if deposition is prevented, the system is purely erosive. If the model is prevented from depositing any eroded material, one stable main channel is eroded which is the product of irreversible entrainment, once eroded material cannot readily be redeposited (Paola, 2001) and without redeposition, once the flow gathers it can never split (Murray and Paola, 1997). Deposition is therefore important in the evolution and maintenance of braided networks.

### **5.5.1.3. Flow splitting ratios.**

The incorporation of flow splitting ratios is unique to *Braided Cascade*. The ability to constrain flow divergence is a purely model parameter and has no equivalence in prototype rivers, however it could serve as a surrogate for momentum in the flow equations. Smaller values of the flow splitting ratios *qratio* ( $Q_r$ ) and *upratio* ( $Q_{ru}$ ) forced the model to produce an incised channel. Higher values allowed greater instances of flow splitting. Forcing flow along negative slopes seems to be the most important mechanism to produce sheet flow in the model and may imply that braiding is a flux divergence phenomenon and not a lateral erosion phenomenon. In other words, if sediment flux is greater than carrying capacity aggradation occurs and will lead to flow splitting and vice versa. Carson (1984) states that the prerequisite for braiding is a local shoaled thalweg with high relative width, which in turn is dependent primarily upon a threshold state of bedload transport. A high rate of imposition of bedload may lead to local aggradation and flow splitting. Bedload may be sourced from the reach itself through bank scour, or from upstream. Carson (1984) states that the balance between bedload supply rates and capacity allows the possibility of coexistence of different channel patterns along the same reach of constant slope, discharge and sediment type.

#### **5.5.1.4. Lateral transport (Diffusivity).**

Model results are very sensitive to diffusion erosion (lateral sediment transport). Lateral sediment transport has been approximated in *Braided Cascade* as diffusive sediment transport, following the style of the implementation of lateral sediment transport in the model of Murray and Paola (1994, 1997). The original version of *Cascade* contained an allowance for diffusive sediment transport and this has been incorporated into *Braided Cascade* as an analogy for lateral sediment transport. Once again, in the absence of valid data from prototype rivers it is difficult to make a useful comparison between the numerical values of the diffusivity constant implemented in the model and lateral sediment transport from channel banks. However, if flow splitting is easy diffusion is not essential to produce braiding as vertical changes in the bed elevation produce channel dynamism. If this is the case then results from *Braided Cascade* differ from the model of Murray and Paola (1994, 1997).

#### **5.5.1.5. Grid gradient.**

Higher grid gradients are needed to continue to allow channel evolution. Channels formed on lower gradients tend to remain stable, even if the discharge-slope product remains the same.

#### **5.5.1.6. Sediment input.**

Runs with sediment feed tended to produce less stable channel networks (i.e. the channel pattern evolved throughout the run) at the upstream end of the grid. Sediment input to the model is therefore important for braiding, however braiding can occur without sediment feed (Brotherton, 1979).

### **5.6. Conclusions.**

Most combinations of model results will produce basic braiding. However, the model will reach a static steady state if the length scales are sufficiently short for the

carrying capacity of the flow to be reached almost instantaneously and also if the splitting ratios (qratio and upratio) are set to disallow flow to split if the ratios between channel slopes are very low (Table 5.12).

When erosion length scale is short (i.e. carrying capacity is reached almost instantaneously) the model produces very similar results to when the system is purely erosional (i.e. no deposition allowed). Therefore an imbalance in the amount of sediment the river is carrying and the carrying capacity AND a reworking of the deposits is needed for a braided network to form. Lateral erosion and gradient are important for braiding; high slopes and sediment transport from channel banks are needed for channel evolution to continue (Table 5.12).

	Maximum braiding	Minimum Braiding	Conditions used in chapter 6
Slope	High	Low	0.02855
Spatial lag	c. model length*	c. node spacing	c. 100 x nodal spacing*
Splitting: Upslope	0.95	0.5	0.95
Splitting: downslope	0.95	0.5	0.95
Sediment feed	On	Off	On
Diffusion	c. $1 \times 10^{-8}$	$\geq 1 \times 10^{-6}$	$1 \times 10^{-8}$
Deposition	On	Off	On

Table 5.12. The effect of model conditions on channel network patterns.

\*a long spatial lag creates numerous braided channels, however these channels are stable and do not change position, therefore a shorter lag that creates numerous channels which continually evolve has been chosen for use in Chapter 6.

It is difficult to compare the parameter values used in the model with data from prototype rivers due to a lack of field measurements. Therefore, the parameter values do not have any significance beyond the model.

## CHAPTER 6.

### TESTING *BRAIDED CASCADE*.

#### 6.1. Introduction.

Chapter 5 has shown that *Braided Cascade* may produce channel morphologies that are qualitatively similar to prototype braided rivers but that the details depends upon the parameter settings. In this Chapter, further questions are asked and the model is used to ascertain conditions influencing braiding and a new quantitative analysis of model results is developed.

#### 6.2. Linking spatial and temporal bedload transport variability.

Bedload transport in braided rivers has been shown to be highly variable, even under steady flow conditions (see section 2.3.1 and Ashmore, 1998; Hoey and Sutherland, 1991; Young and Davies, 1991; Goff and Ashmore, 1994; Warburton 1996). Fluctuations under steady flow conditions in flume experiments have been attributed to processes within in the river such as the migration of individual bedforms or bed waves, although there is considerable uncertainty in ascribing particular types of fluctuation to particular types of event (e.g. Hoey 1992).

There is some evidence from formal time-series analysis that the structure of bedload time series reflects channel configuration. Warburton (1996) reported a relationship between the shape of the autocorrelation function and the standard deviation of bedload transport rates in laboratory experiments, and Ashmore (1988) found a similar, although weaker, pattern. Recently Ashmore (2001) speculated on the relationship of channel morphology (especially pool-bar units and bar-confluence features) to spatial and temporal variations in bedload transport rate.

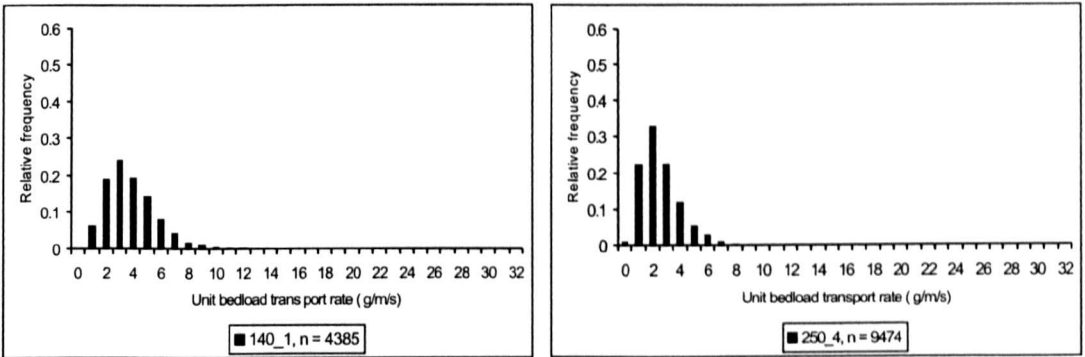
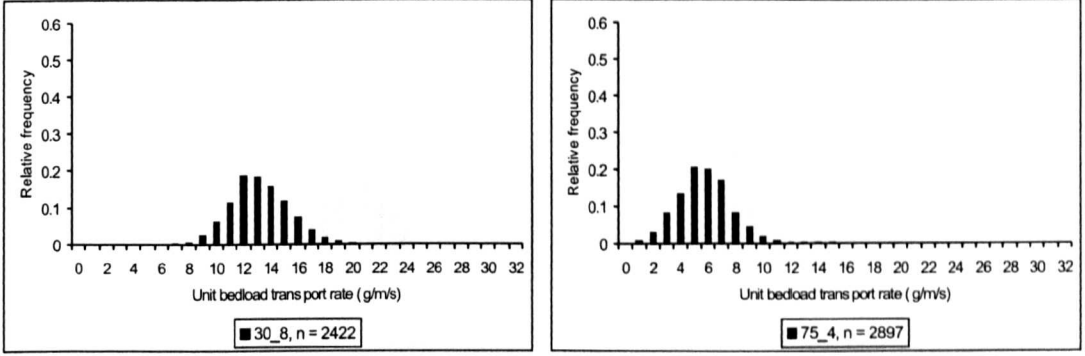
This section will attempt to develop a model of sediment transport by linking spatial and temporal sediment transport together. Primary data (Arolla field data)

and secondary data (flume data from Zarn, 1997) will be used in an attempt to ascertain differences between bedload transport time series from single thread and braided channel planforms, and new runs of *Braided Cascade* are undertaken to determine whether or not the model has captured the essential features of the dynamic braided systems.

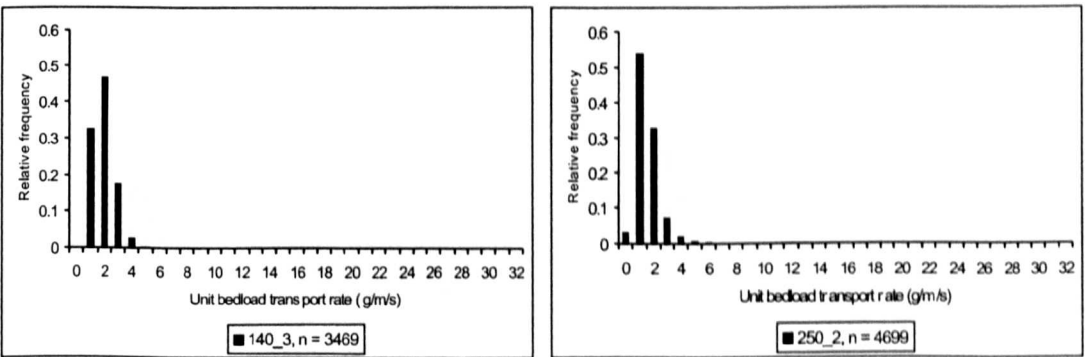
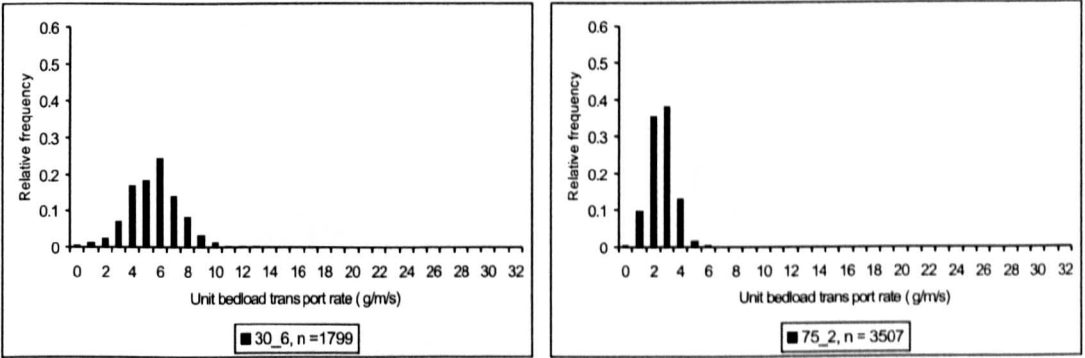
### 6.2.1. Flume data: Zarn (1997)

The flumes experiments of Zarn (1997) have been described in Chapter 4. Variation of bedload transport rate within each run is summarised in histograms in Figure 6.1; these show relative frequency (standardised frequency due to unequal sample sizes) and are grouped according to discharge. Inspection of Figure 6.1 shows that for a given discharge, the histograms are generally symmetrical for narrower runs (30 and 75 cm) and gradually become more positively skewed (biased towards lower transport rates) as the width of the flume increases. Positively skewed data are partly due to the influence of natural phenomena having a lower limit and being unconstrained, theoretically, in the upper range. In this case the natural phenomena are probably scour holes (Zarn, 1997) creating areas of no or very little sediment transport. The positive skew is also reflected in the values for median transport rate, which are similar to the values for mean transport rate for runs of width equal to 30 cm but become less than the mean as flume width increases (Table 6.1).

Time series plots (Figure 6.2) indicate that bedload transport rates are highly variable. Within-run transport rates are summarised in Table 6.1 and vary from zero to just over seven times the mean rate (run 250\_4). Wider runs with more channels experience the greatest variability in bedload transport rates while for runs with one to two channels (30 cm and 75 cm wide runs) the variability in bedload transport rates ranges from just over the mean rate to nearly four times the mean rate.

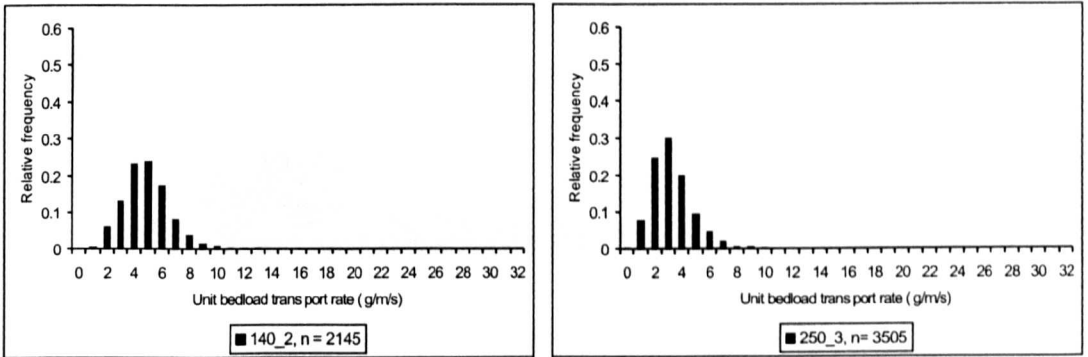
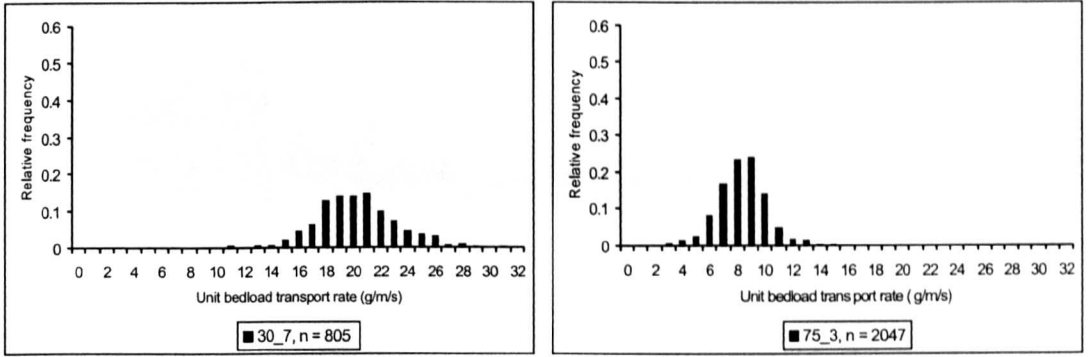


$Q = 2.3 \text{ l s}^{-1}$

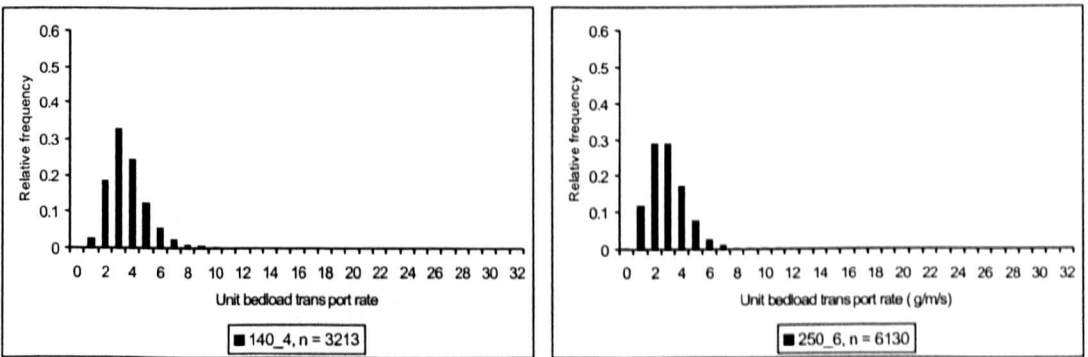
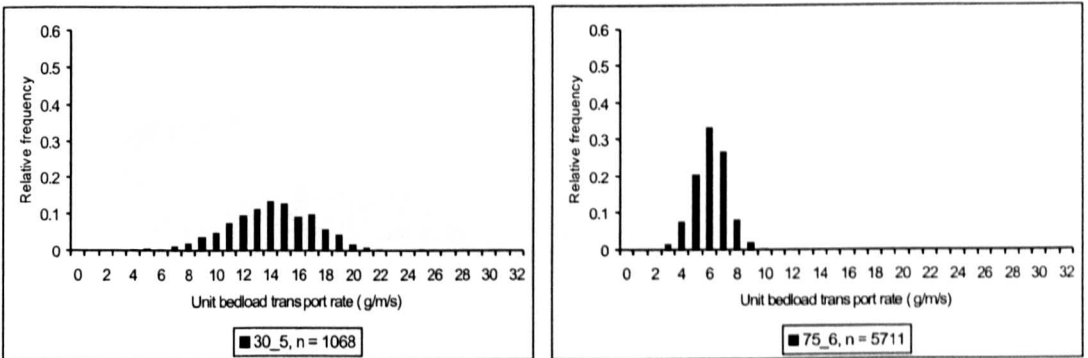


$Q = 4 \text{ l s}^{-1}$

Figure 6.1. Histograms of unit bedload transport rates in experiments of Zarn (1997). Relative frequencies are used due to unequal sample sizes. Histograms are grouped by discharge. Histogram legends contain the run name and number of bedload samples.

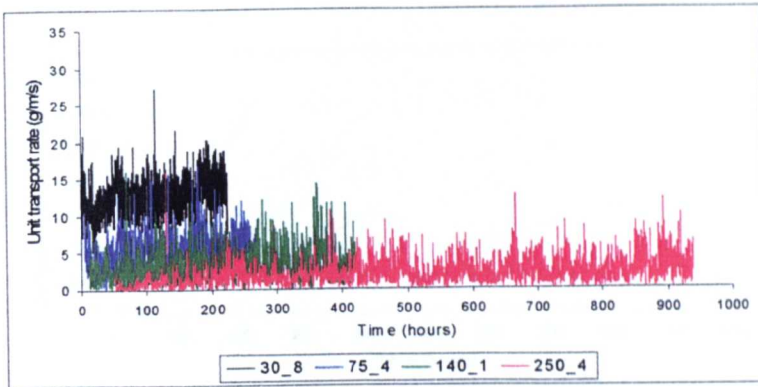


$Q = 5 \text{ l s}^{-1}$

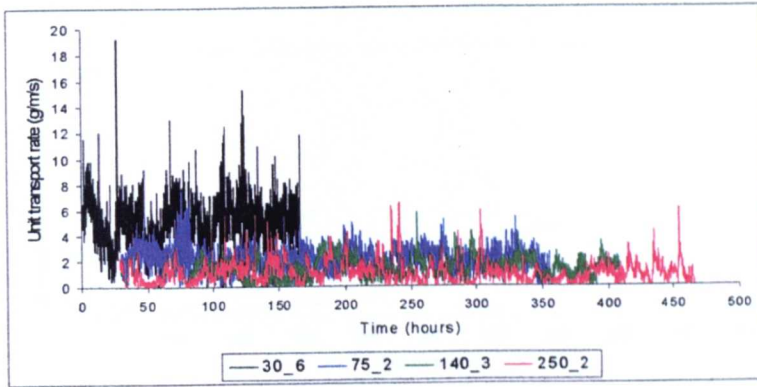


$Q = 7 \text{ l s}^{-1}$

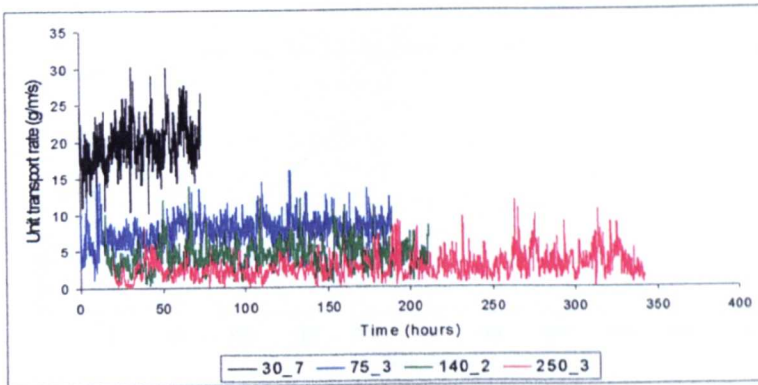
Figure 6.1. Histograms of unit bedload transport rates in experiments of Zarn (1997). Relative frequencies are used due to unequal sample sizes. Histograms are grouped by discharge. Histogram legends contain the run name and number of bedload samples.



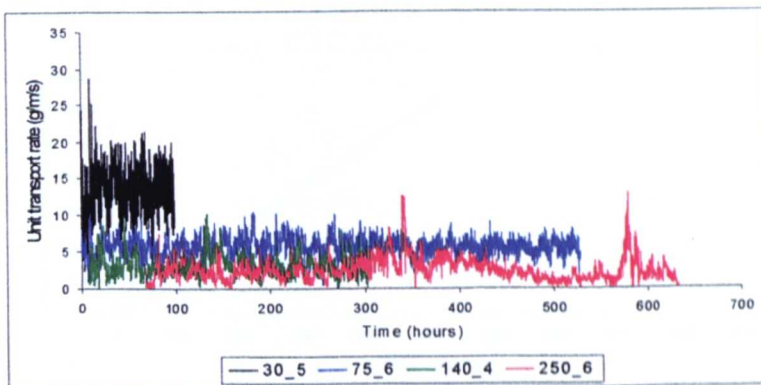
$Q = 2.3 \text{ l s}^{-1}$



$Q = 4 \text{ l s}^{-1}$

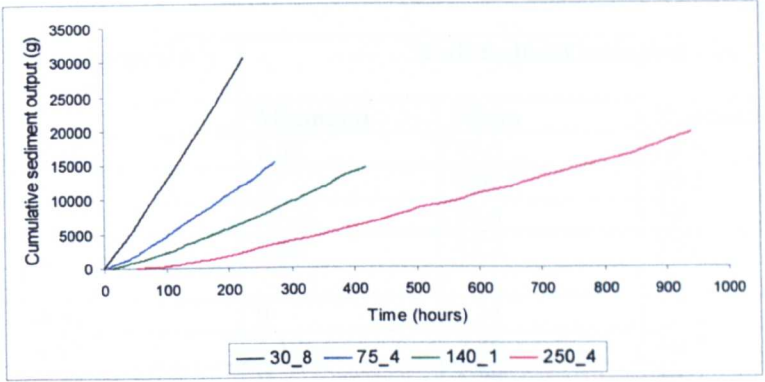


$Q = 5 \text{ l s}^{-1}$

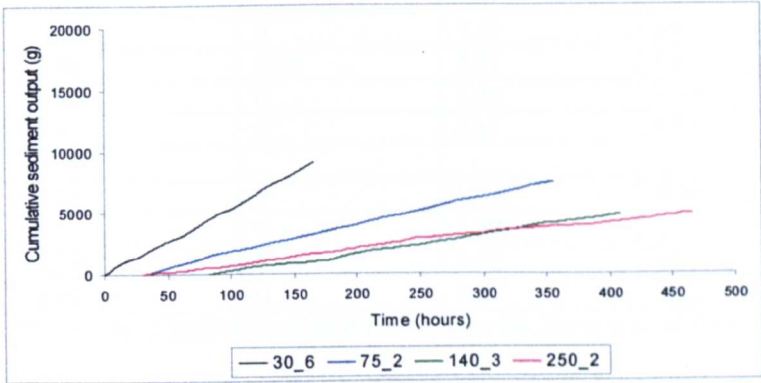


$Q = 7 \text{ l s}^{-1}$

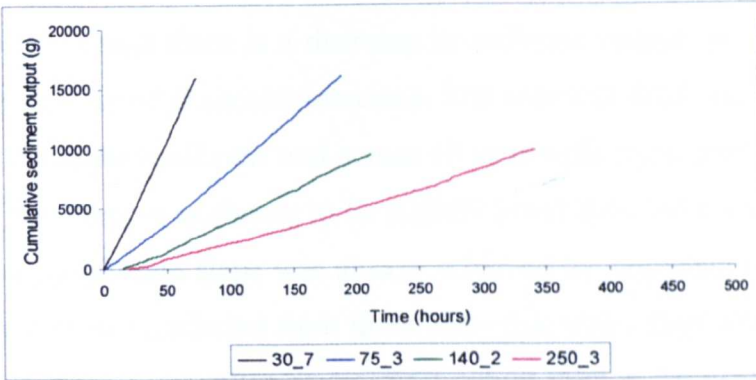
Figure 6.2. Time series of unit bedload transport rate for all runs of Zarn (1997) grouped according to discharge. Note the change of scales between graphs.



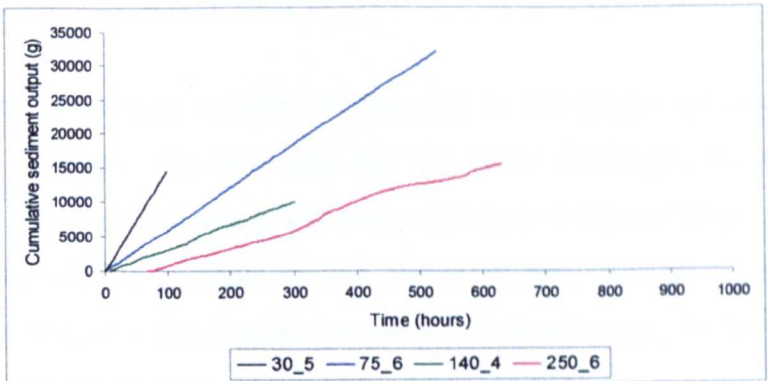
$Q = 2.3 \text{ ls}^{-1}$



$Q = 4 \text{ ls}^{-1}$



$Q = 5 \text{ ls}^{-1}$



$Q = 7 \text{ ls}^{-1}$

Figure 6.3. Cumulative sediment transport curves for all Zarn's (1997) runs. Runs are grouped according to discharge. Note different scales between plots for discharges of 2 and 7  $\text{ls}^{-1}$  and 4 and 5  $\text{ls}^{-1}$ .

Run name	Discharge ( $l s^{-1}$ )	Unit bedload transport rate ( $g m^{-1} s^{-1}$ )			
		Minimum	Mean	Maximum	Max/mean
30 5	6.89	2.37	13.5	28.8	2.13
30 6	4	0	5.08	19.2	3.79
30 7	5	10.2	19.8	30.2	1.52
30 8	2.37	5.09	12.7	27.2	2.14
75 2	4.01	0	2.13	7.52	3.53
75 3	4.97	1.12	7.85	16.3	2.08
75 4	2.34	0	5.29	16.7	3.12
75 6	6.89	0	5.59	10.4	1.85
140 1	2.34	0	3.33	16	4.80
140 2	4.98	0.24	4.41	14	3.17
140 3	3.95	0	1.40	5.75	4.11
140 4	6.9	0	3.11	10.1	3.25
250 2	4.02	0	1.05	6.55	6.24
250 3	5	0	2.80	12	7.71
250 4	2.29	0	2.07	16	4.27
250 6	6.91	0	2.50	13.1	5.24

Table 6.1. Variability of bedload transport rates across the flume runs of Zarn (1997).

The plots of cumulative sediment output from each run (Figure 6.3) show that, for the same discharge there is a decrease in sediment output as flume width (and therefore number of channels) increases. The sediment feed rate into the flume is constant throughout all runs and across all runs with equal discharge. The initial slope of the flume was chosen to be slightly lower than the expected equilibrium slope and equilibrium slope was always achieved by aggradation (Zarn, 1997). It can therefore, be concluded from these plots that wider runs with more channels experience more aggradation as sediment output from wider runs is less than that for narrower runs with fewer channels and the same initial conditions.

Thus, as the average number of channels in the flume increases, the average bedload transport rate decreases for the same discharge, but the relationship between number of channels and transport rate is not linear (Figure 6.4). This may reflect the greater aggradation and the increasing number of sediment storage reservoirs (bars) as the channel geometry switches from single thread to braided.

Figure 6.5 shows that neither is there a linear relationship between bedload transport rate and discharge, all sediment transport curves show the same pattern: transport decreases as discharge increases from 2 l s<sup>-1</sup> to 4 l s<sup>-1</sup>, then rises to a peak at a discharge of 5 l s<sup>-1</sup> before decreasing when discharge is raised to 7 l s<sup>-1</sup>.

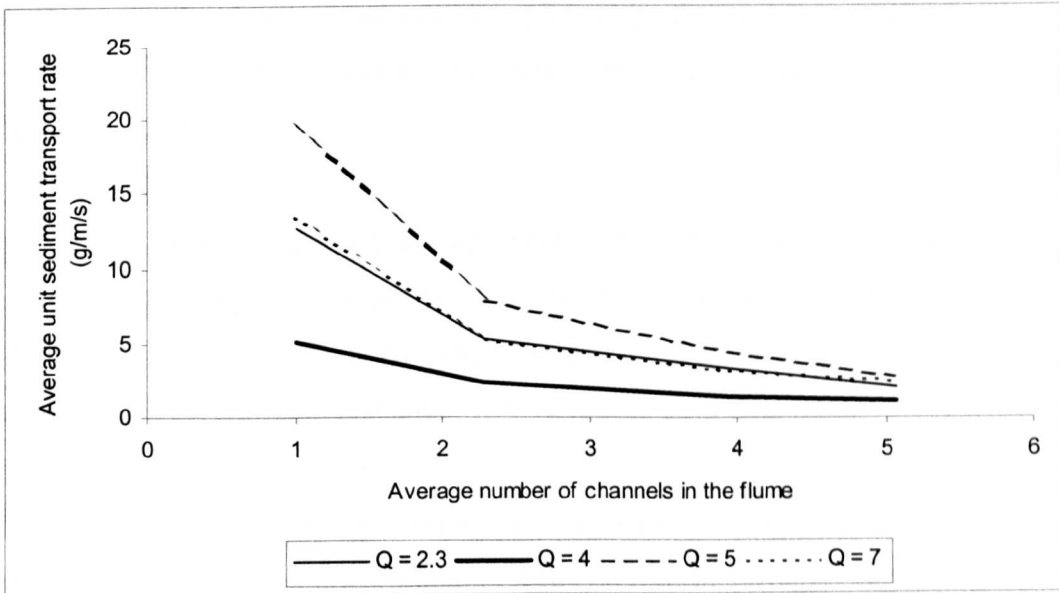


Figure 6.4. Average unit sediment transport rate versus average number of channels for each discharge (Q). Average number of channels for each flume width is as follows: 30 cm – 1 channel; 75 cm – 2.3 channels; 140 cm – 3.9 channels, 250 cm – 5.1 channels.

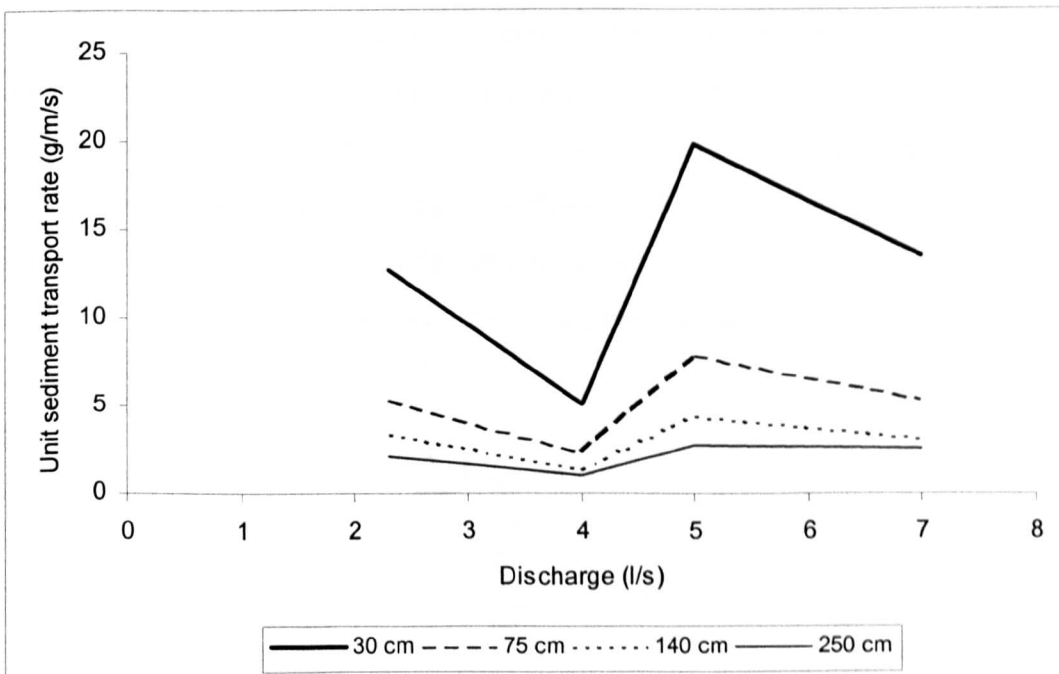


Figure 6.5. Mean unit bedload transport rate versus discharge for different flume widths.

Therefore, it may be concluded that variability in bedload transport rates is related to channel geometry. If one or two channels dominate, sediment transport rates are relatively high and relatively less variable. As the number of channels increases, transport rates become lower and more variable; this is reflected in a gradual skewing of the histograms of bedload transport rate towards lower values as flume width increases, and can be explained by the increasing aggradation due to the greater number of storage reservoirs in the flume as the planform geometry becomes braided.

However, superimposed upon the pattern of decreasing transport rate for increasing channel number is the fact that, for a given flume width, sediment transport is not linearly related to discharge. This may reflect braid intensity but may also reflect experimental conditions (e.g. sediment feed rate).

Further analysis of the time series was carried out using standard time series analysis, specifically autocorrelation. Autocorrelation provides an indication of any aperiodicity of the time series and is the first step in spectral analysis. The theory of autocorrelation has been outlined by Chatfield (1996) amongst others and is briefly reviewed here. Autocorrelation coefficients measure the correlation between observations of the time series at different distances apart. Given  $N$  observations,  $x_1, \dots, x_N$  on a discrete time series it is possible to form  $N-1$  pairs of observations,  $(x_1, x_2), \dots, (x_{N-1}, x_N)$  of successive data points, and also to find the correlation between observations at a distance  $k$  apart, where  $k$  is a lag at a constant interval. The autocorrelation coefficient  $r$ , may be calculated in several ways, the simplest and the one subject to the greatest variance is:

$$r_k = \frac{\sum_{t=1}^{n-k} (x_t - \bar{x})(x_{t+k} - \bar{x})}{\sum_{t=1}^n (x_t - \bar{x})^2} \quad (6.1)$$

where  $n$  is the sample size,  $r_k$  is termed the autocorrelation coefficient at lag  $k$  and  $\bar{x}$  is the mean of the time series (Chatfield, 1996); all of the autocorrelation coefficients must lie in the range  $[-1$  to  $1]$ .  $r_k$  can be plotted against the lag,  $k$  to produce the autocorrelation function (acf), the plot of which is termed the correlogram. The correlogram is used to identify lags at which the series correlates with itself. Autocorrelation coefficients are not valid for  $k$  greater than about  $n/4$  (Bennett 1979; Chatfield 1996)

One assumption of autocorrelation is stationarity i.e. the statistical character of the time series is unchanged throughout the time series. This means that the probability density function (pdf) associated with any part of the series is identical to that for any other part of the series. Usually for the purpose of analysis, a series must obey second order stationarity, i.e. the mean and variance remain unchanged throughout the series. Therefore if there exists an obvious trend in the mean or the variance of a series, this must be removed prior to analysis (assuming that the interest lies in the underlying series and not the trend).

The significance testing of autocorrelation functions is often accomplished by assuming that mean  $r_k = 0$  and it can be shown that the 95% confidence limits are at  $\pm 2/\sqrt{n}$  (Richards 1979; Chatfield, 1980), and that correlations outside this are significantly different from zero. Even if the series is completely random it is expected that  $\approx 1$  of every 20 values to lie outside the 95% confidence limits.

Autoregressive models were also fitted to each of Zarn's (1997) data sets. Suppose that  $\{Z_t\}$  is a purely random process with mean zero and variance  $\sigma_z^2$ . Then a process  $\{X_t\}$  is said to be an autoregressive process of order  $p$  if

$$X_t = \alpha_1 X_{t-1} + \dots + \alpha_p X_{t-p} + Z_t \quad (6.2)$$

This is rather like a multiple regression model but  $X_t$  is not regressed onto independent variable but onto past values of  $X_t$ . An autoregressive process of order  $p$  is termed an AR( $p$ ) process. For a first order process ( $p = 1$ )

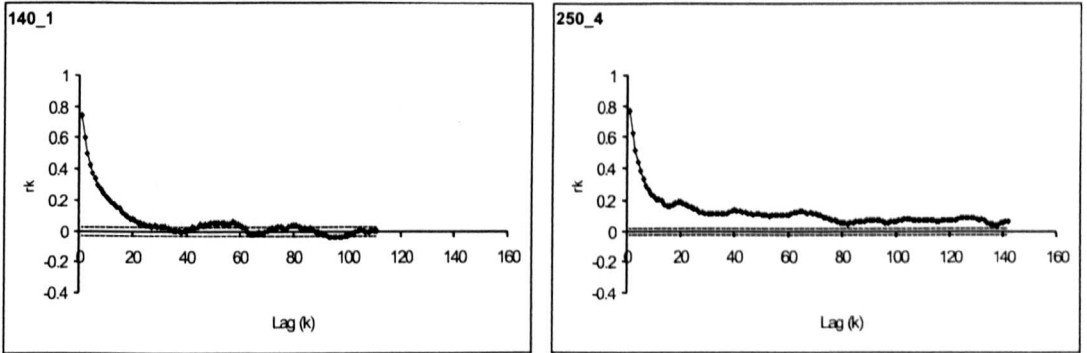
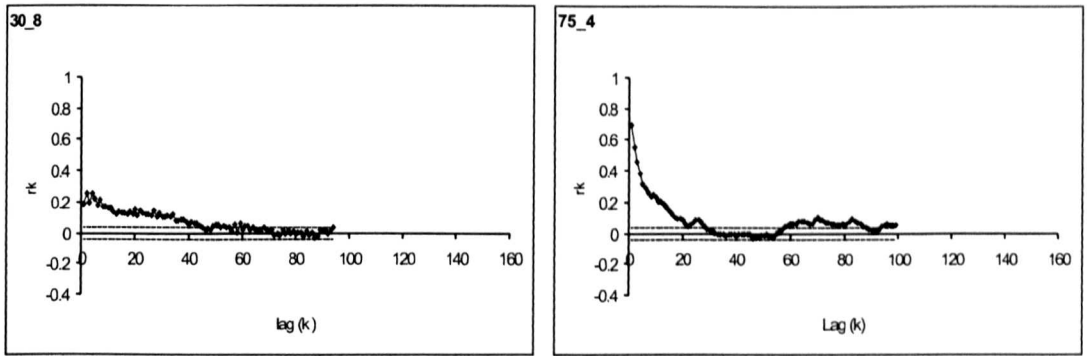
$$X_t = \alpha X_{t-1} + Z_t \quad (6.3)$$

This is sometimes called the Markov process.

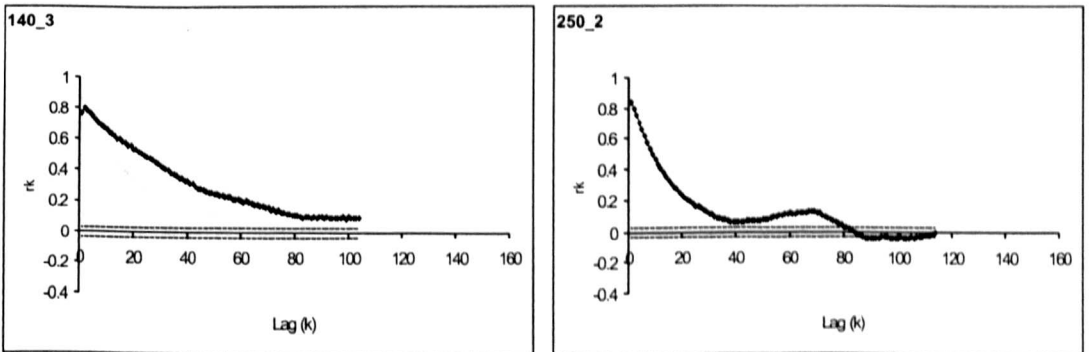
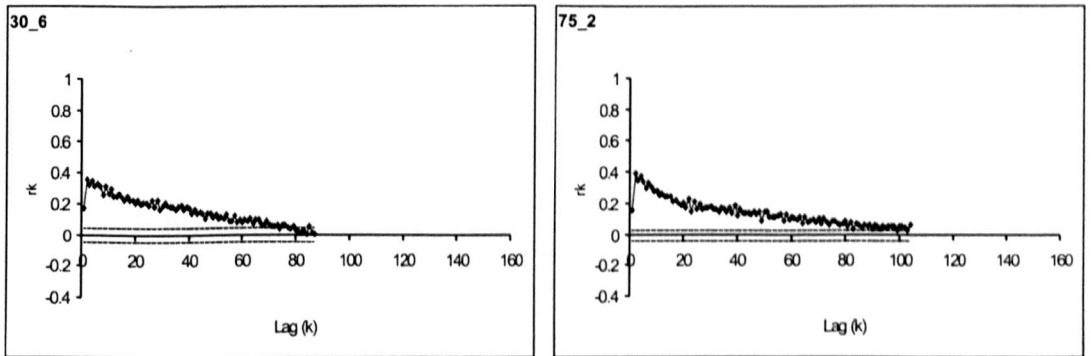
As a first attempt, autocorrelation analysis was undertaken on the raw data, however, inspection of the correlogram indicated that the series were not stationary. Autocorrelations and partial autocorrelations of the first differences of each series were undertaken, however these also displayed non-stationarity so further investigations were carried out using the residuals of a linear regression fitted to the series (see Young and Davies 1991 for an example of using autocorrelation on residuals). Correlograms of the autocorrelation function (ACF) and partial autocorrelations function (PACF) can be seen in Figure 6.6. Partial autocorrelation coefficients measure the degree of association between  $x_t$  and  $x_{t+k}$  when the effect of other time lags on  $x$  are held constant. Partial autocorrelation coefficients are defined in terms of the last autoregressive term of an AR model of  $m$  lags.

Inspection of the correlograms (Figure 6.6) indicates that none of the time series is completely random (if this was so then for a large sample size,  $r_k \approx 0$  for all non-zero values of  $k$ ). Stationary series often exhibit short-term correlation characterised by a fairly large value of  $r_1$  followed by a few further coefficients which, while greater than zero, tend to get successively smaller (Chatfield 1996). Most of the braided runs fall into this category; they show slow initial damping which suggests that they have less frequent fluctuations in the bedload transport rate. However for some runs (especially run 250\_6) the values of  $r_k$  do not come down to zero. This indicates non-stationarity, even though the autocorrelation has been performed on the linear residuals of the series to remove linear trends.

Examination of the PACF (Figure 6.7) indicates that most runs show significant PACF values at lags  $k = 1$  and  $k = 2$ . This indicates that there is greater

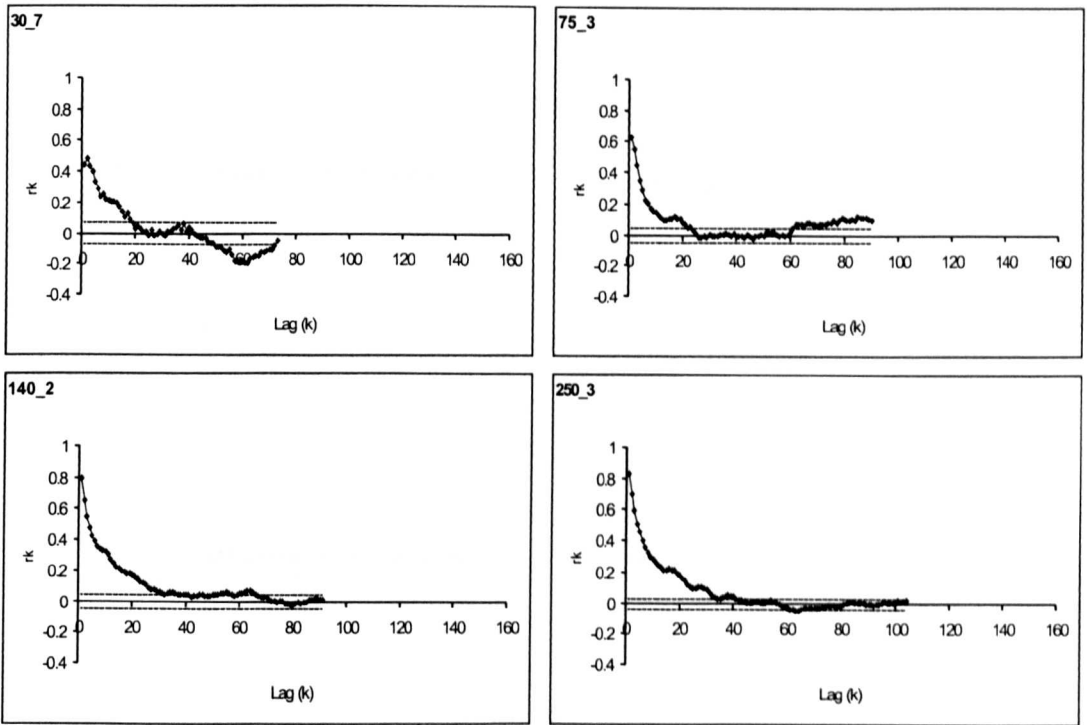


$Q = 2.3 \text{ l s}^{-1}$

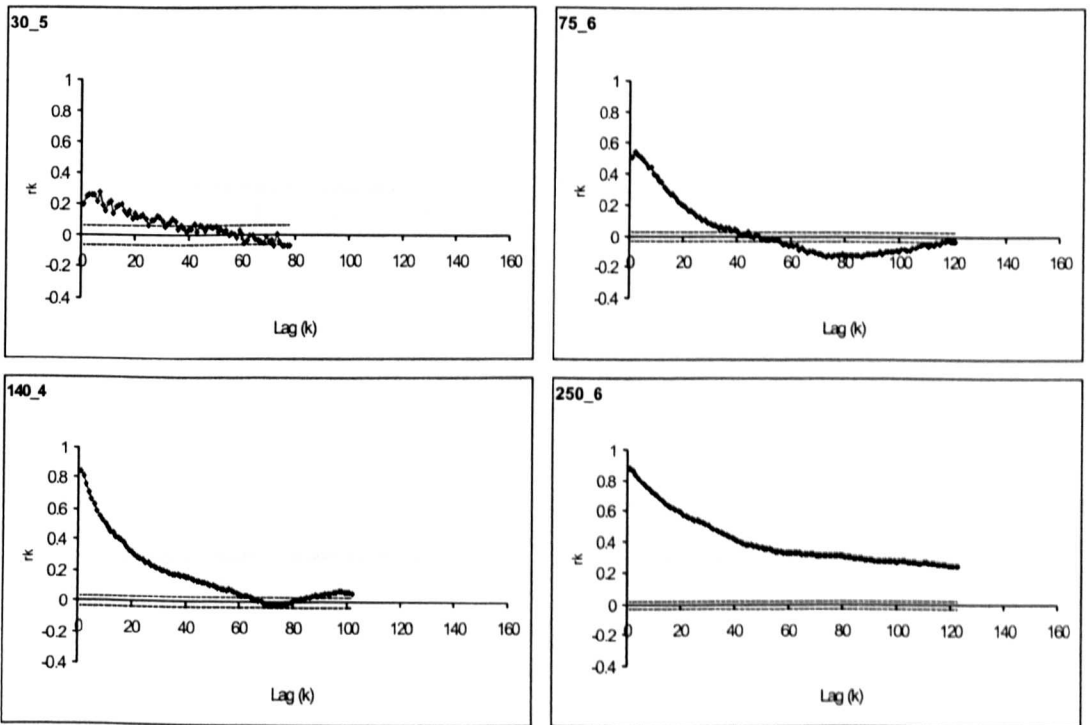


$Q = 4 \text{ l s}^{-1}$

Figure 6.6. Autocorrelation functions of the linear residuals of the bedload transport time series of Zarn (1997). Each lag ( $k$ ) is approximately 6 minutes. Confidence limits are  $\pm 2/n^{0.5}$  where  $n$  is the sample size. The confidence units are narrow due to the large sample size.

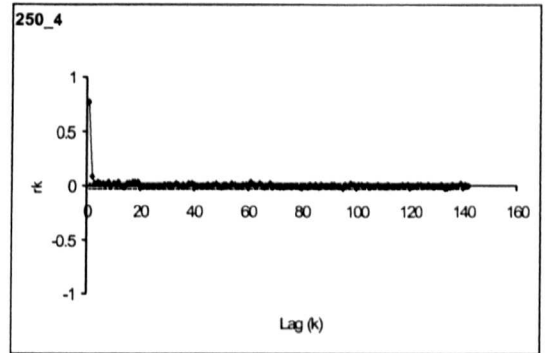
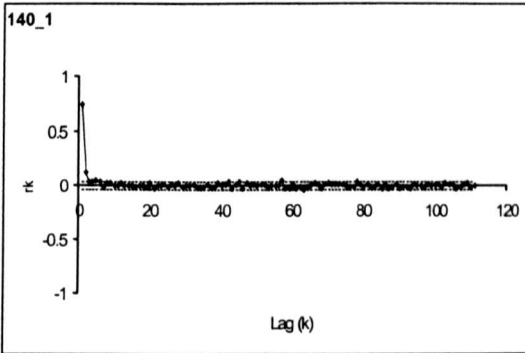
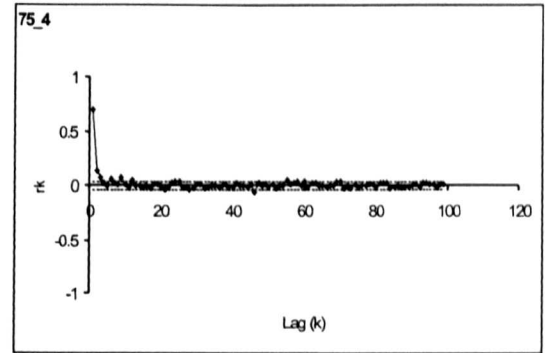
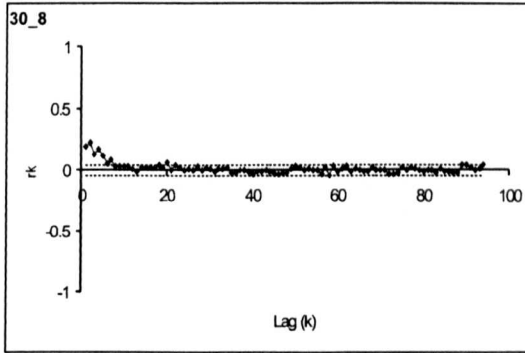


$Q = 5 \text{ l s}^{-1}$

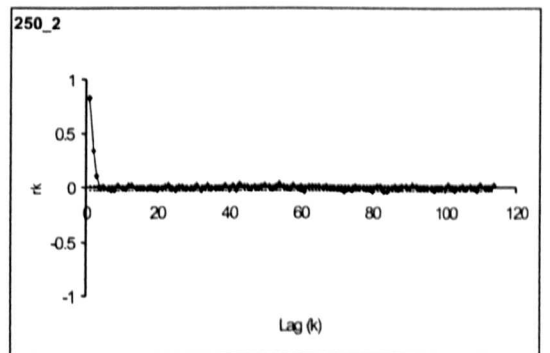
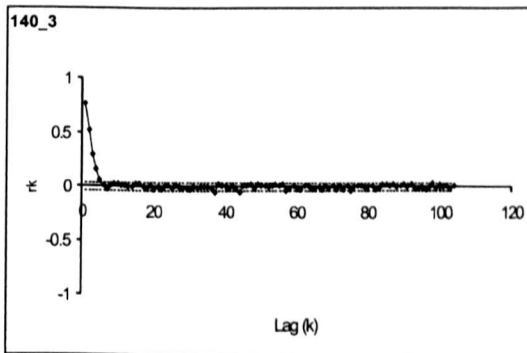
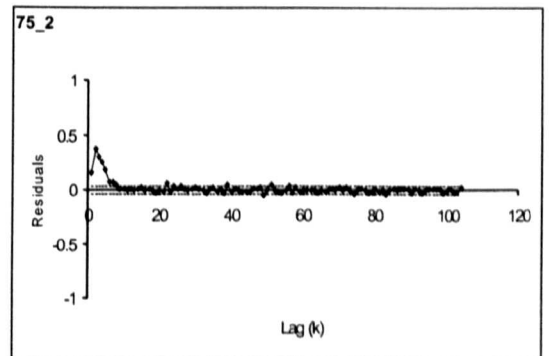
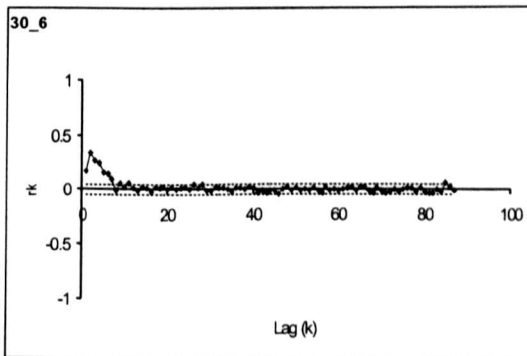


$Q = 7 \text{ l s}^{-1}$

Figure 6.6. Autocorrelation functions of the linear residuals of the bedload transport time series of Zarn (1997). Each lag ( $k$ ) is approximately 6 minutes. Confidence limits are  $\pm 2/n^{0.5}$  where  $n$  is the sample size. The confidence units are narrow due to the large sample size.

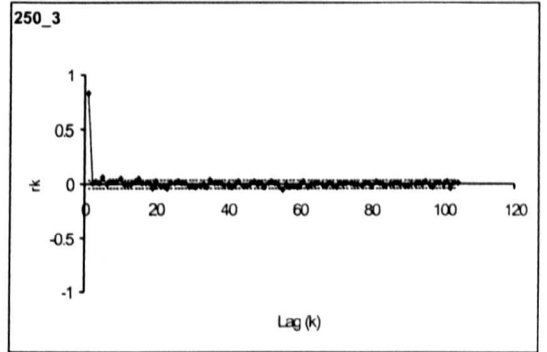
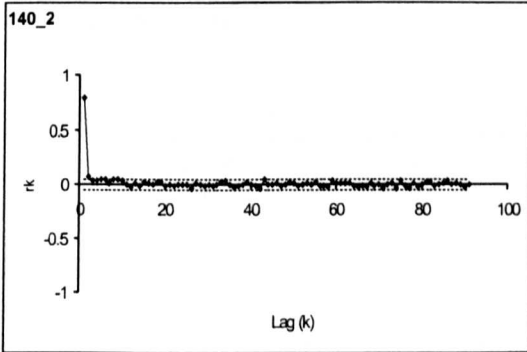
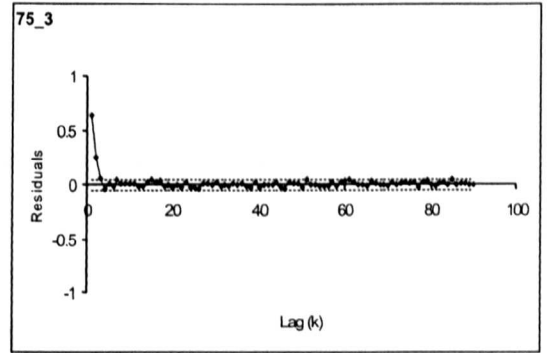
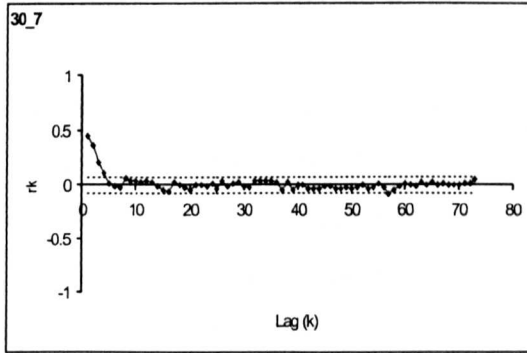


$Q = 2.3 \text{ l s}^{-1}$

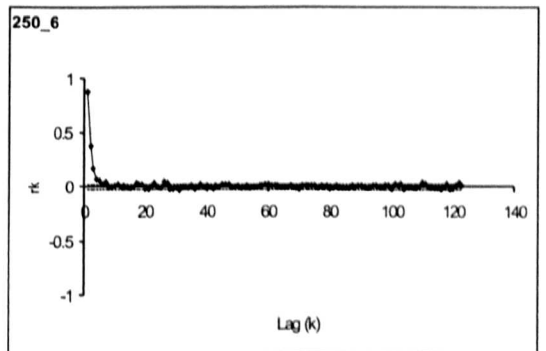
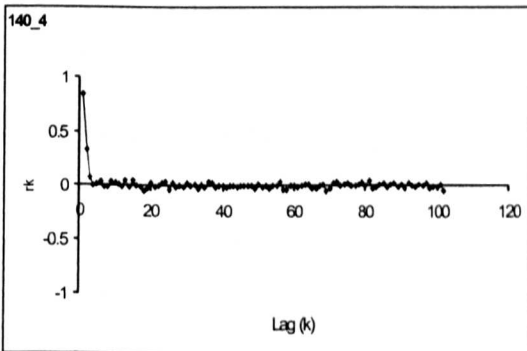
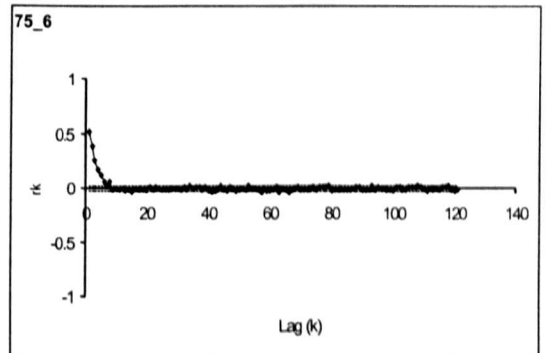
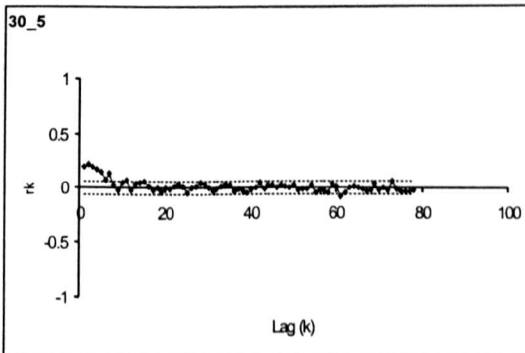


$Q = 4 \text{ l s}^{-1}$

Figure 6.7. Partial autocorrelation functions of the linear residuals of the bedload transport time series of Zarn (1997). Each lag ( $k$ ) is approximately 6 minutes. Confidence limits are  $\pm 2/n^{0.5}$  where  $n$  is the sample size. Confidence limits are narrow due to the large sample size.



$Q = 5 \text{ l s}^{-1}$



$Q = 7 \text{ l s}^{-1}$

Figure 6.7. Partial autocorrelation functions of the linear residuals of the bedload transport time series of Zarn (1997). Each lag ( $k$ ) is approximately 6 minutes. Confidence limits are  $\pm 2/n^{0.5}$  where  $n$  is the sample size. Confidence limits are narrow due to the large sample size.

persistence in the series, and that bedload transport rate is statistically dependent on the previous two transport rates.

AR(1) models (autoregression models with a lag of 1) were fitted to each raw data set (Table 6.2). Fitting an AR(1) model entails undertaking a regression analysis on a data set using the raw data at time =  $t$  for the dependent variable and the raw data at time =  $t + 1$  for the independent variable. From Table 6.2 it can be seen that as the number of channels increases the correlation of the data set with the lag of itself becomes better.

Run name	Constant, ( $Z_t$ in equation 6.3)	AR (1) term, ( $\alpha$ in equation 6.3)	P-value for AR (1) term	$R^2$
30 5	10.8	0.20	$2.98 \times 10^{-11}$	0.04
30 6	4.19	0.18	$7.26 \times 10^{-14}$	0.03
30 7	9.46	0.52	$1.76 \times 10^{-57}$	0.27
30 8	8.89	0.30	$3.36 \times 10^{-51}$	0.08
75 2	1.75	0.18	$2.14 \times 10^{-26}$	0.03
75 3	2.58	0.67	$6 \times 10^{-268}$	0.45
75 4	1.52	0.71	0	0.51
75 6	2.71	0.51	0	0.26
140 1	0.79	0.76	0	0.58
140 2	0.89	0.80	0	0.64
140 3	0.33	0.77	0	0.59
140 4	0.47	0.85	0	0.72
250 2	0.17	0.83	0	0.70
250 3	0.42	0.85	0	0.72
250 4	0.42	0.80	0	0.64
250 6	0.29	0.88	0	0.78

Table 6.2. Results of fitting AR(1) models to residuals from linear regression applied to each data set of Zam (1997).

All coefficients are significantly different from zero at  $p < 0.01$ . The overall goodness of fit of each regression is indicated by the  $R^2$  value and it can be seen that all as flume widths increase the  $R^2$  value of the data set regressed onto itself improves. There is a gradual increase in the AR(1) coefficient from single thread to braided channels but the constant decreases reflecting the smaller sediment transport rates in braided flume runs.

The correlogram is useful in identifying which type of ARIMA model gives the best representation of an observed time series. However, the interpretation of correlograms is one of the hardest aspects of time-series analysis and practical experience is important (Chatfield, 1996). It is necessary to have a stationary series to perform autocorrelation and removing trends from the data may be difficult to achieve as in some of the data here. Although inspection of the partial difference autocorrelation function may help it is difficult to assess the order of an AR process from the sample acf alone. This makes the comparison of different data sets difficult.

Finally, a quantitative comparison of distances between different time series distributions was undertaken using dynamical systems theory, specifically by comparing the time series of different runs plotted in state space. As an example, Figure 6.8 shows the time series of run 30\_7 (a run with one channel and discharge equal to  $5 \text{ l s}^{-1}$ ), plotted against itself in state space using delay embedding with a delay of 1 (i.e. plotting sediment transport at time =  $t$  versus sediment transport at time =  $t+1$ ). When the delay is equal to 1 time period it can be seen that the attractor presents a certain thickening on the first bisectrix (the 1:1 line, corresponding to periods during which the sediment transport rate has no considerable variation). Other delay times may be chosen and the application of delay embedding is not straightforward in practise because of the interaction of noise and delay time (time interval between values used in plotting an attractor). If the chosen delay time is too short, the actual change in the time series is small (a phenomena termed redundancy), and low levels of noise may mask the local structure of the attractor. If the delay time is too large (termed irrelevancy), then exponential divergence of trajectories means that the future state of the system may have little or no relation to the first values in a sequence of lagged values used to represent the initial conditions (Rubin, 1999). However, the shape of the attractor with a delay of 1 resembles that of other physical systems in which evidence of chaotic dynamics has been recognised, e.g. the Rössler attractor and a lag of 1 has been used by other workers (e.g. Porporato and Ridolfi, 1996).

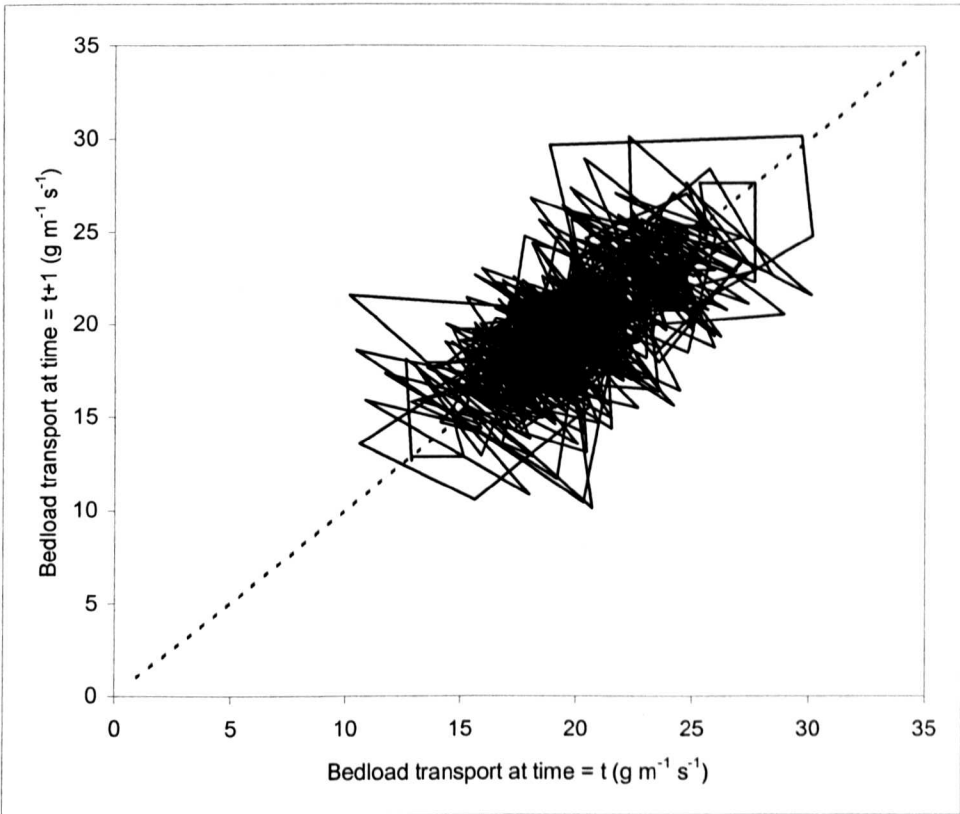


Figure 6.8. Time series of bedload transport rate for run 30\_7 plotted in state space with a delay of 1.

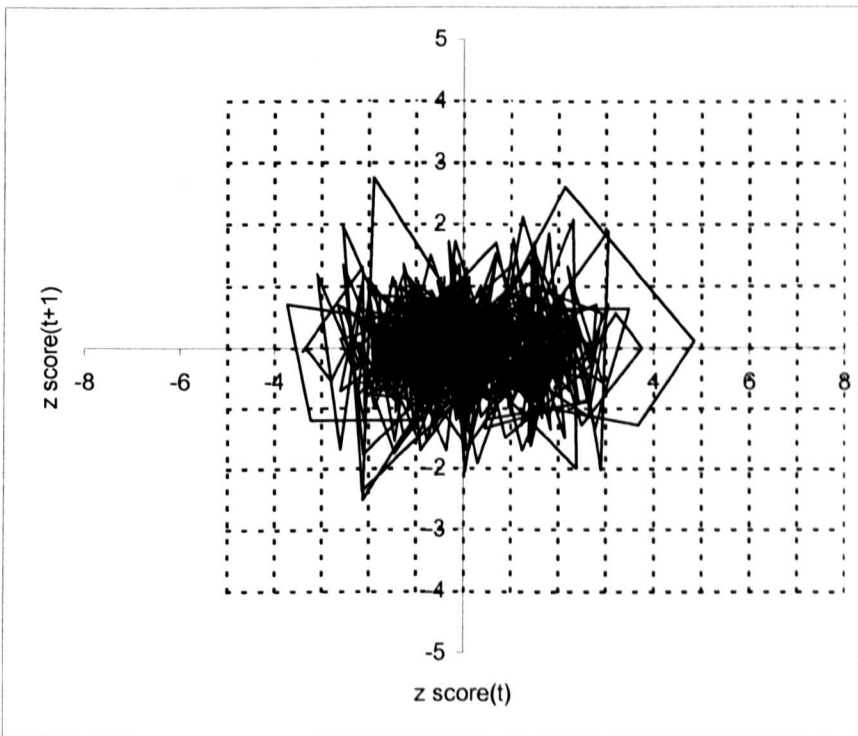


Figure 6.9. Time series data for run 30\_7 plotted as z scores and rotated clockwise so that the 1:1 line is now horizontal. Boxes are one z standard deviation square.

To quantitatively compare plots each delay embedded time series was plotted as z scores and rotated by - 45 degrees to centre each time series on the origin of the graph (Figure 6.9); the 1:1 line is now horizontal (following the x-axis). Rotation of the plot does not affect the distribution of the data set but allows for easier writing of automatic analysis routines. The formula for converting a given value of x into its corresponding z score is:

$$z_x = \frac{x - \bar{x}}{s_x} \quad (6.4)$$

where  $x$  is an observation taken from a sample with mean  $\bar{x}$  and standard deviation  $s_x$ . Z-scores are especially informative when the distribution to which they refer is normal. In every normal distribution, the distance between the mean and a given z score cuts off a fixed proportion of the total area under the curve. All normal density curves satisfy the following property (often referred to as the *Empirical Rule*); 99.7% of the of the observations fall within three standard deviations of the mean, that is, between  $\mu - 3\sigma$  and  $\mu + 3\sigma$ . To compare time series from different runs, the raw data was converted to z-scores. As the data for some runs is not normally distributed, some data will necessarily fall outside three standard deviations of the mean. Summary statistics of z scores for all runs are summarised in Table 6.3a to Table 6.3d and are grouped according to discharge, it should be noted that a normal distribution has a skew of 0.

Run name	Z-scores.			Crossing period
	min	max	skew	
30_8	-3.43	6.55	0.33	1.46
75_4	-2.59	5.58	0.66	1.65
140_1	-1.80	6.84	1.10	1.71
250_4	-1.47	9.92	1.33	1.73

Table 6.3a Summary statistics of z scores for runs with a discharge of approximately  $2.3 \text{ l s}^{-1}$ .

Run name	Z-scores.			Crossing period
	min	max	skew	
30_6	-2.63	7.31	0.49	1.42
75_2	-2.32	5.85	0.52	1.40
140_3	-1.82	5.64	0.52	1.43
250_2	-1.24	6.52	1.89	1.50

Table 6.3b Summary statistics of z scores for runs with a discharge of approximately  $4 \text{ l s}^{-1}$ .

Run name	Z-scores.			Crossing period
	min	max	skew	
30_7	-3.27	3.51	0.26	1.49
75_3	-3.79	4.77	0.19	1.53
140_2	-2.39	5.49	0.83	1.70
250_3	-1.83	6.04	1.19	1.79

Table 6.3c Summary statistics of z scores for runs with a discharge of approximately  $5 \text{ l s}^{-1}$ .

Run name	Z-scores.			Crossing period
	min	max	skew	
30_5	-3.49	4.77	-0.07	1.42
75_6	-4.69	3.99	-0.01	1.47
140_4	-2.20	4.95	1.08	1.54
250_6	-1.69	7.17	1.71	1.53

Table 6.3d Summary statistics of z scores for runs with a discharge of approximately  $7 \text{ l s}^{-1}$ .

The crossing period is defined as the average number of times the data series crosses the 1:1 line, (the line on the state space plot along which there is no change in transport rate between data points). If transport rate remained steady at all times, all points in the state space plot would plot along the 1:1 line. Therefore, when there is a marked change in the time series (i.e. moving from a peak in the

transport rate series to a trough), the time series plotted against itself will cross the 1:1 line. The crossing period is calculated as the total number of times the time series crosses the 1:1 line divided by the total number of data points in the series. The crossing period thus gives another indication of the variability in the time series; a smaller crossing period indicates a higher frequency fluctuation in transport rate (i.e. a more frequent movement between peaks and troughs in the time series).

From Tables 6.3a to 6.3d it can be seen that in general for the same discharge, the crossing period becomes larger as flume width increases, indicating that the periods of the fluctuations in transport rate decrease as the channel geometry becomes braided. For runs with one channel (the 30 cm wide flume) the crossing period is relatively similar for all discharges and is small, indicating a highly fluctuating transport rate.

Results from the crossing period may be contrasted with the variability in transport rate calculated as maximum transport rate divided by mean transport rate (see Table 6.1). Here, it was shown that as planform geometry changes from single thread to braided, variability in transport rate increases, with respect to the overall mean of the time series. However, if the crossing period is taken into account, it may be seen that, although transport rate variability increases (maximum divided by mean transport rate) as the number of channel increases, the time series structure includes fewer crossings of the 1:1 line (the crossing period increases). This finding is reinforced if the probability of each type of transition between data points is examined (Table 6.4), it may be seen that, the proportion of movements across the 1:1 line in either direction (from above to below or vice versa) decreases as the flume width (and therefore the number of channels) increases.

Figure 6.10 is a schematic diagram of the appearance of a bedload pulse in state space. It should be noted that sampling interval relative to fluctuation frequency) has an effect by determining the number of points on each limb. However as a

consistent approach is used to analyse all runs it is assumed that this is not a great issue here.

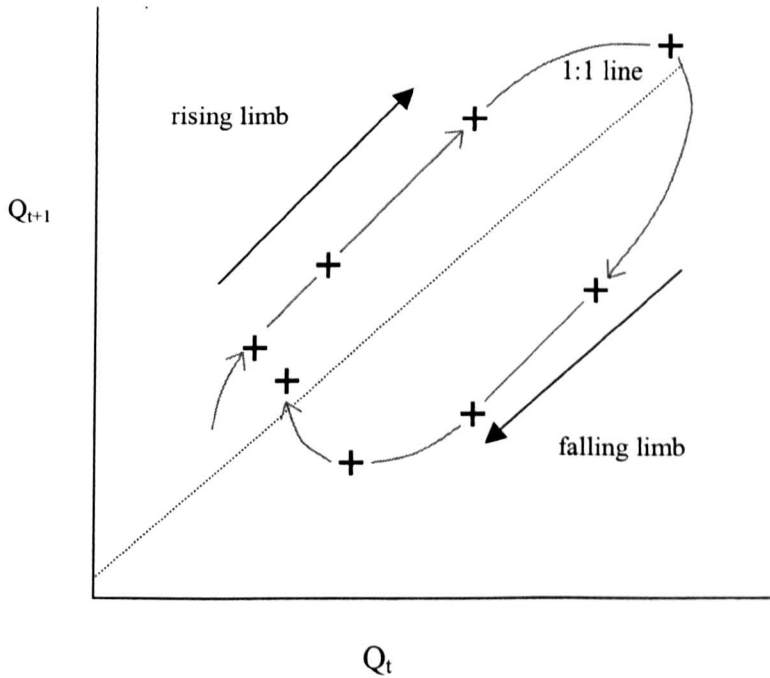


Figure 6.10. Schematic diagram of the appearance of a bedload pulse in state space.

Run name	Discharge l s <sup>-1</sup>	Proportion of each type of movement around the 1:1 line between data points in state space			
		above→above	above→below	below→above	below→below
30_8	2.3	0.171	0.343	0.343	0.143
75_4	2.3	0.195	0.303	0.303	0.200
140_1	2.3	0.206	0.292	0.293	0.209
250_4	2.3	0.211	0.290	0.288	0.211
30_6	4	0.179	0.352	0.352	0.117
75_2	4	0.165	0.357	0.357	0.122
140_3	4	0.169	0.350	0.350	0.131
250_2	4	0.175	0.334	0.334	0.157
30_7	5	0.207	0.336	0.335	0.122
75_3	5	0.187	0.326	0.326	0.161
140_2	5	0.217	0.294	0.294	0.195
250_3	5	0.215	0.280	0.280	0.225
30_5	7	0.169	0.354	0.353	0.125
75_6	7	0.171	0.340	0.340	0.150
140_4	7	0.187	0.325	0.325	0.164
250_6	7	0.178	0.327	0.328	0.167

Table 6.4. Proportion of each type of movement between data points in state space.

Therefore, there is a greater range of transport rate values for braided networks, but within the time series for these planforms, there are fewer transitions from high to low or low to high rates (i.e. there are prolonged periods of high or low transport rates, which are probably related to the channel geometry at the flume outlet). For single thread planforms, there is a smaller range of transport rate values overall, however the internal structure of the time series indicates a greater number of fluctuations from high to low (or low to high) transport rate.

If crossing period is examined with respect to discharge it may be seen that there is no simple relationship. Rather the patterns of crossing period tend to follow those of transport rate versus discharge (see Figures 6.5 and 6.11). For a given flume width, as discharge increases crossing period falls to a minimum when discharge is equal to  $4 \text{ l s}^{-1}$ , then rises to a peak at  $5 \text{ l s}^{-1}$  before falling again when discharge reaches  $7 \text{ l s}^{-1}$ . In other words, the time series of transport rate fluctuates more at discharges of 4 and  $7 \text{ l s}^{-1}$  than at discharges of 2.3 and  $5 \text{ l s}^{-1}$ . Figure 6.11 also shows the variability in crossing periods for different flume widths for a given discharge. There is a clear transition from single thread systems (30 cm wide flume) to braided systems (140 and 250 cm wide flume) reinforcing the earlier statement that, as channel planform changes from a single channel to a braided network, the time series of transport rate becomes less peaked.

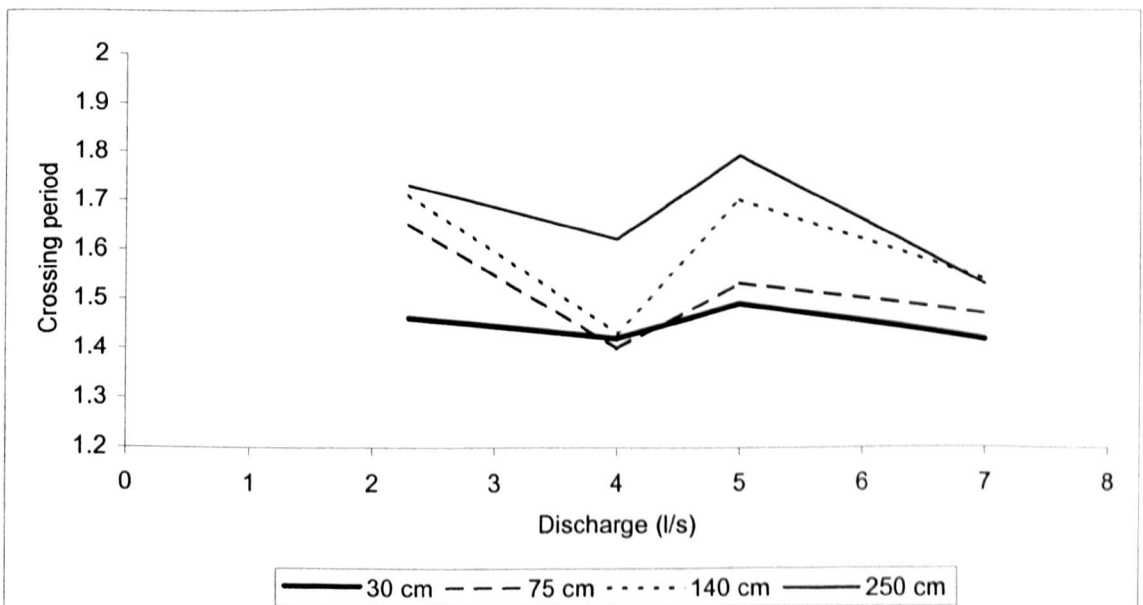
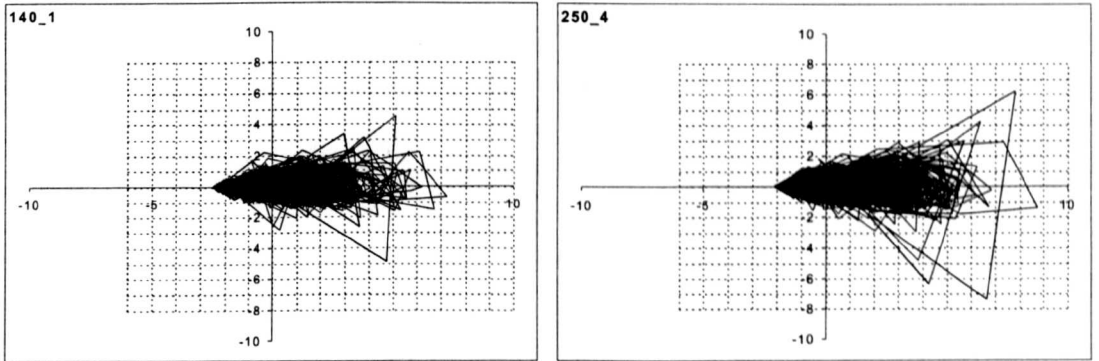
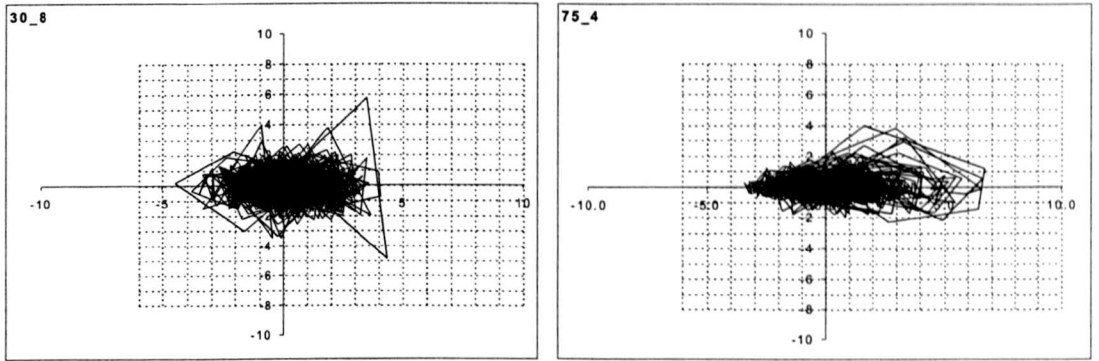


Figure 6.11. Crossing period versus discharge for runs grouped by flume width.

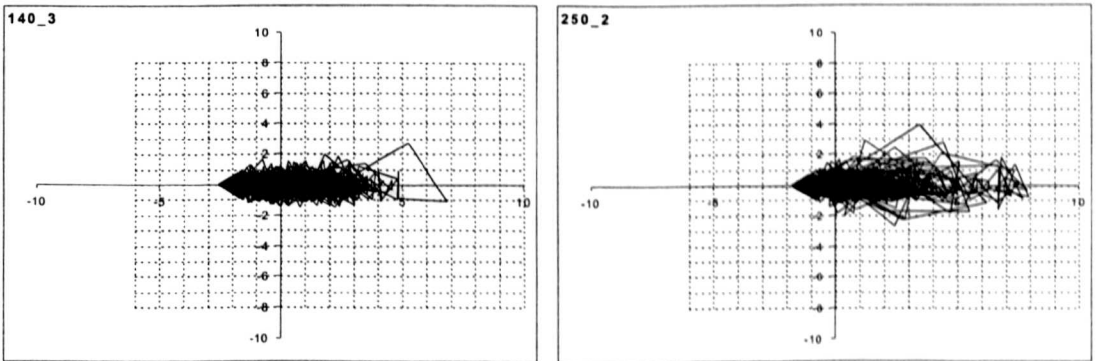
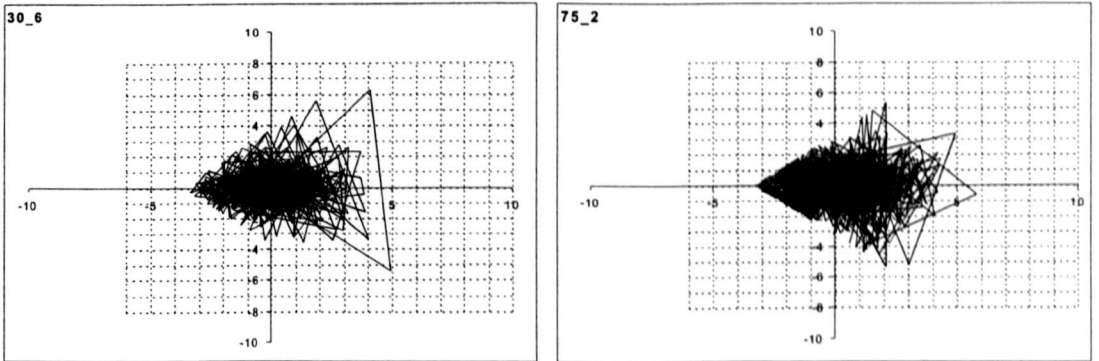
To quantitatively compute the difference between each data series in state space the state-space plots were transformed into discrete probability distributions by dividing the state space into square boxes of one z score in size (Figure 6.8) and assigning a probability to each cell that is equal to the number of points in the cell divided by the total number of points in the state space plot (cf Saphozhnikov *et al.*, 1998).

This was repeated for all boxes for two data sets at a time and the differences in percentages between the data sets were summed. An ANSI standard FORTRAN77 program RelaxIV (Bertsekas and Tseng, 1994) was then employed to calculate the distance between the two time series under investigation. This is the minimum average distance that the nodes of one distribution must move to duplicate the other distribution (Sapozhnikov *et al.*, 1998). All rotated time series plotted in state space may be seen in Figure 6.12. A visual comparison of the plots in Figure 6.12 reveals that there are differences in time series structure between runs of different width for the same input discharge. In general, for a given discharge as flume width increases, the data plot in state space moves from being centred on the origin to spreading along the positive x-axis. This reflects the movement from a normal to a positively skewed distribution.

Flume data sets were compared according to discharge. There are four different discharges and at each discharge, there are four runs with different flume widths. Therefore, within each discharge class, there are six possible comparisons between runs at different widths.

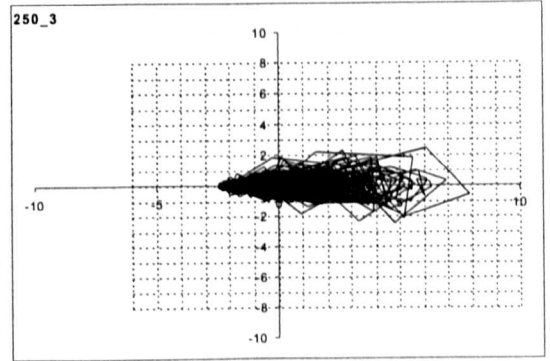
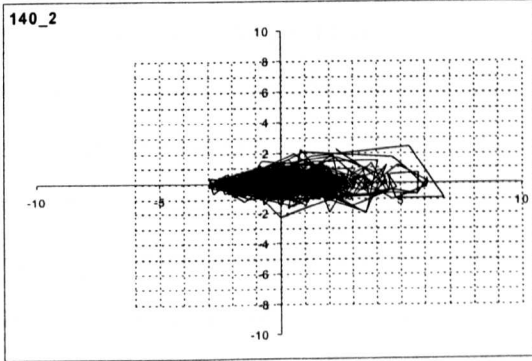
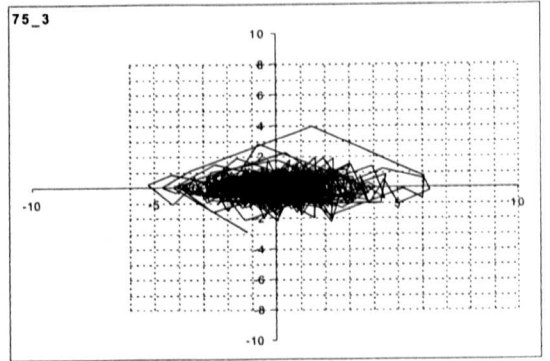
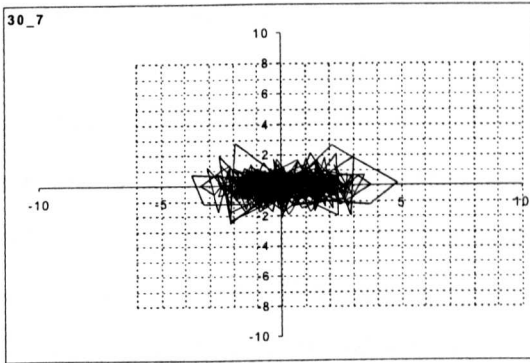


$Q = 2.31 \text{ s}^{-1}$

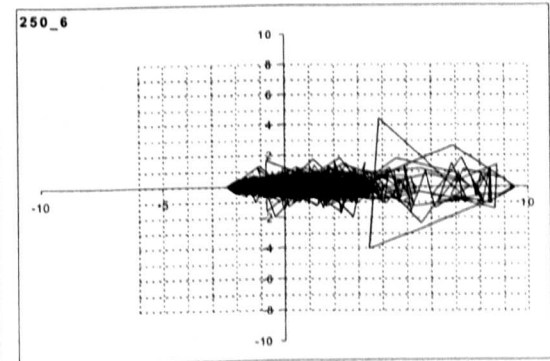
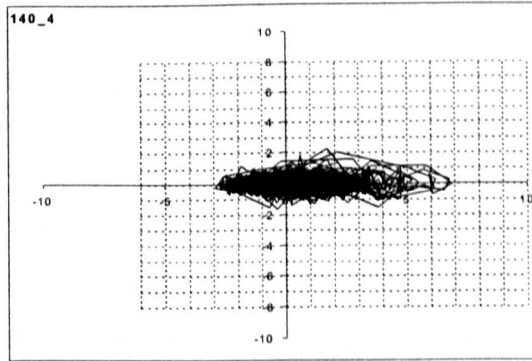
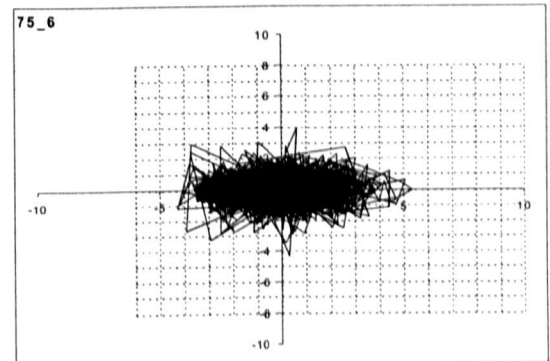
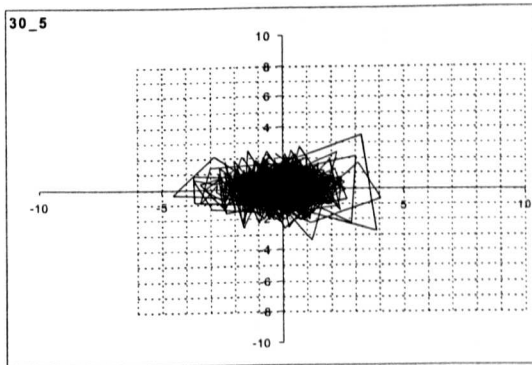


$Q = 4 \text{ l s}^{-1}$

Figure 6.12. State space plots of  $t$  versus  $t+1$  for all runs of Zarn (1997) grouped by discharge. Plots are rotated so the 1:1 line is horizontal (along the x-axis). Boxes are one z score square.



$Q = 5 \text{ l s}^{-1}$



$Q = 7 \text{ l s}^{-1}$

Figure 6.12. State space plots of  $t$  versus  $t+1$  for all runs of Zam (1997) grouped by discharge. Plots are rotated so the 1:1 line is horizontal (along the x-axis). Boxes are one z score square.

RelaxIV computes the least minimum cost flow of a set of data. On the graph of a vector data set comprising a set of nodes and directed arcs (linking the nodes), each arc has a cost which may be defined as the distance along the arc (between the nodes) and a capacity. In the utilisation of RelaxIV that follows, the capacity of each arc is set at 100 %, this allows datasets with differing numbers of data points to be compared directly. For two data sets projected onto the same number of boxes, it is possible to find the minimum cost flow between each data set. In other words, it is possible to find the minimum distance each node of one data set would have to move to replicate the second data set. The movements between nodes are weighted according to whether the flow is vertical, horizontal or diagonal. Horizontal and vertical flows have the same weight (set at 100, for a square box of side 1 multiplied by 100, as arc capacity is specified as a percentage), diagonal flows are weighted as 141, which is the length of the hypotenuse of a square of side 1 multiplied by 100 (Figure 6.13).

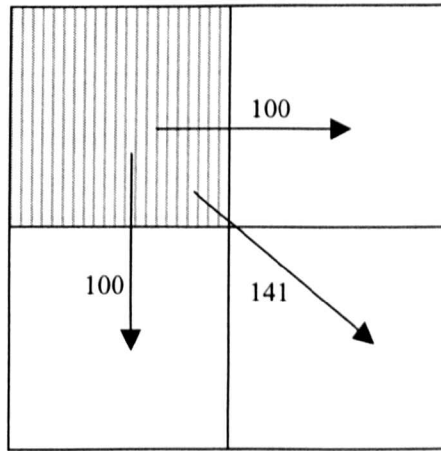


Figure 6.13. Schematic diagram of weighted node movement between cells on the state space plot. Note diagonal moves are included. Sapozhnikov *et al.*, (1998) do not include diagonal moves.

Delay embedding involves plotting a time series against a lag of itself. This replaces a scalar time series with a vector time series and gives an idea of the underlying attractor of a dynamical system (Moeckel and Murray, 1997, Rubin 1999). Therefore, it is feasible to use RelaxIV to compare time series of different runs when plotted in state space with a delay of 1.

Results from the implementation of RelaxIV are given in matrices below (Tables 6.5a-d). The greater the output value from RelaxIV the greater the difference in time series structure of the two data sets under examination. Each value is therefore the distance that needs to be moved in z-score units.

Run name					
250_4				-	
140_1			-	2.92	
75_4		-	3.20	2.25	
30_8	-	2.28	3.90	10.93	
	30_8	75_4	140_1	250_4	Run name

Table 6.5a. Matrix of RelaxIV results for runs with a discharge of approximately  $2.3 \text{ l s}^{-1}$ .

Run name					
250_2				-	
140_3			-	2.43	
75_2		-	3.24	4.01	
30_6	-	1.08	3.62	4.40	
	30_6	75_2	140_3	250_2	Run name

Table 6.5b. Matrix of RelaxIV results for runs with a discharge of approximately  $4 \text{ l s}^{-1}$ .

Run name					
250_3				-	
140_2			-	1.25	
75_3		-	1.40	2.55	
30_7	-	1.68	1.54	2.09	
	30_7	75_3	140_2	250_3	Run name

Table 6.5c. Matrix of RelaxIV results for runs with a discharge of approximately  $5 \text{ l s}^{-1}$ .

Run name					
250_6				-	
140_4			-	69.51	
75_6		-	303.59	300.33	
30_5	-	186.21	458.13	431.15	
	30_5	75_6	140_4	250_6	Run name

Table 6.5d. Matrix of RelaxIV results for runs with a discharge of approximately  $7 \text{ l s}^{-1}$ .

Some general trends can be identified from the matrices above. Firstly when comparing a single thread channel network to networks with more than one channel, the differences in time series structure increase as the number of channels increases. In other words, when comparing a single thread network (30 cm flume) to a network with on average two channels (75 cm flume), there is a greater similarity between these time series than if a single thread network was compared to a braided network of five channels (250 cm flume). For example for a discharge of  $5 \text{ l s}^{-1}$ , the distance between run 30\_7 (single thread channel) and 75\_3 (where the average number of channels throughout the run 2.34) is 168.01 z scores but is 208.90 between run 30\_7 and run 250\_3 (where the average number of channels throughout the run is 5.48). The results also indicate that there is a greater statistical similarity between networks with more channels (4, 140 cm flume and 5, 250 cm flume). For example for a discharge of  $7 \text{ l s}^{-1}$  the distance between run 250\_3 and 140\_2 is 69.51 z-scores but is 431.15 z scores between runs 250\_3 and 30\_7. Therefore, networks with a similar number of channels are more statistically similar than networks with a greater difference in channel number.

### 6.2.2. Field data: Arolla 1999.

Two time series of bedload transport rates were collected in the braided proglacial stream of the Haut Glacier d’Arolla in 1999. Data were collected on the 18<sup>th</sup> and 20<sup>th</sup> of July 1999, the methodology is outlined in Chapter 4 and time series of unit bedload transport rates for each day are shown in Figures 6.14 and 6.15. Data were collected from a single anabranch (the bridge reach) of a wide braidplain (see Figure 4.1). These data are examined below and a summary of each data set is given in Table 6.6.

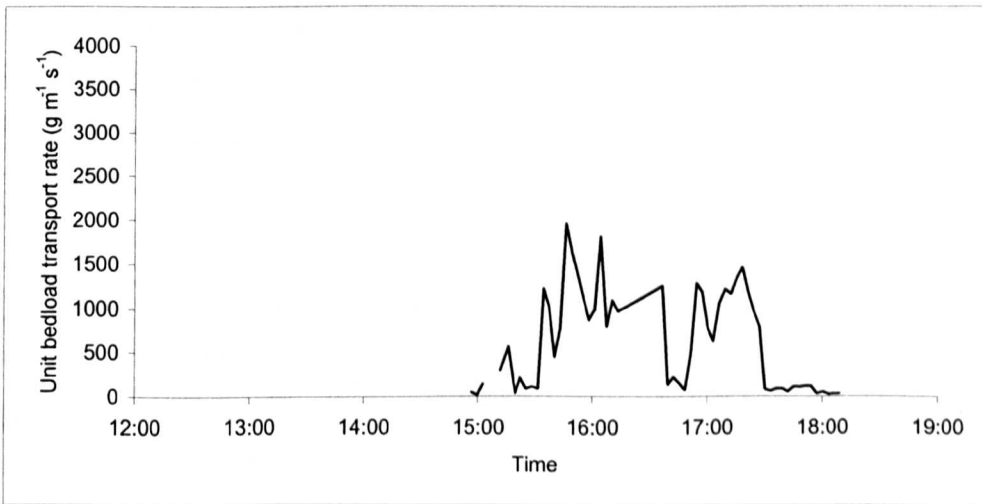


Figure 6.14. Time series of unit bedload transport rate from Arolla, 18/7/99.

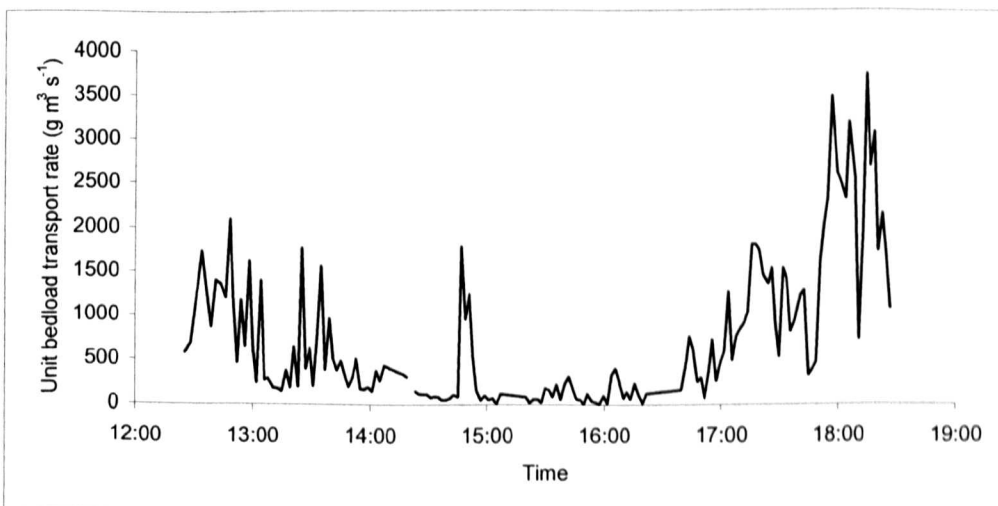


Figure 6.15. Time series of unit bedload transport rate from Arolla 20/7/99.

	18/7/99	20/7/99
Number of samples	54	157
<b>Unit bedload transport rate (g m<sup>-1</sup> s<sup>-1</sup>)</b>		
Minimum	21.08	13.5
Mean	590.3	724.5
Maximum	1964	3735
Median	378.7	387.6
St. dev	558.2	797.2
Max / mean	3.33	5.16
Average discharge* (m <sup>3</sup> s <sup>-1</sup> )	3925	3845

Table 6.6. Summary of unit bedload transport rates at Arolla, 1999. \*Average discharge is calculated as the average over the whole sampling period.

Variation of bedload transport rate is summarised in histograms in Figure 6.16. It is clear that both data sets are positively skewed; this is also apparent from Table 6.6 if the values of median transport rate are compared to the mean value in each data set. The data set of the 20<sup>th</sup> July is more variable than the data of the 18<sup>th</sup> of July when compared to the mean rate of each set (Table 6.6). Some of the bedload pulses during the 20<sup>th</sup> July reflect changes in hydraulics although sediment availability (bedforms) clearly play a role. However pulses at c. 1445 and after c. 1745 (20/7/99) are due to advection of material eroded from an undercut moraine bank 10 – 40 m upstream of the measuring station (Hoey *et al.*, 2001) and may result in greater variability of the data set.

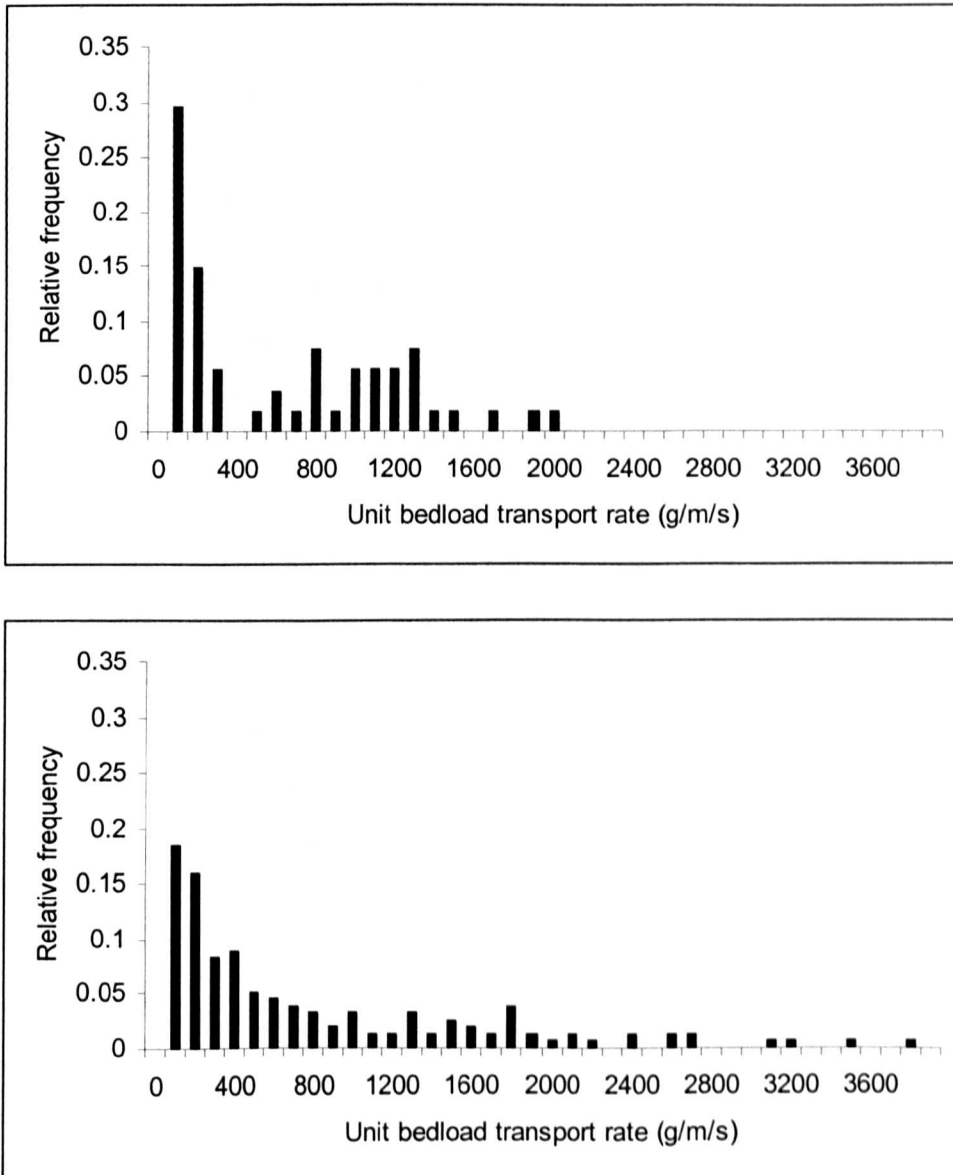


Figure 6.16. Histograms of unit bedload transport rate from Arolla **TOP** 18/7/99. **BOTTOM**: 20/7/99. Relative frequency is used due to unequal sample sizes between data sets. Sample size 18/7/99:  $n = 54$ . Sample size 20/7/99:  $n = 157$ .

Each raw data set was converted to z-scores and plotted in state space using delay embedding with a delay of 1. Raw data was used instead of transformed data to keep the analysis consistent between different data sets (i.e. between the analysis of Zarn's data and the field data). Summary statistics of z-scores and the crossing periods are summarised in Table 6.7; the proportion of each type of movement is summarised in Table 6.8.

Date	Z-scores			Crossing period
	Min	Max	Skew	
18/7/99	-1.02	2.46	0.62	1.56
20/7/99	-0.89	3.78	1.54	1.64

Table 6.7 Summary statistics of z-scores for Arolla 1999 data sets.

Date	Proportion of each type of movement around the 1:1 line between data points in state space.			
	above → above	above → below	below → above	below → below
18/7/99	0.154	0.308	0.327	0.212
20/7/99	0.168	0.310	0.303	0.219

Table 6.8. Proportion of each type of movement between data points in state space for field data from Arolla 1999.

The crossing periods for both data sets are similar to each other and are also similar to crossing periods for the braided flume runs of Zarn (1997). The crossing period is greater for 20/7/99 indicating that, although the time series of transport rates is more variable for the 20<sup>th</sup> (when measured as maximum transport rate divided by mean rate), the periods of the fluctuation increase (i.e. there are longer periods of high or low transport rates and relatively few transitions from high to low or low to high rates).

Autocorrelations were performed on the raw data (i.e. there was not a significant trend to remove) and correlograms are shown in Figures 6.17. Inspection of the correlograms indicates that both cases show slow initial dampening however values of  $r_k$  in both correlograms eventually come down to zero (cf Zarn's 1997 braided runs, Figure 6.6). Examination of the PACF (Figure 6.18) indicates that both data series show significant lags at  $k = 1$  and  $k = 2$ . This indicates that there is a greater persistence in the series, and that the bedload transport rate is statistically dependent on the previous two transport rates and is a similar results to that discovered for Zarn's (1997) data for braided flume runs.

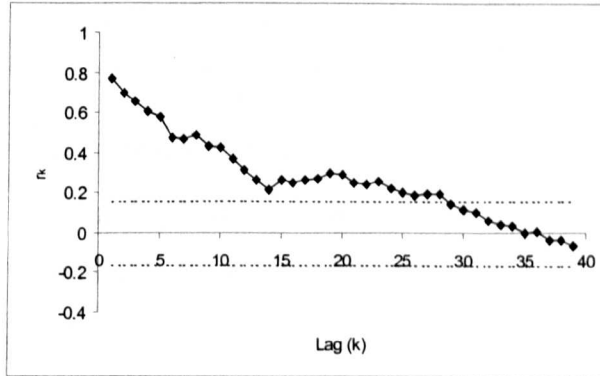
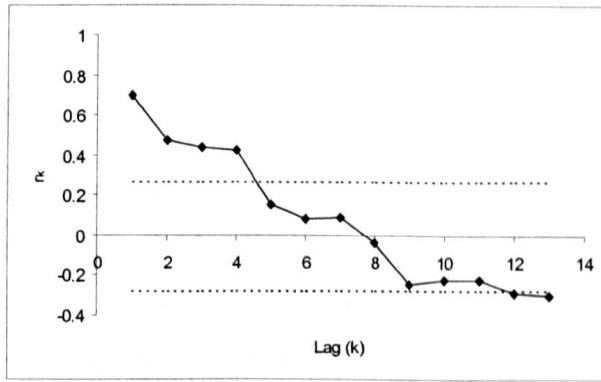


Figure 6.17. Correlograms for Arolla data. TOP: 18/7/99. BOTTOM 20/7/99. Note different scales for x axes.

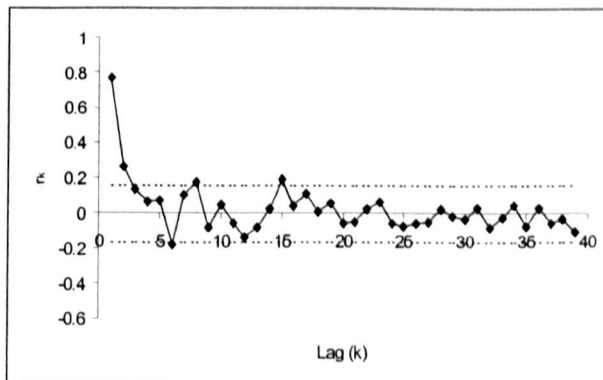
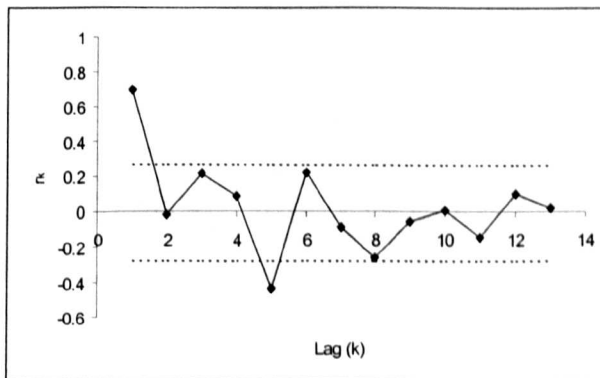


Figure 6.18. Partial autocorrelations for Arolla data. TOP: 18/7/99. BOTTOM 20/7/99. Note different scales for x axes.

AR(1) models were fitted to both Arolla datasets and the results are given in Table 6.9. Both coefficients are significantly different from zero at  $p < 0.01$ . The  $R^2$  value and the AR(1) term are similar to those of Zarn's (1997) data for braided runs, however the constant is much larger than that of the constants for Zarn's (1997) data reflecting the larger transport rates in the field.

Date	Constant	AR(1) term	P-value for AR(1) term	$R^2$
18/7/99	174.4	0.71	$2.3 \times 10^{-9}$	0.50
20/7/99	163.0	0.77	$4.67 \times 10^{-32}$	0.59

Table 6.9. Summary statistics of first order autoregression models fitted to the data from Arolla 1999.

When drawn in state space, both raw data sets are spread along the x-axis and are qualitatively more similar to the braided flume runs of Zarn (1997) than to the single thread runs (Figures 6.19 and 6.20).

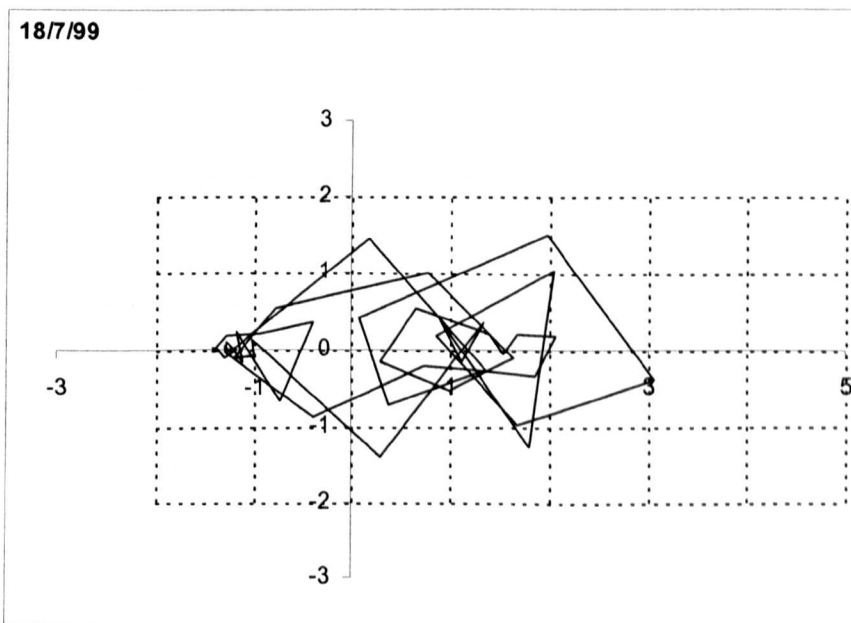


Figure 6.19 Rotated state space plot of  $t$  versus  $t + 1$  for Arolla data, 18/7/99. Boxes are one standard deviation square.

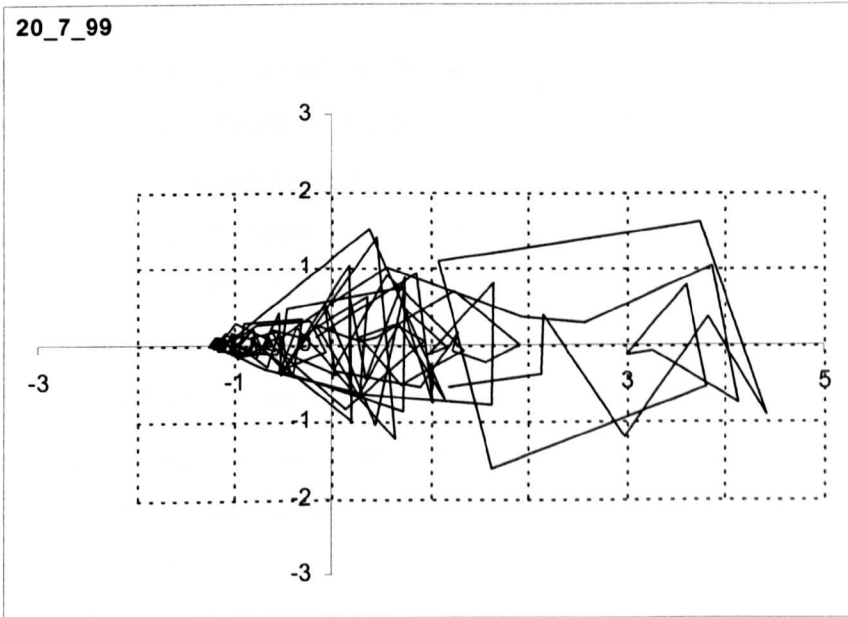


Figure 6.20 Rotated state space plot of  $t$  versus  $t + 1$  for Arolla data, 20/7/99.

RelaxIV was used to compare the two data sets from Arolla with each other; the RelaxIV result was 443.89 indicating that the data sets are dissimilar. When compared to the RelaxIV results obtained from Zarn’s (1997) data result is similar to those obtained when comparing single thread flume runs with braided flume runs.

Each data set was compared with flume data from Zarn (1997) for one discharge ( $5 \text{ l s}^{-1}$ ). This discharge was chosen to avoid the extreme low or high discharges used in the flume runs; raw data was used (i.e. no transformations were undertaken on the either the field or flume data). It is important to remember that this is not an exact comparison as laboratory models trap bedload across the entire braidplain width, and provide spatial integration that is not present when point sampling is used (Hoey *et al.*, 2001). Table 6.10 gives a matrix of results for these comparisons.

Date				
18/7/99	474	491	470	465
20/7/99	348	409	infeasible	229
Run name	30_7	75_3	140_2	250_3

Table 6.10. Matrix of results of Arolla field data compared to Zarn’s (1997) flume data using RelaxIV. An infeasible result indicates that the numerical program could not resolve the problem.

The matrix of results suggests that the structure of the field data is dissimilar to that of the flume runs. An “infeasible” result is returned for the comparison of the field data from 20<sup>th</sup> July 1999 and flume run 140\_2 and indicates that RelaxIV could not resolve the problem. The majority of results returned are of a similar magnitude to the comparisons of Zarn’s (1997) flume runs with single thread and braided channel networks. The one exception is the comparison of the field data from 20<sup>th</sup> July 1999 with the narrowest flume width (30\_7) and the widest flume run (250\_3); smaller output values from RelaxIV reveal that structure of the these data sets are more similar than any of the other comparisons made. In other words, the structure of the time series data from 20<sup>th</sup> July 1999 shows some similarity to the single thread flume run but more similarity to the braided flume run, however the comparisons indicate that the nature of both similarities are weak. Overall RelaxIV shows that the internal structures of the time series of the field data differ from each other and are also are unlike the time series structure of any of the flume data sets. This may be a consequence of the different sampling methods used.

### **6.2.3. *Braided Cascade* runs.**

Model runs were undertaken with different grid dimensions (length to width ratios) to ascertain whether or not the numerical model results followed a similar pattern to the data of Zarn (1997), obtained by physical modelling using flumes with different braidplain widths, and field data from Arolla. Three runs were undertaken and their results examined in detail. As the grids used for two of these runs were large the time taken to process each run was high (e.g. 9 days for Run 3) therefore, only three runs have been undertaken for this chapter. Run conditions are given in Table 6.11.

Parameter values	Run 1	Run 2	Run 3
<b>Grid dimensions</b>			
Length, L	500	500	500
Width, W	3	6	14
Mean nodal spacing (delta)	1.002	1.002	1.002
<b>Overall DEM/grid</b>			
Slope, Si	0.02855	0.02855	0.02855
Amplitude of white noise random topography	0.071375	0.071375	0.071375
Timestep, dt (secs)	1	1	1
<b>Upstream boundary conditions</b>			
Discharge	5	5	5
Sediment input	Sedeqb at time t = 1	Sedeqb at time t = 1	Sedeqb at time t = 1
<b>Initial conditions</b>			
Qratio	0.95	0.95	0.95
Upratio	0.95	0.95	0.95
Erosion length scale	100.02	100.02	100.02
Deposition	ON	ON	ON
Diffusion	ON	ON	ON
Diffusion constant	$1 \times 10^{-8}$	$1 \times 10^{-8}$	$1 \times 10^{-8}$
Run length (iterations)	250 000	250 000	250 000

Table 6.11. Run conditions for long *Braided Cascade* runs.

Run conditions were chosen to force the model to either braid or remain in a single channel. The model grid for Run 1 was three nodes wide, however two nodes are situated on either side boundary effectively confining the channel to one node wide, this run was used to simulate a single thread channel. Runs 2 and 3 are wider, allowing differing degrees of channel bifurcation and therefore braiding. Water was introduced at all nodes along the upstream boundary that were not situated on side boundaries. Hence, all water was introduced at node 2 in Run 1; in Runs 2 and 3 total discharge was divided by available nodes (4 in Run 2 and 12 in Run 3) and an equal amount of water was added at each node. Water was added at each timestep at a constant rate. Sediment was also introduced at all available nodes on the upstream boundary at a constant rate which was set to equal the equilibrium sediment transport of each node at time  $t = 1$ . Sediment output was monitored at the downstream end of

the grid. In this respect the method of obtaining model output is similar to that of obtaining flume data, i.e. the output data are spatially integrated across the entire braidplain.

### **6.2.3.1. Model results.**

#### **6.2.3.1.1. Run 1.**

Run 1 was used to simulate the case of a single thread channel planform. Confining the channel to one node throughout the run forced the production of a single thread channel. It may be expected that the temporal sediment transport rates would settle into a static state throughout the run, however a constant sediment input produced a varying sediment outflux throughout the run (Figure 6.21). As the side boundaries cannot erode and the channel in Run 1 is only one node wide, no sediment can be supplied to the channel from the sides. Therefore, diffusion erosion is not relevant in this run, and all erosion can be thought of as fluvial.

The time series of sediment outflux from the (Figure 6.21) shows that there was an initial peak in sediment outflux before the model reached a “steady” state from 37 000 to 117 000 (however it should be noted that sediment outflux was increasing very slowly during this time period). Sediment outflux oscillates between 119 000 and 140 000 iterations before steadily climbing to reach another “steady” state at 140 000 until 200 000 iterations (again sediment outflux rates were slowly increasing). The run was stopped after 250 000 iterations (approximately 69 hours or 2.89 days). It is possible that, had the run been allowed to continue, the sediment outflux would have become more variable (as the model had appeared to settle into a steady state between approximately 100 000 to 200 000 iterations), however this is not certain. The approach to steady state may reflect a gradual slope adjustment. What is apparent is that model output is very dissimilar to output from single thread channels modelled in the flume by Zarn (1997) and may reflect a limitation of the model, i.e. that the small scale processes that are not modelled are actually important.

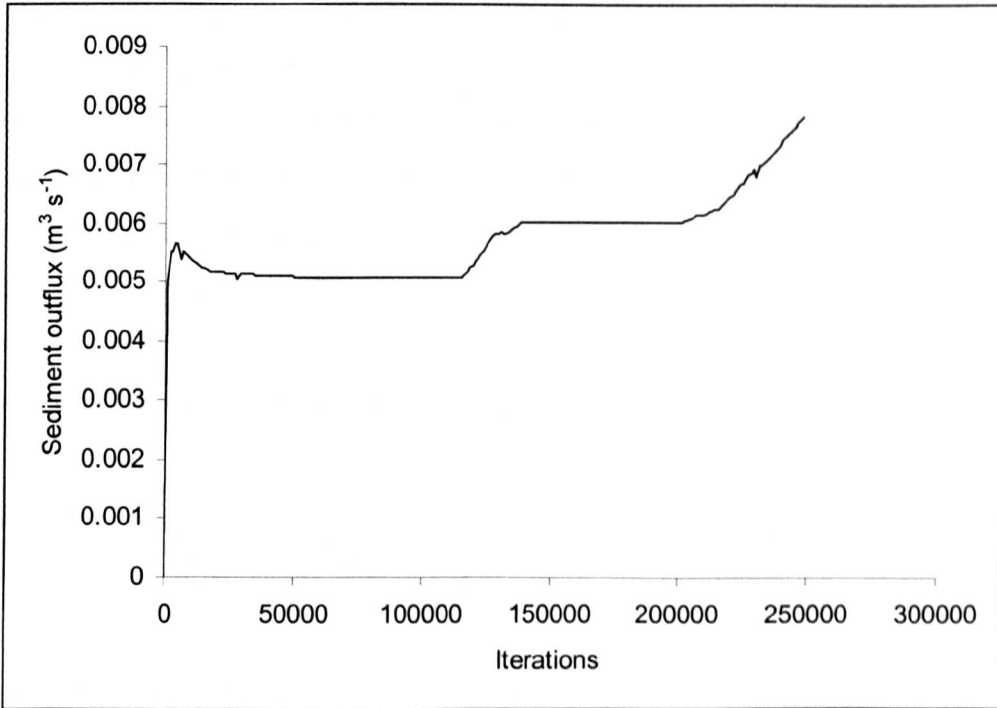


Figure 6.21. Time series of sediment outflux from the grid for a run with a single channel.

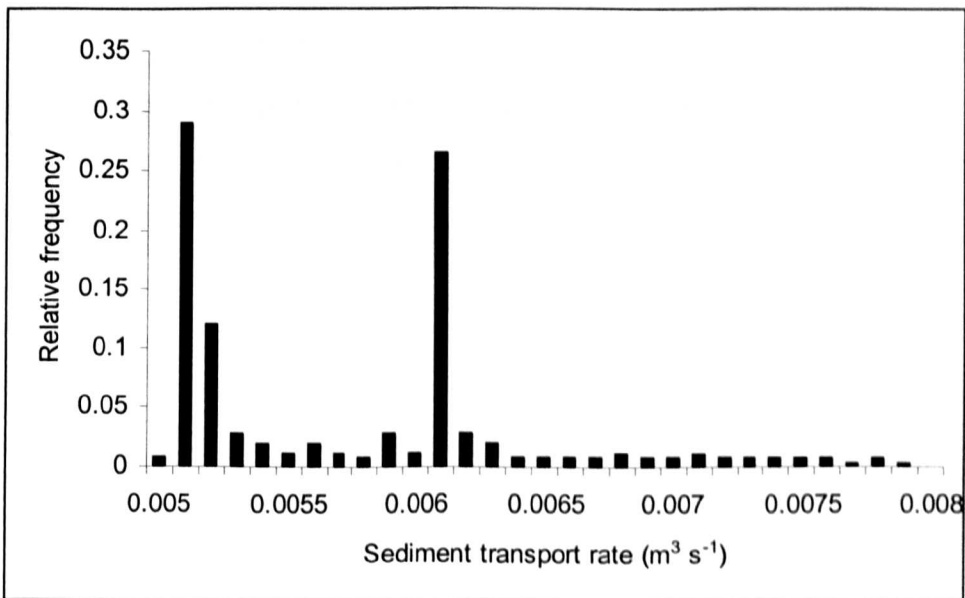


Figure 6.22. Histogram of sediment outflux from model run 1 with a single thread channel. Note that relative frequency is used on the y-axis.

The sediment outflux rates are bimodal, due to long periods in which the model reached a static state (Figure 6.22). The bimodality of the data leads to the values for median transport rate being similar to those for mean transport rate (Table 6.12), a result that would be expected if the data series were normally distributed. However, the shape of the histogram indicates that the model result is dissimilar result as that of Zarn's (1997) data for single thread channels, which produced normally distributed histograms. Variability in sediment outflux rates is not great, within the model run the sediment outflux rates varied from just under the mean rate to just over the mean rate (Table 6.12) again reflecting long periods of constant outflux rate.

Run name	Sediment outflux ( $\text{m}^3 \text{s}^{-1}$ )				
	Min	Mean	Maximum	Median	Max/mean
Run 1	0.0050	0.0057	0.0078	0.0056	1.37

Table 6.12. Variability of sediment outflux from Run 1.

Inspection of the time series plot indicates that the series is not stationary (Figure 6.19), therefore to carry out formal time series analysis the data was transformed and autocorrelation was undertaken on the first differences of the series. Inspection of the correlogram (Figure 6.23) shows that there are significant lags at  $k = 2$  and  $k = 3$ . The partial autocorrelation function (PACF, Figure 6.24) shows that there is a significant lag at  $k = 1$ , i.e. the value of sediment outflux is statistically dependent on the previous outflux rate.

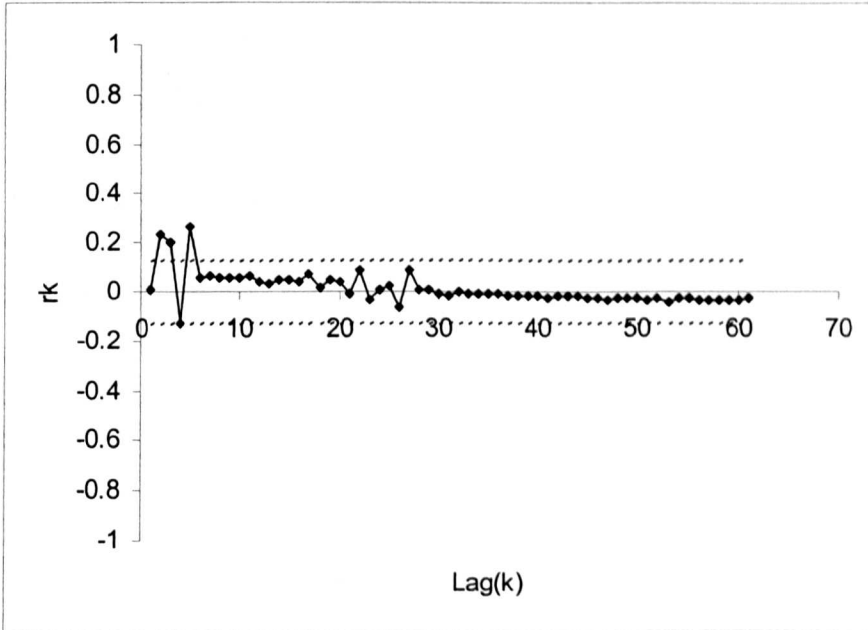


Figure 6.23. Correlogram for *Braided Cascade* Run 1, using first differencing.

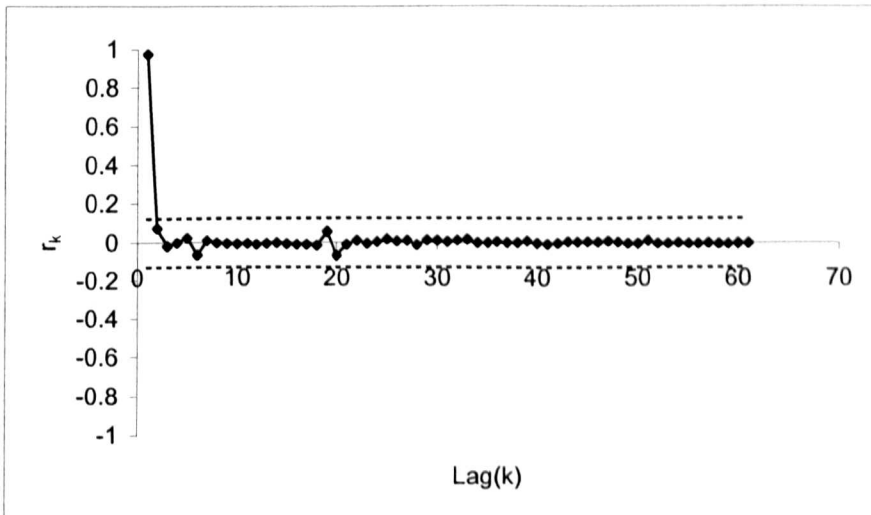


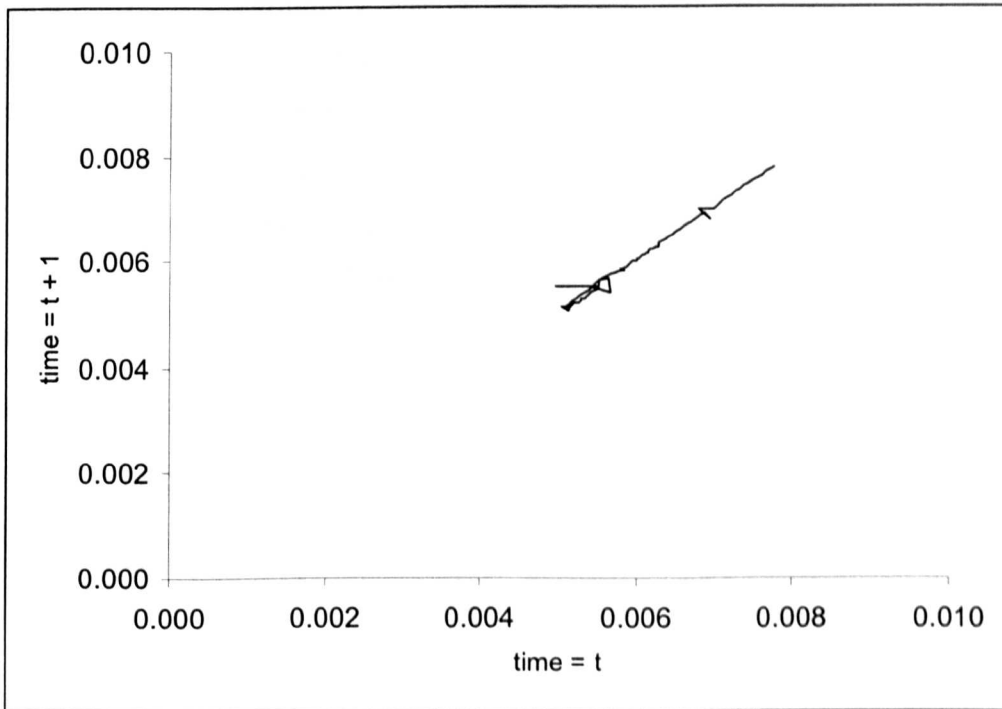
Figure 6.24. Partial autocorrelation function for *Braided Cascade* Run 1 using first differencing.

Using an AR(1) model on the sediment outflux indicates that the regression model explains nearly all of the variance in transport rate ( $R^2$  is 0.99, Table 6.13), and the coefficient is significantly different from zero. The success of the AR(1) model at explaining variation in transport rate is due to the long periods of steady transport rate causing most data points to plot along the 1:1 line in state space.

Run name	Constant	AR(1) term	P-value for AR (1) term	R <sup>2</sup>
RUN 1	0.0001	0.98	$4.2 \times 10^{-280}$	0.99

Table 6.13. Summary statistics of AR(1) regression for *Braided Cascade* run 1.

If the model results are plotted in state space (Figure 6.23) the majority of data points plot along the 1:1 line (i.e. a line attractor) indicating long periods when outflux changes only slightly. This is reinforced by the large crossing period (14.53).

Figure 6.25. Sediment outflux from *Braided Cascade* Run 1 plotted in state space.

Overall Run 1 fails to produce realistic results for a single thread channel. The results produced are qualitatively very different from single thread channel runs produced in the flume by Zarn (1997). The sediment outflux from Run 1 is stepped in appearance and may reflect slope changes that progress upstream along the grid.

### 6.2.3.1.2. Run 2.

The grid used for Run 2 was composed of 500 nodes long and 6 nodes wide to simulate a similar effect as the narrower runs of Zarn (1997) but to allow the model to braid. Water and sediment were added at every node on the upstream boundary (i.e. nodes 2 to 5) at a rate given in Table 6.10. Time series of sediment output from the grid is shown in Figure 6.26. Figure 6.26 indicates that sediment output fluctuates for the first third of the run until a peak is reached after 85 000 iterations and declines steadily thereafter until a steady state is reached around 172 000 iterations. Figure 6.27 shows channel pattern at certain times throughout the run (20 000, 37 000, 85 000 and 210 000 iterations, see Figure 6.26 for an indication of where these points lie in the time series). It may be seen that channel pattern does not change greatly as the run progresses and areas of braiding and single thread channels remain relatively constant.

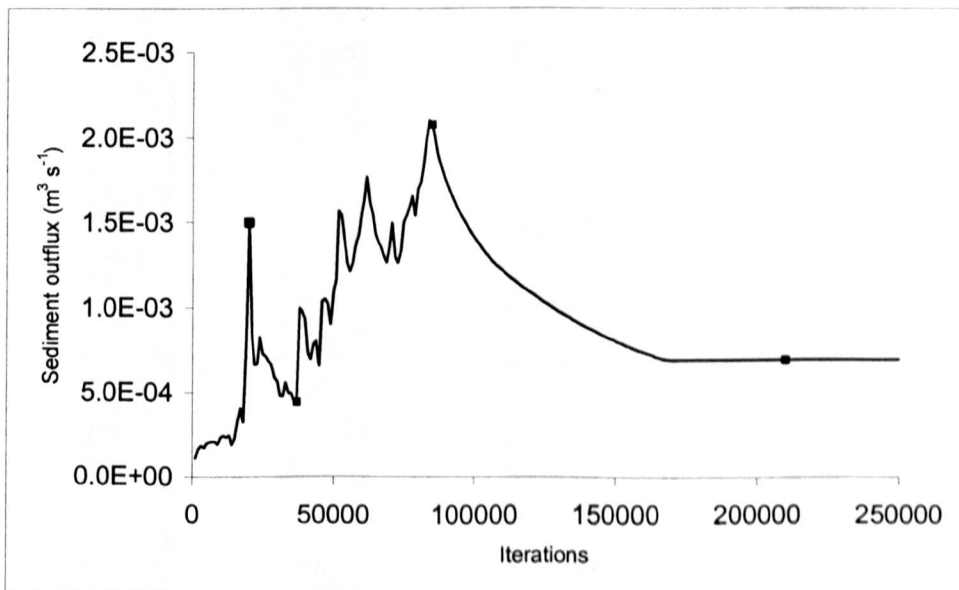


Figure 6.26. Time series of sediment outflux from the grid for *Braided Cascade* Run 2. Points indicated by a square marker are those points in time where channel pattern has been plotted in Figure 6.27.

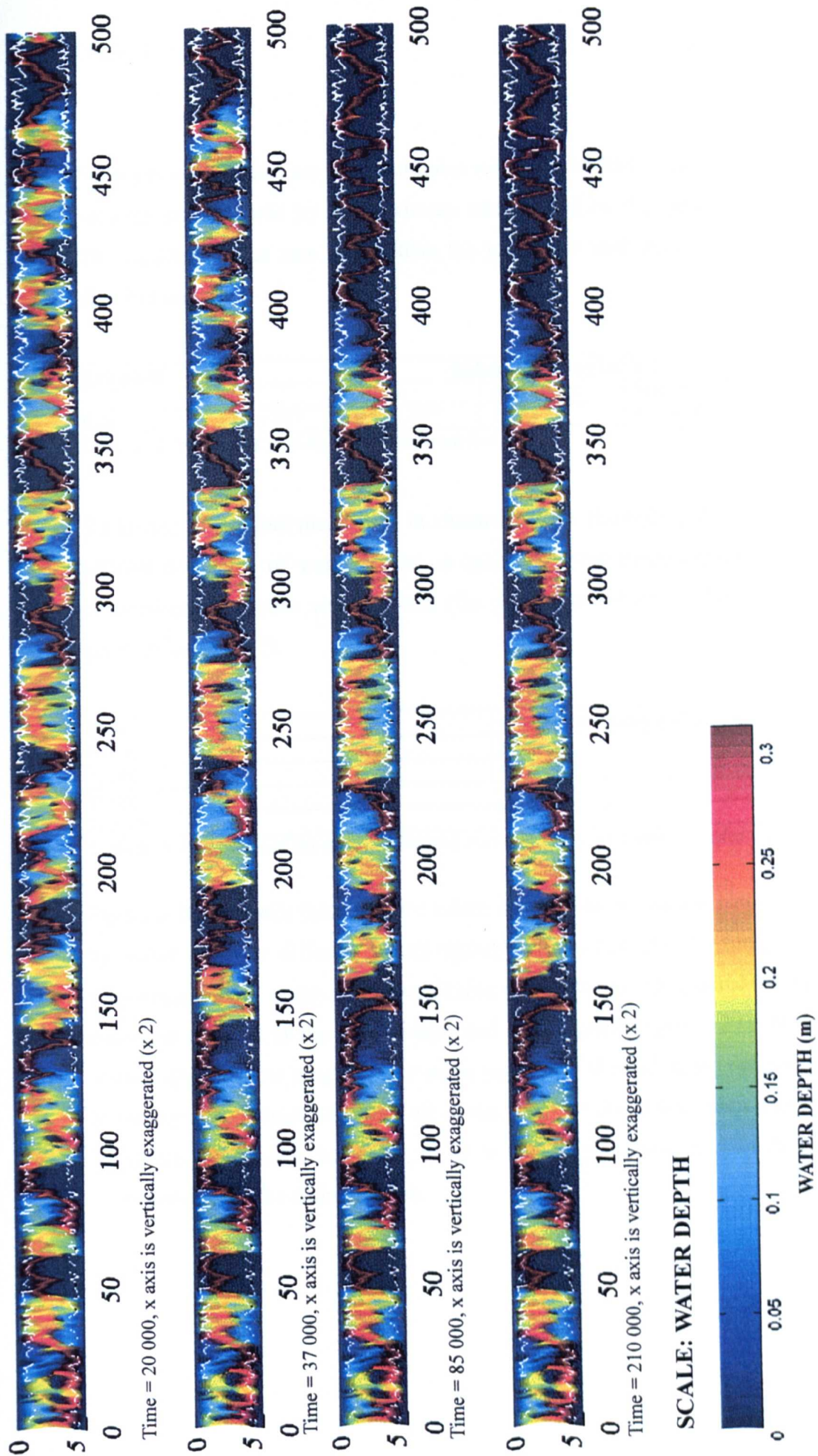


Figure 6.27. Plots of water depth on the grid at different times throughout Run 2.

Sediment output rates are less than those recorded for Run 1, however they are more variable as calculated by the maximum rate divided by the mean rate (Table 6.14). The median outflux rate is less than the mean rate indicating a positively skewed distribution.

Run name	Sediment outflux ( $\text{m}^3 \text{s}^{-1}$ )				
	Min	Mean	Maximum	Median	Max/mean
Run 2	$1.06 \times 10^{-4}$	$9.57 \times 10^{-4}$	$2.10 \times 10^{-3}$	$8.38 \times 10^{-4}$	2.20

Table 6.14. Variability of sediment outflux from Run 2.

To further investigate the change in channel pattern throughout Run 2 histograms of relative frequency of water depths on each grid were plotted (Figure 6.28), to aid comparison dry nodes were omitted (the proportion of dry nodes in each grid are given in Table 6.15).

Time	Proportion of dry nodes on grid
20 000	0.52
37 000	0.52
85 000	0.57
210 000	0.57

Table 6.15. Proportion of dry nodes on the grid at certain times throughout *Braided Cascade* Run 2.

Figure 6.28 indicates that there are subtle differences in channel pattern as indicated by water depth at differing points throughout the run. As the run progresses the proportion of dry nodes increases (Table 6.15) due to the gradual incision of one dominant channel at the downstream end of the grid (Figure 6.27). Histograms of water depth become progressively more negatively skewed as the run progresses due to the incised channel capturing all of the water at the downstream end of the grid. Therefore, there does not seem to be a direct link between channel pattern and sediment output rate from the grid.

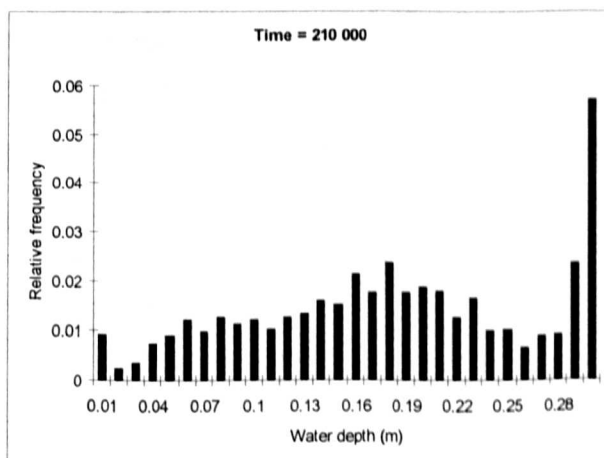
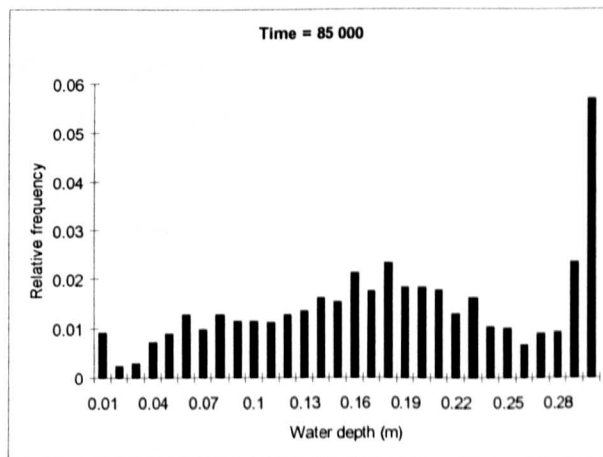
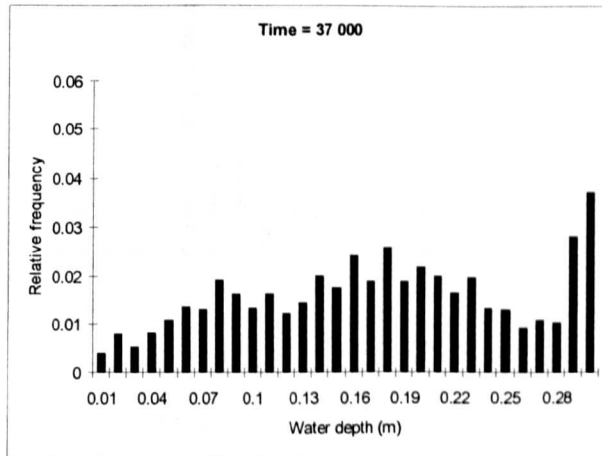
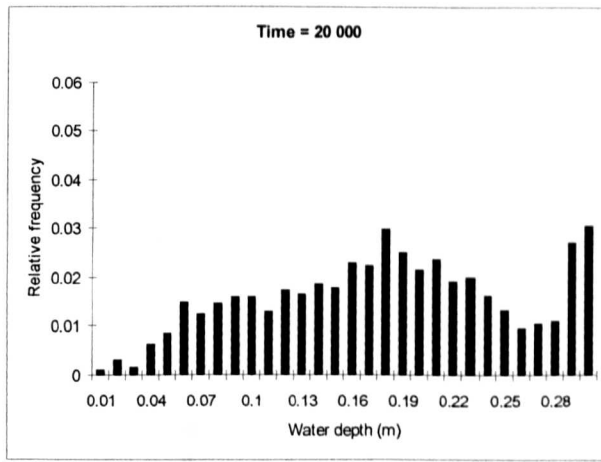


Figure 6.28. Histograms of relative frequency of water depths at different times on the grid for Braided Cascade run 2.

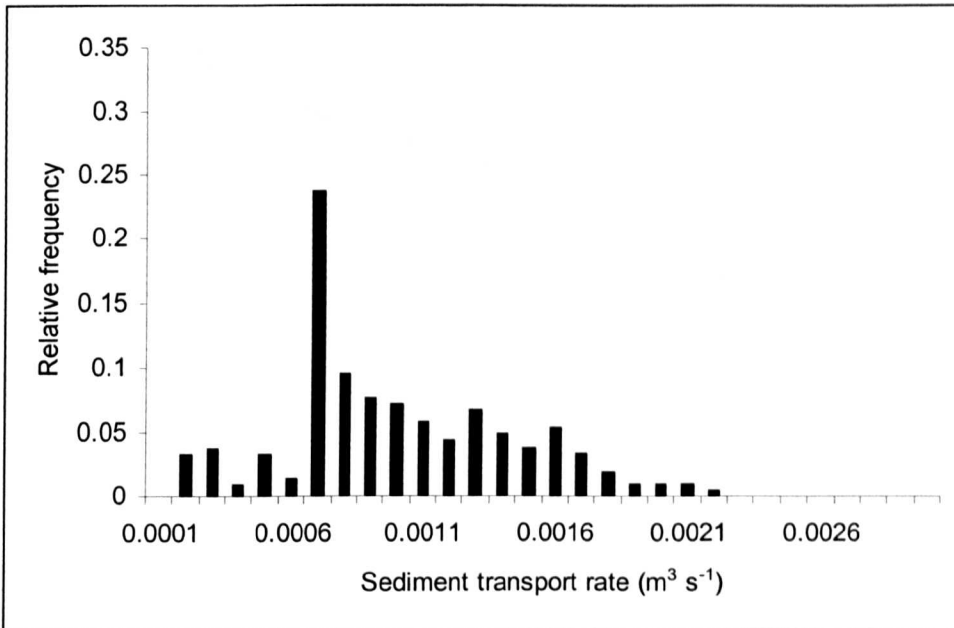


Figure 6.29. Histogram of sediment outflux from *Braided Cascade* run 2 with a braided channel pattern. Note that relative frequency is used on the y-axis.

The histogram of sediment transport outflux rates shows a slightly positively skewed distribution (Figure 6.29), which is qualitatively similar to Zarn's (1997) braided runs. There is one modal class at  $7 \times 10^{-4} \text{ m}^3 \text{ s}^{-1}$  corresponding to the steady state reached towards the end of the run.

Autocorrelation analysis on the raw data shows that the values of  $r_k$  slowly come down to zero (Figure 6.30). Examination of the PACF (Figure 6.31) indicates that the run shows a significant PACF value at lag  $k = 1$  indicating that sediment outflux rate is statistically dependent on the previous transport rate. An AR(1) model was fitted to the raw data (Table 6.16). The  $R^2$  value is not as good as that obtained for Run 1 (probably due to a shorter period of constant sediment output) but is still high.

Run name	Constant	AR (1) term	P-value for AR (1) term	$R^2$
Run 2	$1.91 \times 10^{-5}$	0.977	$2.18 \times 10^{-127}$	0.94

Table 6.16. Summary statistics of AR(1) regression for *Braided Cascade* run 2.

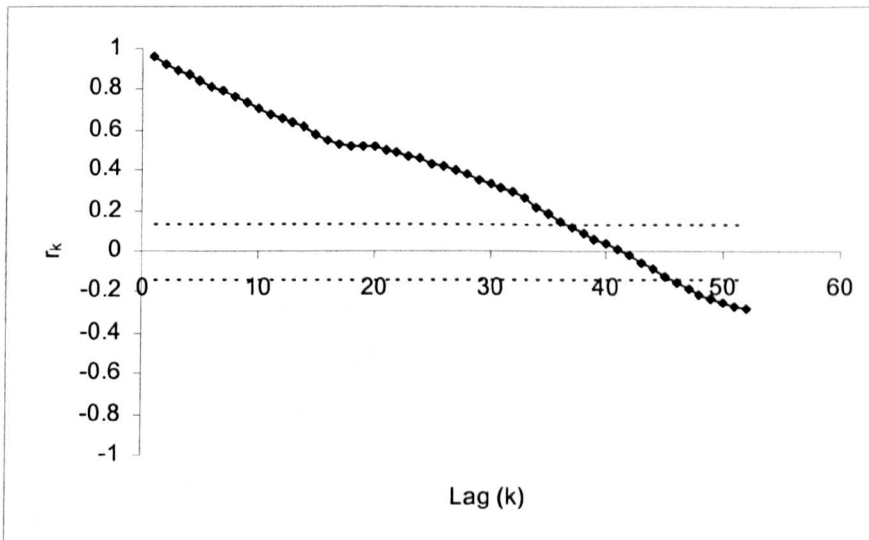


Figure 6.30. Correlogram for *Braided Cascade* Run 2.

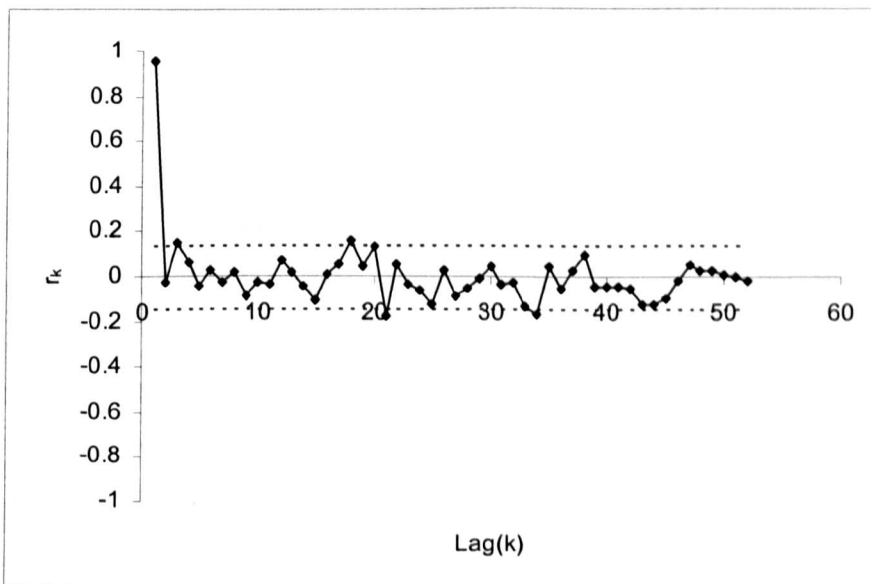


Figure 6.31. Partial autocorrelation function for *Braided Cascade* Run 2.

When plotted in state space the sediment output rate shows a slight thickening on the first bisectrix (Figure 6.32), however some points that plot along the 1:1 line due to the near steady state of sediment outflux reached towards the end of the run. The crossing period (7.11) is large compared to the flume runs of Zarn (1997) but is shorter than that for Run 1 due to the more variable sediment output.

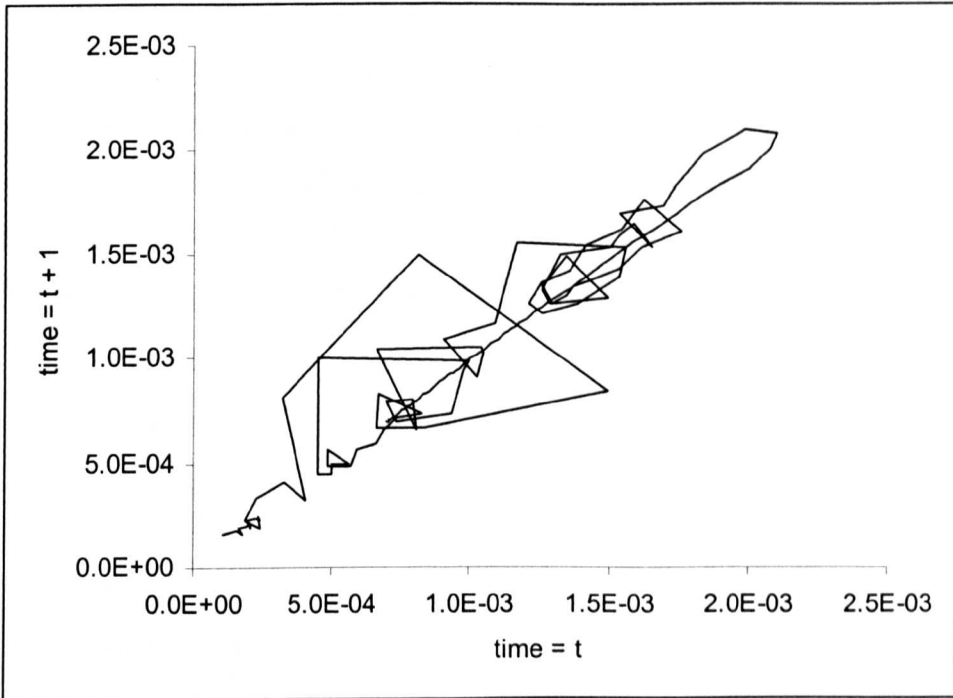


Figure 6.32. Sediment outflux from *Braided Cascade* Run 2 plotted in state space.

### 6.2.3.1.3. Run 3.

The grid for Run 3 was 500 nodes long and 14 nodes wide and was designed to simulate wider braided runs. Again, water and sediment were added at every node along the upstream boundary (12 nodes) at a rate given in Table 6.11. Time series of sediment output from the grid is shown in Figure 6.33. There is an initial peak in sediment output from the grid, sediment output then drops before climbing and reaching a steady state at a relatively early period in the run. It should be noted that in this run a true steady state was reached, i.e. the sediment outflux rates from 27 000 iterations onwards does NOT change. The interpretation of steady state may be that averaged processes in a deterministic model produce steady equilibrium, whereas detailed representations of small-scale processes would produce more instability. The histogram of sediment outflux (Figure 6.34) shows a strong modal class which is due to the steady state reached by the model. An inspection of the channel pattern at varying times throughout the run (Figure 6.35, these points in time are marked on

Figure 6.33) indicates that channel pattern does not change significantly throughout the run. Histograms of relative frequency of water depths at these points in time are shown in Figure 6.36, to aid comparison dry nodes were omitted but the proportion of each grid that contains dry nodes is given in Table 6.17. it can be seen from Table 6.17 and from Figures 6.35 and 6.36 that the channel pattern, proportion of dry nodes and the histograms of water depth change very little throughout the course of the run.

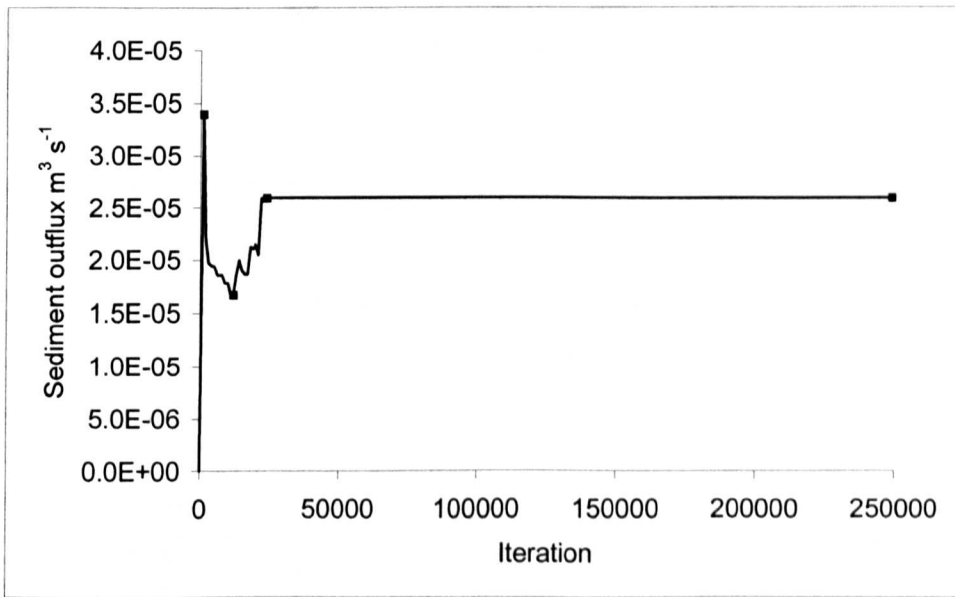


Figure 6.33. Time series of sediment outflux from the grid for *Braided Cascade* Run 3. Points indicated by a square marker are those points in time where channel pattern has been plotted in Figure 6.35.

Time	Proportion of dry nodes on grid
1000	0.33
12 000	0.34
26 000	0.34
250 000	0.34

Table 6.17. Proportion of dry nodes on the grid at certain times throughout *Braided Cascade* Run 3.

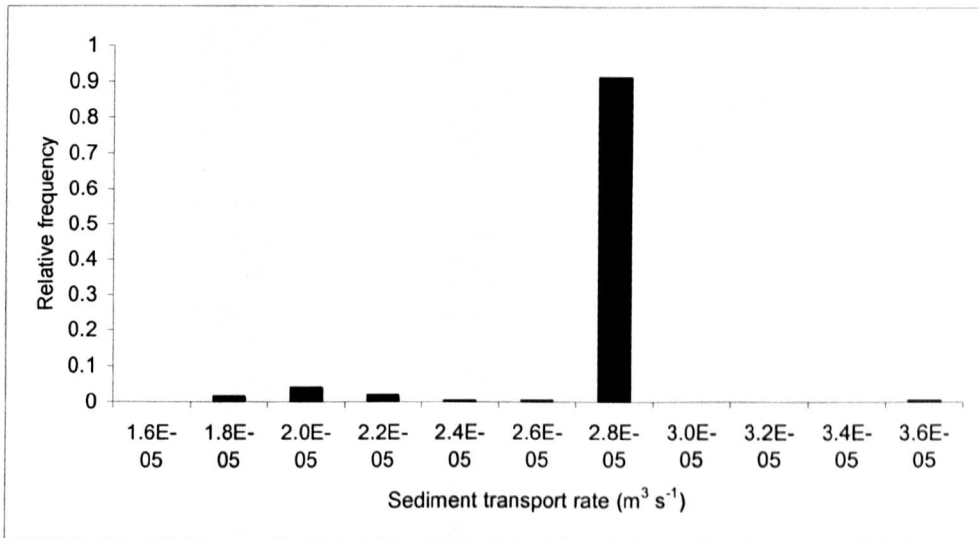


Figure 6.34. Histogram of sediment outflux from *Braided Cascade* run 3 with a braided channel pattern. Note that relative frequency is used on the y-axis.

Sediment transport rates recorded are the lowest for the three *Braided Cascade* runs and the least variable (Table 6.18) The median and mean rates are approximately the same reflecting the large modal class created by the model reaching a steady state.

Run name	Sediment outflux (m³ s⁻¹)				
	Min	Mean	Maximum	Median	Max/mean
<b>Run 3</b>	1.68 x 10 <sup>-5</sup>	2.55 x 10 <sup>-5</sup>	3.4 x 10 <sup>-5</sup>	2.6 x 10 <sup>-5</sup>	1.33

Table 6.18. Variability of sediment outflux from Run 3.

The data are clearly not stationary so autocorrelation analysis was performed on the first differences of the data. Inspection of the correlogram (Figure .37) indicates that there is a significant lag at k = 1 but that the acfs very quickly reach zero and then do not change. This reflects the static state reached by the model. The partial autocorrelation (Figure 6.38) shows a significant lag at k = 1 but both results indicate that the sediment outflux rate is not strongly statistically dependent any previous transport rates.

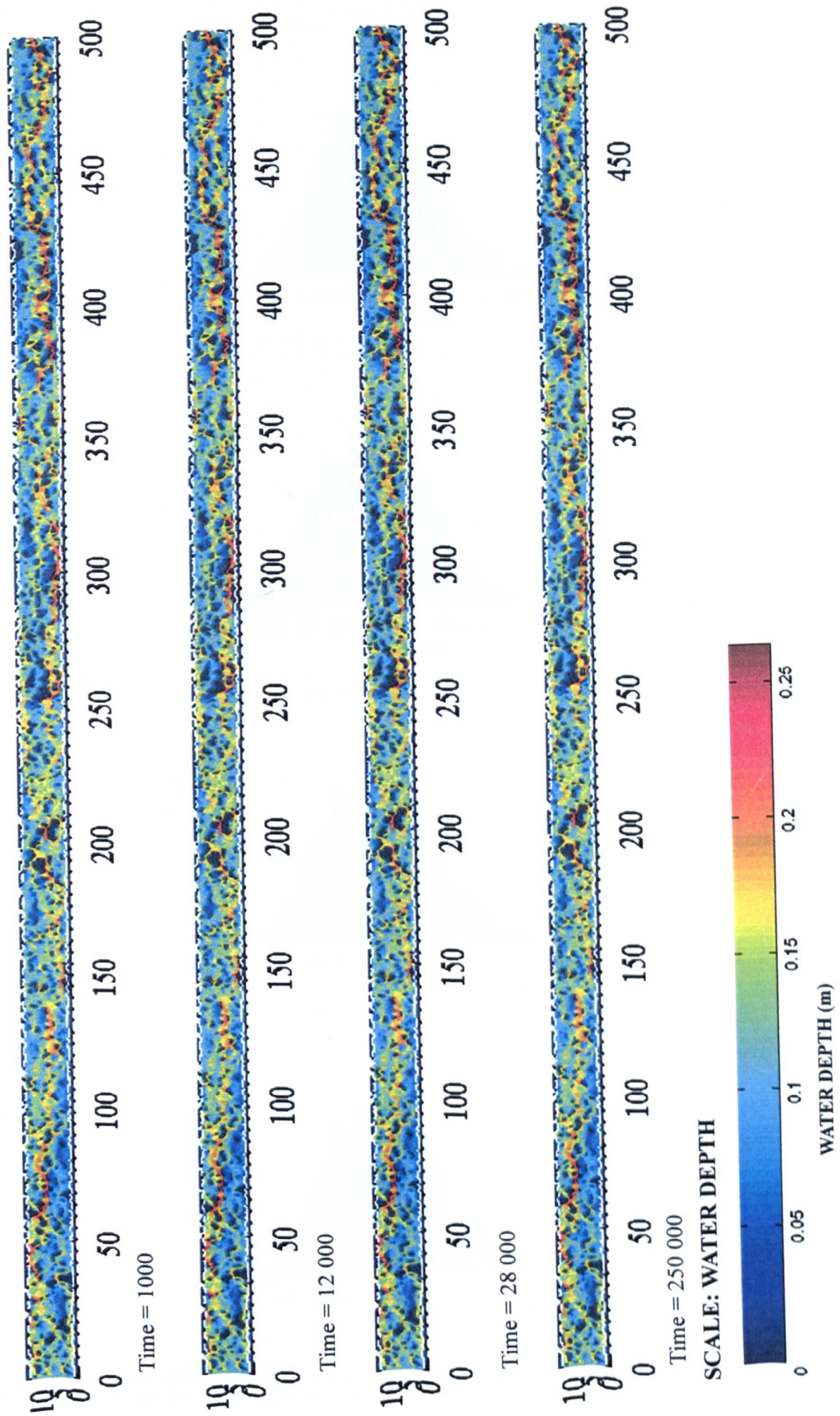


Figure 6.35. Plots of water depth on the grid at different times throughout *Braided Cascade* Run 3.

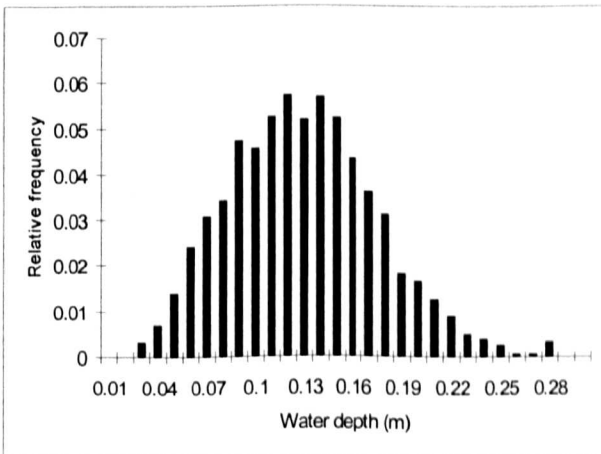
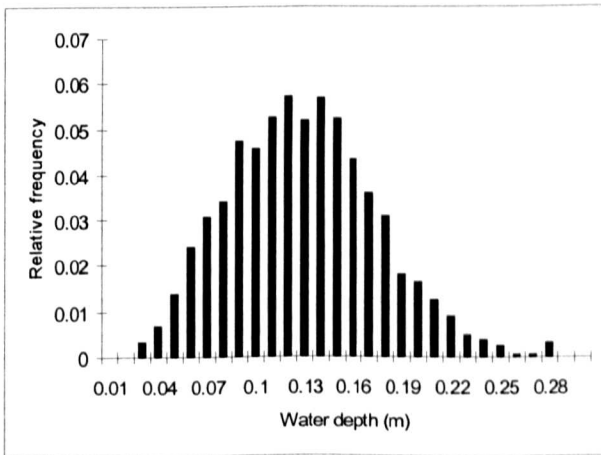
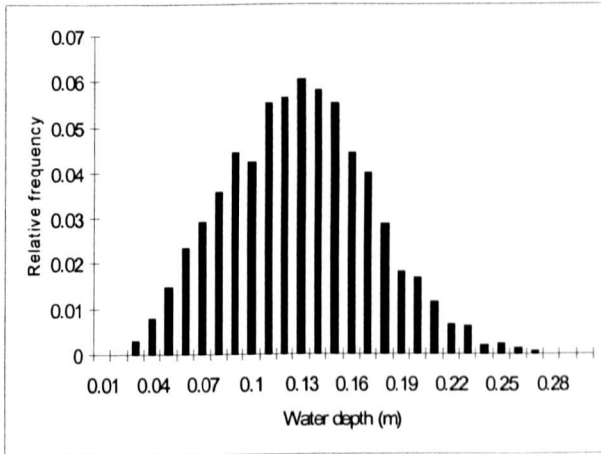
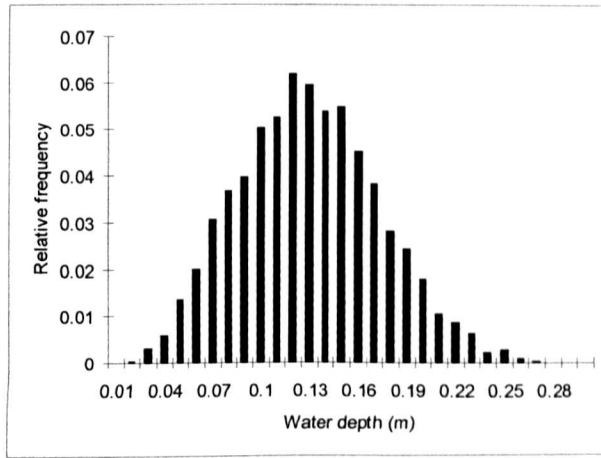


Figure 6.36. Histograms of relative frequency of water depths at different times on the grid for Braided Cascade run 3. From the top times are: 1000, 12 000, 28 000 and 250 000s.

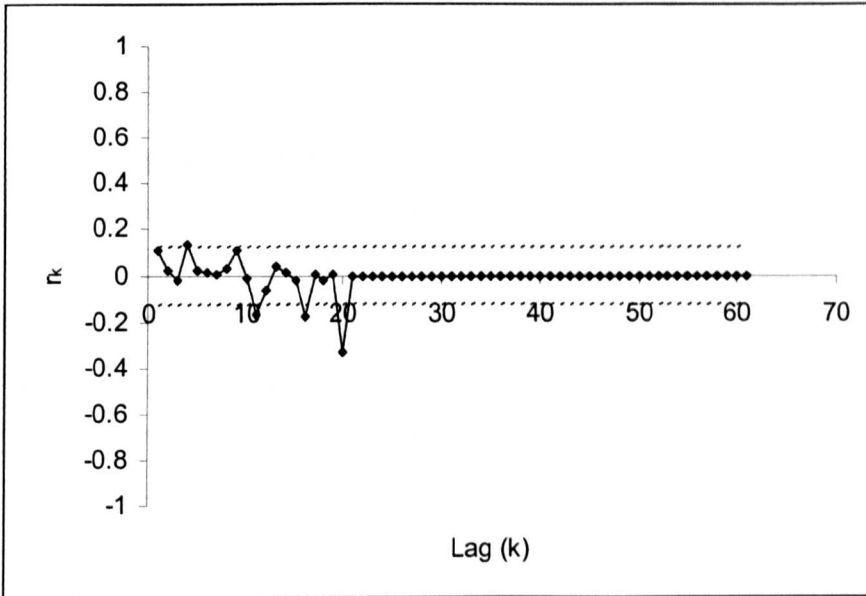


Figure 6.37. Correlogram for *Braided Cascade* Run 3.

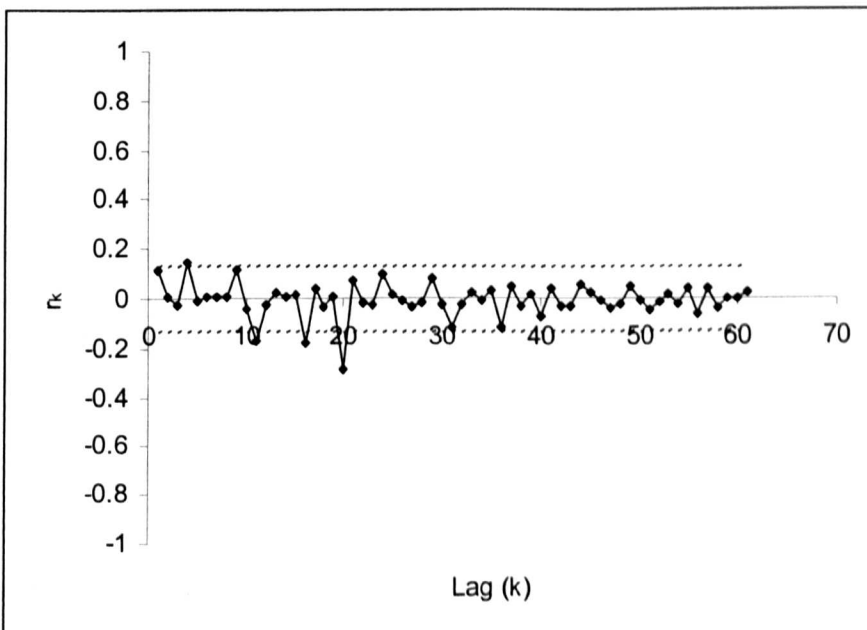


Figure 6.38. Partial autocorrelation function for *Braided Cascade* Run 3.

An AR(1) model fitted to the raw data gives a lower constant, AR(1) term and  $R^2$  value than that calculated for both Runs 1 and 2 (Table 6.19).

Run name	Constant	AR(1) term	P-value for AR (1) term	R <sup>2</sup>
RUN 3	$1.83 \times 10^{-6}$	0.93	$2.6 \times 10^{-87}$	0.80

Table 6.19. Summary statistics of AR(1) regression for *Braided Cascade* run 3.

In state space the model results show some variation around the 1:1 line (Figure 6.39); the results qualitatively fall between the extreme results of Run 1 where the majority of the points plotted on the 1:1 line and Run 2 which shows more variation in sediment output than Run 3. There is not a pronounced trend to plot along the 1:1 line as in Runs 1 and 2. This is probably due to the long period in which the sediment outflux results do not vary; these results will all plot at the same *point* (i.e. a point attractor) in state space and will be hard to make out on the state space plot.

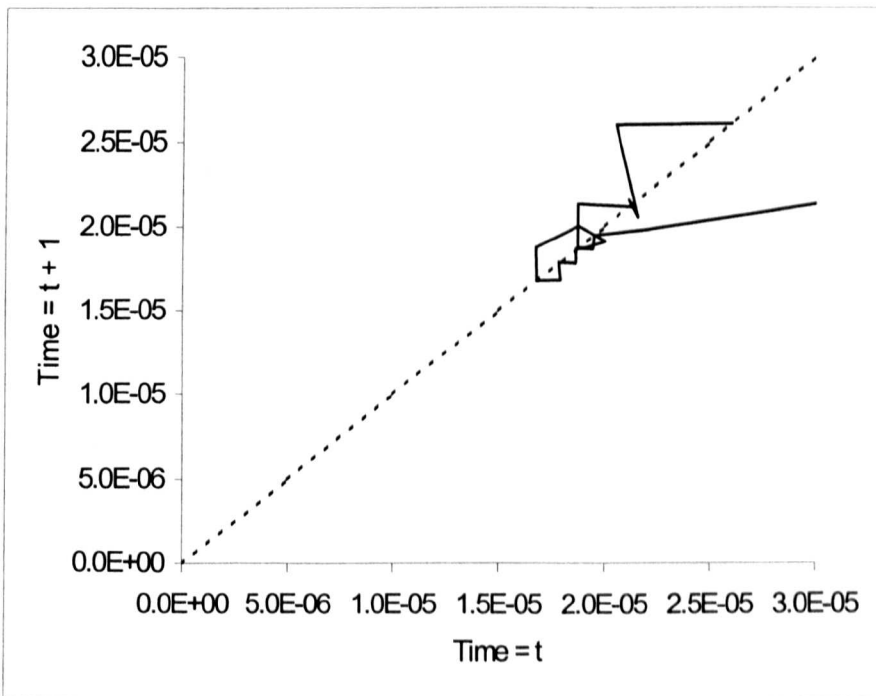


Figure 6.39. Sediment outflux from *Braided Cascade* run 3 plotted in state space.

#### 6.2.3.1.4. Comparisons of all *Braided Cascade* runs.

Z-scores calculated on the raw data of each run indicate that none of the runs show a normal distribution (Table 6.20). Run 1 has a skew of zero due to it the sediment transport rate results being bimodal; both Runs 2 and 3 are skewed. The crossing period for Run 3 is the largest for any of the *Braided Cascade* runs in this Chapter (20.67) indicating that the model reaches a steady state for a period longer in than that attained in either Runs 1 or 2. This is also confirmed by the proportion of each type of movement around the 1:1 line (Table 6.21). Run 2 has a greater proportion of movements across the 1:1 line than movements on one side of the line, however both Runs 1 and 3 have a greater proportion of movements on one side of the line and not across it.

Run name	Z-scores			Crossing period
	Min	Max	Skew	
Run 1	-1.10	3.01	1.00	14.53
Run 2	-1.98	2.67	0.42	7.11
Run 3	-4.48	4.36	-2.68	20.67

Table 6.20. Summary statistics of z-scores for *Braided Cascade* runs.

Run name	Discharge $\text{m}^3 \text{ s}^{-1}$	Proportion of each type of movement around the 1:1 line between data points in state space			
		above → above	above → below	below → above	below → below
Run 1	5	0.748	0.033	0.033	0.187
Run 2	5	0.427	0.069	0.069	0.435
Run 3	5	0.923	0.020	0.024	0.032

Table 6.21. Proportion of each type of movement between data points in state space for *Braided Cascade* runs.

The plots of cumulative sediment output from each run (Figure 6.40) show that, for the same discharge, there is a decrease in sediment output as the width of the model grid (and number of channels on the grid) increases. Discharge and sediment input rate are constant throughout all runs and across all runs with equal discharge. Therefore, as in the flume data, wider runs with more channels experience more

aggradation than narrower runs with fewer channels and the same initial conditions. This may reflect the increasing number of sediment storage reservoirs (bars) as the channel geometry switches from single thread to a braided network.

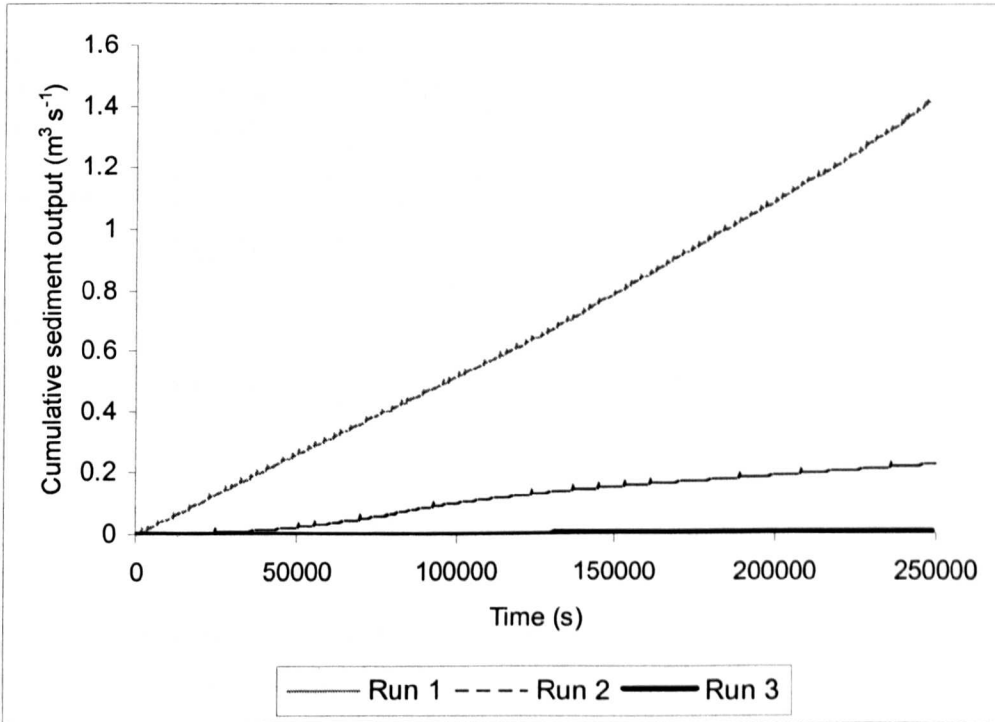


Figure 6.40. Cumulative sediment output from *Braided Cascade* runs.

Runs were compared using RelaxIV and a matrix of results is shown in Table 6.22. It can be seen that all data sets are dissimilar and that the magnitude of results is much larger than those for either Zarn’s (1997) flume data sets or for the Arolla field data.

<b>Run name</b>				
<b>Run 3</b>			-	
<b>Run 2</b>		-	2104.82	
<b>Run 1</b>	-	911.13	1837.39	
	<b>Run 1</b>	<b>Run 2</b>	<b>Run 3</b>	<b>Run name</b>

Table 6.22. Matrix of RelaxIV results for Braided Cascade runs.

Comparing the *Braided Cascade* runs to the braided data of Zarn (1997) and the Arolla data sets produced the following results (Table 6.23). The Zarn (1997) data for

flume runs with a discharge of  $5 \text{ l s}^{-1}$  was used for comparison. Run 1 was not compared to the braided flume runs as it is obviously qualitatively different to any other data set. Runs 2 and 3 were not compared to the single thread channel run as they were meant to simulate braided channel networks.

<b>Arolla field data</b>				
18/7/99	1026.60	871.68	infeasible	
20/7/99	1042.03	657.37	infeasible	
<b>Flume data (Zarn 1997)</b>				
30_7	940.79	-	-	
75_3	-	655.75	infeasible	
140_2	-	579.76	infeasible	
250_3	-	569.28	infeasible	
	<b>Run 1</b>	<b>Run 2</b>	<b>Run 3</b>	<b>Run name</b>

Table 6.23. Matrix of RelaxIV results for Braided Cascade runs.

From Table 6.23 it is clear that the model results are very different to either the field or flume data. Run 2 produces results that are the most similar to either data set, however the similarities are weak with the RelaxIV output values higher than for any previous comparison (except for flume runs 30\_8 and 250\_4). Comparisons using Run 3 produce infeasible results. This is due to the materialisation of a point attractor in state space after 27 000 iterations causing problems with the numerical program RelaxIV.

### 6.3. Discussion and summary of Chapter 6.

This chapter has attempted to link spatial and temporal bedload transport together. It has been shown that, using the flume data of Zarn (1997), different flume widths produce different time series structures of transport rate. As the number of channels increases the histogram of the time series structure becomes positively skewed, due the greater aggradation experienced in these runs and the increase in sediment storage areas (bars) within the flume. As the planform geometry changes from single thread to braided, variability in transport rate increases if measured as the maximum

transport rate divided by the mean rate, however dynamical systems analysis shows that the period of the fluctuations in transport rate increase indicating fewer transitions from low to high transport rates (or vice versa). Formal time series analysis (autocorrelation and partial autocorrelation analysis) indicates that braided runs show short-term correlation, with significant lags at  $k = 1$  and  $k = 2$ . A first order autoregression model fitted to each data set indicates that as the flume width increases the overall goodness of fit of the regression model improves. Finally, a modified box counting technique employed to measure the differences between time series indicates that, for a given discharge, planforms with a similar number of channels are more statistically similar than networks with a greater difference in channel number.

Field data from Arolla, Switzerland that was sampled from a single anabranch of a braided reach show variability in transport rates reflecting bedforms and changes in hydraulics. Histograms of both data sets are positively skewed and are qualitatively similar to histograms from the braided flume runs. Autocorrelations performed on the raw data show that, like the braided flume runs, both data sets have significant lags at  $k = 1$  and  $k = 2$ . The constant and AR(1) term from a first order regression are similar to those obtained for Zarn's (1997) braided flume runs. In state space, both data sets are qualitatively similar to the braided flume runs of Zarn (1997) however when compared using RelaxIV it was shown that the field data sets are dissimilar to each other and also to the flume runs. The magnitude of the RelaxIV output values is similar to the output obtained when comparing single thread and braided flume runs. Therefore it can be concluded that, although qualitatively similar, time series data from a single anabranch has a different internal structure than spatially integrated data obtained by trapping sediment across the entire braidplain width.

Finally *Braided Cascade* was tested to investigate if the numerical model could produce results similar to those obtained by either field sampling or flume investigations. Three long runs were undertaken on grids with different length:width

ratios to try and simulate a single thread channel and two braided channel networks. Time series of sediment output produced by mode runs were analysed using formal time series analysis and dynamical systems methods. It was found that the model has a tendency to reach a steady state in all runs (i.e. in state space the trajectories of model output are tend to move towards line or point attractors). Using both qualitative and quantitative analyses it was found that an intermediate grid produced model output that gave the best comparison with the field data or the flume data for braided rivers, however overall *Braided Cascade* fails to adequately reproduce realistic results. However it was found that the differences between model results and the field and flume data indicate that the model does not always match the physical systems as closely as the physical systems match each other.

## CHAPTER 7.

### CONCLUSIONS AND RECOMMENDATIONS.

#### 7.1. Introduction.

Braided rivers are highly dynamic systems characterised by high rates of erosion, sediment transport and deposition (Paola, 2001, Ashmore, 2001). Despite the importance of braided rivers to the work of geomorphologists, engineers, sedimentologists, and geologists they have been less extensively studied than single channel rivers, largely due to the difficulties in undertaking fieldwork in such a rapidly changing environment. Consequently most studies of braided river evolution to date have been qualitative or semi-qualitative in nature.

Within this context it is important to note that fieldwork in braided river systems has also largely been carried out in a reductionist framework, with the scale of investigation typically one bar-chute complex. The use of physical models by some workers has provided useful qualitative data on braided river evolution and whole reach scale sediment transport. Quantitative data may be collected but this is usually on averaged properties. However it is clearly recognised that there is a difficulty in making distributed spatial measurements in a shallow, rapidly changing flume setting.

Numerical modelling of braided river systems is a fairly recent phenomenon and a variety of approaches has been used:

1. CFD models.

These models have been successfully used to predict short-term fluid flow behaviour in small, narrow channels at scales of 1-10 m, (e.g. Lane and Richards, 1998). These models generally require very detailed field measurements for both input data and validation that may be difficult to obtain. However it is computationally difficult to couple these models to models of sediment transport.

## 2. Random walk models.

Channel patterns grow sequentially as a consequence of user-defined statistical rules. These models may reproduce the planar features of braided systems, and may reproduce topologically based statistics. However they are largely empirical and give no insight into the geomorphic processes responsible for network evolution.

## 3. Deterministic models of sedimentation and landscape evolution.

These models allow for growth and meaningful three-dimensional river basin structures. However, they are fundamentally reductionist in spirit, and require detailed specification of the dominant dynamics and the calibration of the relative importance of many key processes.

## 4. Cellular automata models.

These models have been applied to the evolution of braided river networks, most notably by Murray and Paola (1994, 1997). These models are synthesist in character, with the braided channel network emerging from a highly simplified model of the dynamics. The representation of fluid flow may be simple but this allows for fast calculation and a deformable mesh. Thomas and Nicholas (2002) have developed a cellular automata model similar to Murray and Paola's (1994, 1997) model but, at the time of writing this model does not transport sediment.

Modelling braided river systems is a key theme of this research, and the main findings here relate to the thesis aims and objectives presented in Chapter 1. The main aim was to develop a numerical model of water and sediment transport that incorporates physically realistic transport rules for water and sediment and can simulate the evolution of braided channel networks. Subordinate to this were three objectives:

1. to test the sensitivity of model parameters;
2. to use the model to answer specific questions about the formation and evolution of braided channel networks in order to gain insight into the mechanics of braided rivers, for example to attempt to understand the relationship between unsteady sediment transport and morphology; and

3. to investigate the relationship between spatial and temporal structure in bedload transport using the model results, field data and results from a physical modelling study.

To address these objectives a new hybrid model of water and sediment transport encapsulating these rules that is capable of producing braided channel networks was developed; this model is named *Braided Cascade*.

## 7.2. Model development: *Braided Cascade*.

*Braided Cascade* is a large scale numerical model that is capable of simulating the evolution of braided channel networks and incorporates various physically realistic processes of a real river. *Braided Cascade* is synthesisist in spirit was developed from *Cascade* (Braun and Sambridge, 1997), a finite-difference long-term (timesteps on the order of 100 years) landscape evolution model. *Braided Cascade* has been modified so that it can be applied to relatively short term process modelling. New routines were written to initialise the grid, incorporate physically realistic sediment transport and fluvial erosion rules and to allow the flow to bifurcate around local topographic highs. *Braided Cascade* improves upon previous models of braided networks in four main areas:

- the use of Delaunay triangulation to generate a computational grid allowing flexible lateral movement. The inclusion of an irregular triangulated network (TIN) for the model grid allows channels to form in all directions. In this respect *Braided Cascade* is unique among other previously published large scale models of braided rivers where square grids are used and channel network growth is constrained by angles that exist between cells;
- the inclusion of water height and thus routing of water and sediment due to water surface slopes is unique to *Braided Cascade*;
- the incorporation of spatial lag effects, (also termed step lengths, or length scales for erosion), is again unique to *Braided Cascade*. Spatial lag effects are defined as the inability of an alluvial system to immediately overcome the presence of constrained sediment boundary conditions (Phillips and

Sutherland 1989). A certain distance is required before the alluvial system reaches equilibrium (Phillips and Sutherland, 1989). The step length method identifies a typical distance of travel between sediment source (erosion) and sediment sink (deposition) and has been applied to meandering (e.g. Neill 1971) and braided channels (e.g. Carson and Griffiths 1989; Ferguson and Ashworth 1992; Goff and Ashmore 1994). No temporal lags are included, which is equivalent to a steady flow assumption; and

- the incorporation of flow splitting ratios. The ability to constrain flow divergence is a purely model parameter and has no equivalence in prototype rivers, however it can serve as a surrogate for momentum in the flow equations. Channels can bifurcate or join (more than two channels may join but one channel cannot be split into more than two anabranches). Discharge in the original channel is assigned to each of the two new channels according to channel bed slope, sediment is assigned according to water surface slope, which is calculated using hydraulic geometry relations. Thus, discharge and sediment are conserved throughout the network. The movement of water is determined by local gradient, and fluxes of water and sediment are determined by the water surface slopes between a donor and receiving node.

Although *Braided Cascade* improves upon previous cellular automata models of braiding, the model contains some problems. Shortcomings of *Braided Cascade* include:

- the model cannot accommodate the effects of channel width. Each node is treated as being one channel even if the nodes are adjacent and should be treated as part of the same channel.
- the model does not explicitly include a sediment size; however there is a maximum amount of material that can be deposited during one timestep and this is equivalent to a notional grain size.

Overall the modelling approach used here is simplified and takes no account of detailed flow hydraulics. The intention was to model the overall spatial patterns of sediment transport, deposition and erosion and to analyse these in terms of their

net statistical properties, rather than to produce accurate predictions of processes at particular localities. In this respect, the modelling approach is synthesisist and braiding is an emergent phenomenon.

### 7.3. Model sensitivity analysis and testing. What causes braiding?

A formal sensitivity analysis was undertaken to investigate the sensitivity of the model results for a range of values of the model parameters: slope, erosion length scale, deposition, diffusion (lateral sediment transport), discharge splitting ratios and sediment input and has investigated the parameter values needed to give styles and timescales for model evolution that are comparable to the evolution of braided channel networks. It was found that most combinations of model parameters produce basic braiding, however the model has a tendency to reach a static state in certain circumstances.

The most significant parameters for braiding were found to be:

- **the erosion length scale:** The model will reach a static steady state if the length scales are sufficiently short for the carrying capacity of the flow to be reached almost instantaneously;
- **the splitting ratios:** The model will reach a static steady state if the splitting ratios (*qratio* and *upratio*) are set to disallow flow to split if the ratios between channel slopes are very low; and
- **deposition:** If deposition is suppressed and the system is purely erosive, the model erodes a canyon down the grid and produces very similar results to when the erosion length scale is short.

#### 7.3.1. Parameter values.

It should be noted that the parameter values do not have any significance beyond that model. A lack of field measurements and the presence of lumped parameters (e.g. the erosion length scale) make it difficult to compare the parameter values used in the model with data from prototype rivers, therefore the best that can be

done is to make approximate estimates of the scale dependence from existing data and to show that these are consistent with the model behaviour.

### **7.3.2. Comparison of model data with field and flume data.**

To address the third objective above field and flume data were used as a comparison of model output to input results. Sediment output from model runs was monitored across the entire downstream boundary of the grid. Using both qualitative and quantitative analyses it was found the similarities between model data and other data sets are weak and all runs tended to reach static equilibrium. *Braided Cascade* therefore failed to adequately reproduce realistic data sets. This may reflect a limitation of the model, i.e. that the small scale processes that are not included in *Braided Cascade* are actually important.

It was found that the differences between model results and the flume data indicate that the model does not always match the physical systems as closely as physical systems match each other.

### **7.3.3. Summary of conclusions.**

Therefore main conclusions of this work are:

1. requirements for a braided network to form are an imbalance between the amount of sediment the river is carrying and the carrying capacity as well as a reworking of the deposits;
2. parameter values do not have any significance beyond the model;
3. the model tends to reach a static state implying that the small scale processes that are not modelled are actually important; and
4. the model does not always match the physical systems as closely as physical systems match each other.

### **7.4. Braided river modelling: recommendations for future work.**

A numerical model for braided channel network growth has been developed here. With hindsight a number of potential improvements can be identified, which may

improve the ability of the model to produce more realistic results (i.e. results that resemble data from physical systems).

- In this study *Braided Cascade* has been used to simulate flume experiments by allowing the braided network to be developed within a rectangular space having lateral no-flow boundaries and a random white noise initial elevation. This methodology was decided upon to constrain parameters for sensitivity testing and to enable comparisons with flume data. *Cascade* however has the ability to read in digital elevation models of topography. If a pre-existing topography is read in this should control channel location and may allow the model to produce more realistic results (i.e. not move towards a steady state). It should therefore be possible to input riverbed topography into *Braided Cascade*.
- The inclusion of more than one sediment size. *Braided Cascade* contains a notional sediment size defined as the maximum amount of deposition allowed during one time step. This notional sediment size was set to equal the median sediment size ( $D_{50}$ ) of the Arolla grain size (0.07751 m) to try to avoid computational instability. The transport equation used in *Braided Cascade* was developed for gravel braids, so a grain size is implicit here. The inclusion of more than one sediment size would be useful for sedimentary sequence modelling (this has been done for landscape evolution models) and would be very useful in the context of modelling sequences as have been studied in the flume.
- The input of hydrographs. All model development and testing was carried out using constant input discharges. Longer model runs tended to reach a steady state which may be a consequence of the ability of the model to aggrade and absorb all sediment input. If discharge input rates were controlled by hydrographs and sediment input rates were controlled by a sediment-discharge relation this may effect sediment output rates and prevent a steady state being reached.
- Further testing of *Braided Cascade* against other similar models using the same input data. It would be interesting to carry out runs using *Braided*

*Cascade* and other braided river models (e.g. the model of Murray and Paola, (1994, 1997) random walk models) with the same initial parameter and input data to see the differences in outcome.

Synthesist style models therefore have the potential to lead to a greatly improved understanding of braided rivers, however it has been shown in this model that the exclusion of small scale processes from the model may be important when trying to produce braided networks. Modelling can gain from new technologies providing better field data (e.g. Lane 2001) and synthesist modelling can compliment reductionist modelling techniques (Paola 2001).

## REFERENCES.

- Aldrin, M., Damsleth, E. and Sæbø, H.V. (1989) Time series analysis of unequally spaced observations – with applications to copper contamination of the River Gaula in central Norway. *Environmental Monitoring and Assessment* **12**, 227-243.
- Anderson, R.S. (1994) Evolution of the Santa Cruz Mountains, California, through tectonic growth and geomorphic decay. *Journal of Geophysical Research*, **99**, 20161-20179.
- Anderson, M.G. and Burt, T.P. (1985) *Hydrological Forecasting*. Wiley, Chichester.
- Anderson, M.P., Aitken, J.S., Webb, E.K. and Mickelson, D.M. (1999) Sedimentology and hydrogeology of two braided stream deposits. *Sedimentary Geology* **129**, 187-199.
- Ashmore, P.E. (1982) Laboratory modelling of gravel braided stream morphology. *Earth Surface Processes and Landforms* **7**, 201-225.
- Ashmore, P.E. (1988) Bed load transport in braided gravel-bed stream models. *Earth Surface Processes and Landforms* **13**, 677-695.
- Ashmore, P.E. (1991a) How do gravel-bed rivers braid? *Canadian Journal of Earth Science* **28**, 326-341.
- Ashmore, P.E. (1991b) Channel morphology and bed load pulses in braided, gravel-bed streams. *Geografiska Annaler* **73A** (1), 37-52.
- Ashmore, P.E. (1993) Anabranch confluence kinetics and sedimentation processes in gravel-bed streams. In Best, J.L. and Bristow, C.S. (eds.) *Braided Rivers*. Geological Society Special Publication, **75**, 129-146.
- Ashmore, P.E. (2001) Braiding phenomena: statics and kinetics. In Mosley, P (ed.) *Gravel Bed Rivers V*, 95-120.
- Ashmore, P.E. and Parker, G. (1983) Confluence scour in coarse grained braided streams. *Water Resources Research* **19** (2), 392-402.
- Ashworth, P.J. (1996) Mid-channel bar growth and its relationship to local flow strength and direction. *Earth Surface Processes and Landforms* **21**, 103-123.
- Ashworth, P.J., Best, J.L., Leddy, J.O. and Geehan, G.W. (1994) The physical modelling of braided rivers and deposition of fine-grained sediment. In Kirkby, M.J. (ed.) *Process models and theoretical geomorphology*. John Wiley and Sons Limited, Chichester, 115-139.

- Ashworth, P.J. and Ferguson, R.I. (1986) Interrelationships of channel processes, changes and sediments in a proglacial braided river. *Geografiska Annaler* **68** (A), 361-371.
- Ashworth, P.J., Ferguson, R.I., Ashmore, P.E., Paola, C. Powell, D.M. and Prestegard, K.L. (1992a) Measurements in a braided river chute and lobe. 2. Sorting of bed load during entrainment, transport and deposition. *Water Resources Research* **28** (7), 1887-1896.
- Ashworth, P.J., Ferguson, R.I. and Powell, D.M. (1992b) Bedload transport and sorting in braided channels. In Billi, P., Hey, R.D., Thorne, C.R. and Tacconi, P. (eds.) *Dynamics of Gravel-bed Rivers*. 1992. John Wiley and Sons Limited, Chichester, 497-515.
- Bak, P., Tang, C. and Wisenfeld, K. (1987) Self-organized criticality: an explanation of  $1/f$  noise. *Physical Review Letters* **59** (4), 381-384.
- Barzini, G.N. and Ball, R.C. (1993) Landscape evolution in flood - a mathematical model. *Journal of Physics A. Mathematical and General*, **26**, 6777-6787.
- Bates, P. D. and Lane, S.N. (1998) High resolution flow modelling 1: Preface. *Hydrological Processes* **12**, 1129-1130.
- Beaumont, C. Fullsack, P. and Hamilton, J. (1992) Erosional control of active compressional orogens. In McClay, K.R. (ed.) *Thrust Tectonics*. Chapman and Hall, London, 1-18.
- Belova, N.N., Jaoshvili, S.V., Kiknadze, A.G. and Orlova, G.A. (1975) On the amount of bedload of the Byzb River. *Bulletin of the Academy of Sciences of the Georgian SSR*, **77**, 637-640. (in Russian)
- Benda, L. and Dunne, T. (1997a) Stochastic forcing of sediment supply to channel networks from landsliding and debris flow. *Water Resources Research* **33** (12), 2849-2863.
- Benda, L. and Dunne, T. (1997b) Stochastic forcing of sediment routing and storage in channel networks. *Water Resources Research* **33** (12), 2865-2880.
- Bertsekas D.P. and Tseng, P. (1994) RELAX-IV: *A faster version of the RELAX code for solving minimum cost flow problems*. LIDS Technical Report, LIDS-P-2276.
- Best, J.L. (1986) The morphology of river channel confluences. *Progress in Physical Geography* **10**, 157-174.

Best, J.L. (1988) Sediment transport and bed morphology at river channel confluences. *Sedimentology* **35**, 481-498.

Brasington, J., Rumsby, B.T. and McVey, R.A. (2000) Monitoring and modelling morphological change in a braided gravel-bed river using high-resolution GPS-based survey. *Earth Surface Processes and Landforms* **25** (9), 973-990.

Braun, J. and Sambridge, M. (1997) Modelling landscape evolution on geological time scales: a new method based on irregular spatial discretization. *Basin Research* **9**, 27-52.

Bridge, J.S. (1993) The interaction between channel geometry, water flow, sediment transport and deposition in braided rivers. In Best, J.L. and Bristow, C.S. (eds.) 1993, *Braided Rivers*. Geological Society Special Publication **75**, 13-71.

Bridge, J.S. and Gabel, S.L. (1992) Flow and sediment dynamics in a low sinuosity, braided river: Calamus River, Nebraska Sandhills. *Sedimentology* **39**, 125-142.

Brierley, G.J. (1989) River planform facies models: the sedimentology of braided, wandering and meandering reaches of the Squamish River, British Columbia. *Sedimentary Geology*, **61**, 17-35.

Bristow, C.S. and Best, J.L. (1993) Braided Rivers: perspectives and problems. In Best, J.L. and Bristow, C.S. (eds.) 1993, *Braided Rivers*. Geological Society Special Publication **75**, 1-11.

Brotherton, D.I. (1979) On the origin and characteristics of river channel patterns. *Journal of Hydrology* **44**, 211-230.

Brown, G.H. and Tranter, M. (1990) *Hydrograph and chemograph separation of bulk meltwaters draining the Upper Arolla Glacier, Switzerland*. International Association of Hydrological Sciences Publication **193**, 429-437.

Carey, W.P. and Hubbell, D.W. (1986) Probability distributions for bedload transport. *Proceedings of the 4<sup>th</sup> Federal Inter-Agency Sedimentation Conference*, U.S. Government Printing Office, Washington, D.C., **2**, 4131-4140.

Carson, M.A. and Griffiths, G.A. (1989) Gravel transport in the braided Waimakariri River: mechanisms, measurements and predictions. *Journal of Hydrology* **109**, 201-220.

Chase, C.G. (1992) Fluvial land sculpting and the fractal dimension of topography. *Geomorphology* **5**, 39-57.

Chatfield, C. (1989) The analysis of time series: an introduction. Chapman and Hall, London.

Church, M. (1983) Pattern of instability in a wandering gravel bed river. *Special Publications of the Institute of Sedimentology* 6, 169-180.

Church, M. and Jones, (1982) Channel bars in gravel-bed rivers. In Hey, R.D., Bathurst, J.C. and Thorne, C.R. (eds.) 1982, *Gravel-Bed Rivers*. John Wiley, Chichester, 291-338.

Church M.A., McLean, D.G. and Wolcott, J.F. (1987) River bed gravels:sampling and analysis. In Thorne, C.R. and Bathurst, J.C. and Hay, R.D. (eds.) *Sediment Transport in Gravel-Bed Rivers*. John Wiley and Sons, Chichester, 43-48.

Coulthard, T.J., Kirkby, M.J. and Macklin, M.G. (1998) Non-linearity and spatial resolution in a cellular automaton model of a small upland basin. *Hydrology and Earth System Sciences*, 2 (2-3), 257-264.

Coulthard, T.J., Kirkby, M.J. and Macklin, M.G. (1999) Modelling the impacts of Holocene environmental change in an upland catchment, using a cellular automaton approach. In Brown, A.G. and Quine, T.A. (eds.) *Fluvial processes and Environmental Change*. John Wiley and Sons Limited, Chichester, 31-46.

Davoren, A. and Mosley, M.P. (1986) Observations of bedload movement, bar development and sediment supply in braided Ohau River. *Earth Surface Processes and Landforms* 11, 643-652.

Delaunay, B.N. (1934) Sur la sphere vide. *Izvestia Akademii Nauk SSSR. Otdelenie Matematicheskii I Estestvennyka Nauk*, 7, 793-800.

Desai, C.S. (1979) *Elementary finite element method*. Prentice-Hall, New Jersey.

Einstein, H.A. (1937) Der Geschiebetrieb als Wahrscheinlichkeitsproblem (Bedload transport as a probability problem). Mitteilung der Versuchsanstalt für Wasserbau und der Eidgenössische Technische Hochschule, Zurich. English translation in: Shen, H.W. (ed.) 1972, *Sedimentation*, Water Resources Publications, Fort Collins, Colorado, C1-C105.

Emmett, W.W. (1979) A field calibration of the sediment trapping characteristics of the Helley-Smith bedload sampler. *United States Geological Survey, Professional Paper* 1139.

Ergenzinger, P. (1987) Chaos and order. The channel geometry of gravel bed braided rivers. *Catena Supplement* 10, 85-98.

Ferguson, R.I. (1993) Understanding braiding processes in gravel-bed rivers: progress and unsolved problems. In Best, J.L. and Bristow, C.S. (eds.) 1993, *Braided Rivers*. Geological Society Special Publication 75, 73-87.

Ferguson, R.I. and Ashworth, P.J. (1992) Spatial patterns of bedload transport and channel change in braided and near-braided rivers. In Billi, P., Hey, R.D., Thorne,

C.R. and Tacconi, P. (eds.) *Dynamics of Gravel-bed Rivers*. John Wiley and Sons Limited, Chichester, 477-496.

Ferguson, R.I., Ashworth, P.J. and Prestegard, K.L. (1989) Influence of sand on hydraulics and gravel transport in a braided gravel bed river. *Water Resources Research* **25**, 635-643.

Ferguson, R.I. and Paola, C. (1997) Bias and precision of bulk grain size distributions. *Earth Surface Processes and Landforms* **22**, 1061-1077.

Flemings, P.B. and Jordan, T.E. (1989) A synthetic stratigraphic model of foreland basin development. *Journal of Geophysical Research*, **94**, 3851-3866.

Freer, J., Beven, K.J. and Ambrose, B. (1996) Bayesian estimation of uncertainty in runoff prediction and the value of data: an application of the GLUE approach, *Water Resources Research*, **32**(7), 2161-2173.

Gee, D.M., Anderson, M.G. and Baird, L. (1990) Large-scale floodplain modelling. *Earth Surface Processes and Landforms* **15**, 513-523.

Gilbert, G.K. (1917) Hydraulic mining debris in the Sierra Nevada. *US Geological Survey Professional Paper*, **105**.

Goff, J.R. and Ashmore, P.E. (1994) Gravel transport and morphological change in braided Sunwapta River, Alberta, Canada. *Earth Surface Processes and Landforms* **19**, 195-212.

Gomez, B. (1991) Bedload transport. *Earth Science Reviews* **31**, 89-132.

Gomez, B., Naff, R.L. and Hubbell, D.W. (1989) Temporal variations in bedload transport rates associated with the migration of bedforms. *Earth Surface Processes and Landforms* **14**, 135-156.

Griffiths, G.A. (1979) Recent sedimentation history of the Waimakariri River, New Zealand. *Journal of Hydrology (New Zealand)* **18**, 6-28.

Griffiths, G.A. (1993) Sediment translation waves in braided gravel-bed rivers. *Journal of Hydraulic Engineering* **119** (8), 924-935.

Hamamori A. (1962) *A theoretical investigation on the fluctuations of bedload transport*. Delft Hydraulics Laboratory Report R4, 21 p.

Hardisty, J. (1993) Time series using spectral techniques: oscillatory currents. *Earth Surface Processes and Landforms* **18**, 855-862.

Henderson, F.M. (1961) Stability of alluvial channels. *Journal of the Hydraulics Division, American Society of Civil Engineers*, **87** 109-138.

- Hilborn, R. (1994) *Chaos and Non-Linear Dynamics. An introduction for scientists and engineers*. Oxford University Press, Oxford.
- Hodskinson, A. (1996) Computational fluid dynamics as a tool for investigating separated flow in river bends. *Earth Surface Processes and Landforms* **21**, 993-1000.
- Hodskinson, A. and Ferguson, R.I. (1998) Numerical modelling of flow in separated meander bends: model testing and experimental investigation of geometric controls on the extent of flow separation at the concave bank. *Hydrological Processes* **12**, 1323-1338.
- Hoey, T.B. (1992) Temporal variations in bedload transport rates and sediment storage in gravel-bed rivers. *Progress in Physical Geography* **16** (3), 319-338.
- Hoey, T.B. (1994) Patterns of sediment storage in the Kowai River, Torlesse Range, New Zealand. *Journal of Hydrology (New Zealand)* **32** (1), 1-15.
- Hoey, T.B. and Ferguson, R.I. (1994) Numerical simulation of downstream fining by selective transport in gravel bed rivers: model development and illustration. *Water Resources Research* **30** (7), 2251-2260.
- Hoey, T.B. and Sutherland, A.J. (1991) Channel morphology and bedload pulses in braided rivers: a laboratory study. *Earth Surface Processes and Landforms* **16**, 447-462.
- Hoey, T.B., Cudden J.R. and Shvidchenko, A. (2001) The consequences of unsteady sediment transport in braided rivers. In Mosley, P (ed.) *Gravel Bed Rivers V*, 121-142.
- Howard, A.D. (1994) A detachment-limited model of drainage basin evolution. *Water Resources Research* **30** (7), 2261-2285.
- Howard, A.D. (1997) Badland morphology and evolution: interpretation using a simulation model. *Earth Surface Processes and Landforms* **22**, 221-227.
- Howard, A.D., Keetch, M.E. and Vincent, C.L. (1970) Topological and geometrical properties of braided streams. *Water Resources Research* **6** (6), 1674-1688.
- Ibbitt, R.P., Willgoose, G.R. and Duncan, M.J. (1999) Channel network simulation models compared with data from the Ashley River, New Zealand. *Water Resources Research* **35** (12) 3875-3890.
- Iseya, F. and Ikeda, H. (1987) Pulsations in bedload transport rates induced by a longitudinal sediment sorting: a flume study using sand and gravel mixtures. *Geografiska Annaler* **69A** (1), 15-27.

- Jackson, R.G. (1975) Hierarchical attributes and a unifying model of bed forms composed of cohesionless material and produced by shearing flow. *Geological Society of America Bulletin* **86**, 1523-1533.
- James, L.A. (1989) Sustained storage and transport of hydraulic gold mining sediment in the Bear River, California. *Annals of the Association of American Geographers* **79** (4), 570-592.
- James, L.A. (1991a) Incision and morphologic evolution of an alluvial channels recovering from hydraulic mining sediment. *Geological Society of America Bulletin* **103**, 723-736.
- James, L.A. (1991b) Quartz concentration as an index of sediment mixing: hydraulic mine-tailings in the Sierra Nevada, California. *Geomorphology* **4**, 125-144.
- Jaoshvili, S.V., Belova, N.N., Kiknadze, A.G. and Orlova, G.A. (1976) Measurement of bedload transport in a mountain using tracers. In V.P. Zenkovich (ed.) *Problems of the Study of the Georgian Coast*, Tblisi, Metsniereba, 59-74 (in Russian).
- Jaoshvili, S.V. and Zenginidze, A.G. (1981) Bedload of the Kodori River. *Bulletin of the Academy of Sciences of the Georgian SSR* **103**, 85-88 (in Russian).
- Kirkby, M.J. (1972) Alluvial and nonalluvial meanders. *Area* **4**, 284-288.
- Kirkby, M.J., Naden, P.S., Burt, T.P. and Butcher, D.P. (1993) *Computer Simulation in Physical Geography*. Wiley, Chichester.
- Knighton, A.D. (1994) *Fluvial forms and processes. A new perspective*. Arnold, London.
- Knighton, A.D. and Nanson, G.C. (1993) Anastomosis and the continuum of channel pattern. *Earth Surface Processes and Landforms* **18**, 613-625.
- Kondolf, G.M. and Matthews, W.V.G. (1986) Transport of tracer gravels on a coastal California river. *Journal of Hydrology* **85**, 265-280.
- Kooi, H. and Beaumont, C. (1994) Escarpment evolution on a high-elevation rifted margins: Insights derived from a surface processes model that combines diffusion, advection and reaction. *Journal of Geophysical Research*, **99** (B6), 12191-12209.
- Krumbein, W.C. and Orme, A.R. (1972) Field mapping and computer simulation of braided-stream networks. *Geological Society of America Bulletin* **83**, 3369-3380.

Kuhnle, R.A. and Southard, J.B. (1988) Bed load transport in a gravel bed laboratory channel. *Water Resources Research* **24** (2), 247-260.

Kuhnle, R.A., Willis, J.C. and Bowie, A.J. (1989) Variations in the transport of bed load sediment in a gravel-bed stream, Goodwin Creek, Northern Mississippi, USA. *Fourth International Symposium on River Sedimentation*, June 5-9, Beijing, China.

Lane, E.W. (1957) *A study of the shape of channels formed by natural streams flowing in erodible material*. Missouri River Division Sediment Series No. 9, U.S. Army Corps of Engineers, Omaha, Nebraska.

Lane, S.N. (1998) Hydraulic modelling in hydrology and geomorphology: A review of high resolution approaches. *Hydrological Processes* **12**, 1131-1150.

Lane, S.N. and Richards, K.S. (1998) High resolution, two-dimensional spatial modelling of flow processes in a multi-thread channel. *Hydrological Processes* **12**, 1279-1298.

Lane, S.N., Chandler, J.H. and Richards, K.S. (1994) Developments in monitoring and modelling small-scale river bed topography. *Earth Surface Processes and Landforms* **19**, 349-368.

Lane, S.N., Richards, K.S. and Chandler, J.H. (1995) Morphological estimation of time-integrated bed load transport rate. *Water Resources Research* **31** (3), 761-772.

Lane, S.N., Richards, K.S. and Chandler, J.H. (1996) Discharge and sediment supply controls on erosion and deposition in a dynamic alluvial channel. *Geomorphology* **15**, 1-15.

Lane, S.N. (2001) The measurement of gravel-bed river morphology. In Mosley, P. (ed.) *Gravel Bed Rivers V*, 291-337.

Laronne, J.B. and Duncan, M.J. (1989) Constraints on duration of sediment storage in a wide gravel-bed river, New Zealand. *Sediment and the Environment* (Proceedings of the Baltimore Symposium, May 1989). IAHS Publication **184**.

Lee, D. T. and Preparata, F.P. (1984) Computational geometry – a survey. *IEEE Transactions on Computers*, **C-33** (12) 1072-1101.

Leopold, L.B. and Wolman, M.G. (1957) River channel patterns: Braided, meandering and straight. *US Geological Survey Professional Paper* **282-B**.

Lisle, T.E. (1995) Particle size variations between bed load and bed material in natural gravel bed channels. *Water Resources Research* **31** (4) 1107-1118.

Lisle, T.E., Pizzuto, J.E., Ikeda, H., Iseya, F. and Kodama, Y. (1997) Evolution of a sediment wave in an experimental channel. *Water Resources Research* **33** (8), 1971-1981.

Lorenz M.S.F. (1963) Deterministic non-periodic flow. *Journal of the Atmospheric Sciences* **20**, 130-141

Lucas, C. (2000) Attractors everywhere – order from chaos.

<http://homepages.force9.net/calresco/attract.htm>

Madej, M.A. and Ozaki, V. (1996) Channel response to sediment wave propagation and movement, Redwood Creek, California, USA. *Earth Surface Processes and Landforms* **21**, 911-927.

Mandelbrot, B.B. (1982) *The Fractal Geometry of Nature*. W.H. Freeman, New York.

Mandelbrot, B.B. (1986) Self-affine fractal sets. In Petroniero, L. and Tosatti, E. (eds.) *Fractals and Physics, Proceedings of the Sixth Trieste International Symposium on Fractals in Physics, ICTP, Trieste, Italy*. North-Holland, New York, 3-16.

Martin, Y. and Church, M. (1997) Diffusion in landscape development models: on the nature of basic transport relations. *Earth Surface Processes and Landforms*, **22**, 273-279.

McArdle, B. and Faeh, R. (2001) A computational investigation of river braiding. In Mosley, P. (ed.) *Gravel Bed Rivers V*, 73-93.

Meade, R.H. (1985) Wavelike movement of bedload sediment, East Fork River, Wyoming. *Environmental Geology and Water Science* **7** (4), 215-225.

Miall, A.D. (1977) A review of the braided river depositional environment. *Earth Science Reviews* **13**, 1-62.

Miall, A.D. (1978) Lithofacies types and vertical profile models in braided river deposits: a summary. In Miall, A.D. (ed.) *Fluvial Sedimentology*. Canadian Society of Petroleum Geologists Memoir. **5**, 597-604.

Moeckel, R. and Murray, A.D. (1997) Measuring the distance between time series. *Physica D*, **102** 187-194.

Mosley, M.P. (1976) An experimental study of channel confluences. *Journal of Geology* **84**, 535-562.

Mosley, M.P. (1982) Analysis of the effect of changing discharge on channel morphology and instream uses in a braided river, Ohau River, New Zealand. *Water Resources Research* **18** (4), 800-812.

- Murray, A.B. and Paola, C. (1994) A cellular model of braided rivers. *Nature*, **371**, 54-57.
- Murray, A.B. and Paola, C. (1996) A new quantitative test of geomorphic models, applied to a model of braided streams. *Water Resources Research*, **32** (8), 2579-2587.
- Murray, A.B. and Paola, C. (1997) Properties of a cellular braided-stream model. *Earth Surface Processes and Landforms*, **22**, 1001-1025.
- Nicholas, A.P. (2000) Modelling bedload yield in braided gravel bed rivers. *Geomorphology* **36** (1-2), 89-106.
- Nicholas, A.P., Ashworth, P.J., Kirkby, M.J., Maclin, M.G. and Murray, T. (1995) Sediment slugs: large-scale fluctuations in fluvial sediment transport rates and storage volumes. *Progress in Physical Geography* **19** (4), 500-519.
- Nicholas, A.P. and Sambrook Smith, G.H. (1999) Numerical simulation of three-dimensional flow hydraulics in a braided channel. *Hydrological Processes* **13**, 913-929.
- Nienow, P., Sharp, M. and Willis, I. (1998) Seasonal changes in the morphology of the subglacial drainage system, Haut Glacier d'Arolla, Switzerland. *Earth Surface Processes and Landforms*, **23**, 825-843.
- Paola, C. (1996) Incoherent structure: turbulence as a metaphor for stream braiding. In Ashworth, P.J., Bennett, S.J., Best, J.L. and McLelland, S.J. (editors) *Coherent Flow Structures in Open Channels*. John Wiley and Sons, Chichester, 705-723.
- Paola, C. (2000) Quantitative models of sedimentary basin filling. *Sedimentology* **47**, (Supplement 1), 121-178.
- Paola, C. (2001) Modelling stream braiding over a range of scales. In Mosley, P. (ed.) *Gravel Bed Rivers V*, 11-46.
- Paola, C. and Fofoula-Georgiou, E. (2001) Statistical geometry and dynamics of braided rivers. In Mosley, P. (ed.) *Gravel Bed Rivers V*, 47-72.
- Parker, G. (1976) On the cause and characteristic scales of meandering and braiding in rivers. *Journal of Fluid Mechanics* **76** (3), 457-480.
- Parker, G. (1984) Lateral bed load transport on side slopes. *Journal of Hydraulic Engineering*, **110**, 197-199.

- Pickup, G. Higgins, R.J. and Grant, I. (1983) Modelling sediment transport as a moving wave - the transfer and deposition of mining waste. *Journal of Hydrology*, **60**, 281-301.
- Phillips, B.C. and Sutherland, A.J. (1989) Spatial lag effects in bed load sediment transport. *Journal of Hydraulic Research*, **27** (1) 115-133.
- Phillips, B.C. and Sutherland, A.J. (1990) Temporal effects in bed load sediment transport. *Journal of Hydraulic Research*, **28** (1) 5-23.
- Porporato, A. and Ridolfi, L. (1996) Clues to the existence of deterministic chaos in river flow. *International Journal of Modern Physics B*, **10** (15), 1821-1862.
- Rachoki, A.R. (1981) *Alluvial Fans*. John Wiley and Sons, Chichester.
- Rice, S. and Church, M. (1996) Sampling surficial fluvial gravels: the precision of size distribution percentile estimates. *Journal of Sedimentary Research* **66** (3), 654-665.
- Rinaldo, A., Dietrich, W.E., Rigon, R. Vogel, G.K. and Rodríguez-Iturbe, I. (1995) Geomorphological signatures of varying climate. *Nature*, **374**, 632-635.
- Rodríguez-Iturbe, I. and Rinaldo, A. (1997) *Fractal River Networks*. Cambridge University Press.
- Rosenbloom, N.A. and Anderson, R.S. (1994) Hillslope and channel evolution in a marine terraced landscape, Santa Cruz, California. *Journal of Geophysical Research*, **99**, 14012-14029.
- Rubin, D.M. (1999) Forecasting techniques, underlying physics and applications. In Middleton, G.V., Plotnick, R.E. and Rubin, D.M. (eds.) *Nonlinear dynamics and fractals - new numerical techniques for sedimentary data*. USGS SEPM Short Course No. 36. <http://walrus.wr.usgs.gov/seds/ch5/ch5.1.html>
- Rundle, A. (1985a) The mechanism of braiding. *Zeitschrift fur Geomorphologie Supplementband* **55**, 1-3.
- Rundle, A. (1985b) Braid morphology and the formation of multiple channels. the Raakaia, New Zealand. *Zeitschrift fur Geomorphologie Supplementband* **55**, 15-37.
- Sapozhnikov, V. and Foufoula-Georgiou, E. (1996) Self-affinity in braided rivers. *Water Resources Research* **32** (5), 1429-1439.
- Sapozhnikov, V. and Foufoula-Georgiou, E. (1997) Experimental evidence of dynamic scaling and indications of self-organized criticality in braided rivers. *Water Resources Research* **33** (8), 1983-1991.

Sapozhnikov, V., Murray, A.B., Paola, C. and Fofoula-Georgiou, E. (1998) Validation of braided-stream models: spatial state-space plots, self-affine scaling and island shapes. *Water Resources Research* **34** (9), 2353-2364.

Schumm, S.A. (1977) *The Fluvial System*. Wiley, New York.

Sharp, M.J., Richards, K., Willis, I., Arnold, N., Nienow, P., Lawson, W. and Tison, J-L. (1993) Geometry, bed topography and drainage system structure of the Haut Glacier d'Arolla, Switzerland. *Earth Surface Processes and Landforms*, **18** (6), 557-571.

Shvidchenko, A.B. (1997) Field measurements of sediment transport in a piedmont reach of the Laba River. *Journal of Hydrology (N.Z.)* **36**, 173-181.

Shvidchenko, A.B. and Kopaliani, Z.D. (1998) Hydraulic modelling of bedload transport in gravel-bed Laba River. *Journal of Hydraulic Engineering* **124**, 778-785.

Southard, J.B., Smith, N.D. and Kuhnle, R.A. (1984) chutes and lobes: newly identified elements of braiding in shallow gravelly streams. In Koster, E.H. and Steel, R.J. (eds.) *Sedimentology of gravels and conglomerates*. Canadian Society of Petroleum Geologists Memoir **10**, 51-59.

Smart, J.S. and Moruzzi, V.L. (1971) *Quantitative properties of delta channel networks*. U.S. Naval Office Research Contr. N00014-70-C-0188, Technical Report **3**, 27p.

Smith, R. (1991) Short Communication. The application of cellular automata to the erosion of landforms. *Earth Surface Processes and Landforms* **16**, 273-281.

Takens, F. (1980) Detecting strange attractors in turbulence. In Rand, D. and Young L.S. (eds.), *Dynamical Systems and Turbulence*. Berlin, Springer-Verlag, 366-381.

Tang, C. and Bak, P. (1988) Critical exponents and scaling relations for self-organised critical phenomena. *Physical Review Letters*, **60** (23) 2347-2350.

Thomas, R. and Nicholas, A.P. (2002) Simulation of braided river flow using a new cellular routing scheme. *Geomorphology* **43**, 179-195.

Tucker, G.E., Lancaster, S.T., Gasparini, N.M. Bras, R. and Rybarczyk, S.M. (1999) An object orientated framework for distributed hydrologic and geomorphic modelling using triangulated irregular networks. *Computers and Geosciences*, **27** (8), 959-973.

Tucker, G.E. and Slingerland, R. (1997) Drainage basin responses to climate change. *Water Resources Research* **33** (8) 2031-2047.

- van den Berg, J.H. (1995) Prediction of alluvial channel patterns of perennial river. *Geomorphology* **12**, 259-279.
- Vernard, J.K. and Street, R.L. (1961) *Elementary Fluid Mechanics*. John Wiley and Sons Ltd, New York, 689 pp.
- Voronoi, M.G. (1908) Nouvelles applications des paramètres continus à la théorie des formes quadratiques. *Journal reine Angew Mathematiques* **134**, 198-287.
- Warburton, J. and Davies, T. (1994) Variability of bedload transport and channel morphology in a braided river hydraulic model. *Earth Surface Processes and Landforms* **19**, 403-421.
- Wathen, S.J. and Hoey, T.B. (1998) Morphological controls on the downstream passage of a sediment wave in a gravel-bed stream. *Earth Surface Processes and Landforms* **23**, 715-730.
- Webb, E.K. (1994) Simulating the three-dimensional distribution of sediment units in braided-stream deposits. *Journal of Sedimentary Research* **B64** (2), 219-231.
- Webb, E.K. (1995) Simulation of braided channel topology and topography. *Water Resources Research* **31** (10), 2603-2611.
- Webb, E.K. and Anderson, M P. (1996) Simulation of preferential flow in three-dimensional, heterogeneous conductivity fields with realistic internal architecture. *Water Resources Research* **32** (3), 533-545.
- Westaway, R.M., Lane, S.N. and Hick, D.M. (2000) Development of an automated correction procedure for digital photogrammetry for the study of wide, shallow gravel-bed rivers. *Earth Surface Processes and Landforms*, **25**, 200-226.
- Whiting, P.J., Dietrich, W.E., Leopold, L.B., Drake, T.G. and Shreve, R.L. (1988) Bedload sheets in heterogeneous sediment. *Geology* **16**, 105-108.
- Willgoose, G., Bras, R.L. and Rodriguez-Iturbe, I. (1991a) A coupled channel network growth and hillslope evolution model 1. Theory. *Water Resources Research* **27** (7), 1671-1684.
- Willgoose, G., Bras, R.L. and Rodriguez-Iturbe, I. (1991b) A coupled channel network growth and hillslope evolution model 2. Nondimensionalisation and applications. *Water Resources Research* **27** (7), 1685-1696.
- Willgoose, G., Bras, R.L. and Rodriguez-Iturbe, I. (1991c) Results from a new model of river basin evolution. *Earth Surface Processes and Landforms* **16**, 237-254.

Willgoose, G., Bras, R.L. and Rodriguez-Iturbe, I. (1991d) A physical explanation of an observed link area-slope relationship. *Water Resources Research* **27** (7), 1697-1702.

Willgoose, G., Bras, R.L. and Rodriguez-Iturbe, I. (1994) Hydrogeomorphology modelling with a physically based river basin evolution model. pp 271-294 in Kirkby, M.J. (ed.) *Process models and theoretical geomorphology*. John Wiley and Sons, Chichester.

Wolcott, J. and Church, M. (1991) Strategies for sampling spatially heterogeneous phenomena – the example of river gravels. *Journal of Sedimentary Petrology*, **61** (4), 534-543.

Wolfram, S. (1983) Statistical mechanics of cellular automata. *Reviews of Modern Physics* **55** (3) 601-642.

Wolfram, S. (1984) Universality and complexity in cellular automata. *Physica* **10D**, 1-35.

Wolman, M.G. (1954) A method for sampling coarse river-bed material. *American Geophysical Union Transactions*, **35**, 951-956.

Young, W.J. and Davies, T.H. (1991) Bedload transport processes in a braided gravel-bed river model. *Earth Surface Processes and Landforms* **16**, 499-511.

Zarn, B. (1997) *Influence of the river bed width on the interaction of discharge, morphology and bed load transport capacity*. Laboratory of Hydraulics, Hydrology and Glaciology of the Swiss Federal Institute of Technology, Report number **154**, 240pp.

Zielke, W. and Urban, C. (1981) Two dimensional modelling of rivers with floodplains. *Numerical Modelling of River Channel and Overland Flow for Water and Environmental Applications*. IAHR, Delft, Netherlands.

**APPENDIX.****CASCADE AUTHORSHIP AND FORTRAN CODE.****1. Authorship of *Cascade* and *Braided Cascade*.**

This notice concerning the development and authorship of the original version of *Cascade* is inserted at the start of the code for the main program. Please note that the important note below (by Jean Braun) is still valid and anyone wishing to use *Cascade* must gain permission from Jean Braun at the address below.

**1.1. Cascade.**

The program *Cascade* was developed by:

Jean Braun  
Research School of Earth Sciences  
Australian National University  
Canberra, ACT, 0200  
Australia  
Tel: +61-2-6249-5512  
Fax: +61-2-6249-5443  
email: [Jean.Braun@anu.edu.au](mailto:Jean.Braun@anu.edu.au)

(Canberra, June 1st, 1995)  
(Present version September 27, 1999)

**IMPORTANT NOTE:**

Please, note that this software CANNOT be freely distributed. You must obtain Jean Braun's permission to use it (or part of it) or to give to other potential users. Please respect this condition of use. I am trying to protect parts of the Delaunay/Voronoi algorithms that we are using in a commercial venture with Malcolm Sambridge. This means that some of our "clients" had to pay to use this software commercially.

---

**1.2. Braided Cascade.**

The program *Braided Cascade* was developed by:

Judith Cudden  
Department of Geography and Topographic Science  
University of Glasgow  
Glasgow  
G12 8QQ.

As I am no longer at the University of Glasgow, the code is currently being administered by Dr. Trevor Hoey:

Dr. Trevor Hoey  
Department of Geography and Topographic Science  
University of Glasgow  
Glasgow  
G12 8QQ.

e-mail: [thoey@geog.gla.ac.uk](mailto:thoey@geog.gla.ac.uk)

Anyone wishing to use the code for *Braided Cascade* should contact both Jean Braun AND Trevor Hoey (who will then contact myself).

Thanks.

Judith Cudden.

July 2002.

## 2. FORTRAN code for altered subroutines.

The following routines are the altered routines *only*. The original version of *Cascade* contains 31 other routines, 7 calculate tectonic movement and have been switched off in *Braided Cascade*, 21 are unaltered.

### 2.1. FORTRAN code for the grid initialisation subroutine.

c This is a the FORTRAN CODE for the subroutine to generate  
 c a grid of specified dimensions, with known slope, and then to add  
 c white noise of specified amplitude.  
 c Lines beginning with c are comment lines and are inserted to explain  
 c the code. These lines are not read by the program.

```

subroutine makegrid (sidex,sidey,gradient,ampnoise,
&                 randnum,x,y,h,nnode,
&                 delta,surfscale,fix,h2)

```

```

common /vocal/ ivocal

```

```

real  x(nnode),y(nnode),h(nnode)
real  fix(nnode),sidex,sidey,ampnoise,gradient
real  randnum(nnode),delta
real  h2(nnode)

```

c Specify grid details. Units are m, and m/m for gradient.

```

nx=250
ny=10
nnode=nx*ny
sidex=250
sidey=10
gradient=0.02855
delta=sidex/float(nx-1)
surfscale=sidex*sidey/nnode
htop=100

```

c Define nodes, and calculate x, y, h without noise.

```

if(ivocal.eq.1) call debug('random$',0)
call random (x,nnode)
call random (y,nnode)
call random (randnum,nnode)
if(ivocal.eq.1) call debug('makegrid$',1)

```

c Add white noise.

```

ampnoise=0.01*gradient*sidex

do i=1,nx
do j=1,ny
ishake=1
if (i.eq.1 .or. i.eq.nx .or. j.eq.1 .or. j.eq.ny) ishake=0
ij=(i-1)*ny+j

if (i.eq.1 .or. i.eq.nx .or. j.eq.1 .or. j.eq.ny) then

```

```

x(ij)=(float(i-1)/float(nx-1))*sidex
y(ij)=(float(j-1)/float(ny-1))*sidey

else
x(ij)=((x(ij)-0.5)/float(nx-1)
& +float(i-1)/float(nx-1))*sidex
y(ij)=((y(ij)-0.5)/float(ny-1)
& +float(j-1)/float(ny-1))*sidey
endif

```

c Define boundary nodes.

```

fix(ij)=1
if(i.eq.1) fix(ij)=2
if(j.eq.1 .or. j.eq.ny) fix(ij)=0

dh=gradient*x(ij)
h(ij)=(htop-dh)+ampnoise*(randnum(ij)-0.5)
if(fix(ij).eq.0) h(ij)=h(ij)+100

enddo
enddo

close(5)

return
end

```

## 2.2. FORTRAN code for the node ordering subroutine.

c This is the FORTRAN code for the subroutine to calculate the proper  
c order in which the nodes must be stored to perform the river  
c erosion calculations.

c Lines beginning with c are comment lines and are inserted to explain  
c the code. These lines are not read by the program.

```
subroutine find_order (ibucket,ndon,iorder,
&                    nnode,norder,x,xtx,orderin,
&                    outorder,shorttime)
```

c INPUT:

```
c      ndon          = donor array
c      fix           = boundary condition array
c      nnode         = total number of nodes
c      ibucket       = working array
c      orderin       = working array
c      outorder      = working array
c      xtx           = working array
```

```
c OUTPUT:   iorder      = node ordering
c           norder      = number of nodes in the ordering
```

c subroutines called:

c NONE

```
common /vocal/ ivocal
```

```
integer    ibucket(nnode,2)
integer    ndon(nnode,2),iorder(nnode)
integer    orderin(nnode),outorder(nnode)
real       x(nnode),xtx(nnode)
```

```
dimension orderin(nnode)
```

c Set the number of nodes ordered to 0 to start.

```
norder=0
```

c Loop over all the nodes and their receiving nodes. Set the ibucket  
c values of all nodes to 1. If the receiving nodes of a donor nodes are  
c either self donors (local minima) or if a node donates to only one  
c receiver, set the ibucket values of the donor nodes to 0.

```
do i=1,nnode
do j=1,2
ibucket(i,j)=1
enddo
if (ndon(i,1).eq.i) ibucket(i,1)=0
if (ndon(i,2).eq.0) ibucket(i,2)=0
enddo
```

c Loop over all the nodes. If the ibucket value of the node is not 0  
c set it to -1. If

```
do i=1,nnode
```

```

do j=1,2
  if (ibucket(i,j).ne.0) ibucket(ndon(i,j),1)=-1
enddo
if (ibucket(i,2).ne.0) ibucket(i,2)=0
enddo

```

c Loop over all nodes and set the order of nodes equal to the order in c which they were looped over.

```

do ii=1,nnode
  orderin(ii)=ii
enddo

```

c If the node is not a self donor set the xtx value of the FIRST node c to 1000 and loop over nodes 2 to nnode (nnode is the maximum c number of nodes). Set xtx of the ALL OTHER nodes to 0.

```

if(ndon(i,1).ne.i) then
  xtx(1)=1000

```

```

do 16 j=2,nnode
  xtx(j)=0

```

```

16 continue

```

c Loop over all nodes. If the ibucket value of the first receiving node c is 0 then jump out of the loop. Otherwise look at the x co-ordinates c of each node.

```

do 20 jj=1,nnode
  if(ibucket(jj,1).eq.0) goto 20

```

```

  xttest=x(jj)

```

c Loop over all nodes. In the first pass through the loop if the x c co-ordinate of the node is less than the xtx value of the node c (i.e. 1000 for the first node) then loop over the nodes (loop kk) c backwards from the node in question to the first node.

c Set the xtx value of the node in question to the xtx value of the c next node.

```

do 25 k=1,nnode

```

```

  if(xttest.lt.xtx(k)) then

```

```

    do 30 kk=nnode-1,k,-1
      xtx(kk+1)=xtx(kk)

```

```

      outorder(kk+1)=outorder(kk)

```

```

30 continue

```

```

  xtx(k)=xttest

```

```

  outorder(k)=jj

```

```

  goto 20
endif

```

```
25  continue
20  continue
    endif

    do k=1,mnode
        norder=norder+1
        iorder(norder)=outorder(k)
    enddo

return
end
```

### 2.3. FORTRAN code for the fluvial erosion subroutine.

c This is the FORTRAN code for the subroutine to calculate  
 c the amount of fluvial erosion at each node.  
 c Lines beginning with c are comment lines and are inserted to explain  
 c the code. These lines are not read by the program.

```

subroutine fluvial_erosion (xkf,xlf_BR,xlf_AL,
&          x,y,h,h0,hi,ndon,nnode,
&          surface,slope,length,
&          water,sediment,
&          ibucket,dt,fix,
&          dhh,
&          nb,nn,nbmax,
&          iorder,itype_node,
&          dhminfluv,dhmaxfluv,
&          nlake,
&          sea_level,outflux,ideposition,q,
&          ahw,a,b,prewater,hold,xtx,
&          orderin,outorder,wsslope,
&          shorttime)

```

c INPUT:

```

c  xkf          = diffusivity
c  xlf_BR      = bedrock erosion length scale
c  xlf_AL      = alluvials erosion length scale
c  x,y         = x- and y-nodal positions
c  h           = present topography
c  h0          = bedrock-alluvion interface
c  hi          = initial topography (at time 0)
c  ndon        = donor array
c  nnode       = number of nodes
c  surface     = surface associated with each node
c  slope       = slope associated with each nodal link (stream)
c  length      = length associated with each nodal link (stream)
c  ibucket     = working array used to find node ordering
c  dt          = time step length
c  fix         = boundary condition array
c  dhh         = amount of material eroded/deposited over the time step
c  nb          = number of natural neighbours per node
c  nn          = list of natural neighbours
c  nbmax       = maximum of natural neighbours
c  iorder      = working array containing the proper sequence in node
c               number in which to perform the river erosion operations
c  itype_node  = type associated to each node (see later in code)
c  dhminfluv  = minimum amount removed by river erosion
c  dhmaxfluv  = maximum amount removed by river erosion
c  nlake       = determines whether a node is part of a lake or not
c  sea_level   = sea level
c  ideposition = to prevent deposition by rivers (=0)
c  q           = input reading of water at each node (in data file)
c  qn          = n parameter from Murray and Paola water splitting
c  ahw         = water depth
c  a           = coefficient for water depth calculations
c               (from Ergenzinger 1987)
c  b           = exponent for water depth calculations
c               (from Ergenzinger 1987)
c  prewater    = water at each node (before amount is updated)

```

```

c   hold      = old topography
c   xtx       = working array used to find order of nodes
c   orderin   = working array used to find order of nodes
c   outorder  = used to find order of nodes
c   wsslope   = water surface slope
c   shorttime = used to check timestep

c OUTPUT: several arrays are updated:
c   h         = new current topography
c   outflux   = the contribution from river incision to outflux is calculated
c   The following arrays are filled:
c   water     = water discharge at each point
c   sediment  = sediment load at each point

```

c subroutines called:

```

c - debug
c - find_order

```

```

common /vocal/ ivocal

```

```

real  x(nnode),y(nnode),h(nnode),h0(nnode),hi(nnode)
real  xkf(nnode),xlf_BR(nnode)
real  surface(nnode),dhh(nnode)
real  slope(nnode,2),length(nnode,2),qn,a,b
real  fix(nnode),q,water(nnode),rain
real  ahw(nnode),prewater(nnode),hold(nnode)
real  xtx(nnode),wsslope(nnode,2)

```

```

integer  ibucket(nnode,2),split
integer  ndon(nnode,2)
integer  nb(*),nn(nbmax,*)
integer  iorder(nnode),itype_node(nnode)
integer  nlake(nnode)
integer  orderin(nnode),outorder(nnode)

```

```

double precision  sediment(nnode),sedeqb,sedqb1,sedqb2

```

c Initialises parameter values.

```

qn=0.5
akm=2.428e-10
exp=3.606
a=0.16
b=0.37
maxdh=0.1

```

```

c Definition of qn from Murray and Paola (1994,1997),
c called n in their papers).
c akm is the constant in the sediment transport equation and
c exp is the exponent (Hoey et al. 2001).

```

```

c Initialises arrays. Sets water to 1 and sediment to 0 at every node.
c Sets the thickness of the alluvial layer to 50 m.

```

```

do i=1,nnode
h(i)=h(i)
water(i)=0

```

```

sediment(i)=0.
dhh(i)=0.
alluvialthickness=50
h0(i)=(h(i)-alluvialthickness)

```

c Sets all ibucket to 0.

```

do j=1,2
  ibucket(i,j)=0
enddo
enddo

```

c Opens file to read in water for each node.

```

  iread=1

  if(iread.eq.1 .and. time.le.endtime) then
    open(39,file='RUN1//newwater',status='old')

    do j=1,nnode
      read(39,*,end=1999)j,rain,sed
      water(j)=rain
      sediment(j)=sed
    enddo
1999    close(39)
  endif

```

c Sets the minimum and maximum amount of erosion to 0.

```

  dhminfluv=0.
  dhmaxfluv=0.

```

c Orders nodes using the new node ordering subroutine.

```

  if (ivocal.eq.1) call debug ('find_order$',0)
  call find_order (ibucket,ndon,iorder,
&                nnode,norder,x,xtx,orderin,
&                outorder)
  if (ivocal.eq.1) call debug ('fluvial_erosion$',1)

```

c itype\_node determines the type of node:

```

c -2: local minima
c -1: node below sea level (sea level = 0)
c 0: diffusion only
c 1: channel because one of its parents was a channel

```

c Sets all nodes to type 0 .

```

do i=1,nnode
  itype_node(i)=0
enddo

```

c Loops over all nodes in order to determine if they donate to any receiving nodes (array of receiving nodes = ndon).

```

do jorder=1,norder
  i=iorder(jorder)

```

- c If the node donates to one node only the set the splitting function (split)  
 c to 0.  
 c If the node donates to itself (i.e. is a local minima) set split to 4.

```
if(ndon(i,2).eq.i .or. ndon(i,2).eq.0) split=0
if(ndon(i,1).eq.i) split=4
```

- c If the node has two receiving nodes and they are both downslope from  
 c the donor then calculate the slope ratios, the discharge ratios and set  
 c split to equal 1.

```
if((-slope(i,1)).gt.0 .and. (-slope(i,2)).gt.0) then
slopesum=(-slope(i,1)**qn)+((-slope(i,2))**qn)
splitq=(-slope(i,1)**qn)/(slopesum)
splitq2=(-slope(i,2)**qn)/(slopesum)
```

```
qratio=splitq/(splitq+splitq2)
split=1
```

- c If the discharge ratio is greater than the threshold then all water is  
 c routed to the first donor and split is set to 0.

```
if (qratio.gt.0.8) then
ndon(i,2)=0
split=0
endif
```

- c If the node has two upslope receiving nodes, calculate slope ratios,  
 c calculate upslope discharge ratio and set split to 2.

```
elseif((-slope(i,1)).lt.0 .and. (-slope(i,2)).lt.0) then
upslopesum=((slope(i,1)**(-qn))+((slope(i,2))**(-qn)))
upsplit1=((slope(i,1))**(-qn))/upslopesum
upsplit2=((slope(i,2))**(-qn))/upslopesum
upratio=upsplit1/(upsplit1+upsplit2)
split=2
```

- c If the upslope discharge ratio is greater than the threshold then  
 c all water is routed to the first receiving node and split is set to 3.

```
if (upratio.gt.0.8) then
ndon(i,2)=0
split=3
endif
```

- c If the slope to the first receiver is positive and the slope to the  
 c second receiver is negative then all water is routed to the first  
 c receiving node. Split is set to 0.

```
elseif((-slope(i,1)).gt.0 .and. (-slope(i,2)).lt.0) then
ndon(i,2)=0
split=0
```

- c If the slope to the first receiver is negative and the slope to the  
 c second receiver is positive then all water is routed to the second  
 c receiver. THIS SHOULD NEVER HAPPEN but has been left as  
 c a check.

```
elseif((-slope(i,1)).lt.0 .and. (-slope(i,2)).gt.0) then
  ndon(i,1)=0
  split=0
```

c If the slope to the first receiver is approximately 0 and the slope  
c to the second receiver is negative, all water is routed to the first  
c receiver, split is set to 0.

```
elseif (abs(-slope(i,1)).gt.0.000001 .and.
& (-slope(i,2)).lt.0) then
  split=0
  ndon(i,2)=0
```

c If the slope to the first receiver is positive and there is NO second donor,  
c all water is routed to the first receiver. Split is set to 3.

```
elseif((-slope(i,1)).lt.0 .and.
& ndon(i,2).eq.0) then
  split=3
  ndon(i,2)=0

endif
```

c If all water is routed to the first receiver then calculate water and  
c water depth at the receiver.

```
ahw(i)=h(i)+(a*(water(i))**b)

if(split.eq.0 .or. split.eq.3) then
  water(ndon(i,1))=water(ndon(i,1))+water(i)
  ahw(ndon(i,1))=h(ndon(i,1))+(a*(water(ndon(i,1))))**b)
```

c If there are two downslope receiving nodes then iterate to calculate  
c water passed to each receiver. Prewater is the amount of water already  
c at each receiving node (before they receive any more).

```
elseif (split.eq.1) then
```

```
  qrest=qratio
```

```
  prewater1=water(ndon(i,1))
```

```
  prewater2=water(ndon(i,2))
```

```
  count=0
```

```
200    do 150, kk=1,2
```

```
  count=count+1
```

```
  water(ndon(i,1))=(water(i)*qrest)
```

```
  water(ndon(i,2))=(water(i)*(1-qrest))
```

```
  ahw(i)=h(i)+(a*(water(i))**b)
```

```
  ahw(ndon(i,1))=h(ndon(i,1))+(a*(water(ndon(i,1))))**b)
```

```
  ahw(ndon(i,2))=h(ndon(i,2))+(a*(water(ndon(i,2))))**b)
```

```

slopest1=(ahw(ndon(i,1))-ahw(i))/length(i,1)
slopest2=(ahw(ndon(i,2))-ahw(i))/length(i,2)
slopestsum=((-slopest1)**qn)+((-slopest2)**qn)

```

```

splitq1calc=(-slopest1)**qn/(slopestsum)
splitq2calc=(-slopest2)**qn/(slopestsum)

```

```

qrcalc=splitq1calc/(splitq1calc+splitq2calc)

```

```

qrrror=(abs(qrcalc-qrest))

```

c If the error between the calculated value of the discharge ratio (qrcalc)  
c and the user specified value (qrest) is greater than the user specified  
c threshold, update the value of qrest and perform the iteration again,  
c if it is below the threshold, exit the iterative loop and set qratio to  
c equal the new value of qrest.  
c If the program becomes stuck in the loop print an error message.

```

if(qrrror.gt.0.05) then
qrest=qrest+0.5*(qrcalc-qrest)
goto 200
else
goto 300
endif

```

```

if (kk.eq.100) print*, "error in fluvial erosion"

```

```

150    continue
300    qratio=qrest

```

```

water(ndon(i,1))=water(ndon(i,1))+prewater1
water(ndon(i,2))=water(ndon(i,2))+prewater2

```

c If there are two upslope receiving nodes then iterate to calculate  
c water passed to each receiver. upprewater is the amount of water already  
c at each receiving node (before they receive any more).

```

elseif(split.eq.2) then

```

```

upprewater1=water(ndon(i,1))
upprewater2=water(ndon(i,2))

```

```

ahw(i)=h(i)+(a*(water(i))**b)

```

```

ahw(ndon(i,1))=h(ndon(i,1))+a*(water(ndon(i,1)))**b
ahw(ndon(i,2))=h(ndon(i,2))+a*(water(ndon(i,2)))**b

```

```

upslopest1=(ahw(ndon(i,1))-ahw(i))/length(i,1)
upslopest2=(ahw(ndon(i,2))-ahw(i))/length(i,2)

```

c For two upslope receiving nodes.

```

if((-upslopest1).gt.0 .and.
&  (-upslopest2).gt.0) then
upslopesum=((-upslopest1)**qn)+((-upslopest2)**qn)
upsplithw1=(-upslopest1)**qn/upslopesum
upsplithw2=(-upslopest2)**qn/upslopesum

```

```
upratiohw=upsplithw1/(upsplithw1+upsplithw2)
```

```
water(ndon(i,1))=water(i)*upratiohw
water(ndon(i,2))=water(i)*(1-upratiohw)
```

```
water(ndon(i,1))=water(ndon(i,1))+upprewater1
water(ndon(i,2))=water(ndon(i,2))+upprewater2
```

c For the first receiving node with a positive slope from the donor node  
c and the second with a negative slope.

```
elseif((-upslopest1).gt.0 .and.
&      (-upslopest2).lt.0) then
  upsplithw1=0
  upsplithw2=0
  upratiohw=0
  water(ndon(i,1))=water(ndon(i,1))+water(i)
  water(ndon(i,2))=0
```

```
water(ndon(i,1))=water(ndon(i,1))+upprewater1
water(ndon(i,2))=water(ndon(i,2))+upprewater2
```

c For the first receiving node with a negative slope and the  
c second with a positive slope.

```
elseif((-upslopest1).lt.0 .and.
&      (-upslopest2).gt.0) then
  upsplithw1=0
  upsplithw2=0
  upratiohw=0
  water(ndon(i,2))=water(ndon(i,2))+water(i)
  water(ndon(i,1))=0
```

```
water(ndon(i,1))=water(ndon(i,1))+upprewater1
water(ndon(i,2))=water(ndon(i,2))+upprewater2
```

c Both receiving nodes have negative slopes.

```
elseif((-upslopest1).lt.0 .and.
&      (-upslopest2).lt.0) then
  upslopesum1=(upslopest1**(-qn))+ (upslopest2**(-qn))
  upspliq1calc=((upslopest1)**(-qn))
&  /(upslopesum1)
  upspliq2calc=((upslopest2)**(-qn))
&  /(upslopesum1)
```

```
upqrcalc=upspliq1calc/(upspliq1calc+upspliq2calc)
```

```
water(ndon(i,1))=water(i)*upqrcalc
water(ndon(i,2))=water(i)*(1-upqrcalc)
```

```
water(ndon(i,1))=water(ndon(i,1))+upprewater1
water(ndon(i,2))=water(ndon(i,2))+upprewater2
```

```
endif
endif
```

c Special treatment for self donors.

c Self donating nodes: type of node is set to -2.

```

if (ndon(i,1).eq.i) then
  dh=0.
  water(i)=water(i)
  sediment(i)=sediment(i)
  itype_node(i)=-2

```

c Special treatment for boundary nodes Upstream boundary nodes, fix = 2.

c Side boundary nodes, fix = 0.

```

if (fix(i).eq.1 .or. fix(i).eq.2) then
  outflux=outflux+sediment(i)
  if(fix(i).eq.2) dh=0

```

```

else if (fix(i).eq.0) then
  outflux=outflux
endif

```

c Special treatment for nodes below sea level. Node type is set to -1.

```

elseif (h(i).lt.sea_level) then
  dh=sediment(i)/surface(i)
  h(i)=h(i)+dh
  itype_node(i)=-1
  sediment(i)=0.

```

c If the node is not a self donor or below sea-level then

c node type is set to 1.

```

else
  if (itype_node(i).ne.0) itype_node(i)=1

```

c Sediment transport calculation.

c sedeqb is how much sediment the river can carry (carrying capacity).

c 1000 is water density.

c First calculate carrying capacity for nodes that donate to one

c downslope node only.

```

if(split.eq.0) then
  if(slope(i,1) .lt. -0.0457) slope(i,1)=-0.0457
  sedeqb=(akm*((( -slope(i,1))) * water(i) * 1000)**exp)*dt
  sedqb1=0
  sedqb2=0

```

c Now calculate carrying capacity for nodes with two downslope

c receiver nodes.

```

elseif (split.eq.1) then

```

```

if(slope(i,1) .lt. -0.0457) slope(i,1)=-0.0457
if(slope(i,2) .lt. -0.0457) slope(i,2)=-0.0457

```

```

sedqb1=(akm*(-slope(i,1)*water(i)*qratio*1000)**exp)*dt
sedqb2=(akm*(-slope(i,2)*water(i)*(1-qratio)*1000)**exp)
& *dt
sedeqb=sedqb1+sedqb2

```

c Calculate carrying capacity for nodes with two upslope receiver nodes.

```

elseif(split.eq.2) then
sedqb1=0
sedqb2=0
sedeqb=0

```

c Calculate carrying capacity for nodes with one upslope receiver node.

```

elseif(split.eq.3) then
sedqb1=0
sedqb2=0
sedeqb=0

```

```
endif
```

c If carrying capacity is very small set it equal to 0.

c If the receiver node(s) is/are downslope from the donor node

c calculate amount of sediment donated to each receiver node.

c If the receiving node(s) is/are upslope from the donor node, NO

c sediment is moved to the receiver node(s).

```

if(sedeqb.lt.1.e-100) then
sdratio1=0
sdratio2=0
elseif(split.eq.1 .or. split.eq.2) then
sdratio1=sedqb1/sedeqb
sdratio2=sedqb2/sedeqb
elseif(split.eq.0 .or. split.eq.3) then
sedqb1=0
sedqb2=0
sdratio1=0
sdratio2=0
endif

```

c Special treatment for lake nodes. No ponding is allowed in the model

c so the next section should not be used, it is included to trap errors.

```

if (nlake(i).eq.1) then
dh=sediment(i)/surface(i)
h(i)=h(i)+dh
sediment(i)=0.

```

c Deposition.

c If the amount of sediment at a node is greater than the carrying capacity

c AND deposition is allowed, then deposition occurs.

```

elseif (sediment(i).ge.sedeqb.and.ideposition.eq.1) then
dh=(sediment(i)-sedeqb)/surface(i)

```

c There is a maximum amount of sediment that can be dumped at one location.

c The maximum is given by the maximum height that the dumping may

c produce such that the slope it creates between this node and its donor is not

c greater than the erosional threshold. In other words, it is assumed that

c by deposition one cannot create a levee so big that at the next time step

c it is going to be eroded down. The maximum amount of erosion that is

c allowed to take place in one timestep is set to equal the D50 of surface

c sediment from Arolla, 1999 (see thesis chapter 3).

```

alluvialthickness=50
h0(i)=(h(i)-alluvialthickness)

if (water(i).ne.0.) then
dhmax=0.07751

else
dhmax=dh
endif
if (dh.le.dhmax) then
sediment(i)=sedeqb
h(i)=h(i)+dh

else
dh=dhmax
sediment(i)=sediment(i)-dhmax*surface(i)
h(i)=h(i)+dh

endif

```

c Erosion.

c There are three cases in which erosion may take place:  
c erosion in bedrock only, erosion in alluvial material only and  
c erosion in both alluvial material and bedrock.  
c In Braided Cascade the alluvial layer is set to be 50 m thick so all  
c erosion should take place within this layer (i.e. the second  
c scenario is true).

```
else
```

c Redefine length scales.

```

xlength_BR=amin1(length(i,1)/xlf_BR(i),1.)
xlength_AL=amin1(length(i,1)/xlf_AL,1.)

```

c First case: eroding bedrock only.

```

alluvialthickness=50
h0(i)=(h(i)-alluvialthickness)

if (h(i).le.h0(i)) then
dsediment=(sedeqb-sediment(i))*xlength_BR
dh=-dsediment/surface(i)
h(i)=h(i)+dh
sediment(i)=sediment(i)+dsediment

```

c Second case: eroding alluvial material only.

```

else
if (fix(i).ne.2) then
dsediment=(sedeqb-sediment(i))*xlength_AL

```

```

dh=-dsediment/surface(i)
if (dh.ge.h0(i)-h(i)) then
h(i)=h(i)+dh
sediment(i)=sediment(i)+dsediment

```

```

else
dh=0

```



```
endif
```

```
else
```

c Third case: eroding alluvial material and bedrock.

```
if(fix(i).ne.2) then
```

```
dh1=h(i)-h0(i)
```

```
dsediment1=dh1*surface(i)/xlength_AL
```

```
& dsediment=(sedeqb-sediment(i)-dsediment1)*  
xlength_BR
```

```
dh=-dsediment/surface(i)
```

```
h(i)=h0(i)+dh
```

```
sediment(i)=sediment(i)+dsediment1+dsediment
```

```
else
```

```
dh=0
```

```
endif
```

```
endif
```

```
endif
```

```
endif
```

```
dhminfluv=amin1(dhminfluv,dh)
```

```
dhmaxfluv=amax1(dhmaxfluv,dh)
```

c From water, sediment and slope update height and sediment.

```
if(split.eq.4) sediment(i)=sediment(i)
```

```
if (split.eq.0) then
```

```
sediment(ndon(i,1))=sediment(ndon(i,1))+sediment(i)
```

```
goto 890
```

```
elseif (split.eq.1) then
```

```
sediment(ndon(i,1))=sediment(ndon(i,1))
```

```
& +sediment(i)*sedratio1
```

```
sediment(ndon(i,2))=sediment(ndon(i,2))
```

```
& +sediment(i)*sedratio2
```

```
elseif (split.eq.2) then
```

```
sediment(ndon(i,1))=sediment(ndon(i,1))
```

```
& +sediment(i)*sedratio1
```

```
sediment(ndon(i,2))=sediment(ndon(i,2))
```

```
& +sediment(i)*sedratio2
```

```
endif
```

```
890 endif
```

```
if((-slope(i,1)).ne.0) itype_node(ndon(i,1))=1
```

```
if((-slope(i,2)).ne.0) itype_node(ndon(i,2))=1
```

c Compute elevation change, dhh.